Ex Vivo Expanded Adult Human Periosteal Cells for Future Use in Craniofacial Bone Repair



- Lisanne Groeneveldt -

Ex Vivo Expanded Adult Human Periosteal Cells for Future Use in Craniofacial Bone Repair

Lisanne Caroline Groeneveldt

Copyright 2023. Erasmus University Medical Center, Rotterdam, and KU Leuven, Group Biomedical Sciences, Leuven.

Uitgegeven in eigen beheer - Publication privately printed – Lisanne Groeneveldt

Cover-design: Mandy van Passel

All rights reserved. No part of the publication may be reproduced in any form of print, photoprint, microfilm, electronic or any other means without prior written permission from the publisher.

Alle rechten voorbehouden. Niets uit deze uitgave mag worden vermenigvuldigd en/of openbaar gemaakt worden door middel van druk, fotokopie, microfilm, elektronisch of op welke andere wijze ook zonder voorafgaande schriftelijke toestemming van de uitgever.

The work presented in this joint doctorate thesis was performed in the Department of Development and Regeneration, Faculty of Medicine, KU Leuven, Leuven, Belgium and the Department of Cell Biology at Erasmus University Medical Center (Erasmus MC), Rotterdam, The Netherlands. In the Leuven department, the PhD training was coordinated by the Doctoral School of Biomedical Sciences. PhD education and training at the Erasmus University Rotterdam (EUR) was coordinated through the Erasmus MC Graduate School. The Department of Cell Biology is also member of the Erasmus MC – Leiden University joint research school *Medisch Genetisch Centrum (MGC) Zuid-West Nederland*. This booklet is the dissertation presented in partial fulfilment of the requirements for the doctorate degree at the KU Leuven and the EUR, respectively.

Printed by

RIDDERPRINT

Ohmweg 17, 2952 Alblasserdam, The Netherlands

www.ridderprint.nl

Ex Vivo Expanded Adult Human Periosteal Cells for Future Use in Craniofacial Bone Repair

Ex vivo gegroeide adulte cellen uit humaan periost voor toekomstig gebruik in herstel van craniofaciaal bot

Thesis

to obtain the joint doctorate degree from the Erasmus University Rotterdam and KU Leuven by command of the rector magnificus Prof. dr. A.L. Bredenoord and rector Prof. dr. L. Sels and in accordance with the decisions of the respective Doctorate Boards

The public defense shall be held on
28 september 2023, at 10:30 a.m. in Rotterdam, The Netherlands, and
tbd in Leuven, Belgium
by

Lisanne Caroline Groeneveldt
born in Rotterdam, The Netherlands

Erasmus University Rotterdam

KU LEUVEN

KU LEUVEN
DOCTORAL SCHOOL BIOMEDICAL SCIENCES

Doctoral promotion committees at the respective universities

Erasmus University Rotterdam

Inner doctorate committee

Promoters:	Prof. dr. D.F.E. Huylebroeck
	Prof. dr. L. Geris
Other members:	Prof. dr. G. Carmeliet
	Assoc. Prof. dr. G. Jansen
	Prof. dr. P. ten Dijke

KU Leuven

Promoter:	Prof. dr. L. Geris
Co-Promoter:	Prof. dr. F.P. Luyten
Other members:	Prof. dr. P. Callaerts
	Prof. dr. G. Carmeliet
	Prof. dr. C.I. Colnot
	Prof. dr. D.F.E. Huylebroeck
	Assoc. Prof. dr. G. Jansen
	Prof. dr. F. Lambert

Table of contents

List of used abbreviations

List of all figures

Chapter 1	Introduction	**1**
Chapter 2	Scope of this thesis	**21**
Chapter 3	The bone-forming properties of periosteum-derived cells differ between harvest sites	**25**
Chapter 4	Schneiderian membrane derived cells have bone-forming capacities not superior to other hPDCs	**55**
Chapter 5	Human periosteum-derived cells do expand and retain their bone-forming properties in platelet lysate	**71**
Chapter 6	Human periosteum-derived cells primed with BMP2 can heal a large bone defect in rats	**87**
Chapter 7	Discussion, and some perspectives	**107**
Appendix	Summary	**120**
	Samenvatting	**122**
	Curriculum vitae and PhD portfolio	**124**
	Acknowledgments	**128**

List of contents

List of used abbreviations

List of all figures

Chapter 1 Introduction

1.1. Situation
1.2. Bone tissue
1.3. Bone tissue formation
1.4. Craniofacial development
1.5. Bone tissue engineering
1.6. Skeletal Stem and Progenitor Cells
1.7. Bone tissue engineering for the craniofacial area

Chapter 2 Scope of this thesis

Chapter 3 The bone-forming properties of periosteum-derived cells differ between harvest sites

3.1. Summary
3.2. Introduction
3.3. Results
    3.3.1. Characterization of the isolated and expanded hPDCs
    3.3.2. Human PDCs can be expanded for 2 months
    3.3.3. *In vitro* analysis of marker genes of expanded hPDCs from three different origins
    3.3.4. Bulk RNA-seq of cultured adult hPDCs reveals differences that reflect different embryonic origins
    3.3.5. *In vivo* bone formation
3.4. Discussion
3.5. Experimental procedures
Supplementary tables
Other supplementary tables
Literature references

Chapter 4 Schneiderian membrane derived cells have bone-forming capacities not superior to other hPDCs

4.1. Summary
4.2. Introduction
4.3. Results
    4.3.1. Primary cells obtained from the inner side of the maxillary sinus can readily be expanded in cell culture
    4.3.2. Cultured sinus membrane cells can be differentiated towards the chondrogenic and osteogenic lineages
    4.3.3. SSPC-marker analysis in sinus membrane cells
    4.3.4. *In vivo* bone formation
4.4. Discussion
4.5. Experimental procedures

Supplementary table
Literature references

Chapter 5 Human periosteum-derived cells do expand and retain their bone-forming properties in human platelet lysate

5.1. Summary
5.2. Introduction
5.3. Results
    5.3.1. Proliferation of cultured hPDCs in the presence of hPL
    5.3.2. Flowcytometrics
    5.3.3. *In vitro* differentiation
    5.3.4. *In vivo* bone formation
5.4. Discussion
5.5. Experimental procedures
Supplementary table
Literature references

Chapter 6 Human periosteum-derived cells primed with BMP2 can heal a large bone defect in rats

6.1. Summary
6.2. Introduction
6.3. Results
    6.3.1. RNA-sequencing of BMP2 and BMP6-primed hPDCs in cell culture
    6.3.2. Knockdown studies
    6.3.3. *In vivo* ectopic bone formation
    6.3.4. *In vivo* orthotopic bone formation
6.4. Discussion
6.5. Experimental procedures
Supplementary table
Literature references

Chapter 7 Discussion, and some perspectives

7.1. Background
7.2. *In vitro* culture of cells
7.3. Priming of cells
    7.3.1. Priming with BMPs
    7.3.2. Angiogenesis
7.4. Perspectives
Literature references

Summary

Samenvatting

Curriculum vitae and PhD portfolio

Acknowledgments

List of used abbreviations

-:	negative
+:	positive
3D:	3-dimensional
ACAN:	aggrecan
ActR:	activin receptor
ALK:	activin receptor like kinase
ALP:	alkaline phosphatase
α-MEM:	Minimum Essential Medium Eagle – alpha modification
AP:	anterior-posterior
ATOH:	Atonal BHLH Transcription Factor
β-gal:	β-galactosidase
BGLAP:	bone gamma-carboxyglutamate protein
BM:	bone marrow
BMP:	bone morphogenetic protein
BMPR:	bone morphogenetic protein receptor
BSA:	bovine serum albumin
BSP:	Bone sialoprotein
CAII:	carbonic anhydrase-II
CaP:	calcium phosphate
CASP:	caspase
CD:	cluster of differentiation
CDM:	chemically defined medium
cDNA:	complementary DNA
CEB:	cell extraction buffer
CI:	confidence interval
COL:	collagen
CPD:	cumulative population doubling
COM:	counts per million
CT:	computer tomography
CTHRC:	Collagen Triple Helix Repeat Containing
CTSK:	cathepsin-K
DEG:	differentially expressed gene
DLX:	distal-less homeobox
DMEM:	Dulbecco's modified Eagle's medium
ECM:	extracellular matrix
EdU:	5-ethynyl-2′ -deoxyuridine
EGF:	epidermal growth factor
EMA:	European Medicines Agency
EMT:	epithelial-to-mesenchymal transformation
EO:	endochondral ossification
Erk:	extracellular signal-regulated kinases
FACS:	fluorescence activated cell sorting
FBS:	fetal bovine serum
FDA:	Food and Drug Administration (USA)
FDR:	false discovery rate
FGF:	fibroblast growth factor
FLT:	Fms Related Receptor Tyrosine Kinase
FMO:	Fluorescence-Minus-One
GAPDH:	glyceraldehyde 3-phosphate dehydrogenase
GDF:	growth and differentiation factor
GelMA:	gelatin methacryloyl
GSEA:	gene-set enrichment analysis
H/E:	hematoxylin/eosin
HIF:	hypoxia-inducible factor
HOTAIR:	*HOX* transcript antisense RNA
hPDC:	human periosteum-derived cell
hPL:	human platelet lysate
HPRT:	Hypoxanthine Phosphoribosyltransferase

hSM:	(cell from the) human maxillary sinus
ID:	inhibitor of DNA-binding
IGF:	insulin-like growth factor
IO:	intramembranous ossification
iPSC:	induced pluripotent stem cell
KI67:	marker of proliferation Ki-67
LEP:	leptin
M-CSF:	macrophage colony-stimulating factor
MD:	mandible
MMP:	metallproteinase
mRNA:	messenger RNA
MSC:	mesenchymal stromal (or stem) cell
MSX:	Msh homeobox
mTOR:	mammalian target of rapamycin
MTT:	3-(4,5-Dimethylthiazol-2-yl)-2,5-diphenyltetrazolium bromide
MX:	maxilla
Nano-CT:	nano-computed tomography
OPG:	osteoprotegerin
OPN:	osteopontin
Padj:	adjusted p-value
PAX:	paired box
PBS:	phosphate-buffered saline
PCA:	principal component analysis
PDC:	periosteum-derived cell
PDGF:	platelet-derived growth factor
PDPN:	podoplanin
PFA:	paraformaldehyde
PIC:	protease inhibitor cocktail
POC:	primary ossification center
PPARG:	peroxisome proliferator activated receptor gamma
PVDF:	polyvinylidene fluoride
qPCR:	quantitative polymerase chain reaction
RANKL:	receptor activator of nuclear factor κB ligand
RNA-seq:	RNA-sequencing
RT:	reverse transcription
RUNX:	Runt-related transcription factor
S1P:	Sphingosine-1 phosphate
SD:	standard deviation
SEMA4D:	Semaphorin-4D
Shh:	sonic hedgehog
SIBLING:	small integrin binding N-linked glycoproteins
siRNA:	small-interfering RNA
SOC:	secondary ossification center
SP7:	transcription factor 7
SPARC:	Secreted protein acidic and cysteine rich
SSPC:	skeletal stem and progenitor cell
T:	tibia
TAK:	TGFβ-activated kinase
TGFβ:	transforming growth factor type β
TP:	tumor protein
VEGF:	vascular endothelial growth factor
VEGFR:	vascular endothelial growth factor receptor
TRAP:	tartrate-resistant acid phosphatase
X-gal:	5-bromo-4-chloro-3-indolyl-β-D-galactopyranoside

List of all figures

Fig. 1.1. Structure of bone.
Fig. 1.2. Osteoclastogenesis, osteoblastogenesis and their interplay.
Fig. 1.3. Schematic overview of intramembranous and endochondral ossification, respectively, and fracture healing.
Fig. 1.4. Development of the mandible.
Fig. 3.1. Characterization of isolated and expanded human periosteum-derived cells.
Fig. 3.2. Further characterization of isolated and expanded hPDCs.
Fig. 3.3. Human PDCs can be expanded for 2 months.
Fig. 3.4. Marker gene analysis in hPDCs.
Fig. 3.5. Bulk RNA-seq results in hPDCs.
Fig. S3.1. Comparative gene ontology analyses. Maxillary versus tibial-derived hPDCs. The bone-forming properties differ between maxillary and tibial hPDCs.
Fig. S3.2. Comparative gene ontology analyses. Mandibular versus tibial-derived hPDCs. The bone-forming properties differ between mandibular and tibial hPDCs.
Fig. S3.3. Comparative gene ontology analyses. Maxillary versus mandibular-derived hPDCs. The bone-forming properties differ between maxillary and mandibular hPDCs.
Fig. 3.6. Validation of RNA-seq results of hPDCs of three different sources.
Fig. 3.7. Bone formation *in vivo* by expanded hPDCs of various origin.
Fig. 4.1. Proliferative characteristics of sinus membrane-derived cells in comparison to hPDCs of other origin.
Fig. 4.2. Trilineage differentiative capacity of cells obtained from the Schneiderian membrane.
Fig. 4.3. Bone formation *i vivo* by hPDCs of various origin (Groeneveldt *et al.,* 2020) and by cells derived from the sinus membrane.
Fig. 5.1. Characterization during the expansion of human periosteum-derived cells in hPL versus FBS (control).
Fig. 5.2. Flow-cytometric analysis of cell cycle in in vitro cultured hPDCs, including in hPL-supplemented DMEM.
Fig. S5.1. Adipogenic differentiation capacities of cultured hPDCs, including in hPL-supplemented DMEM.
Fig. 5.3. Differentiation capacities of cultured hPDCs, including in hPL-supplemented DMEM.
Fig. 5.4. *In vivo* bone-forming capacity of hPDCs expanded in hPL-supplemented DMEM.
Fig. 6.1. RNA-seq profiling of BMP2 and BMP6 primed hPDCs in cell culture.
Fig. 6.2. Comparative expression levels of individual genes in unprimed (control) or BMP-primed mandibular hPDCs based on RNA-seq.
Fig. 6.3. Gene expression levels after knockdown of DLX5 and/or DLX6, including in BMP2 and/or BMP6 priming conditions.
Fig. S6.1. Gene expression levels after knockdown of DLX5 and/or DLX6, including in BMP2 and/or BMP6 priming conditions.
Fig. 6.4. *In vivo* bone formation results 8 weeks after implantation of constructs.
Fig. 7.1. BMP signalling and its crosstalk with WNT

Chapter 1

Introduction

Based on:
Master thesis *Molecular Medicine* (Erasmus University Medical Center Rotterdam), Groeneveldt LC, 2017
Master thesis *Dentistry* (KU Leuven), Groeneveldt LC, 2019
Groeneveldt LC *et al.,* ***Front Cell Dev Biol.*** 2020 Nov 25;8:554984

1.1. Situation

In the clinic, bone grafts are used frequently to treat bone defects primarily in orthopedics and traumatology departments, and also in oral and maxillofacial surgery (Amini *et al.*, 2012; Sallent *et al.*, 2020). In the latter case, important causes for severe bone defects are trauma, oncologic resection, and congenital malformations as well as craniofacial osteonecrosis and impactful prosthetic treatments. About 178 million bone fractures occur each year globally, approximately 5-10% of which are accompanied by delayed healing, with more than 15% of the latter even resulting in a non-healing fracture (Bishop *et al.*, 2012; Buza and Einhorn, 2016; GBD 2019 Fracture Collaborators, 2021). Oncologic treatments in the oral cavity have a yearly incidence of about 4 per 100,000 (van Dijk *et al.*, 2016), about 77% of these being treated by oncologic resection, resulting again in bone defects in the cases where the bone was involved. The palate or gum is involved in 23% of the oncologic cases, which are mostly treated by removal of some bone tissue (due to the resection intervention), because these are body sites where the bone tissue is located immediately below the soft tissue. Congenital malformations, such as an alveolar cleft, have a prevalence of 1.8 to 25 per 10,000 live births, firmly requiring a therapy to close the bony defect, which comes with a success rate of 46 to 63% (Dissaux *et al.,* 2016; Wu *et al.,* 2018). In osteonecrosis of the jaw (*e.g.*, occurring in 1 out of every 1,500 people taking bisphosphonate therapy) a bone-replacement therapy may be required, especially when the jaw structure is interrupted and dental prosthesis is no longer possible (Caldroney *et al.*, 2017; Lo *et al.*, 2023). Taken together, bone-replacing therapies are often required and have several causes. The ideal bone graft material is osteoconductive for its support to the bone structure, and is able to induce bone formation (Moussa and Dym, 2020; Doonquah *et al.,* 2021). The current standard is to use autologous bone tissue for grafting, and to obtain it from different body locations, such as the iliac crest, ribs, fibula, cranial bones or mandible.

Worth noting is that bone is the second-most transplanted tissue worldwide, second only to blood (Liu *et al.,* 2013). Of course, bone transplantation implies the generation of a second surgical site where the tissue is harvested, and this creates the risk for donor site morbidity (including pain) and major complications (in up to 10% of the donor sites). These complications include vascular injuries or deep infection within the donor site, and the possibility of herniation of abdominal contents if iliac crest grafts were used (Arrington *et al.,* 1996). Furthermore, quantities of donor tissue for filling large bone defects are usually inadequate and, in addition, poor vascularization of the tissue graft can lead to necrosis within the transplantation site (Meijer *et al.,* 2008). The use of allogeneic bone donated by post-mortem individuals could be a solution, but due to poor integration of such allografts in general the failure rates can reach up to 30% (Sorger *et al.,* 2001). Allografts potentially also transmit infectious diseases or elicit host-versus-graft reactions (Graham *et al.,* 2010). These problems could be solved by applying irradiation or freeze-drying procedures, but these procedures risk to affect the osteoinductive capacity of such grafts (Finkermeier, 2002). Besides bone tissue, also non-biological osteoconductive biomaterials or osteoinductive implants are used in the management of bony defects. They use hydroxyapatite or other calcium phosphates, demineralized bone or calcium sulfates, with or without added polypeptide growth/differentiation factors (Elsalanty and Genecov, 2009; Tannoury and An, 2014; Johari *et al.,* 2016; Wang and Yeung, 2017; Wu *et al.,* 2017). The used metal (like titanium) in implants also accompanies an increased risk of infection (estimated 16%), and other bone void fillers (such as bioceramics) give only limited bone regeneration (only ~26% more mineralized tissue) compared to non-use of bone substitutes (Rohner *et al.,* 2013; Wiggins *et al.,* 2013). An emerging solution to repair bone defects is therefore to use engineered bone tissue.

1.2. Bone tissue

Bone tissue serves multiple functions, collectively providing structure, stability and, together with the joints and muscular tissue, mobility to the body. Also, bones such as the ribs and the hyoid will protect internal organs and provide an open airway (Genta *et al.,* 2014; Su *et al.,* 2019). Furthermore, bone has hematopoietic, endocrine and storage functions, including calcium and phosphate, which can be released in case their respective concentrations in the blood become too low (Zhou *et al.,* 2021).

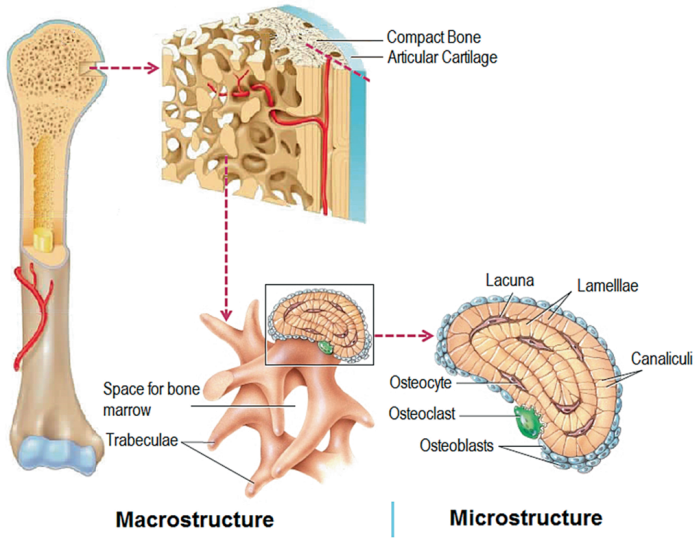

Figure 1.1. Structure of bone.

Bone tissue consists of compact cortical bone and less dense trabecular bone tissue, both consisting of mineralized tissue, osteocytes and canaliculi in-between, and osteoclasts and osteoblasts as bone-lining cells at the outer side. Image adapted from Wang *et al.* (2016).

Bones consist of trabecular bone in the middle, cortical bone tissue at the surroundings, and periosteal tissue that covers the bone tissue. The cortical bone tissue is very dense: it contains plenty of collagen type-1 fibrils on which hydroxyapatite is deposited, with only 3-5% of the space reserved for bone cells (osteocytes), for channels that serve supply of macronutrients via fluid in the bone tissue (canaliculi), and for blood vessels. In trabecular bone, the situation is similar, but here 10-50% of its volume is reserved for osteocytes, canaliculi and blood vessels as well as adipocytes and cells of the bone marrow (**Fig 1.1;** Rho *et al.,* 1998; Wang *et al.,* 2016).

Bone tissue consists of osteoblasts that first deposit the aforementioned collagen type-1 and later, as they mature, mineralize bone with hydroxyapatite crystals. These consist of calcium phosphate for which the phosphates come about by actions of alkaline phosphatases, with alkaline phosphate (ALP) being released by the osteoblasts (Anh *et al.,* 1998; Hessle *et al.,* 2002). Non-collagenous proteins in the extracellular matrix are the Small Integrin Binding N-Linked Glycoproteins (SIBLING) consisting of, among others, bone sialoprotein (BSP, with BSP2 also

known to bind to integrins (I), hence its synonym IBSP) and the highly phosphorylated sialoprotein osteopontin (OPN). These play a role in the continuous mineralization process as well as bone remodeling and maintenance (Bouet *et al.,* 2015).

Next, the osteoblasts can undergo apoptosis or become entrapped by bone tissue; in the latter case they will become terminally differentiated osteocytes or they can line the bone tissue as quiescent cells, waiting for signals that activate them. Osteoblasts also secrete macrophage colony-stimulating factor (M-CSF) and receptor activator of nuclear factor κB ligand (RANKL). Both these cytokines stimulate the formation and subsequent development of osteoclasts. M-CSF also stimulates the differentiation of hematopoietic stem cells towards macrophages and pre-osteoclasts. Together with RANKL, it further directs these pre-osteoclasts towards the bone-resorbing osteoclasts (Feng and Teitelbaum, 2013; Kim *et al.,* 2020; Ma *et al.,* 2022). On the one hand osteoclasts resorb bone by a generating an acidic environment in the cavity between their adhesion site and the cell durface, and by their produced enzymes that accumulate in this cavity (*e.g.*, tartrate-resistant acid phosphatase (TRAP), carbonic anhydrase-II (CAII) and cathepsin-K (CTSK); Bernhardt *et al.,* 2017). Osteoblasts further release osteoprotegerin (OPG), which stimulates osteoclastogenesis (Udagawa *et al.,* 2020). On the other hand, osteoclasts secrete complement component-3 (C3), Collagen Triple Helix Repeat Containing-1 (CTHRC1) and Sphingosine-1 phosphate (S1P), thereby stimulating the differentiation of mesenchymal stromal cells (MSCs) towards osteoblasts or provoking increased osteoblast migration and survival (**Fig. 1.2**). Osteoclasts further produce Semaphorin-4D (SEMA4D), a secreted inhibitor of osteoblast differentiation (Kim *et al.,* 2020). During bone resorption, active Transforming Growth Factor type-β1 (TGFβ1) and Insulin Growth Factor-1 (IGF1) are released from the bone matrix and induce osteoblast differentiation (Kim *et al.,* 2020). As mentioned, osteoclasts originate from the hematopoietic lineage, and also hematopoiesis takes place in the bone marrow (Yu and Scadden, 2016).

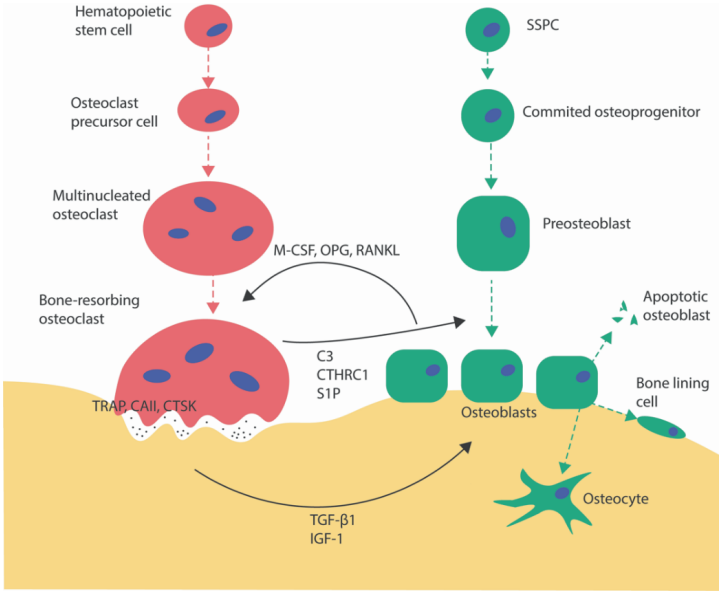

Figure 1.2. Osteoclastogenesis, osteoblastogenesis and their interplay.

Osteoclasts are formed from hematopoietic stem cells, osteoblasts from skeletal stem/progenitor cells (SSPCs). Those osteoblasts can become apoptotic or bone lining cells, or osteocytes, which reside in the bone tissue. Image based on Kim *et al.* (2020).

1.3. Bone tissue formation

Bone tissue arises either by intramembranous or endochondral bone formation. In both processes, the future bone-forming cells are derived from skeletal stem and progenitor cells (SSPCs) capable of self-renewal. In intramembranous ossification (IO), the SSPCs differentiate towards osteoblasts, the bone-producing cells that deposit collagen type-1 and mineralize it with hydroxyapatite (see **section 1.2**). As soon these cells get encapsulated by bone tissue, they become osteocytes that permanently reside within the bone and meanwhile vascularization is triggered (**Fig. 1.3A**). Bones such as the upper jaw (maxilla), some of the skull, and clavicle are formed by IO.

During the process of endochondral ossification (EO), cartilage forms as an intermediate tissue. Here, SSPCs differentiate towards chondroblasts under influence of SRY-box-9 (SOX9) transcription factor and produce extracellular matrix (ECM) consisting of collagen type-2 saturated with glycosaminoglycans. These chondroblasts become encapsulated by the cartilage matrix as chondrocytes, which are still able to proliferate, but progress into mature and even hypertrophic chondrocytes. These latter cells display metabolic changes and swelling, resulting in cells that can get 20 times bigger (Kronenberg, 2006; Cooper *et al.,* 2013; Berendsen and Olsen, 2015). Those cells no longer produce collagen type-2α1 chain (COL2A1), resulting in the ECM typical for cartilage, but now synthesize collagen type-10α1 chain (COL10A1), the transcription factor Runt-related transcription factor-2 (RUNX2), secreted vascular endothelial growth factor (VEGF), and several matrix metalloproteinases (MMPs). The expression of *COL10A1* thus results in the formation of an extracellular network typically consisting of collagen type-10; RUNX2 promotes chondrocyte hypertrophy; VEGF attracts blood vessels and achieves tissue vascularization; MMPs degrade collagen fibers and therefore the ECM (Chen *et al.,* 2014; Kozhemyakina *et al.,* 2015).

After the chondrocytes become hypertrophic, two options are possible, and they both occur. First, some of the hypertrophic chondrocytes die and leave cavities that will later become invaded by osteoprogenitor cells that are supplied by the surrounding cartilaginous matrix (the perichondrium, later becoming periosteum) and by the blood flow in the already vascularized matrix. Further, hematopoietic and endothelial cells invade the tissue, forming the primary ossification center and later on the second ossification center at both ends of the developing bone (Karsenty and Wagner, 2002; Maes *et al.,* 2010). The osteoprogenitor cells differentiate subsequently to osteoblasts under influence of transcription factors RUNX2 and transcription factor 7 (Sp7), leading to the production of bone matrix (Nakashima *et al.,* 2002; Park *et al.,* 2015). Second, another portion of hypertrophic chondrocytes will start to *trans*differentiate (the direct conversion of one differentiated cell type into another), towards osteoblasts (**Fig. 1.3B**; Zhou *et al.,* 2014; Long *et al.,* 2022). Long bones such as the femur and tibia are formed by EO, as does a large portion of the mandible. The bone tissue that is formed by EO gets already vascularized during the hypertrophic cartilage state, while bone that is formed by IO only gets vascularized by the moment bone matrix is already produced.

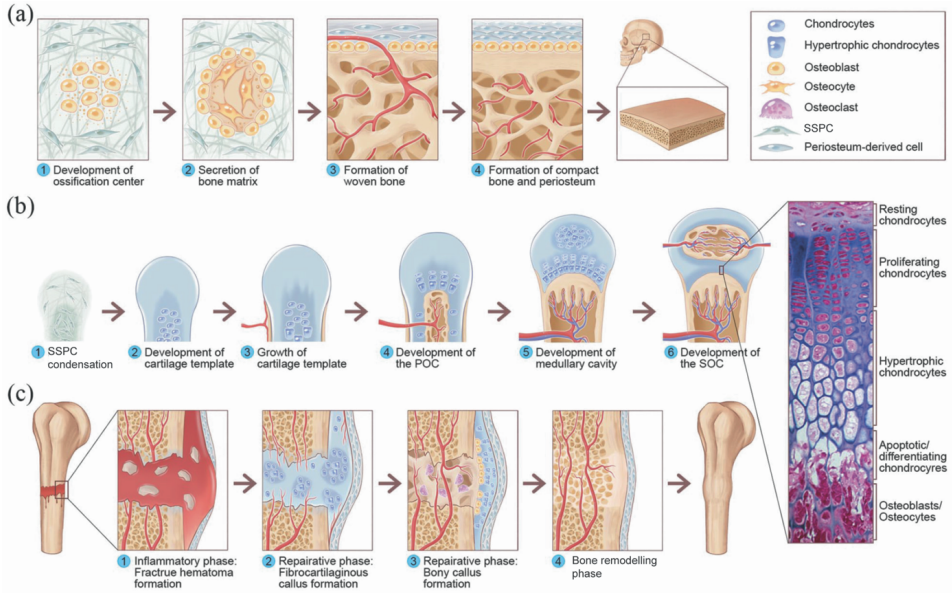

Figure 1.3. Schematic overview of intramembranous and endochondral ossification, respectively, and fracture healing.

(a). Intramembranous ossification showing osteoblasts producing bone matrix and subsequently displaying vascularization. **(b).** Endochondral ossification showing a cartilage template with chondrocytes that increase in size, and blood vessel attraction, together the development of a primary ossification center (POC) and secondary ossification center (SOC). On the right, a histological image of the epiphyseal plate with chondrocytes that proliferate, become hypertrophic and *trans*differentiate towards osteoblasts and subsequently osteocytes. **(c).** Fracture healing showing a hematoma, the formation of callus, which resembles a cartilage intermediate, with the start of the vascularization in the fracture and then the mineralization. Image adapted from Fu *et al.,* 2021.

1.4. Craniofacial development

During the third week of human gestation, three layers of embryonic tissue arise in the inner cell mass between blastocyst formation and the onset of gastrulation: the ectoderm, the mesoderm and the definitive endoderm, respectively. The ectoderm gives rise to the skin and neural plate, the endoderm to *e.g.*, the intestinal system, urinary tract and the airways (Rossant and Tam, 2022). Long bones in the limbs derive from a subregion of mesoderm, the lateral plate mesoderm, while the axial skeleton originates from the sclerotome part of the segmented somites within the paraxial mesoderm. The mesenchymal cells in the outgrowing limbs then differentiate towards chondrogenic and osteogenic, and *e.g.*, *in vitro* also along adipogenic lineages. In contrast, many bones of the skull, in particular those of the face, are derived from multipotent cranial neural crest cells, while the posterior part of the skull is formed by prechordal mesodermal cells that produce cartilage and bone (Berendsen and Olsen, 2015). Neural crest cells arise from those ectodermal cells at the border of the neural plate, which ultimately converges via neurulation into a closed neural tube at the dorsal midline of the elongated embryo, with its dorsal half in the trunk part (posterior to the future brain) of the embryo exposed to Wnt factors and BMPs, exerting downstream effects via Msh homeobox 1 (MSX1) and MSX2, distal-less homeobox 5 (DLX5) and specific paired box (PAX) genes (Villanueva *et al.,* 2002; Tribulo *et al.,* 2003; Meulemans and

Bronner-Fraser, 2004; Green *et al.,* 2015). During neural tube closure, the "mesectodermal" neural crest cells thus obtain properties of mesenchymal cells and are released as individual cells from the edges of the neural plate, typically having undergone epithelial-to-mesenchymal transformation (EMT). From this moment they are sometimes collectively referred to as ectomesenchymal cells. These cells, generated over the entire anterior-posterior (rostral-caudal) axis of the embryo, migrate extensively. In the cranial region they differentiate towards osteoblastic, adipogenic, chondrogenic, odontogenic and muscle cells, but also towards neural cells giving rise to ganglia, and thus neurons and glial cells, and pigment-containing melanocytes (Green *et al.,* 2015).

Long bones, such as the tibia, are formed by endochondral ossification (EO; a process of osteogenesis that uses hypertrophic chondrocytes, see above). In contrast, craniofacial bone tissue of the jaws in particular is formed in two ways: the upper jaw (maxilla) is completely formed by intramembranous ossification (IO, involving direct osteogenesis), whereas the lower jaw (mandible) is formed by IO in combination with the aforementioned EO. Here, the EO centers are positioned in symphysis and at the condyles (**Fig. 1.4**), and at these places cartilage forms first. These chondrocytes become hypertrophic and are subsequently replaced by bone, as previously explained. The other parts of the mandible are formed by IO where, as mentioned above, osteoblasts are directly formed by differentiation of MSCs (Martin *et al.,* 2017).

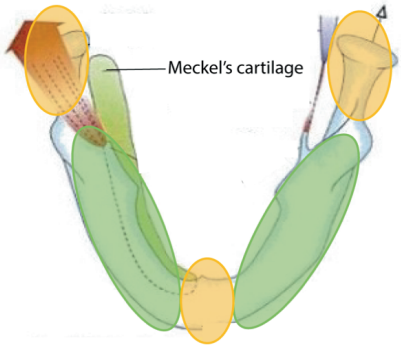

Figure 1.4. Development of the mandible.

The green zones indicate zones of intramembranous ossification, the orange areas zones of endochondral ossification.

Differences in embryonic origin and the respective distinct mechanisms of bone tissue formation could be at the basis of the different properties of the respective progenitor cells, and thus influence adult bone repair strategies for different body sites. In addition, typically descriptive differences between craniofacial bone and skeletal tissue include their respective turnover rate, the level of expression of osteoblast marker genes, and the degree of calcification. Craniofacial bone tissue expresses osteoblast marker genes at higher levels, has a higher rate of cellular proliferation, and "ages" more slowly compared to long bones. Similar observations have been done in engineered bone tissue derived from dental pulp stem cells. The latter cells also develop from cranial neural crest cells and, when they were used for bone tissue engineering strategies, higher proliferation rates and more mineralized tissue have been obtained. Maxillary bone tissue arises by IO and consists of trabecular bone tissue surrounded by a thin cortical layer,

has low bone density and mineral content, and a good vascularization. Mandibular bone tissue develops by both EO and IO (see above), and consists of lamellar bone tissue surrounded by a thick cortical layer, and has high mineral content and bone density (Devlin *et al.,* 1998; Park *et al.,* 2008; Chugh *et al.,* 2013; Lindhe *et al.,* 2013; Kotze *et al.,* 2014). This could also explain the difference in prevalence of osteonecrosis, which occurs more often in mandibular bones.

1.5. Bone tissue engineering

As introduced above, bone tissue engineering presents an alternative and promising treatment option for severe bone defects. Engineered constructs are classically composed of (i) appropriate cells that are able to proliferate as well as differentiate in cell culture, and further (ii) polypeptide growth/differentiation factors that instruct differentiation of the cells, and (iii) a 3-D environment that provides biomechanical support (Leijten *et al.,* 2015).

Bone tissue engineered constructs start to being used in patients in the craniofacial area. They are however only successful in a limited range of indications (Schimming and Schmelzeisen, 2004; Voss *et al.,* 2010; Trautvetter *et al.,* 2011). Therefore, approaches to prime cells with growth/differentiation factors such as bone morphogenetic proteins (BMPs) and the use of more sophisticated scaffolds that not only give 3-D structure to the tissue, but also promote osteoconduction and osteoinduction, are continuously being improved (Shadjou and Hasanzadeh, 2015; Venkatesan *et al.,* 2015; Bolander *et al.,* 2016; Bolander *et al.*, 2017; Diomede *et al.*, 2018). Scaffolds should be well-tolerated (biocompatible) and able to degrade (biodegradable), such that they can be replaced by bone tissue, and preferably also support bone healing. Natural polymers and synthetic polymers have both been considered. The natural polymers, like those based on proteins (*e.g.*, gelatin, collagen, fibrin) or the glycosaminoglycans hyaluronic acid and chondroitin sulfate, and the naturally occurring polysaccharide alginate (most commonly prepared from seaweed) are biocompatible and biodegradable. The use of synthetic polymers (*e.g.*, polyethylene glycol, polyvinyl alcohol, polyacrylamide) offers high controllability of the end product as well as beneficial mechanical properties (Li *et al.,* 2018). Simulations have been made on the osteoinductive effects of calcium phosphate-based scaffolds and their resorption (Sun *et al.,* 2013; Wang *et al.,* 2020).

In order to promote differentiation of SSPCs towards bone-producing cells, priming with polypeptide growth/differentiation factors, in particular BMPs, is commonly used (Rosen *et al.,* 2012; Bolander *et al.*, 2016). BMPs form a special subclass of TGF-b family ligands. Before their identification (and cDNA cloning) as novel cytokines, they were discovered by Urist and co-workers who found that demineralized bone matrix, when implanted ectopically into the muscle or under the skin, could induce bone (Katagiri and Watabe, 2016; for a historical overview, see Grgurevic *et al.*, 2017). BMPs play a role in bone formation, but also in various phases and cellular processes during embryonic development in invertebrates and vertebrates where they act in a dose-dependent fashion (*e.g.*, gastrulation, embryonic patterning and organogenesis, including limb and tooth development; Matsuda *et al.*, 2016; Thesleff, 2018; Economou and Hill., 2020; Madamanchi *et al.*, 2021). Furthermore, they have a role in embryonic and adult angiogenesis, adult iron homeostasis, inflammation, sexual reproduction, and tissue regeneration (Lowery and Rosen, 2018; Sader and Roy, 2022).

In the human skeleton, the genes encoding BMP2, -3, -4, -5, -6, -7, -13 and -14 are expressed (Salazar *et al.,* 2016; Wu *et al.*, 2016; Lowery and Rosen, 2018). BMP13 is also known as GDF6, while BMP14 is better known as GDF5. Besides those 8 BMP genes, also BMP1, 8a, 8b,10, 11, 12

and even 15 exist. For BMP2, -4, -5 and -6 it is known that gene mutations result in skeletal malformations, whereas GDF5 and GDF6 are more connected to cartilage formation, which can be of importance for endochondral ossification (Lowery and Rosen, 2018). For BMP2 and BMP7, the respective regulatory approvals have been given for clinical use in specific treatments. However, BMP7 has been withdrawn from the market (Gillman and Jayasuriya, 2021). For BMP6, promising results are being obtained (Bolander *et al.*, 2016; Pecin *et al.*, 2021) and its effects on endochondral ossification in fracture repair have been explored (Freyria and Maiielin-Gerin, 2012; Mendes *et al.*, 2016). BMP2 and BMP6 both exert their effect via receptor-activated phospho-SMAD1/5/8 (with SMAD8 being renamed to SMAD9; Zou *et al.*, 2021), with sometimes differences between osteogenic and chondrogenic differentiation (Ju *et al.*, 2000), but also non-SMAD pathways involving protein kinases, e.g., p38 MAPK, extracellular signal-regulated kinases (Erk) or TGFβ-activated kinase-1 (Tak1) (Jin *et al.,* 2006; Lou *et al.,* 2000; Shim *et al.,* 2009; Retting *et al.,* 2009; Olsen *et al.,* 2018), the latter also interacting with Smad proteins (Hoffman *et al*., 2005).

Whereas BMP2 is known to bind the BMPR-IA (ALK3) and BMPR-IB (ALK6) type-I receptors, BMP6 also often binds to ActR-IA (ALK2) (Kaps *et al.*, 1998; for reviews, see Heldin and Moustakas, 2016; Yadin *et al.*, 2016). ALK2 and ALK3 are present throughout cartilage and bone formation, ALK6 during chondrogenesis and late osteogenesis, but not during the phase with hypertrophic cartilage (Haaijman *et al.*, 2000; Lin *et al.*, 2016). BMP2 is also necessary for endochondral bone formation and fracture repair (Tsuji *et al.*, 2006; Shu *et al.*, 2011), whereas BMP6 is necessary for periosteal bone formation and the function of the growth plate, which is responsible for growth of the bones in length (Perry *et al.*, 2008). From this, we infer that both BMP2 and BMP6 are each or in combination important factors to direct hPDCs towards bone formation. However, the feasibility of the clinical application of BMPs remains complicated in the field (Bolander *et al.*, 2017; Mata *et al.*, 2017). By using high doses of BMPs, far above physiological levels, side effects might be caused such as bone formation outside the bone defect (ectopic bone), bone resorption by osteoclasts, and/or inappropriate or misbalance in adipogenesis (James *et al.*, 2016).

In the past, many researchers focused on bone tissue engineering via IO. Methods of cell culturing and methods of their priming, and the use of different scaffolds have been explored. However, these constructs failed when up scaled because of lack of vascularization, resulting in significant tissue necrosis (Farrell *et al.,* 2009). Another way to engineer bone tissue is by relying on EO, in which first cartilage intermediate tissue is formed. Chondrocytes live in a hypoxic environment, and when these chondrocytes become hypertrophic, they will, as a consequence of hypoxia, attract blood vessels; osteoblasts are deposited in the nascent cavities, creating in these conditions ultimately a mineralized tissue. Bone tissue engineering via EO is known to give an 8-fold higher bone volume construct *in vivo* as compared to engineering via IO. Several groups have obtained promising results with the ability of SSPCs to guide bone formation along the *in vivo* process of EO (Huang *et al.,* 2006; Gawlitta *et al.,* 2010; Janicki *et al.,* 2010; Scotti *et al.,* 2010; Farrell *et al.,* 2011; Thompson *et al.,* 2014).

1.6. Skeletal Stem and Progenitor Cells

For bone tissue engineering, stem/progenitor cells are often used because of their capabilities to proliferate substantially in cell culture and differentiate after priming towards osteoblasts or chondrocytes. In particular, SSPCs are often used. They are more readily available than embryonal cells and are thus capable of differentiating towards multiple mesenchymal cell types in fact, such as adipogenic cells, chondrogenic cells, osteogenic cells, skeletal myoblasts and smooth muscle

cells (Pittenger *et al.,* 1999; Janeczek Portalska *et al.,* 2012; Williams *et al.,* 2012). SSPCs were originally often obtained from bone marrow and sometimes its adjacent skeletal muscle. Later, it became clear that multipotent mesenchymal cells can be obtained from several other tissues/locations, including adipose tissues, gingiva, dental pulp, the periodontal ligament, and periosteum. These alternative and new sources for multipotent SSPCs are increasingly being used because of the lower impact (less morbidity) upon their collection, and their good availability also in quantity compared to bone marrow-derived SSPCs (Chim *et al.,* 2008).

Multiple cell sources are being used for tissue engineering strategies, and such SSPCs therefore differ in differentiation potential. They are also stimulated (e.g. by polypeptide growth factors) in various ways in cell culture, and different potency assays *in vitro* and *in vivo* are used. Therefore, the field definitely needed refinement of the criteria for MSCs (the previous term for SSPCs). Furthermore, SSPC preparations can bbe heterogeneous in cell types and cell states, with only a fraction of the harvested populations representing true stem cells as SSPCs. First, the field requests that MSCs must be plastic-adherent when maintained in standard culture conditions. Second, MSCs must be positive for CD105, CD73 and CD90, and lack CD45, CD34, CD14 or CD11b, CD79alpha or CD19, and HLA-DR at the cell surface. Third, MSCs must be able to differentiate to osteoblasts, adipocytes and chondroblasts *in vitro* (Dominici *et al.,* 2006).

During the last 20 years,, the focus in cell-based bone tissue engineering strategies shifted progressively towards mimicking, the embryonic development of bone tissue formation and fracture healing processes (Ingber and Levin, 2007; Lenas *et al.,* 2009; Bolander *et al.,* 2017). Since fracture healing at the center of the callus occurs via EO and at the periphery of the callus also by IO, SSPCs will be required that can form bone tissue by both EO and IO (Ferguson *et al.,*, 1999). This means the SSPCS should be capable of forming both bone tissue and cartilage tissue. Although a trilineage differentiation capacity is set as requirement for MSCs already, bone marrow-derived cells show a preference for bone tissue formation over cartilage formation (Duchamp de Lageneste *et al.,* 2018).

Human periosteum derived cells (hPDCs) as a global population, are able to form both cartilage and bone *in vivo* without a need for prior priming. Moreover, after removal of the periosteum, bone fracture healing becomes strongly hindered (Gröngröft *et al.,* 2019). Duchamp de Lageneste and co-workers verified the involvement hPDCs in bone fracture healing by transplantation of GFP-labeled PDCs in mice. This lineage tracing approach has shown that those cells become activated after bone injury during the inflammatory phase (Julien *et al.,* 2022). Also the self-renewal potential of such hPDCs was assessed by colony forming efficiency assays, and this showed a proliferation rate that is even faster than that of bone marrow-derived SSPCs (Duchamp de Lageneste *et al.,* 2018). Therefore, these hDPCs are increasingly recommended for use in bone tissue engineering as a suitable and clinically relevant cell source (Ferguson *et al.,* 1999; Knothe Tate *et al.,* 2008; Colnot *et al.,* 2012; Roberts *et al.,* 2015; Duchamp de Lageneste *et al.,* 2018). Successful isolation of these multipotent hPDCs has been reported by several teams, and bone tissue engineering using these cells and relying on IO and EO formation principles is continuously improving (Nakahara *et al.,* 1991; de Bari *et al.,* 2006; van Gastel *et al.,* 2012).

However, and most importantly, the exact identity of the SSPCs giving rise to both bone and cartilage is still not completely understood. In the early 2010's, there was a surge in research looking to state the criteria for mouse SSPCs as well as human SSPCs. For mice, Chan and co-workers stated that SSPCs should be CD45$^-$Ter119$^-$Tie2$^-$AlphaV$^+$Thy$^-$6C3$^-$. An early progenitor cell should additionally be negative for marker CD105, while later, at less multipotent stages, they become positive for this marker. For the expression of CD200 the opposite occurs: cells are expressing this marker gene at early stages, but lose its expression when they progress more into

specified bone, cartilage and hematopoietic-supportive stroma-producing cells. The criteria for human SSPCs were defined in these studies as $PDPN^{+}CD146^{-}CD73^{+}CD164^{+}$ (Chan *et al.,* 2015; Chan *et al.*, 2018). Later on, adaptations based on these panels have been forwarded by Chan and other workers in the field for periosteum derived cells that are able to form bone tissue; *i.e*. $CD105^{-}CD200^{+}ITGAV^{+}$(Gulati *et al.,* 2018; Long *et al.,* 2022), or $Lin^{-}CD90^{-}CD200^{+}CD105^{-}$ (Debnath *et al.,* 2018). Those cells are capable to self-renew and give rise to bone, cartilage and stromal cells. They can indeed still be isolated from various tissue types, such as bone, articular cartilage and adipose tissue. Induced pluripotent stem cells (iPSCs), after priming with BMP2, also meet these criteria (Luyten and Roberts, 2018).

After these altered criteria for SSPCs, still multiple cell sources did fulfill those criteria and the difference between hPDCs and other SSPCs was still not completely understood. Attempts were made by using markers such as alpha-smooth muscle actin, cathepsin K and paired related homeobox 1, showing the self-renewal potency of cells fulfilling these criteria (Debnath *et al.,* 2018; Duchamp de Lageneste *et al.,* 2018; Ortinau *et al.,* 2019; for a recent comprehensive review on growth factor reactivity and on markers of periosteum derived SSPCs, and further references therein, see Perrin and Colnot, 2022). Despite all efforts, it is not yet known whether, for example, those aforementioned cathepsin K-positive cells are the same cells that are positive for the expression of alpha-smooth muscle actin and paired related homeobox 1. Furthermore, it is still, and rightly so, questioned whether hPDCs are a mixed group of cells from which some give rise to chondrogenic differentiation and others osteogenic differentiation, or whether it is the same (sub)population that gives rise to both bone and cartilage. Single cell RNA sequencing after bone injury shows distinctly different populations present in periosteum derived cells (Julien *et al.,* 2022). In addition, the effects of the environment should not be underestimated, since injury to the skeletal muscle results in altered environmental clues, giving arise more fibrotic tissue and followed by impaired bone healing, even though the required hPDCs are still present at the site of bone injury (Julien *et al.,* 2021).

1.7. Bone tissue engineering for the craniofacial area

Most research in the field of bone tissue engineering was done with tibial-derived hPDCs, also for the purpose of filling bone defects in tibia (or femur). The knowledge emanating from this research cannot, however, automatically be transferred to bone defects such as those in the craniofacial area. Importantly, all bones (except the sesamoid bone) contain a periosteal layer (Nahian and Chauhan, 2022). This means that hPDCs can also be obtained from extra places in the body, as those already mentioned above, including the periosteum covering the maxilla or mandible. Since the expression of HOX-genes differs between cells from the craniofacial area compared to those obtained from the tibia, differences in cellular behaviour can be expected, although cells do also react to environmental clues. This can even result in an altered expression of HOX-genes (Leucht *et al.,* 2008; Bradaschia-Correa *et al.,* 2019). The schneiderian membrane, just like the periosteum, lines the bone tissue. However, this tissue is found at the inner side of the maxillary sinus. It consists of a bone-facing layer and a thin layer of pseudo-stratified columnar ciliated epithelium with vascularized connective tissue (Srouji *et al.,* 2009). When the sinus membrane is partially loosened from the bone tissue during dental implant surgery, this results in a thickening of the bone layer of the maxillary sinus floor (Lundgren *et al.,* 2004; Rong *et al.*, 2015; Zahedpasha *et al.*, 2021). *In vitro* and *in vivo* work has shown that those cells are able to form bone tissue in specific circumstances, making them possibly suitable for bone tissue engineering techniques (Srouji *et al.,* 2009).

Literature references

Amini AR, Laurencin CT, Nukavarapu SP. Bone tissue engineering: recent advances and challenges. Crit Rev Biomed Eng. 2012;40(5):363-408.

Anh DJ, Dimai HP, Hall SL, Farley JR. Skeletal alkaline phosphatase activity is primarily released from human osteoblasts in an insoluble form, and the net release is inhibited by calcium and skeletal growth factors. Calcif Tissue Int. 1998 Apr;62(4):332-340.

Arrington ED, Smith WJ, Chambers HG, Bucknell AL, Davino NA. Complications of iliac crest bone graft harvesting. Clin Orthop Relat Res. 1996 Aug;(329):300-309.

Berendsen AD, Olsen BR. Bone development. Bone. 2015 Nov;80:14-18.

Bernhardt A, Koperski K, Schumacher M, Gelinsky M. Relevance of osteoclast-specific enzyme activities in cell-based in vitro resorption assays. Eur Cell Mater. 2017 Jan 18;33:28-42.

Bishop JA, Palanca AA, Bellino MJ, Lowenberg DW. Assessment of compromised fracture healing. J Am Acad Orthop Surg. 2012 May;20(5):273-282.

Bolander J, Chai YC, Geris L, Schrooten J, Lambrechts D, Roberts SJ, Luyten FP. Early BMP, Wnt and Ca(2+)/PKC pathway activation predicts the bone forming capacity of periosteal cells in combination with calcium phosphates. Biomaterials. 2016 Apr;86:106-118.

Bolander J, Ji W, Leijten J, Teixeira LM, Bloemen V, Lambrechts D, Chaklader M, Luyten FP. Healing of a large long-bone defect through serum-free in vitro priming of human periosteum-derived Ccells. Stem Cell Reports. 2017 Mar 14;8(3):758-772.

Bouet G, Bouleftour W, Juignet L, Linossier MT, Thomas M, Vanden-Bossche A, Aubin JE, Vico L, Marchat D, Malaval L. The impairment of osteogenesis in bone sialoprotein (BSP) knockout calvaria cell cultures is cell density dependent. PLoS One. 2015 Feb 24;10(2):e0117402.

Bradaschia-Correa V, Leclerc K, Josephson AM, Lee S, Palma L, Litwa HP, Neibart SS, Huo JC, Leucht P. Hox gene expression determines cell fate of adult periosteal stem/progenitor cells. Sci Rep. 2019 Mar 25;9(1):5043.

Buza JA 3rd, Einhorn T. Bone healing in 2016. Clin Cases Miner Bone Metab. 2016 May-Aug;13(2):101-105.

Caldroney S, Ghazali N, Dyalram D, Lubek JE. Surgical resection and vascularized bone reconstruction in advanced stage medication-related osteonecrosis of the jaw. Int J Oral Maxillofac Surg. 2017 Jul;46(7):871-876.

Chan CK, Seo EY, Chen JY, Lo D, McArdle A, Sinha R, Tevlin R, Seita J, Vincent-Tompkins J, Wearda T, Lu WJ, Senarath-Yapa K, Chung MT, Marecic O, Tran M, Yan KS, Upton R, Walmsley GG, Lee AS, Sahoo D, Kuo CJ, Weissman IL, Longaker MT. Identification and specification of the mouse skeletal stem cell. Cell. 2015 Jan 15;160(1-2):285-298.

Chan CKF, Gulati GS, Sinha R, Tompkins JV, Lopez M, Carter AC, Ransom RC, Reinisch A, Wearda T, Murphy M, Brewer RE, Koepke LS, Marecic O, Manjunath A, Seo EY, Leavitt T, Lu WJ, Nguyen A, Conley SD, Salhotra A, Ambrosi TH, Borrelli MR, Siebel T, Chan K, Schallmoser K, Seita J, Sahoo D, Goodnough H, Bishop J, Gardner M, Majeti R, Wan DC, Goodman S, Weissman IL, Chang HY, Longaker MT. Identification of the human skeletal stem cell. Cell. 2018 Sep 20;175(1):43-56.e21.

Chen H, Ghori-Javed FY, Rashid H, Adhami MD, Serra R, Gutierrez SE, Javed A. Runx2 regulates endochondral ossification through control of chondrocyte proliferation and differentiation. J Bone Miner Res. 2014 Dec;29(12):2653-2665.

Chim H, Schantz JT, Gosain AK. Beyond the vernacular: new sources of cells for bone tissue engineering. Plast Reconstr Surg. 2008 Sep;122(3):755-764.

Chugh T, Ganeshkar SV, Revankar AV, Jain AK. Quantitative assessment of interradicular bone density in the maxilla and mandible: implications in clinical orthodontics. Prog Orthod. 2013 Oct 20;14(1):38.

Colnot C, Zhang X, Knothe Tate ML. Current insights on the regenerative potential of the periosteum: molecular, cellular, and endogenous engineering approaches. J Orthop Res. 2012 Dec;30(12):1869-1878.

Cooper KL, Oh S, Sung Y, Dasari RR, Kirschner MW, Tabin CJ. Multiple phases of chondrocyte enlargement underlie differences in skeletal proportions. Nature. 2013 Mar 21;495(7441):375-378.

De Bari C, Dell'Accio F, Vanlauwe J, Eyckmans J, Khan IM, Archer CW, Jones EA, McGonagle D, Mitsiadis TA, Pitzalis C, Luyten FP. Mesenchymal multipotency of adult human periosteal cells demonstrated by single-cell lineage analysis. Arthritis Rheum. 2006 Apr;54(4):1209-1221.

Debnath S, Yallowitz AR, McCormick J, Lalani S, Zhang T, Xu R, Li N, Liu Y, Yang YS, Eiseman M, Shim JH, Hameed M, Healey JH, Bostrom MP, Landau DA, Greenblatt MB. Discovery of a periosteal stem cell mediating intramembranous bone formation. Nature. 2018 Oct;562(7725):133-139.

Devlin H, Horner K, Ledgerton D. A comparison of maxillary and mandibular bone mineral densities. J Prosthet Dent. 1998 Mar;79(3):323-327.

Diomede F, Gugliandolo A, Scionti D, Merciaro I, Cavalcanti MF, Mazzon E, Trubiani O. Biotherapeutic Effect of Gingival Stem Cells Conditioned Medium in Bone Tissue Restoration. Int J Mol Sci. 2018 Jan 23;19(2):329.

Dissaux C, Bodin F, Grollemund B, Bridonneau T, Kauffmann I, Mattern JF, Bruant-Rodier C. Evaluation of success of alveolar cleft bone graft performed at 5 years versus 10 years of age. J Craniomaxillofac Surg. 2016 Jan;44(1):21-26.

Dominici M, Le Blanc K, Mueller I, Slaper-Cortenbach I, Marini F, Krause D, Deans R, Keating A, Prockop Dj, Horwitz E. Minimal criteria for defining multipotent mesenchymal stromal cells. The International Society for Cellular Therapy position statement. Cytotherapy. 2006;8(4):315-317.

Doonquah L, Holmes PJ, Ranganathan LK, Robertson H. Bone grafting for implant surgery. Oral Maxillofac Surg Clin North Am. 2021 May;33(2):211-229.

Duchamp de Lageneste O, Julien A, Abou-Khalil R, Frangi G, Carvalho C, Cagnard N, Cordier C, Conway SJ, Colnot C. Periosteum contains skeletal stem cells with high bone regenerative potential controlled by periostin. Nat Commun. 2018 Feb 22;9(1):773.

Economou AD, Hill CS. Temporal dynamics in the formation and interpretation of Nodal and BMP morphogen gradients. Curr Top Dev Biol. 2020;137:363-389.

Elsalanty ME, Genecov DG. Bone grafts in craniofacial surgery. Craniomaxillofac Trauma Reconstr. 2009 Oct;2(3):125-134.

Farrell E, van der Jagt OP, Koevoet W, Kops N, van Manen CJ, Hellingman CA, Jahr H, O'Brien FJ, Verhaar JA, Weinans H, van Osch GJ. Chondrogenic priming of human bone marrow stromal cells: a better route to bone repair?Tissue Eng Part C Methods. 2009 Jun;15(2):285-295.

Farrell E, Both SK, Odörfer KI, Koevoet W, Kops N, O'Brien FJ, Baatenburg de Jong RJ, Verhaar JA, Cuijpers V, Jansen J, Erben RG, van Osch GJ. In-vivo generation of bone via endochondral ossification by in-vitro chondrogenic priming of adult human and rat mesenchymal stem cells. BMC Musculoskelet Disord. 2011 Jan 31;12:31.

Feng X, Teitelbaum SL. Osteoclasts: New Insights. Bone Res. 2013 Mar 29;1(1):11-26.

Ferguson C, Alpern E, Miclau T, Helms JA. Does adult fracture repair recapitulate embryonic skeletal formation? Mech Dev. 1999 Sep;87(1-2):57-66.

Finkemeier CG. Bone-grafting and bone-graft substitutes. J Bone Joint Surg Am. 2002 Mar;84(3):454-64.

Freyria AM, Mallein-Gerin F. Chondrocytes or adult stem cells for cartilage repair: the indisputable role of growth factors. Injury. 2012 Mar;43(3):259-65.

Fu R, Liu C, Yan Y, Li Q, Huang RL. Bone defect reconstruction via endochondral ossification: A developmental engineering strategy. J Tissue Eng. 2021 Mar 30;12:20417314211004211.

Gawlitta D, Farrell E, Malda J, Creemers LB, Alblas J, Dhert WJ. Modulating endochondral ossification of multipotent stromal cells for bone regeneration. Tissue Eng Part B Rev. 2010 Aug;16(4):385-395.

GBD 2019 Fracture Collaborators. Global, regional, and national burden of bone fractures in 204 countries and territories, 1990-2019: a systematic analysis from the Global Burden of Disease Study 2019. Lancet Healthy Longev. 2021 Sep;2(9):e580-e592.

Genta PR, Schorr F, Eckert DJ, Gebrim E, Kayamori F, Moriya HT, Malhotra A, Lorenzi-Filho G. Upper airway collapsibility is associated with obesity and hyoid position. Sleep. 2014 Oct 1;37(10):1673-1678.

Gillman CE, Jayasuriya AC. FDA-approved bone grafts and bone graft substitute devices in bone regeneration. Mater Sci Eng C Mater Biol Appl. 2021 Nov;130:112466.

Gulati GS, Murphy MP, Marecic O, Lopez M, Brewer RE, Koepke LS, Manjunath A, Ransom RC, Salhotra A, Weissman IL, Longaker MT, Chan CKF. Isolation and functional assessment of mouse skeletal stem cell lineage. Nat Protoc. 2018 Jun;13(6):1294-1309.

Graham SM, Leonidou A, Aslam-Pervez N, Hamza A, Panteliadis P, Heliotis M, Mantalaris A, Tsiridis E. Biological therapy of bone defects: the immunology of bone allo-transplantation. Expert Opin Biol Ther. 2010 Jun;10(6):885-901.

Green SA, Simoes-Costa M, Bronner ME. Evolution of vertebrates as viewed from the crest. Nature. 2015 Apr 23;520(7548):474-482.

Grgurevic L, Pecina M, Vukicevic S. Marshall R. Urist and the discovery of bone morphogenetic proteins. Int Orthop. 2017 May;41(5):1065-1069.

Groeneveldt LC, Herpelinck T, Maréchal M, Politis C, van IJcken WFJ, Huylebroeck D, Geris L, Mulugeta E, Luyten FP. The bone-forming properties of periosteum-derived cells differ between harvest sites. Front Cell Dev Biol. 2020 Nov 25;8:554984.

Gröngröft I, Wissing S, Meesters DM, Poeze M, Matthys-Mark R, Ito K, Zeiter S. Development of a novel murine delayed secondary fracture healing in vivo model using periosteal cauterization. Arch Orthop Trauma Surg. 2019 Dec;139(12):1743-1753.

Haaijman A, Burger EH, Goei SW, Nelles L, ten Dijke P, Huylebroeck D, Bronckers AL. Correlation between ALK-6 (BMPR-IB) distribution and responsiveness to osteogenic protein-1 (BMP-7) in embryonic mouse bone rudiments. Growth Factors. 2000;17(3):177-192.

Heldin CH, Moustakas A. Signaling receptors for TGF-β family members. Cold Spring Harb Perspect Biol. 2016 Aug 1;8(8):a022053.

Hessle L, Johnson KA, Anderson HC, Narisawa S, Sali A, Goding JW, Terkeltaub R, Millan JL. Tissue-nonspecific alkaline phosphatase and plasma cell membrane glycoprotein-1 are central antagonistic regulators of bone mineralization. Proc Natl Acad Sci USA. 2002 Jul 9;99(14):9445-9449.

Hoffmann A, Preobrazhenska O, Wodarczyk C, Medler Y, Winkel A, Shahab S, Huylebroeck D, Gross G, Verschueren K. Transforming growth factor-beta-activated kinase-1 (TAK1), a MAP3K, interacts with Smad proteins and interferes with osteogenesis in murine mesenchymal progenitors. J Biol Chem. 2005 Jul 22;280(29):27271-27283.

Ingber DE, Levin M. What lies at the interface of regenerative medicine and developmental biology? Development. 2007 Jul;134(14):2541-2547.

Janicki P, Kasten P, Kleinschmidt K, Luginbuehl R, Richter W. Chondrogenic pre-induction of human mesenchymal stem cells on beta-TCP: enhanced bone quality by endochondral heterotopic bone formation. Acta Biomater. 2010 Aug;6(8):3292-3301.

James AW, LaChaud G, Shen J, Asatrian G, Nguyen V, Zhang X, Ting K, Soo C. A Review of the Clinical Side Effects of Bone Morphogenetic Protein-2. Tissue Eng Part B Rev. 2016 Aug;22(4):284-297.

Janeczek Portalska K, Leferink A, Groen N, Fernandes H, Moroni L, van Blitterswijk C, de Boer J. Endothelial differentiation of mesenchymal stromal cells. PLoS One. 2012;7(10):e46842.

Jin EJ, Lee SY, Choi YA, Jung JC, Bang OS, Kang SS. BMP-2-enhanced chondrogenesis involves p38 MAPK-mediated down-regulation of Wnt-7a pathway. Mol Cells. 2006 Dec 31;22(3):353-359.

Johari B, Kadivar M, Lak S, Gholipourmalekabadi M, Urbanska AM, Mozafari M, Ahmadzadehzarajabad M, Azarnezhad A, Afshari S, Zargan J, Kargozar S. Osteoblast-seeded bioglass/gelatin nanocomposite: a promising bone substitute in critical-size calvarial defect repair in rat. Int J Artif Organs. 2016 Nov 29;39(10):524-533

Ju W, Hoffmann A, Verschueren K, Tylzanowski P, Kaps C, Gross G, Huylebroeck D. The bone morphogenetic protein 2 signaling mediator Smad1 participates predominantly in osteogenic and not in chondrogenic differentiation in mesenchymal progenitors C3H10T1/2. J Bone Miner Res. 2000 Oct;15(10):1889-1899.

Julien A, Perrin S, Martínez-Sarrà E, Kanagalingam A, Carvalho C, Luka M, Ménager M, Colnot C. Skeletal Stem/Progenitor Cells in Periosteum and Skeletal Muscle Share a Common Molecular Response to Bone Injury. J Bone Miner Res. 2022 Aug;37(8):1545-1561.

Kaps C, Lauber J, Ju W, Czichos S, Gross G. The recombinant expression of bone morphogenetic protein type IA receptor (Alk3) in mesenchymal progenitors C3H10T1/2 is sufficient for osteo-/chondrogenic development. Biochem Soc Trans. 1998 Feb;26(1):27-32.

Karsenty G, Wagner EF. Reaching a genetic and molecular understanding of skeletal development. Dev Cell. 2002 Apr;2(4):389-406.

Katagiri T, Watabe T. Bone Morphogenetic Proteins. Cold Spring Harb Perspect Biol. 2016 Jun 1;8(6):a021899.

Kim JM, Lin C, Stavre Z, Greenblatt MB, Shim JH. Osteoblast-Osteoclast Communication and Bone Homeostasis. Cells. 2020 Sep 10;9(9):2073.

Knothe Tate ML, Falls TD, McBride SH, Atit R, Knothe UR. Mechanical modulation of osteochondroprogenitor cell fate. Int J Biochem Cell Biol. 2008;40(12):2720-2738.

Kotze MJ, Bütow KW, Olorunju SA, Kotze HF. A comparison of mandibular and maxillary alveolar osteogenesis over six weeks: a radiological examination. Head Face Med. 2014 Nov 28;10:50.

Kozhemyakina E, Lassar AB, Zelzer E. A pathway to bone: signaling molecules and transcription factors involved in chondrocyte development and maturation. Development. 2015 Mar 1;142(5):817-831.

Kronenberg HM. PTHrP and skeletal development. Ann N Y Acad Sci. 2006 Apr;1068:1-13.

Leijten J, Chai YC, Papantoniou I, Geris L, Schrooten J, Luyten FP. Cell based advanced therapeutic medicinal products for bone repair: Keep it simple? Adv Drug Deliv Rev. 2015 Apr;84:30-44.

Lenas P, Moos M, Luyten FP. Developmental engineering: a new paradigm for the design and manufacturing of cell-based products. Part I: from three-dimensional cell growth to biomimetics of in vivo development. Tissue Eng Part B Rev. 2009 Dec;15(4):381-394.

Leucht P, Kim JB, Amasha R, James AW, Girod S, Helms JA. Embryonic origin and Hox status determine progenitor cell fate during adult bone regeneration. Development. 2008 Sep;135(17):2845-2854.

Li X, Sun Q, Li Q, Kawazoe N, Chen G. Functional Hydrogels With Tunable Structures and Properties for Tissue Engineering Applications. Front Chem. 2018 Oct 22;6:499.

Lin S, Svoboda KK, Feng JQ, Jiang X. The biological function of type I receptors of bone morphogenetic protein in bone. Bone Res. 2016 Apr 5;4:16005.

Lindhe J, Bressan E, Cecchinato D, Corrá E, Toia M, Liljenberg B. Bone tissue in different parts of the edentulous maxilla and mandible. Clin Oral Implants Res. 2013 Apr;24(4):372-377.

Liu Y, Lim J, Teoh S-H. Review: development of clinically relevant scaffolds for vascularized bone tissue engineering. Biotechnol Adv. 2013 Sep-Oct;31(5):688-705.

Lo JC, O'Ryan FS, Gordon NP, Yang J, Hui RL, Martin D, Hutchinson M, Lathon PV, Sanchez G, Silver P, Chandra M, McCloskey CA, Staffa JA, Willy M, Selby JV, Go AS; Predicting Risk of Osteonecrosis of the Jaw with Oral Bisphosphonate Exposure (PROBE) Investigators. Prevalence of osteonecrosis of the jaw in patients with oral bisphosphonate exposure. J Oral Maxillofac Surg. 2010 Feb;68(2):243-53.

Long JT, Leinroth A, Liao Y, Ren Y, Mirando AJ, Nguyen T, Guo W, Sharma D, Rouse D, Wu C, Cheah KSE, Karner CM, Hilton MJ. Hypertrophic chondrocytes serve as a reservoir for marrow-associated skeletal stem and progenitor cells, osteoblasts, and adipocytes during skeletal development. Elife. 2022 Feb 18;11:e76932.

Lou J, Tu Y, Li S, Manske PR. Involvement of ERK in BMP-2 induced osteoblastic differentiation of mesenchymal progenitor cell line C3H10T1/2. Biochem Biophys Res Commun. 2000 Feb 24;268(3):757-762.

Lowery JW, Rosen V. The BMP Pathway and Its Inhibitors in the Skeleton. Physiol Rev. 2018 Oct 1;98(4):2431-2452.

Lundgren S, Andersson S, Gualini F, Sennerby L. Bone reformation with sinus membrane elevation: a new surgical technique for maxillary sinus floor augmentation. Clin Implant Dent Relat Res. 2004;6(3):165-173.

Luyten FP, Roberts SJ. Close to the bone - in search of the skeletal stem cell. Nat Rev Rheumatol. 2018 Dec;14(12):687-688.

Ma TL, Zhu P, Ke ZR, Chen JX, Hu YH, Xie J. Focusing on OB-OC-MΦ Axis and miR-23a to Explore the Pathogenesis and Treatment Strategy of Osteoporosis. Front Endocrinol (Lausanne). 2022 Jul 14;13:891313.

Madamanchi A, Mullins MC, Umulis DM. Diversity and robustness of bone morphogenetic protein pattern formation. Development. 2021 Apr 6;148(7):dev192344.

Maes C, Kobayashi T, Selig MK, Torrekens S, Roth SI, Mackem S, Carmeliet G, Kronenberg HM. Osteoblast precursors, but not mature osteoblasts, move into developing and fractured bones along with invading blood vessels. Dev Cell. 2010 Aug 17;19(2):329-344.

Martín AE, del R Pani M, Holgado NR, López Miranda LI, Meheris HE, Garat JA. Facial development disorders due to inhibition to endochondral ossification of mandibular condyle process caused by malnutrition. Angle Orthod. 2014 May;84(3):473-8.

Martin-Iglesias S, Milian L, Sancho-Tello M, Salvador-Clavell R, Martín de Llano JJ, Carda C, Mata M. BMP-2 Enhances Osteogenic Differentiation of Human Adipose-Derived and Dental Pulp Stem Cells in 2D and 3D *In Vitro*Models. Stem Cells Int. 2022 Mar 4:4910399.

Matsuda S, Harmansa S, Affolter M. BMP morphogen gradients in flies. Cytokine Growth Factor Rev. 2016 Feb;27:119-127.

Meijer GJ, de Bruijn JD, Koole R, van Blitterswijk CA. Cell based bone tissue engineering in jaw defects. Biomaterials. 2008 Jul;29(21):3053-61.

Mendes LF, Tam WL, Chai YC, Geris L, Luyten FP, Roberts SJ. Combinatorial Analysis of Growth Factors Reveals the Contribution of Bone Morphogenetic Proteins to Chondrogenic Differentiation of Human Periosteal Cells. Tissue Eng Part C Methods. 2016 May;22(5):473-86.

Meulemans D, Bronner-Fraser M. Gene-regulatory interactions in neural crest evolution and development. Dev Cell. 2004 Sep;7(3):291-299.

Moussa NT, Dym H. Maxillofacial bone grafting materials. Dent Clin North Am. 2020 Apr;64(2):473-490.

Nahian A, Chauhan PR. Histology, Periosteum And Endosteum. 2022 May 8. In: StatPearls [Internet]. Treasure Island (FL): StatPearls Publishing; 2023 Jan.

Nakahara H, Goldberg VM, Caplan AI. Culture-expanded human periosteal-derived cells exhibit osteochondral potential in vivo. J Orthop Res. 1991 Jul;9(4):465-476.

Nakashima K, Zhou X, Kunkel G, Zhang Z, Deng JM, Behringer RR, de Crombrugghe B. The novel zinc finger-containing transcription factor osterix is required for osteoblast differentiation and bone formation. Cell. 2002 Jan 11;108(1):17-29.

Ono N, Balani DH, Kronenberg HM. Stem and progenitor cells in skeletal development. Curr Top Dev Biol. 2019;133:1-24.

Ortinau LC, Wang H, Lei K, Deveza L, Jeong Y, Hara Y, Grafe I, Rosenfeld SB, Lee D, Lee B, Scadden DT, Park D. Identification of Functionally Distinct Mx1+αSMA+ Periosteal Skeletal Stem Cells. Cell Stem Cell. 2019 Dec 5;25(6):784-796.e5.

Olsen OE, Sankar M, Elsaadi S, Hella H, Buene G, Darvekar SR, Misund K, Katagiri T, Knaus P, Holien T. BMPR2 inhibits activin and BMP signaling via wild-type ALK2. J Cell Sci. 2018 Jun 11;131(11):jcs213512.

Park HS, Lee YJ, Jeong SH, Kwon TG. Density of the alveolar and basal bones of the maxilla and the mandible. Am J Orthod Dentofacial Orthop. 2008 Jan;133(1):30-37.

Park J, Gebhardt M, Golovchenko S, Perez-Branguli F, Hattori T, Hartmann C, Zhou X, deCrombrugghe B, Stock M, Schneider H, von der Mark K. Dual pathways to endochondral osteoblasts: a novel chondrocyte-derived osteoprogenitor cell identified in hypertrophic cartilage. Biol Open. 2015 Apr 16;4(5):608-621

Pecin M, Stokovic N, Ivanjko N, Smajlovic A, Kreszinger M, Capak H, Vrbanac Z, Oppermann H, Maticic D, Vukicevic S. A novel autologous bone graft substitute containing rhBMP6 in autologous blood coagulum with synthetic ceramics for reconstruction of a large humerus segmental gunshot defect in a dog: The first veterinary patient to receive a novel osteoinductive therapy. Bone Rep. 2021 Feb 25;14:100759.

Perrin S, Colnot C. Periosteal Skeletal Stem and Progenitor Cells in Bone Regeneration. Curr Osteoporos Rep. 2022 Oct;20(5):334-343.

Perry MJ, McDougall KE, Hou SC, Tobias JH. Impaired growth plate function in bmp-6 null mice. Bone. 2008 Jan;42(1):216-225.

Pittenger MF, Mackay AM, Beck SC, Jaiswal RK, Douglas R, Mosca JD, Moorman MA, Simonetti DW, Craig S, Marshak DR. Multilineage potential of adult human mesenchymal stem cells. Science. 1999 Apr 2;284(5411):143-147.

Retting KN, Song B, Yoon BS, Lyons KM. BMP canonical Smad signaling through Smad1 and Smad5 is required for endochondral bone formation. Development. 2009 Apr;136(7):1093-1104.

Rho JY, Kuhn-Spearing L, Zioupos P. Mechanical properties and the hierarchical structure of bone. Med Eng Phys. 1998 Mar;20(2):92-102.

Roberts SJ, van Gastel N, Carmeliet G, Luyten FP. Uncovering the periosteum for skeletal regeneration: the stem cell that lies beneath. Bone. 2015 Jan;70:10-8.

Rohner D, Hailemariam S, Hammer B. Le Fort I osteotomies using Bio-Oss® collagen to promote bony union: a prospective clinical split-mouth study. Int J Oral Maxillofac Surg. 2013 May;42(5):585-91.

Rong Q, Li X, Chen SL, Zhu SX, Huang DY. Effect of the Schneiderian membrane on the formation of bone after lifting the floor of the maxillary sinus: an experimental study in dogs. Br J Oral Maxillofac Surg. 2015 Sep;53(7):607-612.

Rossant J, Tam PPL. Early human embryonic development: Blastocyst formation to gastrulation. Dev Cell. 2022 Jan 24;57(2):152-165.

Sader F, Roy S. Tgf-β superfamily and limb regeneration: Tgf-β to start and Bmp to end. Dev Dyn. 2022 Jun;251(6):973-987.

Salazar VS, Gamer LW, Rosen V. BMP signalling in skeletal development, disease and repair. Nat Rev Endocrinol. 2016 Apr;12(4):203-21

Sallent I, Capella-Monsonís H, Procter P, Bozo IY, Deev RV, Zubov D, Vasyliev R, Perale G, Pertici G, Baker J, Gingras P, Bayon Y, Zeugolis DI. The Few Who Made It: Commercially and clinically successful innovative bone grafts. Front Bioeng Biotechnol. 2020 Sep 1;8:952.

Schimming R, Schmelzeisen R. Tissue-engineered bone for maxillary sinus augmentation. J Oral Maxillofac Surg. 2004 Jun;62(6):724-729.

Scotti C, Tonnarelli B, Papadimitropoulos A, Scherberich A, Schaeren S, Schauerte A, Lopez-Rios J, Zeller R, Barbero A, Martin I. Recapitulation of endochondral bone formation using human adult mesenchymal stem cells as a paradigm for developmental engineering. Proc Natl Acad Sci USA. 2010 Apr 20;107(16):7251-7256.

Shadjou N, Hasanzadeh M. Silica-based mesoporous nanobiomaterials as promoter of bone regeneration process. J Biomed Mater Res A. 2015 Nov;103(11):3703-3716.

Shim JH, Greenblatt MB, Xie M, Schneider MD, Zou W, Zhai B, Gygi S, Glimcher LH. TAK1 is an essential regulator of BMP signalling in cartilage. EMBO J. 2009 Jul 22;28(14):2028-2041.

Shu B, Zhang M, Xie R, Wang M, Jin H, Hou W, Tang D, Harris SE, Mishina Y, O'Keefe RJ, Hilton MJ, Wang Y, Chen D. BMP2, but not BMP4, is crucial for chondrocyte proliferation and maturation during endochondral bone development. J Cell Sci. 2011 Oct 15;124(Pt 20):3428-2440.

Sorger JI, Hornicek FJ, Zavatta M, Menzner JP, Gebhardt MC, Tomford WW, Mankin HJ. Allograft fractures revisited. Clin Orthop Relat Res. 2001 Jan;(382):66-74.

Srouji S, Kizhner T, Ben David D, Riminucci M, Bianco P, Livne E. The Schneiderian membrane contains osteoprogenitor cells: in vivo and in vitro study. Calcif Tissue Int. 2009 Feb;84(2):138-145.

Su N, Yang J, Xie Y, Du X, Chen H, Zhou H, Chen L. Bone function, dysfunction and its role in diseases including critical illness. Int J Biol Sci. 2019 Jan 29;15(4):776-787.

Sun X, Kang Y, Bao J, Zhang Y, Yang Y, Zhou X. Modeling vascularized bone regeneration within a porous biodegradable CaP scaffold loaded with growth factors. Biomaterials. 2013 Jul;34(21):4971-81.

Tannoury CA, An HS. Complications with the use of bone morphogenetic protein 2 (BMP-2) in spine surgery. Spine J. 2014 Mar 1;14(3):552-559.

Thesleff I. From understanding tooth development to bioengineering of teeth. Eur J Oral Sci. 2018 Oct;126 Suppl 1:67-71.

Thompson EM, Matsiko A, Farrell E, Kelly DJ, O'Brien FJ. Recapitulating endochondral ossification: a promising route to in vivo bone regeneration. J Tissue Eng Regen Med. 2015 Aug;9(8):889-902.

Trautvetter W, Kaps C, Schmelzeisen R, Sauerbier S, Sittinger M. Tissue-engineered polymer-based periosteal bone grafts for maxillary sinus augmentation: five-year clinical results. J Oral Maxillofac Surg. 2011 Nov;69(11):2753-2762.

Tribulo C, Aybar MJ, Nguyen VH, Mullins MC, Mayor R. Regulation of Msx genes by a Bmp gradient is essential for neural crest specification. Development. 2003 Dec;130(26):6441-6452.

Tsuji K, Bandyopadhyay A, Harfe BD, Cox K, Kakar S, Gerstenfeld L, Einhorn T, Tabin CJ, Rosen V. BMP2 activity, although dispensable for bone formation, is required for the initiation of fracture healing. Nat Genet. 2006 Dec;38(12):1424-1429.

Udagawa N, Koide M, Nakamura M, Nakamichi Y, Yamashita T, Uehara S, Kobayashi Y, Furuya Y, Yasuda H, Fukuda C, Tsuda E. Osteoclast differentiation by RANKL and OPG signaling pathways. J Bone Miner Metab. 2021 Jan;39(1):19-26.

van Dijk BA, Brands MT, Geurts SM, Merkx MA, Roodenburg JL. Trends in oral cavity cancer incidence, mortality, survival and treatment in the Netherlands. Int J Cancer. 2016 Aug 1;139(3):574-83.

van Gastel N, Torrekens S, Roberts SJ, Moermans K, Schrooten J, Carmeliet P, Luttun A, Luyten FP, Carmeliet G. Engineering vascularized bone: osteogenic and proangiogenic potential of murine periosteal cells. Stem Cells. 2012 Nov;30(11):2460-2471.

Venkatesan J, Bhatnagar I, Manivasagan P, Kang KH, Kim SK. Alginate composites for bone tissue engineering: a review. Int J Biol Macromol. 2015 Jan;72:269-281.

Villanueva S, Glavic A, Ruiz P, Mayor R. Posteriorization by FGF, Wnt, and retinoic acid is required for neural crest induction. Dev Biol. 2002 Jan 15;241(2):289-301.

Voss P, Sauerbier S, Wiedmann-Al-Ahmad M, Zizelmann C, Stricker A, Schmelzeisen R, Gutwald R. Bone regeneration in sinus lifts: comparing tissue-engineered bone and iliac bone. Br J Oral Maxillofac Surg. 2010 Mar;48(2):121-126.

Wang C, Huang W, Zhou Y, He L, He Z, Chen Z, He X, Tian S, Liao J, Lu B, Wei Y, Wang M. 3D printing of bone tissue engineering scaffolds. Bioact Mater. 2020 Jan 15;5(1):82-91.

Wang W, Yeung KWK. Bone grafts and biomaterials substitutes for bone defect repair: a review. Bioact Mater. 2017 Jun7;2(4):224-247.

Wang X, Xu S, Zhou S, Xu W, Leary M, Choong P, Qian M, Brandt M, Xie YM. Topological design and additive manufacturing of porous metals for bone scaffolds and orthopaedic implants: A review. Biomaterials. 2016 Mar;83:127-141.

Wiggins A, Austerberry R, Morrison D, Ho KM, Honeybul S. Cranioplasty with custom-made titanium plates: 14 years experience. Neurosurgery. 2013 Feb;72(2):248-256.

Williams LA, Davis-Dusenbery BN, Eggan KC. SnapShot: directed differentiation of pluripotent stem cells. Cell. 2012 May 25;149(5):1174-1174.e1.

Wu C, Pan W, Feng C, Su Z, Duan Z, Zheng Q, Hua C, Li C. Grafting materials for alveolar cleft reconstruction: a systematic review and best-evidence synthesis. Int J Oral Maxillofac Surg. 2018 Mar;47(3):345-356.

Wu M, Chen G, Li YP. TGF-β and BMP signaling in osteoblast, skeletal development, and bone formation, homeostasis and disease. Bone Res. 2016 Apr 26;4:16009.

Yadin D, Knaus P, Mueller TD. Structural insights into BMP receptors: Specificity, activation and inhibition. Cytokine Growth Factor Rev. 2016 Feb;27:13-34.

Yu VW, Scadden DT. Hematopoietic Stem Cell and Its Bone Marrow Niche. Curr Top Dev Biol. 2016;118:21-44.

Zahedpasha A, Ghassemi A, Bijani A, Haghanifar S, Majidi MS, Ghorbani ZM. Comparison of bone formation after sinus membrane llifting without graft or using bone substitute "histologic and radiographic evaluation". J Oral Maxillofac Surg. 2021 Jun;79(6):1246-1254.

Zhou R, Guo Q, Xiao Y, Guo Q, Huang Y, Li C, Luo X. Endocrine role of bone in the regulation of energy metabolism. Bone Res. 2021 May 20;9(1):25.

Zhou X, von der Mark K, Henry S, Norton W, Adams H, de Crombrugghe B. Chondrocytes transdifferentiate into osteoblasts in endochondral bone during development, postnatal growth and fracture healing in mice. PLoS Genet. 2014 Dec 4;10(12):e1004820.

Zou ML, Chen ZH, Teng YY, Liu SY, Jia Y, Zhang KW, Sun ZL, Wu JJ, Yuan ZD, Feng Y, Li X, Xu RS, Yuan FL. The Smad Dependent TGF-β and BMP Signaling Pathway in Bone Remodeling and Therapies. Front Mol Biosci. 2021 May 5;8:593310.

Chapter 2

Scope of this thesis

Cell-based tissue and organ repair based on insights from the instructed differentiation of specific cell types during embryogenesis, and incorporation and maturation of these latter cells during organogenesis, the later phase of development of the embryo, are promising avenues to improved medical therapies. This emerging knowledge provides ways to either rely on reactivation of resident stem/progenitor cells in tissues and organs for the repair after injury of or on repair strategies using cells that are cultured *ex vivo*. For the latter, this starts with the isolation of appropriate stem/progenitor cells and the *ex vivo* expansion of these cells whilst maintaining their characteristics, and subsequently instruct their differentiation via exposure to appropriate growth/differentiation factors and transplant them back into the patient. The creation of cell-based tissue constructs to repair bone tissue defects forms the basis for the bone tissue engineering field. Furthermore, an exciting interface exists with biomaterials research that aims at providing suitable or optimized mechanical carriers for the obtained transplantable cells. Importantly, depending on their body location and thus tissue of origin where these cells are harvested (such as from bone marrow, adipose tissue, gingiva, dental pulp), different types of skeletal stem/progenitor cell (SSPC) have been explored already for many years (for a discussion, see **Chapter 1**).

The **general objectives** of this PhD research are to investigate whether the principles that result from the focus on treating critical size defects in long bone with PDCs, can be applied to craniofacial bone tissue and whether it can be improved.

With this in mind, the **specific objectives** are as follows:

- To investigate **intrinsic differences between hPDCs** of the various aforementioned adult tissue sources (tibia, maxilla, mandibula) originating from different embryonic cell lineages (**Chapter 3**).
- To explore **another source of hPDC-like cells**, *i.e.* those located in the Schneiderian membrane, as a potential candidate for cranio-maxillofacial bone tissue engineering. Like in the case of the periosteum, the cells of this membrane line the bone tissue, but they do this on the inner side of the maxillary sinus cavity. Older work by others has shown that lifting of this sinus membrane (without the insert of osteo-conductive/ inductive materials) results in augmentation of the maxillary sinus floor. *In vitro* and *in vivo* work further demonstrated that those cells are able to form bone tissue in specific circumstances. Our extra hypothesis is that those cells, although their harvesting procedure is giving more post-operative discomfort than the presently used hPDC collection from long bones, are better suited for bone tissue engineering than the maxillary-derived hPDCs investigated in this PhD research. Therefore, we started to investigate the cells obtained from the Schneiderian membrane in this PhD research, with focus on their proliferative properties *in vitro* and their bone-forming properties *in vitro* and *in vivo* (**Chapter 4**).
- To test the feasibility of **replacing fetal bovine serum (FBS) by human platelet lysate (hPL) in cell culture protocols for hPDCs**. The assembly of tissue engineering constructs consisting of a scaffold, supplemented with growth-differentiation factors and seeded with cells, requires cell numbers. To obtain these cell numbers from otherwise limited tissue samples, cells are expanded in culture first. This is normally done in FBS. Many groups are searching for FBS-free optimized cell culture protocols, and these are not yet available for hPDCs. Specifically, we tested the replacement of FBS by hPL (**Chapter 5**).
- To document the transcriptional response to growth/differentiation factors (*i.e.* Bone Morphogenetic Proteins, BMPs, i.e. BMP2 and/or BMP6) of cultured tibial *vs.* maxillary and mandibular hPDCs. Such priming strategy with BMPs is also tested with the purpose of

directing these respective hPDCs towards bone tissue formation *in vivo*. Furthermore, we included a comparison of different scaffolds *in vivo* in ectopic bone formation after transplantation in recipient mice as well as in a (for our laboratory) new orthotopic rat model with a critical sized bone defect in the mandible (**Chapter 6**).

Rather than recapitulating the discussion of each chapter, **Chapter 7** at the end of this PhD thesis attempts to integrate all elements of this PhD research and its current experimental results in a more general discussion and future perspectives of the bone tissue engineering field, with focus - where possible - on applications in cranio-maxillofacial surgery.

Chapter 3

The bone-forming properties of periosteum-derived cells differ between harvest sites

Lisanne C. Groeneveldt [1,2,3,4,5], Tim Herpelinck [1,2], Marina Maréchal [1,2], Constantinus Politis [3,4], Wilfred F. J. van Ijcken [5,6], Danny Huylebroeck [5,7], Liesbet Geris [1,2,8,9*], Eskeatnaf Mulugeta [5], Frank P. Luyten [1,2,7]

[1] Prometheus, Division of Skeletal Tissue Engineering, KU Leuven, Leuven, Belgium;
[2] Skeletal Biology and Engineering Research Center, KU Leuven, Leuven, Belgium;
[3] OMFS IMPATH Research Group, Department of Imaging and Pathology, KU Leuven, Leuven, Belgium;
[4] Oral and Maxillofacial Surgery, University Hospitals Leuven, Leuven, Belgium;
[5] Department of Cell Biology, Erasmus University Medical Center, Rotterdam, Netherlands;
[6] Center for Biomics, Erasmus University Medical Center, Rotterdam, Netherlands;
[7] Department of Development and Regeneration, KU Leuven, Leuven, Belgium;
[8] Biomechanics Research Unit, GIGA-R In Silico Medicine, Université de Liège, Liège, Belgium;
[9] Biomechanics Section, KU Leuven, Leuven, Belgium

Published in
Front. Cell Dev Biol. 2022;8:554984

3.1. Summary

The development of alternatives for autologous bone grafts is a major focus of bone tissue engineering. To produce living bone-forming implants, skeletal stem and progenitor cells (SSPCs) are envisioned as key ingredients. SSPCs can be obtained from different tissues including bone marrow, adipose tissue, dental pulp, and periosteum. Human periosteum-derived cells (hPDCs) exhibit progenitor cell characteristics and have well-documented *in vivo* bone formation potency. Here, we have characterized and compared hPDCs derived from tibia with craniofacial hPDCs, from maxilla and mandible, respectively, each representing a potential source for cell-based tissue engineered implants for craniofacial applications. Maxilla and mandible-derived hPDCs display similar growth curves as tibial hPDCs, with equal trilineage differentiation potential toward chondrogenic, osteogenic, and adipogenic cells. These craniofacial hPDCs are positive for SSPC-markers CD73, CD164, and Podoplanin (PDPN), and negative for CD146, hematopoietic and endothelial lineage markers. Bulk RNA-sequencing identified genes that are differentially expressed between the three sources of hPDC. In particular, differential expression was found for genes of the *HOX* and *DLX* family, for *SOX9* and genes involved in skeletal system development. The *in vivo* bone formation, 8 weeks after ectopic implantation in nude mice, was observed in constructs seeded with tibial and mandibular hPDCs. Taken together, we provide evidence that hPDCs show different profiles and properties according to their anatomical origin, and that craniofacial hPDCs are potential sources for cell-based bone tissue engineering strategies. The mandible- derived hPDCs display - both *in vitro* and *in vivo* - chondrogenic and osteogenic differentiation potential, which supports their future testing for use in craniofacial bone regeneration applications.

3.2. Introduction

The development of effective treatments for large bone defects incurred by trauma, osteonecrosis or tumor resection remains a challenge, which is further complicated by factors such as infections and congenital abnormalities. Currently, autografts are considered as the standard treatment of these bone defects, however, this approach requires large volumes of bone. In addition, it also requires a second surgical site where donor tissue is harvested, thereby introducing donor site morbidity (including pain) and potential major complications (in up to 10% of the cases; Arrington *et al.*, 1996). These include vascular injuries or deep infection in the donor site, and the possibility of herniation of abdominal contents in case an iliac crest graft is used. Furthermore, usually these donor sites provide insufficient quantities of tissue for filling large bone defects and, in addition, poor vascularization of the tissue graft can lead to necrosis (Meijer *et al.*, 2008).

Bone tissue engineering presents an opportunity for the repair of large bone defects, with the engineered constructs classically being composed of appropriate cells that are able to proliferate and differentiate, and growth factors to instruct cell differentiation in a 3D environment that provides some biomechanical support (Leijten *et al.*, 2015). Skeletal stem and progenitor cells (SSPCs), often referred to as mesenchymal stromal cells (MSCs), whereas these originate from various tissues including bone marrow, adipose tissue, gingiva, dental pulp and the periosteum, are being assessed for their potential in bone tissue engineering. Recently, a *bona fide* human skeletal stem cell characterized by a PDPN+CD146−CD73+CD164+ signature was identified (Chan *et al.*, 2018). This stem cell population demonstrates significant amplification properties in response to fracture. Similarly, periosteum-derived cells (PDCs) undergo a rapid

expansion to assist in callus formation (Colnot *et al.*, 2012), suggesting the presence of a stem or progenitor cell population among PDCs.

Depending on their tissue of origin, differences in the properties of SSPCs regarding cellular proliferation, differentiation and senescence, as well as cytokine release and gene/mRNA expression profiles have been documented (Dominici *et al.*, 2006; Kern *et al.*, 2006; Tsai *et al.*, 2007). Although bone marrow-derived SSPCs (BM-SSPCs) are osteogenic *in vitro* and form bone tissue *in vivo,* the bone forming cells in a long bone fracture forming the callus are predominantly PDCs (Colnot *et al.*, 2012). Furthermore, periosteum forms a larger callus with a higher mineral content compared to bone marrow (Guichet *et al.*, 1998), and cells in the periosteum display higher proliferation following injury (Brighton and Hunt, 1997). Ultimately, some data suggests that PDCs contain a higher bone regenerative potential than BM-SSPCs (Duchamp de Lageneste *et al.*, 2018). For these reasons PDCs are increasingly studied as a clinically relevant source for bone tissue engineering purposes (Nakahara *et al.*, 1991; De Bari *et al.*, 2006; van Gastel *et al.*, 2012; Owston *et al.*, 2019; Bolander *et al.*, 2020).

The anatomical location and other types (e.g., developmental molecular signatures) of positional information are important factors when studying *in vivo* bone formation (Leucht *et al.*, 2008). During development, facial cartilage and bone are predominantly derived from cranial neural crest, unlike long bones, such as the tibia, that originate from limb skeletal precursors derived from the somatic layer of the lateral plate mesoderm (Noden, 1982; Couly *et al.*, 1993). In the neural plate stage embryo, neural crest and placodal cells develop in the future cranial region at the border of the neural plate with the non-neural ectoderm under the influence of FGF signaling together with precisely dosed Wnt and/or BMP signaling. The actions of these signals converge on specific gene families of Msh-type homeobox (MSX1, MSX2), distal-less homeobox (DLX) and paired domain (PAX) transcription factors (Villanueva *et al.*, 2002; Tribulo *et al.*, 2003; Meulemans and Bronner-Fraser, 2004; Green *et al.*, 2015). The cranial neural crest cells extensively migrate to the pharyngeal arches and form multiple ectomesenchymal cell types including thymus cells, odontoblasts, osteoblastic, adipogenic and chondrogenic cells, muscle cells and neuronal ganglia (Green *et al.*, 2015). Craniofacial bone tissue has a higher turnover rate, "ages" more slowly, and has higher levels of osteoblastic markers compared to appendicular skeletal bone tissue such as that from tibia (Aghaloo *et al.*, 2010). Furthermore, substantial differences in structure and bone biology exist between maxillary and mandibular bone tissue. Maxillary bone tissue arises by intramembranous ossification and consists of trabecular bone surrounded by a thin cortical layer, has low bone density and mineral content, and is highly vascularized. Mandibular bone tissue develops by both endochondral ossification and intramembranous ossification. It consists of lamellar bone tissue that is surrounded by a thick cortical layer, has a high mineral content and bone density, and shows more centralized vascularization (Park *et al.*, 2008; Lindhe *et al.*, 2013). In a first step to assess the implications of these differences on tissue regeneration strategies, Leucht *et al.* (2008) performed cross-grafting of tibial periosteum onto craniofacial defects and *vice versa*, and further have shown that embryonic origin and homeobox gene expression influenced the regeneration potential. Despite these well-known differences in bone origin, structure and biology – and their effect on tissue regeneration strategies – many bone tissue engineering therapies intended for use in maxillofacial context continue using the same cell source as their long bone counterparts.

In this study, we built on the work of Leucht *et al.* (2008), toward clinical translation. We investigate the molecular differences of *in vitro* expanded periosteal cells from maxilla and mandibula in the context of their potential use as cell source for maxillofacial tissue engineering applications, using tibial hPDCs as benchmark. Cell surface markers, growth curves, trilineage

differentiation potential, gene/mRNA expression and *in vivo* bone formation were assessed. We show that craniofacial PDCs meet essential criteria of SSPCs (Chan *et al.*, 2018). In addition, *in vitro* differentiation and the mRNA profiling by bulk RNA-sequencing (RNA-seq) show that hPDCs exhibit different properties depending on their retrieval site.

3.3. Results

3.3.1. Characterization of the isolated and expanded hPDCs

Flow cytometric analysis was performed on culture expanded hPDCs to confirm the presence of SSPCs (**Fig. 3.1A-I**). 88.9% of the maxillary hPDCs were positive (+) for CD73, CD164 and PDPN, while negative (-) for CD31, CD45, CD235ab, and CD146 (**Fig. 3.1J**). In contrast, 87.7% of the mandibular cells and 62.0% of the tibial hPDCs met the SSPC criteria. All cells were selected based on their capacity to adhere to plastic (**Fig. 3.1K-M**).

Alcian Blue-positive micromasses from maxillary and mandibular and tibial hPDCs indicated their ability to differentiate toward the chondrogenic lineage (**Fig. 3.2A-C**; controls in **Fig. 3.2D-F**). Adipogenic differentiation of hPDC cultures in monolayer was verified by staining with Oil Red O of hPDCs obtained from the three different origins (**Fig. 3.2G-I**; controls in **Fig. 3.2J-L**). Calcium phosphate formed by osteogenic primed cells in monolayer was stained by Alizarin Red (**Fig. 3.2M-O**; controls in **Fig. 3.2P-R**) and showed mineral deposition by the hPDCs, independent of their origin. Additional RT-qPCR on chondrogenically differentiated micromasses at days 1 (control), 3, 5, and 7 showed that *RUNX2* (**Fig. 3.2U**) and *COL10A1* (**Fig. 3.2T**) were expressed at higher levels after chondrogenic differentiation in comparison to undifferentiated micromasses at day 1. Also *ACAN* was expressed from day 5, at statistically significantly higher levels compared to the controls (**Fig. 3.2S**). These results indicated that plastic-adherent hPDCs derived from maxilla and mandible could be expanded, and that these cultured hPDCs were positive for acknowledged SSPC surface markers and able to differentiate towards three different cell types.

3.3.2. Human PDCs can be expanded for 2 months

We have tested the ability to expand hPDCs obtained from maxilla versus mandible and tibia. The proliferation rates of hPDCs during *in vitro* expansion under the culture conditions used, measured in cumulative population doublings (CPDs), were similar and independent of their origin (**Fig. 3.3A,B;** *see* next page). After 6, 9 and 12 weeks of expansion, staining with X-gal for senescence-associated β-Gal was carried out. During the first 9 weeks the average rates of such cells remained below 5%. After 12 weeks, significantly higher rates were found, up until 28% of the cells ($p=0.045$; **Fig. 3.3C**). Quantification of proliferation was measured by staining for incorporated EdU, again after expansion for 6, 9 and 12 weeks, respectively. About 75% of the cells were EdU+ after 6 and 9 weeks of expansion (**Fig. 3.3D**) with a significantly higher proliferation rate for maxillary hPDCs after 6 weeks in comparison to mandibular and tibial hPDCs.

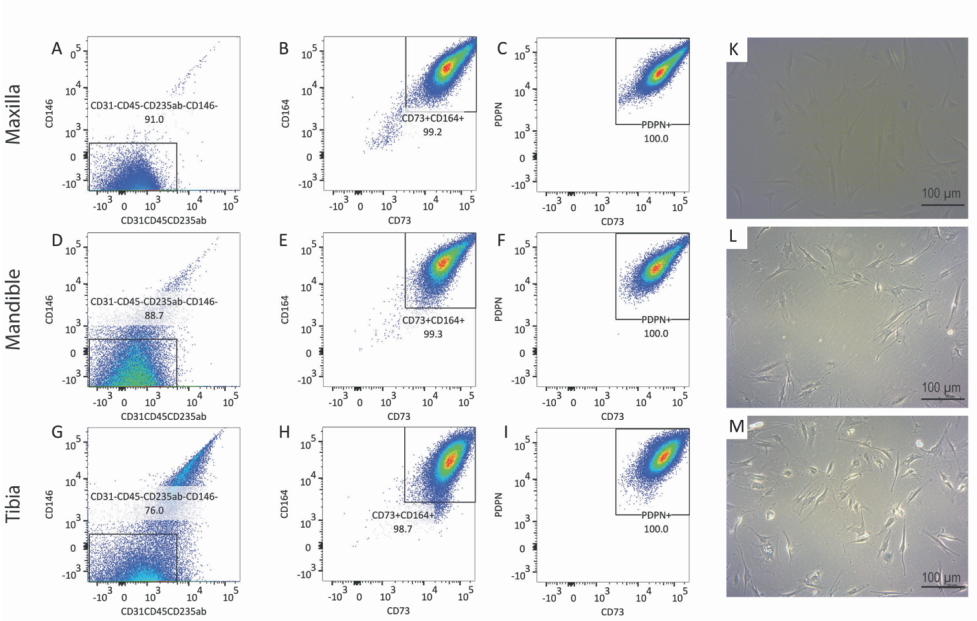

J

	Single cells	CD31- CD45- CD235ab- CD146-	CD73 + CD164 +	PDPN+	Single cells fulfilling SSPC criteria
Maxilla	95.6%	89.7%	99.1%	100%	88.9%
Mandible	92.0%	89.1%	98.7%	100%	87.7%
Tibia	96.1%	65.8%	94.2%	100%	62.0%

Figure 3.1. Characterization of isolated and expanded human periosteum-derived cells.

(A-I) Flow-cytometric analysis of periosteal-derived cells obtained from maxilla (A–C), mandible (D–F) and tibia (G–I). Gating is performed using FMOs for each run. n = 3; 100,000 events were read for each sample. **(J)** Summary of flow-cytometric analysis, n = 3 for each origin. **(K-M)** Staining of β-gal in periosteal cells derived from maxilla (K), mandible (L), and tibia (M) demonstrating the absence of X-gal precipitate.

Assessing cellular metabolic activity using the MTT colorimetric assay, we saw a trend toward lower mitochondrial metabolic rates in tibia-derived hPDCs, however, no statistically significant differences were found between the maxillary, mandibular and tibia-derived hPDCs (**Fig. 3.3E**). Furthermore, no decline in the metabolic activity was observed after 12 weeks. From this, we conclude that hPDCs, regardless of their tissue source, can be expanded during at least 9 weeks, with an expected yield of about 350 million cells after 50 days of proliferation. This yield is sufficient for typical applications in bone tissue engineering (Lammens *et al.*, 2020).

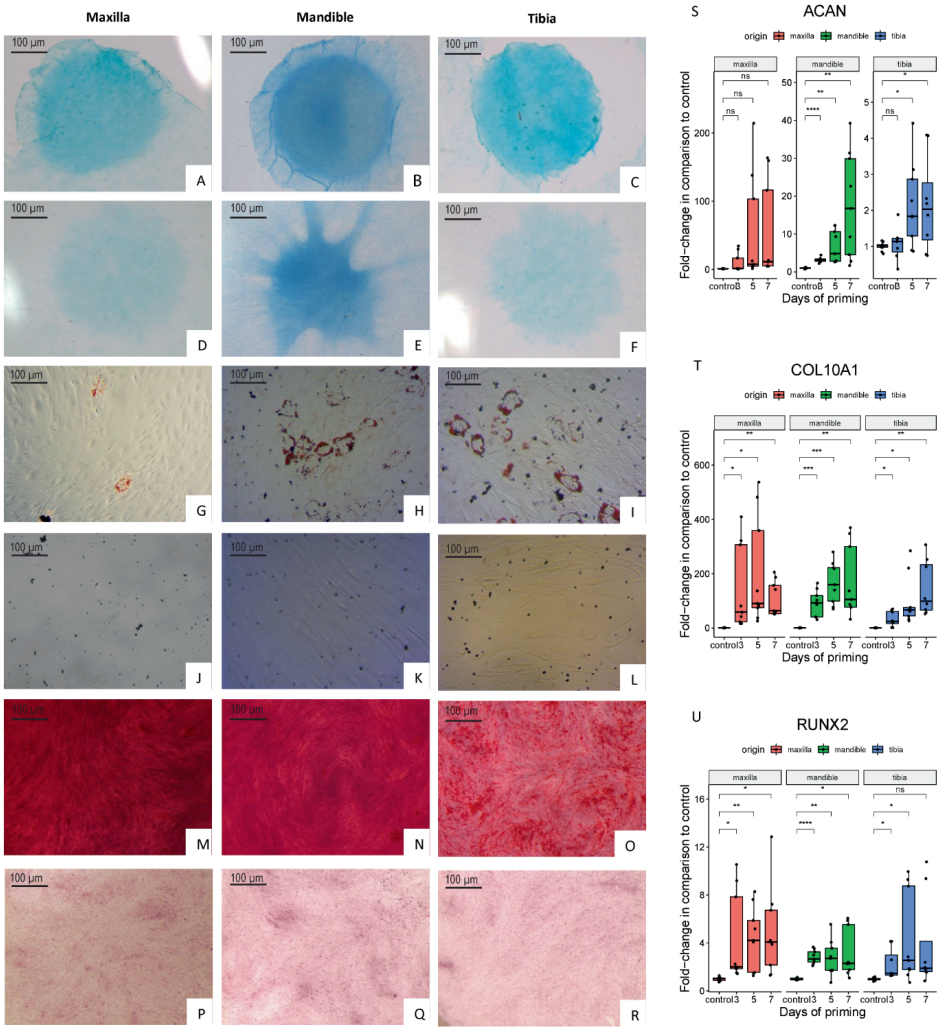

Figure 3.2. Further characterization of isolated and expanded hPDCs.
(A-F) Alcian Blue staining of chondrogenically differentiated hPDCs obtained from maxilla, mandible and tibia (A–C) and cells cultured in DMEM-C (D-F). **(G-L)** Oil Red O staining of adipogenically differentiated hPDCs (G-I) and cells cultured in DMEM-C as controls (J-L). **(M-R)** Cells stained with Alizarin Red staining to detect calcium phosphate deposition of osteogenically differentiated hPDCs (M-O) and controls cultured in DMEM-C (P-R). **(S-U)** RT-qPCR performed at days 1 (control), 3, 5 and 7, respectively, for the chondrogenic genes *RUNX2*, *COL10A1* and *ACAN* showed as fold-change compared to the control after correction for *GAPDH*, n = 3 in biological triplicates. *p ≤ 0.05, **p ≤ 0.01, ***p ≤ 0.001, ****p ≤0.0001).

3.3.3. *In vitro* analysis of marker genes of expanded hPDCs from three different origins

In order to investigate further the differences in mRNA profiles between the respective *in vitro* expanded hPDCs, we performed RT-qPCR on acknowledged marker genes for bone. These include *ALP*, a marker gene of osteogenic differentiation; *BGLAP*, coding for a protein secreted in bone solely by osteoblasts; and *SPP1*, a gene expressed by multiple cell types including osteoblasts and osteoclasts. The steady-state transcript levels of *ALP* are higher in maxillary compared to mandibular (p=0.025) and tibial hPDCs (p=0.0013) (**Fig. 3.4A**), whereas *BGLAP* transcripts showed no statistically significant differences (**Fig. 3.4B**). *SPP1* was upregulated for tibia-derived cells when compared to hPDCs from mandible (p=0.014; **Fig. 3.4C**). For the adipogenic receptor *PPARG* no differences were seen that are statistically significant (**Fig. 3.4D**). *SOX9* was upregulated in both maxillary and mandibular cells compared to tibial hPDCs (p=0.03 and p=0.008, respectively; **Fig. 3.4E**). *VEGFR-1* transcripts were higher in maxillary compared to tibial (p=0.007) and mandibular hPDCs (p=0.04) (**Fig. 3.4F**). Also for *COL10A1* an upregulation was seen for maxillary hPDCS compared to mandibular and tibial hPDCs (p=0.016 and 0.013, respectively, **Fig. 3.4G**).

3.3.4. Bulk RNA-seq of cultured adult hPDCs reveals differences that reflect different embryonic origins

We have also performed bulk RNA-seq on expanded cells. Principal component analysis (PCA; **Fig. 3.5A**) and the hierarchical clustering (dendrogram in **Fig. 3.5B**) show that the differences in anatomical origin of the hPDCs are reflected in bulk mRNA expression differences. To capture the maxilla and mandible-derived hPDCs genes that contribute to this distinction, we have carried out differential gene expression analysis between the hPDCs. 780 differentially expressed genes (DEGs; FDR < 0.05, log fold change > 1) were identified between tibial and maxillary hPDCs. 291 of these were down and 489 up regulated in maxilla-derived hPDCs. Between mandible and tibia-derived hPDCs 841 DEGs were identified, with 361 genes down and 480 genes up regulated in mandibular hPDCs (**Fig. 3.5C**; **Tables S3.2, S3.3**). In these comparisons only around 33% of the DEGs are common between maxilla and mandible derived hPDCs compared to tibial hPDCs, attesting to the large difference that exists between maxilla and mandible-derived hPDCs. Finally, the comparison between mandibular and maxilla-derived hPDCs identified 438 DEGs; 236 of these genes were up and 202 genes were down regulated in maxilla-derived hPDCs (**Fig. 3.5C**; **Table S3.4**).

Next, we performed gene enrichment analysis on the DEGs to capture the biological processes and molecular functions that show significant changes. Genes that show up- and down-regulation in both maxillary and mandibular hPDCs, compared to tibial hPDCs, are involved in skeletal system development, extracellular structure organization, vascular development and related pathways (**Figs. S3.1, S3.2**). Upregulated genes in tibia showed more significant enrichment in bone development related pathways (**Figs. S3.1, S3.2**). In the comparison between maxillary and mandibular hPDCs, genes that are up regulated in mandibular (and also down regulated in maxillary) were enriched for terms related to skeletal system development, bone remodeling, ossification (**Fig. S3.3**). This reflects the chondrogenic and osteogenic differentiation potential of mandible-derived hPDCs compared to maxillary hPDCs. Down regulated genes in

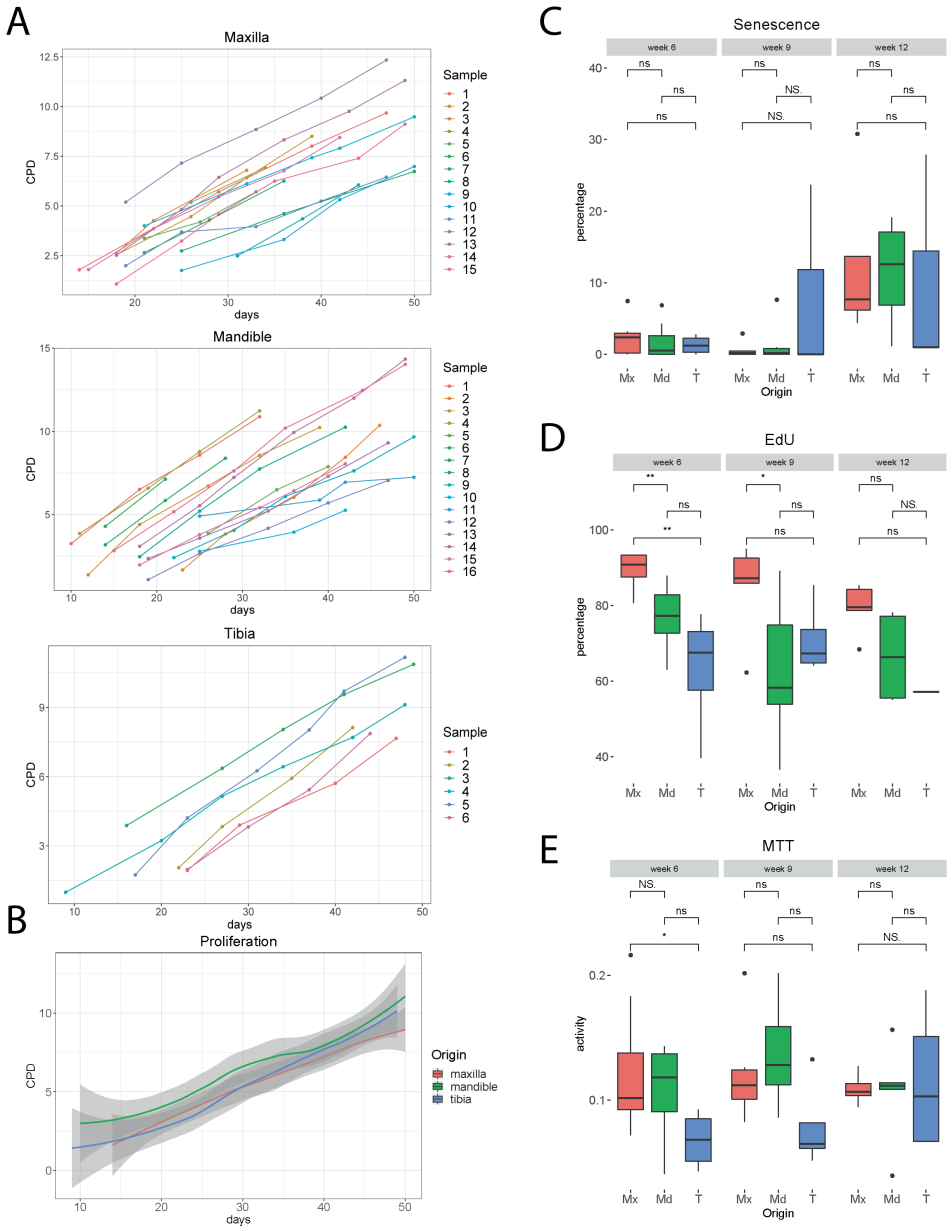

Figure 3.3. Human PDCs can be expanded for 2 months.

(A) Proliferation curves of hPDCs obtained from maxilla, mandible and tibia, wherein the X-bar displays the time in days and the vertical axis the cumulative population doublings (CPD). **(B)** Mean proliferation curves of hPDCs from maxilla (red), mandible (green) and tibia (blue), with confidence interval showed in gray. **(C)** Percentage of SA-β-gal staining-positive cells at 6, 9 and 12 weeks of expansion in DMEM-C. **(D)** Proliferation-capacity of hPDCs showed by the percentage of EdU+ cells after 6, 9, and 12 weeks of expansion in DMEM-C. **(E)** Metabolic activity shown by MTT-test of hPDCs obtained from maxilla (Mx), mandible (Md) and tibia (T) after 6, 9 and 12 weeks of expansion in DMEM-C. *p ≤ 0.05, **p ≤ 0.01.

mandibular (and also up regulated in maxillary) were involved for terms that are not related to bone development (**Fig. S3.3**).

The list of DEGs also pointed to differences among *HOX*- and *DLX*-family genes between craniofacial and tibial hPDCs. The majority of the *HOX*-family genes showed upregulation in tibial hPDCs. However, some *HOX* genes (*HOXC8, HOXD8, HOXC9, HOXD9,* and *HOXA10*) showed also higher expression in craniofacial hPDCs (**Fig. 3.5D**). From the *DLX* family, the *DLX1* gene was highly expressed in craniofacial and tibial hPDCs, and *DLX5* in mandibular hPDCs.

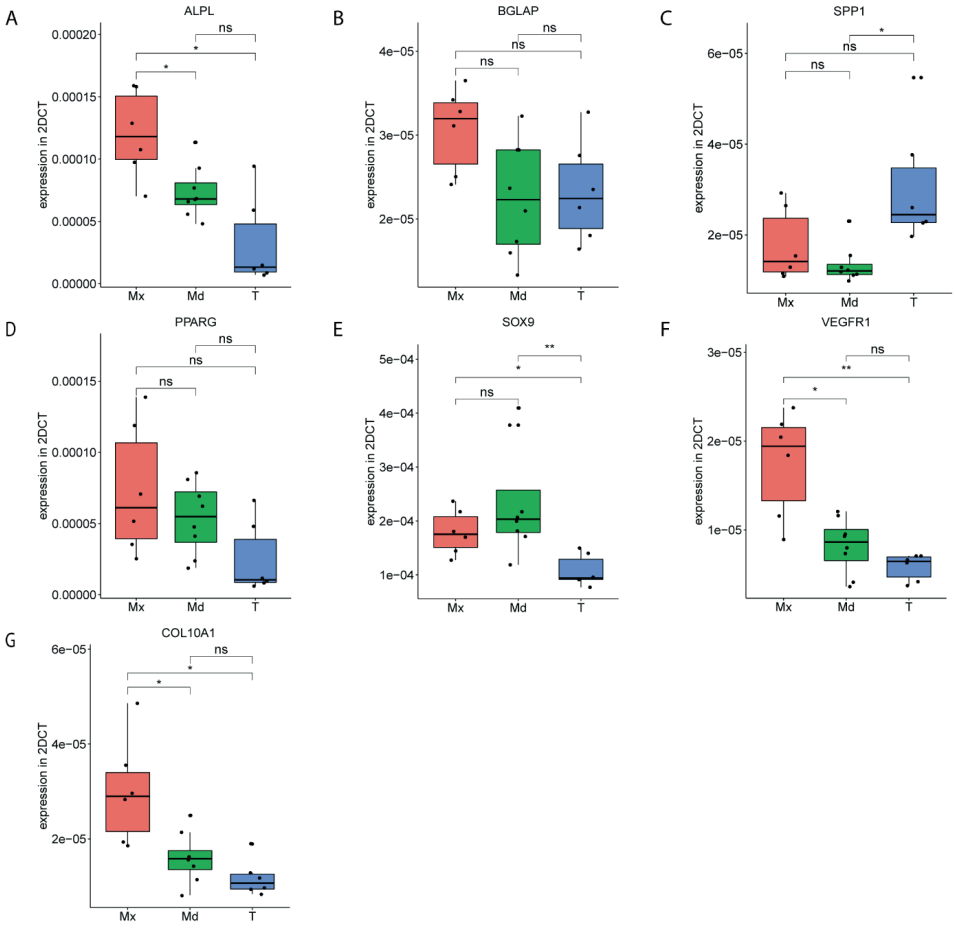

Figure 3.4. Marker gene analysis in hPDCs.

(A-G) Expression level of *ALPL* (A), *BGLAP* (B), *SPP1* (C), *PPARG* (D), *SOX9* (E), *VEGFR-1* (F) and *COL10A1* (G) of hPDCs from maxilla (Mx), mandible (Md) and tibia (T) after expansion in DMEM-C at PD=10, n=3 in biological duplicates for each origin corrected for *GAPDH*. *p ≤ 0.05, **p ≤ 0.01, ***p ≤ 0.001, ****p ≤ 0.0001.

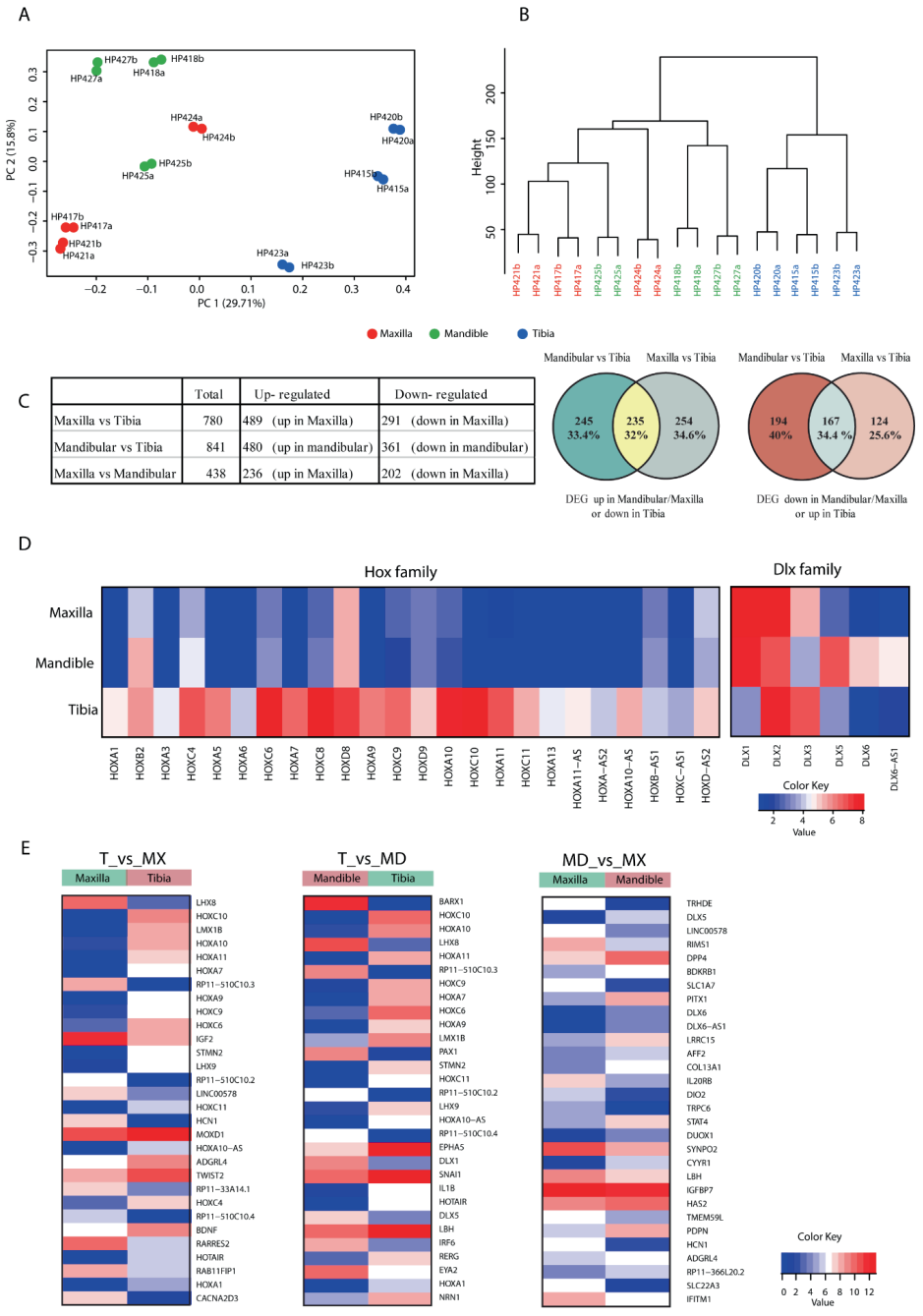

	Total	Up- regulated	Down- regulated
Maxilla vs Tibia	780	489 (up in Maxilla)	291 (down in Maxilla)
Mandibular vs Tibia	841	480 (up in mandibular)	361 (down in mandibular)
Maxilla vs Mandibular	438	236 (up in Maxilla)	202 (down in Maxilla)

Figure 3.5. Bulk RNA-seq results in hPDCs.

(A) Principal component (PC) analysis of RNA-sequencing on hPDCs obtained from maxilla (red), mandible (green) and tibia (blue). Each dot represents the sample mean from a single donor. **(B)** Cluster dendrogram based on RNA-sequencing results. **(C)** Table showing the number of DEGs, and Venn diagrams of DEGs between maxillary, mandibular and tibial hPDCs based on RNA-seq. **(D)** Heatmap of *HOX* and *DLX* family

genes based on RNA-seq data. **(E)** Heatmap of the 30 most-DEGs in the comparisons tibia (T) vs. maxilla (MX) and mandible (MD), and MD vs. MX.

Supplementary figure 1

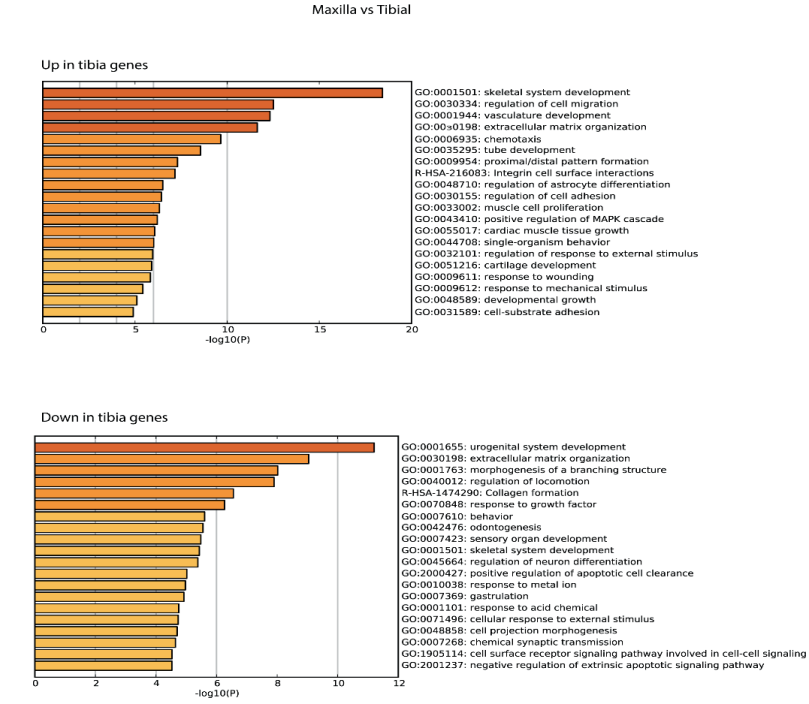

Supplementary figure 2

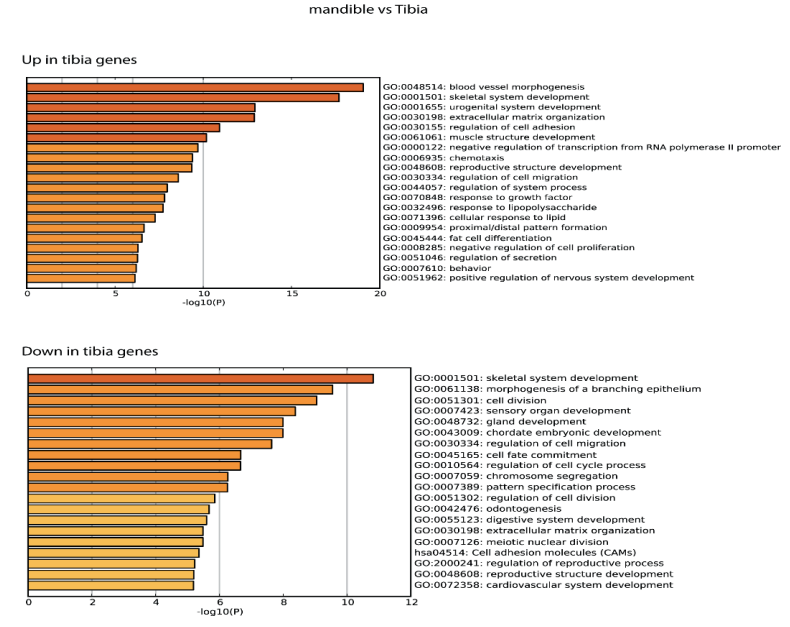

Supplementary figure 3

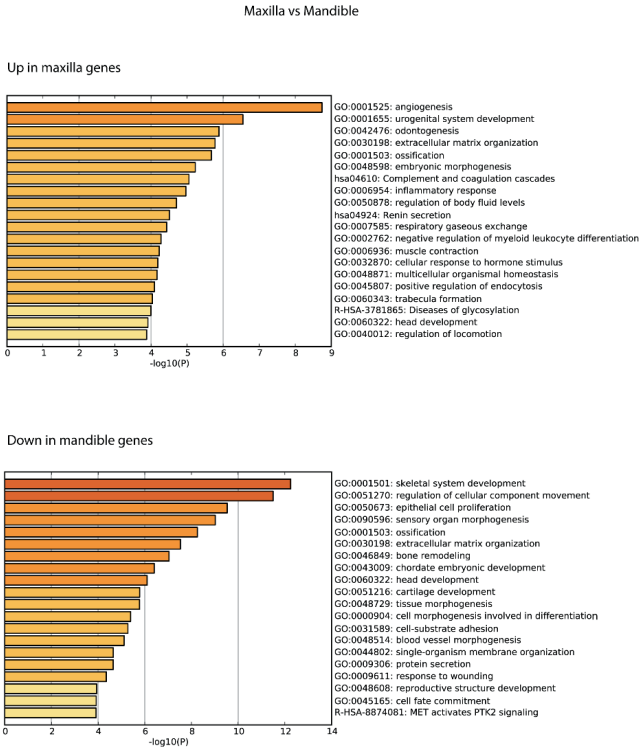

Figures S3.1-S3.3. Comparative gene ontology analyses.

Fig. S3.1 (***top panel of previous page***): Maxillary versus tibial-derived hPDCs. The bone-forming properties differ between maxillary and tibial hPDCs.

Fig. S3.2 (***bottom panel of previous page***): Mandibular versus tibial-derived hPDCs. The bone-forming properties differ between mandibular and tibial hPDCs.

Fig. S3.3 (***this page***): Maxillary versus mandibular-derived hPDCs. The bone-forming properties differ between maxillary and mandibular hPDCs

The RNA-seq data were validated by RT-qPCR by taking the top-10 DEGs in the 3 comparisons (see **Fig. 3.5E**; **Table S3.5**). Expression of *HOXA11*, encoding a transcription factor regulating positional cell identity along the anterior-posterior (AP) axis of embryonic segments (Liatsikos *et al.*, 2010; Raines *et al.*, 2015), was elevated in tibial compared to maxillary and mandibular hPDCs (p=0.007 for both; **Fig. 3.6A**). Also, significantly higher expression values of *HOXA7, HOXA10, HOXC10*, and the *HOX* transcript antisense RNA (*HOTAIR*) were obtained for tibial hPDCs compared to those from the craniofacial area, which confirmed the RNA-seq results (**Fig. 2.6B-E**). We conclude that tibia-derived periosteal cells isolated from patients still express genes that are involved in AP patterning in the embryo. *DLX1*, encoding a transcriptional regulator and an acknowledged downstream target of multiple transforming growth factor beta (TGF-β) family members (including BMPs; Mimura *et al.*, 2016), was more highly expressed in mandibular compared to tibial hPDCs (p=0.007; **Fig. 3.6F**). *DLX5* is an early-BMP responsive gene and encodes a transcription factor involved in osteoblast differentiation (Li *et al.*, 2008). This gene was more strongly expressed by mandibular compared to tibial hPDCs (p=0.013; **Fig. 3.6G**). *DLX6*, often proposed as paralog of *DLX1* (Li *et al.*, 2008), did not show any statistically significant difference (**Fig. 2.6H**), but the antisense RNA encoded by *DLX6* (*DLX6-AS1*) was down regulated in mandibular compared to tibial hPDCs (p=0.007; **Fig. 3.6I**). The latter is in accordance with the trend toward a higher expression of *DLX6* in mandibular hPDCs.

BARX1 is expressed during tooth development and in neural crest-derived craniofacial mesenchymal tissues, but is also known for its inhibition of canonical Wnt signaling (Woo *et al.*, 2011; Lin *et al.*, 2019). Expression of *BARX1* was higher in mandibular compared to tibial hPDCs (p=0.007; **Fig. 3.6J**). *LHX8* encodes a transcription factor that plays a role in the development of the palate, in oogenesis and neuronal differentiation (Choi *et al.*, 2008; Flandin *et al.*, 2011; Cesario *et al.*, 2015). However, *LHX8* is also known to stimulate the proliferation of MSCs, while a drop in *LHX8* expression level combined with increased levels of BMP2 promotes osteogenesis (Wang *et al.*, 2019). For *LHX8* higher expression was found in maxillary compared to tibial hPDCs (p=0.013; **Fig. 3.6K**).

PAX1, a target of Sonic Hedgehog (Shh) signaling that plays a role in axial skeletogenesis (Wallin *et al.*, 1994), showed a trend toward downregulation in hPDCs originating from the mandible, compared to those from tibia (**Fig. 3.6L**). PAX1 also positively regulates the chondrogenic marker genes *SOX5*, *ACAN, COL2A1,* and *WW domain-containing protein 2* (*WWP2*) (Takimoto et al., 2019). *COL13A1* encodes the alpha-chain of one of the non-fibrillar collagens and has previously been implicated in bone mass and bone formation rate (Ylönen *et al.*, 2005), but did not show any statistically significant differences (**Fig. 3.6M**). *DPP4* plays an important role in glucose metabolism. Administration of inhibitors against DPP4 results in an increase in bone mass by upregulation of *IL-10* and subsequent stimulation of chondrocyte hypertrophy (Jung *et al.*, 2013; Wang *et al.*, 2018). *DPP4* was expressed less by maxillary compared to mandibular hPDCs (p=0.015; **Fig. 3.6N**). *GPC3*, encoding an antagonist of DPP4 and involved in limb patterning and skeletal development via BMP4 (Paine-Saunders *et al.*, 2000), did not show statistically significant differences, but an opposing trend to *DPP4* (**Fig. 3.6P**). No statistically significant differences were found for the G-protein coupled receptor encoding gene *GPRC5C* (**Fig. 3.6O**). *VEGFB*, the encoded factor being involved in angiogenesis and endothelial cell physiology (Hagberg *et al.*, 2010), showed an upregulated trend in maxillary compared to tibial and mandibular hPDCs (**Fig. 3.6Q**). In total, we could confirm, using RT-qPCR and after Bonferroni-correction, statistically significant differences in expression for 11 out of the 30 DEGs selected from the RNA-seq lists.

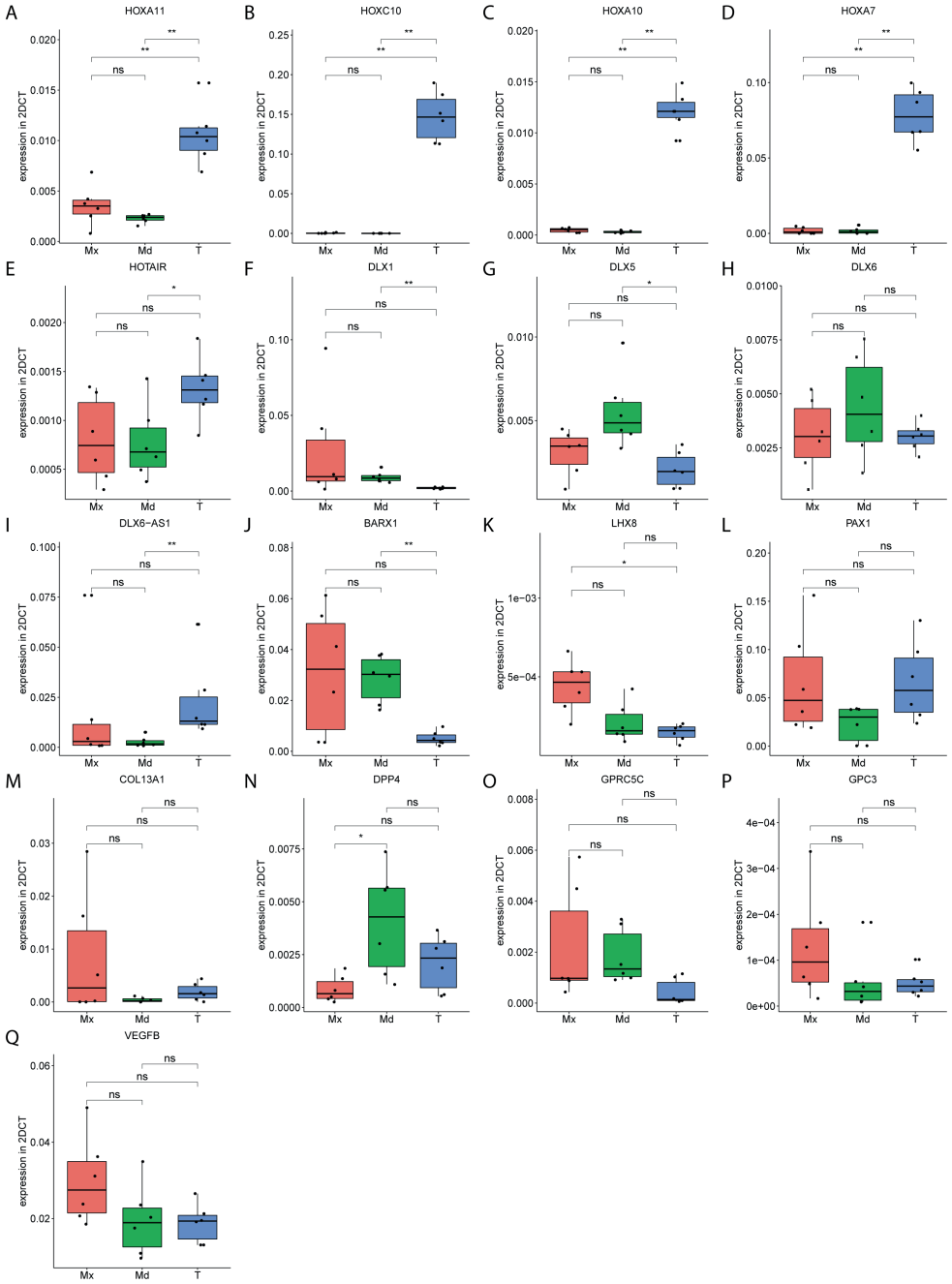

Figure 3.6. Validation of RNA-seq results of hPDCs of three different sources.

(A-Q) Expression level of genes found in top-10 from RNA-seq for each comparison, forming in total a top-30 list, confirmed on maxillary (Mx), mandibular (Md) and tibial (T) hPDCs obtained from different donors at PD = 10, n = 3 in biological duplicates for each origin corrected for *GAPDH*. *$p \leq 0.05$, **$p \leq 0.01$.

3.3.5. *In vivo* bone formation

We assessed whether after 8-weeks bone formation in scaffolds seeded with tibial hPDCs did occur; for this, we used Nano-CT analysis of ectopically implanted scaffolds (**Fig. 2.7A,B**). No *in vivo* mineralized tissue was detected with maxilla-derived hPDCs, whereas it was present, as a positive control, in constructs seeded with tibial hPDCs ($p=0.04326$) at an average of 0.0736 mm^3 bone tissue (**Fig. 3.7A,B**). Importantly, bone formation by mandibular hPDCs was detected in 6 out of the 12 retrieved constructs, averaging 0.06 mm^3 bone tissue in those 12 constructs. Staining with hematoxylin/eosin (HE) confirmed that the mineralized tissue seen on CT-scans was indeed bone tissue (**Fig. 3.7C-E**). Staining of cartilage with Alcian Blue showed more staining in scaffolds seeded with mandibular hPDCs (**Fig. 3.7F-H**). Staining for bone tissue with Masson's Trichrome confirmed the results obtained from both staining with HE and Alcian Blue (**Fig. 2.7I-K**).

3.4. Discussion

Research toward cell-based bone tissue-engineering recently focused strongly on the properties of SSPCs and proposed hPDCs as candidate cells (Roberts *et al.*, 2015; Bolander *et al.*, 2020). We have documented the differences between PDCs obtained from different anatomical locations (maxilla, mandible and tibia, respectively) *in vitro* and also *in vivo*. FACS on markers on SSPCs was shown by others to underlie further cellular differentiation accompanied by loss of stem cell state (van Lochem *et al.*, 2004). We concluded that 88% of our *in vitro* expanded craniofacial cells fulfilled the applied SSPC criteria, and 62% of our *in vitro* expanded tibial hPDCs, but also acknowledged the limited relevance of these markers for stem cell function (Ambrosi *et al.*, 2019).

Our hPDCs were able to proliferate *in vitro* at comparable rates to each other, they did not display senescence during 9 weeks of culture, and were able to differentiate at CPD 8 to osteogenic, chondrogenic and adipogenic lineages. *ALPL* and *BGLAP* displayed higher mRNA expression *in vitro* cultured hPDCs obtained from maxilla compared to tibia, which could underlie the higher *in vitro* osteogenic potential of maxilla-derived hPDCs. For *in vivo* endochondral bone formation, the mandibular hPDCs showed a higher potential, possibly due to higher *SOX9* expression by these cells *in vitro*, again compared to tibial hPDCs. The steady-state mRNA levels of Fms Related Receptor Tyrosine Kinase 1 *(FLT1)*, encoding the decoy receptor VEGFR-1, and that are normally upregulated during healing of fractured bones, were highest in maxillary hPDCs compared to hPDCs of other sites. This can be of interest when scaling-up tissue engineering constructs that have diffusion limits of oxygen and nutrients, since cell death or apoptosis in the center of the implant has been reported if good vascularization is not achieved quickly (Potier *et al.*, 2007; Giannoni *et al.*, 2010).

RNA-seq and further validation by RT-qPCR on separate *in vitro* cultured samples thus reveal notable differences in gene expression between hPDCs obtained from the three sites. These are represented mostly by the higher expression of *HOX* and *DLX* family genes steering skeletal system and other connective tissue development, but also co-determine extracellular matrix organization, collagen formation, and responses to growth factors. Overall, these sets of genes are irrefutably relevant to *in vivo* bone regeneration and form a solid basis for future experiments that aim at improving bone tissue engineering applications. *HOXA7, HOXA10, HOXC10,* and *HOTAIR*

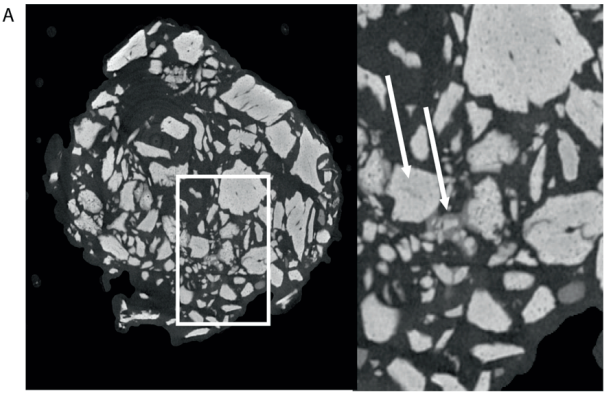

B

	Mean	SD
Maxilla		
Mandible	1,10%	1,44%
Tibia	1,72%	1,14%

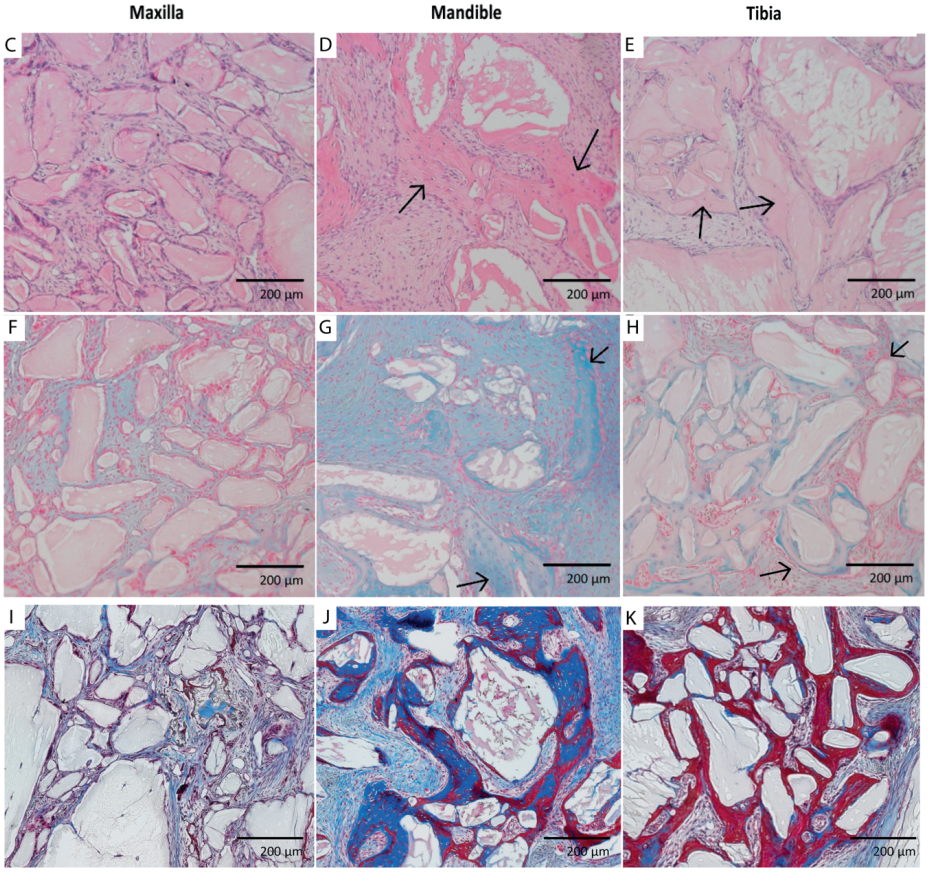

Figure 3.7. Bone formation *in vivo* by expanded hPDCs of various origin.

(A) Shown is Nano-CT imaging of scaffolds seeded with hPDCs obtained after 8 weeks of ectopic implantation with scaffold grains in light gray (white arrow) and mineralized tissue in dark gray (white dashed arrow). **(B)** Volumetric percentage of mineralized tissue in each cell construct. **(C-K)** Histological imaging of those cell constructs stained with Hematoxylin/Eosin **(C-E),** Alcian Blue **(F-H)** with bony tissue pointed by black arrows, and Masson's Trichrome **(I-K).**

were each upregulated in tibial hPDCs compared to those from the craniofacial area. Hence, tibia-derived periosteal cells isolated from adult patients still express genes that are involved in several other processes, including anterior-posterior patterning in the embryo, or these genes also have additional functions in cell differentiation. Leucht *et al.* (2008) grafted periosteum from the tibia onto craniofacial bone defects (and *vice versa*) and demonstrated that *HOXA11*-expressing cells maintain their *HOX* status after changing the environment, but *HOXA11*-non-expressing cells can start to express *HOXA11* after changing the environment. In this study, the change of environment, which *in vitro* expansion is, could explain the presence of low expression of *HOX* genes by hPDCs obtained from the maxilla and mandible.

DLX1 was expressed at a higher level in maxilla-derived hPDCs. This could explain the higher osteogenic potential of these cells *in vitro*. DLX5 acts as an early BMP-responsive transcriptional activator driving osteoblastic differentiation of cells, while *DLX6* has been proposed as paralog of *DLX1* (Li *et al.*, 2008). These results suggest favoring the use of mandibular hPDCs in craniofacial applications, since *DLX5* and *DLX6* were both up-regulated in these cells. However, *PAX1*, a target of Shh signaling, but also positively regulating the chondrogenic effector or marker genes *SOX5, ACAN, COL2A1*, and *WWP2* (Wallin *et al.*, 1994; Takimoto *et al.*, 2019), was expressed at higher levels in tibial hPDCs. Taken together, hPDCs obtained from maxilla, mandible and tibia showed different gene/mRNA expression profiles, including of relevant effector or marker genes, which could lead to different direct or endochondral bone forming properties. This could be exploited in bone tissue engineering strategies for various anatomical locations. For a number of selected genes, based on RNA-seq, we also could not reproduce the results by RT-qPCR. We hypothesize that this is due to our use of different donors throughout these comparisons, which made the validation more stringent.

Analysis of hPDC-seeded scaffolds showed bone formation 8 weeks after ectopic implantation when seeded with tibial and mandibular cells, but unexpectedly not with maxilla-derived hPDCs. For the latter, cells show *in vitro* upregulation of osteogenic genes compared to tibia-derived cells. We hypothesize that maxilla-derived periosteal cells are less prone for endochondral bone formation when the cells are not stimulated by growth factors. Also local environmental cues influence the ability of these cells to form bone, as demonstrated previously through periosteal grafting experiments (Leucht *et al.*, 2008). In addition, the choice of the carrier or any coincidence in view of the generally observed biological variability of the *in vivo* ectopic bone formation assays, could account for the documented difference (Ji *et al.*, 2018).

To our knowledge, *in vivo* results of ectopic bone formation using *in vitro* expanded maxilla-derived periosteal cells have not been reported yet. Additional work is needed to investigate if priming of hPDCs prior to implantation could be optimized for craniofacial-derived hPDCs, as was shown for tibial hPDCs (Bolander *et al.*, 2016). The effects of priming tibia-derived periosteal cells with different concentrations of calcium in the medium on their bone-forming capacities *in vivo*, and when using calcium phosphate scaffolds, have been documented previously (Chai *et al.*, 2012). Mandibular periosteal cells, obtained from the region near the wisdom tooth, yield more bone tissue *in vivo* when co-cultured with CD34+ endothelial progenitors obtained from the umbilical cord, while a trend toward a better osteogenic potential of mandibular periosteum-derived cells cultured using cyclic tension force has also been reported (Lee *et al.*, 2014; Lee *et al.*, 2017). For tibia-derived periosteal cells, the effects of different calcium phosphate scaffolds on *in vivo* bone formation capacities of such cells was also reported (Kerckhofs *et al.*, 2016). Others have stated the importance of the combination of mesenchymal lineage-derived cells with type of scaffold (Mattioli-Belmonte *et al.*, 2015), but this has not yet been explored with maxilla and/or mandible-

derived cells. Furthermore, many features of scaffolds contribute to the *in vivo* outcome, including bio-compatibility, porosity, pore size, surface properties, osteo-inductivity and mechanical properties (Salgado *et al.*, 2004). In addition, the predictability and robustness of the *in vivo* formed bone construct as well as possible differences in the speed of bone formation, and bone formation in an orthotopic environment altogether, should also be evaluated and/or improved in order to prepare translation toward the clinic (Geris and Papantoniou, 2019).

We hypothesized that location and tissue of origin are relevant for successful bone repair when using *in vitro* expanded cell-based tissue engineering constructs. hPDCs from different anatomical locations may be interesting sources, but would display different properties and possibly differences in outcome with regard to bone healing *in vivo*. Therefore, we focused on documenting (dis)similarities between *in vitro* expanded periosteum-derived cells from tibia, maxilla and mandible. Progenitor cells from different anatomical sources indeed differ in their transcriptomic signature and *in vivo* differentiation potential (Sacchetti *et al.*, 2016). We have shown that *in vitro* expanded hPDCs obtained from these respective sites do not differ in their capacities to proliferate *in vitro* under the experimental conditions used. However, the cells showed differences in gene expression profiles and *in vivo* bone formation. So, different properties, including embryonic origin and (epi)genetic priming laid down within functionally similar cell types, located at different anatomical sites, can be retained during ex vivo expansion. This then influences the functional outcome, here demonstrated by different skeletogenic potential of SSPCs. It remains to be investigated if these observed differences are critical for clinical outcomes, including remodeling of tissue over time, and for which indications.

3.5. Experimental procedures

Isolation and culture of hPDCs

Periosteal samples (5-10 mm) were obtained from the posterior areas of the maxilla and mandible of 16- to 30-year-old healthy female and male patients who underwent bimaxillary orthognathic surgery, after informed consent was obtained (Belgian registration number B322201731127). The tibial samples were harvested by orthopedic surgeons as described previously from 16- to 30-year-old female and male patients undergoing total knee replacement or distraction osteogenesis (Eyckmans and Luyten, 2006). These samples were digested in medium consisting of Dulbecco's modified Eagle's medium (DMEM) supplemented with 10% Fetal Bovine Serum (FBS; Thermo Fisher Scientific, Waltham, MA, United States) and 1% antibiotics-antimycotics solution (100 units penicillin/ml, 100 µg streptomycin/ml and 0.25 µg amphotericin-B/ml; Invitrogen), from here on referred to as DMEM-complete (DMEM-C), in addition of 4,400 units per 10 ml Collagenase type-IV (Gibco) under constant agitation for 16 h. Cells were from then on cultured in DMEM-C.

Population doublings of these human PDCs (hPDCs) were calculated upon passaging using the formula $\log_2(n_2)$- $\log_2(n_1)$, with n_1 representing the number of cells seeded in the dish/flask and n_2 the number of cells obtained after trypsinization (TrypLE, Thermo Fisher Scientific) of cells from the same dish/flask at 90% confluency.

Cellular senescence

For detection of senescent cells, 10^5 cells were plated per well in a 6-well plate in DMEM-C. After one day, the cells were fixed using 4% paraformaldehyde (PFA) for 5 min, rinsed using PBS and stained with 2 ml/well filtered (0.22 µm; Millex-GP) staining solution consisting of 36 mM citric acid, pH 6.0 (Sigma Aldrich), 4.5 mM potassium ferricyanide (Merck), 0.14 M NaCl, 1.8 mM $MgCl_2$ (Merck) and 1 mg X-gal/ml (Biotium). After 6 h, the cells were imaged using a Primovert inverted microscope (Zeiss).

Cell proliferation

For detection of proliferating cells, staining for incorporated EdU was performed using the Click-iTTM EdU Alexa FluorTM 555 Imaging Kit (Thermo Fisher Scientific) according to the manufacturer's protocol.

In short, 10^5 cells/well were seeded in a 6-well plate in DMEM-C. The following day, medium was replaced with DMEM-C containing 10 µM EdU, followed by an incubation of 72 h. Next, cells were fixated using 3,7% formaldehyde in PBS (VWR) for 15 min, rinsed twice with 3% bovine serum albumin (BSA, Sigma Aldrich) in PBS and lysed with 0.5% Triton X-100 in PBS (Sigma Aldrich) for 20 min. This was followed by adding the Click-iT reaction cocktail for 30 min in absence of light, quick washing steps of 1 min using subsequently 3% BSA dissolved in PBS and later on in PBS, addition of the Hoechst solution for 30 min in a 1:2,000 dilution in PBS and final washing steps using PBS for 1 min.

Cell metabolism

Cell metabolism was measured by using 3-(4,5-dimethylthiazol-2-yl)-2,5-diphenyltetrazolium bromide (MTT) assay. Living cells contain the mitochondrial reductase enzyme, which reduces MTT toward formazan forming salt crystals. By measuring the amount of reduction of MTT toward formazan, the cell metabolism was measured. This was done by removing remaining MTT and solubilizing of the salt crystals in order to get with the different quantities of salt crystals corresponding differences in color intensity (Mosmann, 1983).

Tests were performed as technical replicates 6 times per donor at 6, 9, and 12 weeks of culture. 10,000 cells were seeded in a 24-well plate in 0.5 ml DMEM-C. After 1 day, DMEM-C was replaced with DMEM containing 250 µg MTT/ml (Sigma Aldrich). After 4 h, medium and remaining MTT were removed and 1 ml absolute ethanol was added to each well in order to solubilize the salt crystals. These solutions were transferred to a 96-well plate and absorbance was read at 570 and 670 nm with a Synergy HT reader (BioTek). In order to calculate the metabolic rate, the background absorbance (at 670 nm) was subtracted from the absorbance at 570 nm and corrected for the blank values which were obtained by performing all steps on wells containing no cells.

Flow cytometry

10^6 cells were at passage 6 washed in 500 µl PBS + 1% FBS and incubated at the following dilutions with anti-CD90-APC (1:250), anti-CD164-PE (1:250), anti-CD45-FITC (1:1,000), anti-CD31-FITC (1:1,000), anti-CD235ab-FITC (1:1,000; all from BioLegend), anti-CD146-BV711 (1:250), anti-CD73-BV395 (1:250) and anti-PDPN-BV510 (1:100; all from BD Bioscience) in 200 µl PBS + 1% FBS for 15 min in a dark area. The cells were then washed twice with 1% FBS in PBS. For compensation controls, UltraComp eBeads Compensation Beads (Thermo Fisher Scientific) were used. Gating was performed using Fluorescence-Minus-One (FMO) controls. Fluorescence measurement was performed on a FACS Calibur (BD Biosciences) using 100,000 events.

Differentiation of hPDCs

Human PDCs were primed for adipogenic, osteogenic and chondrogenic differentiation for 14, 21, and 7 days, respectively. Analysis was performed by staining with Oil Red O, Alizarin Red and Alcian Blue, respectively.

For adipogenic differentiation of hPDCs, cells were cultured in 24-well plates at a density of 19,000 cells/well in 0.5 ml DMEM-C. After 2 days, the medium was changed for adipogenic differentiation medium, i.e., Minimum Essential Medium Eagle - alpha modification (α-MEM; Invitrogen supplemented with 10% FBS, 1% antibiotics-antimycotics solution, 1 µM dexamethasone + 10 µg human insulin/ml (Sigma Aldrich), 100 µM indomethacin (Sigma Aldrich) and 25 µM 3-isobutyl- 1-methylxanthine (Sigma Aldrich). The cells were cultured in a humidified atmosphere at 5% CO_2 and 37°C for 14 days and medium was replaced every 2 days. Lipid droplets were stained by Oil Red O. Cells in monolayer were washed in PBS and fixed for 30 min at room temperature in 10% formaldehyde (VWR) diluted in PBS. Next, cells were washed with Milli-Q water and rinsed in 60% isopropanol (VWR) diluted in Milli-Q water. Cells were allowed to dry completely and then stained with 0.2% Oil Red O (Sigma Aldrich) in Milli-Q water for 60 min. These cells were then washed with Milli-Q water before obtaining pictures using the Primovert microscope (Zeiss).

For osteogenic differentiation of hPDCs, cells were cultured in 24-well plates at a density of 8,550 cells per well in 0.5 ml DMEM-C, first allowing them to proliferate. After 1 day, medium was then changed for osteogenic medium consisting of DMEM-C supplied with 100 nM dexamethasone (Sigma Aldrich), 10 mM β-glycerophosphate disodium salt hydrate (Sigma Aldrich) and 50 µg L-ascorbic acid 2-phosphate/ml (Sigma Aldrich). Cells were cultured in a humidified atmosphere at 5% CO_2 and 37°C for 21 days, during which this medium was replaced every 3 days. Cells in monolayer were washed in PBS, fixed with methanol at 20°C (Fisher Scientific), stored for 1 h at 4°C, and washed again with PBS. Cells were stained for 1 h with a 2% Alizarin-S stain (Sigma Aldrich) in Milli-Q water with pH adjusted to 4.2 (Merck) while the plate was

placed on a shaker for constant agitation. After staining, cells were washed with Milli-Q water. Pictures were made using a Discovery.v8 SteREO microscope (Zeiss).

For chondrogenic differentiation of hPDCs, the cells were cultured in micromasses. Micromasses containing 200,000 cells in 10 µl DMEM-C after centrifugation at 260 RCF for 10 min were added to individual wells of 24-well plates. After 2 h, an extra 0.5 ml of DMEM-C was added to each well. After 1 day, this medium was replaced by chondrogenic inductive medium (DMEM-F12 (Invitrogen) containing 2% FBS, antibiotics-antimycotics solution, 1x ITS + premix universal culture supplement (Corning), 100 nM dexamethasone, 10 µM Y27632 (Axon Medchem), 50 µg L-ascorbic acid 2- phosphate/ml, 40 µg proline/ml (Sigma Aldrich) and 10 ng transforming growth factor-β1/ml (TGFβ1; PeproTech). These cells were cultured under humidified conditions at 37°C and 5% CO_2 for 7 days; medium was replaced every 2 days. Sulfated glycosaminoglycans in the micromasses were stained by Alcian Blue (Roth). The cells were rinsed with PBS and fixed with excess ice-cold methanol for 1 h at 4°C. This methanol was removed and cells were rinsed with Milli-Q water prior to adding 0.1% Alcian Blue staining solution (in 0.1 M HCl at pH 2.4) for 1 h on a shaker. Alcian Blue stain was removed and the cells were rinsed with Milli-Q water before pictures were made using the Discovery.v8 SteREO microscope (Zeiss). At days 1 (control), 3, 5 and 7, micromasses were also obtained for confirmation of chondrogenic differentiation by RT-qPCR. Micromasses were individually lysed in 350 µl RLT buffer (Qiagen) containing 1% β-mercaptoethanol (Sigma Aldrich) and homogenized by thoroughly pipetting up and down. Samples were directly placed on ice and frozen at 80°C until further processing.

RNA isolation, cDNA synthesis and quantitative PCR

RNA was isolated from biological duplicates when a cumulative PD 10 was reached for RT-qPCR and at PD 16 for RNA-seq analysis. 106 cells were rinsed twice in PBS and centrifuged at 260 RCF for 10 min. After removing the supernatant, the cell pellet was lysed by adding 350 µl RLT buffer (Qiagen) containing 1% β-mercaptoethanol (Sigma Aldrich) and homogenized by thoroughly pipetting up and down. Samples were directly placed on ice and frozen at 80°C until further processing. The Qiagen RNeasy mini kit was used to isolate RNA according to the manufacturer's instructions. cDNA was obtained by reverse transcription of 500 ng of total RNA, using the RevertAid H Minus First Strand cDNA Synthesis Kit, 1 mM oligo (dT)20 and random hexamer primers (Thermo Fisher Scientific).

RT-qPCR was performed on expanded cells without stimulation for differentiation for RNA encoding alkaline phosphatase (*ALPL*), osteocalcin (*BGLAP*), osteopontin (*SPP1*), peroxisome proliferator activated receptor gamma (*PPARG*), collagen type-X (*COL10A1*), SRY (sex determining region Y)-box 9 (*SOX9*) and vascular endothelial growth factor receptor 1 (*VEGFR-1*). In chondrogenically differentiated cells, the expression of aggrecan (*ACAN*), *Col10A1* and Runt-related transcription factor 2 (*RUNX2*) was defined.
Samples were processed and measured in technical duplicates on a Step-One-Plus PCR machine (Applied Biosystems) using a Sybr Green detection system (Life Technologies) according to the manufacturer's instructions, and normalized using glyceraldehyde 3-phosphate dehydrogenase (*GAPDH*) as a housekeeping gene. The respective primer sequences are listed in the **Table S3.1**.

RNA-sequencing and data analysis

RNA-seq samples were obtained from three donors for the maxillary samples (HP417, HP421, and HP424), four donors for mandibular samples (HP418, HP422, HP425, and HP427), and three tibial donors (HP415, HP420, and HP423). RNA-seq samples were prepared from hPDCs at CPD 16 in technical duplicates (A and B) and cDNA libraries were generated using the Illumina TruSeq Stranded mRNA Library Prep Kit. These libraries were then sequenced (50 bp length) according to the Illumina TruSeq Rapid v2 protocol in 5 runs, 2 lanes each run, on an Illumina HiSeq 2500 sequencer. Low quality reads and contaminants (e.g., sequence adapters) were removed using Trimmomatic (Bolger *et al.*, 2014). Sequences that passed the quality assessment were aligned to the GRCh38 genome using HiSat2 (version 2.1.0) (Kim *et al.*, 2015).

Transcript abundance level (transcript count) was generated using HTSeq (version 0.9.1) (Anders *et al.*, 2015). The transcript counts were further processed using R (version 3.4.0). Data normalization and removal of batch effect was performed using the EDASeq R package (Risso *et al.*, 2011) and RUVseq package (Remove Unwanted Variation from RNA-Seq package). Differential expression analysis was performed using the edgeR R package (Robinson *et al.*, 2010), using the negative binomial generalized linear model approach. Differentially expressed genes with false discovery rate (FDR) 0.05 after Benjamini-Hochberg correction for multiple testing and expression level greater than 1 count per million (CPM) were retained and used for further processing, gene ontology and pathway analysis. Gene enrichment analysis was performed using metascape (Zhou *et al.*, 2019).

The RNA-seq data is deposited at NCBI with GEO accession number GSE149167.

In vivo bone formation

After proliferation, 10^6 cells suspended in 25 µl of DMEM- C were seeded on NuOss scaffolds (21 mm^3; ACEuropa). One hour after seeding, an additional 5 ml of DMEM-C was added. After overnight incubation at 37°C and 5% CO_2, scaffolds were randomly implanted subcutaneously over the available mice in triplicates with a maximum of 4 for each mouse at the shoulder and the back in the limb region of 8-week-old female NMRInu/nu mice (Janvier). All animal procedures were approved by the local ethical committee for Animal Research (KU Leuven). The animals were housed according to the guidelines of the Animal Facilities at Leuven (KU Leuven). Explants were harvested after 8 weeks.

Bone formation was analyzed using the Phoenix NanoTom S CT system (GE measurement) at a voltage of 60 kV and a current of 200 mA. An aluminium filter of 1 mm was used to filter out the low energetic radiation. CTAn and Batch Manager Software programs (Bruker micro-CT, Kontich, Belgium) were used for 3-D quantification of the bone volume and calcium phosphate (CaP) grains of the NuOss scaffold. A three-level automatic Otsu segmentation algorithm was used to segment the newly formed bone tissue and CaP-grains from the background in combination with manually chosen thresholds. Noise was reduced by removing black and white speckles smaller than 200 voxels and a closing operation of 2 voxels was performed to solidify the resulting structure, providing binarized images suitable for the 3-D analysis.

Percentage of bone was calculated with respect to total explant volume (Kerckhofs *et al.*, 2013). After decalcification in EDTA, dehydration through a series of graded ethanol baths, embedding in paraffin and sectioning, histological stainings were performed. Staining with hematoxylin and eosin (HE) was done by a dip in Hematoxylin-solution for 2 min, followed by a wash in water and subsequently a staining in 1% Eosin (Klinipath, Duiven, Netherlands) for 7 min (Bolander *et al.*, 2016). For Alcian Blue staining, samples were rehydrated, stained for 30 min in 0.5% Alcian Blue (Roth) solution in 1 M HCl (pH = 1). Nuclear Fast Red (Vector) was used for staining of the nuclei during 5 min. For staining with Safranin O, samples were dipped in acidic alcohol (1% HCl in 70% ethanol). Next, they were placed in Fast Green (Klinipath) for 3 min, dipped in 1% acetic acid and then stained in 0.1% Safranin O (Sigma Aldrich) for 10 min.

Masson's trichrome staining was performed using Bouin's solution (Sigma Aldrich) as mordant followed by 5-minute-dips in Weigert's Iron Hematocxylin Solution, Biebrich Scarlet-Acid Fuchsin, Phosphotungstic/Phosphomolybdic Acid Solution and Aniline Blue Solution (all from Sigma Aldrich), followed by a dip in 1% acetic acid for 2 min. The sections were cleared in HistoClear (National-Diagnostics) and mounted in Pertex (Histolab). Pictures were made using the IX83 microscope (Olympus).

Statistical analysis

Statistical analysis for cellular senescence, quantitative PCR and *in vivo* bone formation was performed using the Kruskal-Wallis test. In case $p < 0.05$ for Kruskal-Wallis, a two-sided Wilcoxon test was performed to make comparisons for the qPCR validation of the RNA-seq data and to analyze cellular senescence, proliferation and metabolism rate.

Student's t-test was used to make comparisons for the chondrogenically differentiated micromasses. The Bonferroni correction was used to correct for multiple testing.

All statistical analyses were performed in R (version 3.6.0). Results were considered statistically significant at $p < 0.05$. Data are presented as mean values standard deviation (SD) or 95% confidence interval (CI) when stated.

Data availability

The datasets presented in this study can be found in online repositories. The names of the repository/repositories and accession number(s) can be found below: https://www.ncbi.nlm.nih.gov/geo/, under accession number GSE149167.

Ethics statement

The studies involving human participants were reviewed and approved by Ethics Committee Research UZ/KU Leuven. Written informed consent to participate in this study was provided by the participants or their legal guardian. The animal study was reviewed and approved by KU Leuven Animal Ethics Committee.

Conflict of Interest

The authors declare that the research was conducted in the absence of any commercial or financial relationships that could be construed as a potential conflict of interest.

Acknowledgments

We thank Stijn Bellinkx, Melanie Van den Broeck, Orely Vanborren and Janne Vleminckx for their practical support during the experiments. We also thank Carla Geeroms for acquisition of µCT-scans, Samuel Ribeiro Visei for his help with the FACS experiment and Kathleen Bosmans for her help during implantation experiments. We would also thank Louca Verbeeck and Samuel Ribeiro Visei for their help during analysis of FACS data, and Mirjam van den Hout for help with RNA-seq.

Author contribution

LG contributed to conception, design, and data acquisition, drafted and critically revised the manuscript. TH contributed to the data analysis and critically revised the manuscript. MM and FL contributed to conception, design supported in case of problems, and critically revised the manuscript. CP contributed to conception and critically revised the manuscript. WI contributed to data acquisition, initial data analysis, and critically revised the manuscript. DH and EM contributed to conception, design, data acquisition, data analysis, interpretation of results, and critically revised the manuscript. LG contributed to conception, supported in case of problems and critically revised the manuscript. All authors gave final approval and agree to be accountable for all aspects of the work.

Supplementary tables

Table S3.1: Primer sequences used for RT-qPCR.

Gene	Forward	Reverse
ALPL	GCTTCAAACCGAGATACAAGCA	GCTCGAAGAGACCCAATAGGTAGT
BGLAP	GTGCAGCCTTTGTGTCCAA	GCTCACACACCTCCCTCCT
COL10A1	ACGATACCAAATGCCCACAG	GTGGACCAGGAGTACCTTGC
GAPDH	CGATGCTGGCGCTGAGTAC	CGTTCAGCTCAGGGATGACC
PPARG	GCCAAGCTGCTCCAGAAAAT	TGATCACCTGCAGTAGCTGCA
SOX9	TGGAGACTTCTGAACGAGAGC	CGTTCTTCACCCACTTCCTC
SPP1	ACTGATTTTCCCACGGACCT	TCAGGGTACTGGATGTCAGG
VEGFR	ATTTGTGATTTTGGCCTTGC	CAGGCTCATGAACTTGAAAGC
ACAN	GTCTCACTGCCCAACTAC	GGAACACGATGCCTTTCAC
RUNX2	CGCATTCCTCATCCCAGTAT	GCCTGGGGTCTGTAATCTGA

Table S3.5: **Primer sequences of selected top-30 genes after RNA-sequencing, used for RT-qPCR.**

Gene	Forward code	Reverse code
HOXC10	CGGATAACGAAGCGAAAGAGGAG	GCGCTCTCGCGTCAAATACA
HOXA10	AGGATTCCCTGGGCAATTCCAAA	TTGTCTGTCCGTGAGGTGGA
HOXA11	TTTGATGAGCGTGGTCCCTG	AGTATGTCATTGGGCGCGAA
HOXC9	CCCCAGTAAGTTGGGAGCAAT	CCGACGGTCCCTGGTTAAAT
HOXA7	GGAGTTCCACTTCAACCGCT	CGGACCTTCGTCCTTATGCTC
HOTAIR	GCCAGTACCGACCTGGTAGA	GTCTGTGAGTGCCCGTCTTG
TMEM255B	CGTCCTCATAGTCACCGTCG	GCCACCAGCATTTGCCTTC
DPP4	GCTCGGCGCTCACTAATGTT	CACGGTGTCTTCATCGTCGG
DLX5	CACGGCTACTGCTCTCCTAC	CTTCTTTCTCTGGCTGGTTGGTG
DLX6	GAGGGGACGACACAGATCA	GTTCGGCTCTCTCTGGAAGG
DLX6-AS1	GGAGGATTCTGTGTGGGGTTG	ATGGGAGCACTCAGCCTACC
BDKRB1	GCCCCCTCTAGAGCTCCAAT	AAAGGTTCCCTAGGAGGCCG
LRRC15	GAGCTGCTGATGTGTCCCTAGC	GCCCACCAGCAAAAGGAGATAA
AFF2	TCTTGCGGGAGATGACCCATT	GACACTGACTTTGTAGAAGCTCTGG
COL13A1	CCACACCGGGAGTGCCTAAG	CCTGGAACGTCCGCCTTTTT
STAT4	TGGGTGGGAACTGACCCAAG	AGACATGCTAGCGCTCTCTCAG
DLX1	CGCTTCAATGGCAAGGGAAA	ATCTTGACCTGAGTCTGTGTG
TFAP2C	CTCCACGACATGCCTCACCA	TGGAAATGGGACCTTTGCGAAT
SMAGP	TTCAAAAGGACGCGCGGAG	GGGGTGGTCATCAGTTCTTCTCT
HOMER2	TGGGAGAACAGCCCATCT	TATGATCACCTTGGCTCCGTC
VEGFB	TATACTCGCGCTACCTGCCA	TGAGGATCTGCATCCGGACTT
BARX1	CAAAGCCAAGAAGGGGCGTC	ATCTATTCTGTCCGGCGTGGAA
LHX8	CTGGACCACTTGTGCTGGAGT	GGAAGCGTTTCCAGTCAAGCC

PAX1	TGCGCAAGGTCCTCCTCTG	GGAGGCTTCCTTCTCGGCT
HCN1	CTTTGGAGAGATTTGCCTGCT	AGTCGGTCAATGGCAACTGT
SLC1A7	GGCTCTCATGCGTGGAATGG	TAATTTCCTGTGGTGAGAGGCG
PALMD	AGACTCCAGGCCATCACAGATAA	TTCCTGTTCTTTTCCGCTGCT
GPC3	ACCACCACTGAAACTGAGAAGAA	TTGGCGTTGTTGAGAATGGGC
GPRC5C	TGCACAAAGTTCCGTCCGAAG	GTCCCACACGTAGGGGTTTCT
TMEM150C	AGATCCCACCCCTTCCTGA	CCATGCCTGTACCACTGCT

Other supplementary tables

Table S2.2: List of up- and downregulated genes of hPDCs obtained from maxilla compared to tibial hPDCs.

Available via: https://ndownloader.figstatic.com/files/25591937

Table S2.3: List of up- and downregulated genes of hPDCs obtained from mandible compared to tibial hPDCs.

Available via: https://ndownloader.figstatic.com/files/25591940

Table S2.4: List of up- and downregulated genes of hPDCs obtained from mandible compared to maxillary hPDCs.

Available via: https://ndownloader.figstatic.com/files/25591943

Literature references

Aghaloo TL, Chaichanasakul T, Bezouglaia O, Kang B, Franco R, Dry SM, Atti E, Tetradis S. Osteogenic potential of mandibular vs. long-bone marrow stromal cells. J Dent Res. 2010 Nov;89(11):1293-1298.

Ambrosi TH, Longaker MT, Chan CKF. A revised perspective of skeletal stem cell biology. Front Cell Dev Biol. 2019 Sep 13;7:189.

Anders S, Pyl PT, Huber W. HTSeq--a Python framework to work with high-throughput sequencing data. Bioinformatics. 2015 Jan 15;31(2):166-169.

Arrington ED, Smith WJ, Chambers HG, Bucknell AL, Davino NA. Complications of iliac crest bone graft harvesting. Clin Orthop Relat Res. 1996 Aug;(329):300-309.

Bolander J, Herpelinck T, Chaklader M, Gklava C, Geris L, Luyten FP. Single-cell characterization and metabolic profiling of in vitro cultured human skeletal progenitors with enhanced in vivo bone forming capacity. Stem Cells Transl Med. 2020 Mar;9(3):389-402.

Bolander J, Ji W, Geris L, Bloemen V, Chai YC, Schrooten J, Luyten FP. The combined mechanism of bone morphogenetic protein- and calcium phosphate-induced skeletal tissue formation by human periosteum derived cells. Eur Cell Mater. 2016 Jan 5;31:11-25.

Bolger AM, Lohse M, Usadel B. Trimmomatic: a flexible trimmer for Illumina sequence data. Bioinformatics. 2014 Aug 1;30(15):2114-2120.

Brighton CT, Hunt RM. Early histologic and ultrastructural changes in microvessels of periosteal callus. J Orthop Trauma. 1997 May;11(4):244-253.

Cesario JM, Landin Malt A, Deacon LJ, Sandberg M, Vogt D, Tang Z, Zhao Y, Brown S, Rubenstein JL, Jeong J. Lhx6 and Lhx8 promote palate development through negative regulation of a cell cycle inhibitor gene, p57Kip2. Hum Mol Genet. 2015 Sep 1;24(17):5024-5039.

Chai YC, Roberts SJ, Desmet E, Kerckhofs G, van Gastel N, Geris L, Carmeliet G, Schrooten J, Luyten FP. Mechanisms of ectopic bone formation by human osteoprogenitor cells on CaP biomaterial carriers. Biomaterials. 2012 Apr;33(11):3127-3142.

Chan CKF, Gulati GS, Sinha R, Tompkins JV, Lopez M, Carter AC, Ransom RC, Reinisch A, Wearda T, Murphy M, Brewer RE, Koepke LS, Marecic O, Manjunath A, Seo EY, Leavitt T, Lu WJ, Nguyen A, Conley SD, Salhotra A, Ambrosi TH, Borrelli MR, Siebel T, Chan K, Schallmoser K, Seita J, Sahoo D, Goodnough H, Bishop J, Gardner M, Majeti R, Wan DC, Goodman S, Weissman IL, Chang HY, Longaker MT. Identification of the human skeletal stem cell. Cell. 2018 Sep 20;175(1):43-56.e21.

Choi Y, Ballow DJ, Xin Y, Rajkovic A. Lim homeobox gene, *Lhx8*, is essential for mouse oocyte differentiation and survival. Biol Reprod. 2008 Sep;79(3):442-449.

Colnot C, Zhang X, Knothe Tate ML. Current insights on the regenerative potential of the periosteum: molecular, cellular, and endogenous engineering approaches. J Orthop Res. 2012 Dec;30(12):1869-1878.

Couly GF, Coltey PM, Le Douarin NM. The triple origin of skull in higher vertebrates: a study in quail-chick chimeras. Development. 1993 Feb;117(2):409-429.

De Bari C, Dell'Accio F, Vanlauwe J, Eyckmans J, Khan IM, Archer CW, Jones EA, McGonagle D, Mitsiadis TA, Pitzalis C, Luyten FP. Mesenchymal multipotency of adult human periosteal cells demonstrated by single-cell lineage analysis. Arthritis Rheum. 2006 Apr;54(4):1209-1221.

Dominici M, Le Blanc K, Mueller I, Slaper-Cortenbach I, Marini F, Krause D, Deans R, Keating A, Prockop Dj, Horwitz E. Minimal criteria for defining multipotent mesenchymal stromal cells. The International Society for Cellular Therapy position statement. Cytotherapy. 2006;8(4):315-317.

Duchamp de Lageneste O, Julien A, Abou-Khalil R, Frangi G, Carvalho C, Cagnard N, Cordier C, Conway SJ, Colnot C. Periosteum contains skeletal stem cells with high bone regenerative potential controlled by periostin. Nat Commun. 2018 Feb 22;9(1):773.

Eyckmans J, Luyten FP. Species specificity of ectopic bone formation using periosteum-derived mesenchymal progenitor cells. Tissue Eng. 2006 Aug;12(8):2203-2213.

Flandin P, Zhao Y, Vogt D, Jeong J, Long J, Potter G, Westphal H, Rubenstein JL. Lhx6 and Lhx8 coordinately induce neuronal expression of Shh that controls the generation of interneuron progenitors. Neuron. 2011 Jun 9;70(5):939-950.

Geris L, Papantoniou I. The third era of tissue engineering: reversing the innovation drivers. Tissue Eng Part A. 2019 Jun;25(11-12):821-826.

Giannoni P, Scaglione S, Daga A, Ilengo C, Cilli M, Quarto R. Short-time survival and engraftment of bone marrow stromal cells in an ectopic model of bone regeneration. Tissue Eng Part A. 2010 Feb;16(2):489-499.

Green SA, Simoes-Costa M, Bronner ME. Evolution of vertebrates as viewed from the crest. Nature. 2015 Apr 23;520(7548):474-482.

Guichet JM, Braillon P, Bodenreider O, Lascombes P. Periosteum and bone marrow in bone lengthening: a DEXA quantitative evaluation in rabbits. Acta Orthop Scand. 1998 Oct;69(5):527-531.

Hagberg CE, Falkevall A, Wang X, Larsson E, Huusko J, Nilsson I, van Meeteren LA, Samen E, Lu L, Vanwildemeersch M, Klar J, Genove G, Pietras K, Stone-Elander S, Claesson-Welsh L, Ylä-Herttuala S, Lindahl P, Eriksson U. Vascular endothelial growth factor B controls endothelial fatty acid uptake. Nature. 2010 Apr 8;464(7290):917-921.

Ji W, Kerckhofs G, Geeroms C, Marechal M, Geris L, Luyten FP. Deciphering the combined effect of bone morphogenetic protein 6 and calcium phosphate on bone formation capacity of periosteum derived cells-based tissue engineering constructs. Acta Biomater. 2018 Oct 15;80:97-107.

Jung YK, Kim GW, Park HR, Lee EJ, Choi JY, Beier F, Han SW. Role of interleukin-10 in endochondral bone formation in mice: anabolic effect via the bone morphogenetic protein/Smad pathway. Arthritis Rheum. 2013 Dec;65(12):3153-3164.

Kerckhofs G, Chai YC, Luyten FP, Geris L. Combining microCT-based characterization with empirical modelling as a robust screening approach for the design of optimized CaP-containing scaffolds for progenitor cell-mediated bone formation. Acta Biomater. 2016 Apr 15;35:330-340.

Kerckhofs G, Sainz J, Maréchal M, Wevers M, Van de Putte T, Geris L, Schrooten J. Contrast-Enhanced Nanofocus X-Ray computed tomography allows virtual three-dimensional histopathology and morphometric analysis of osteoarthritis in small animal models. Cartilage. 2014 Jan;5(1):55-65.

Kern S, Eichler H, Stoeve J, Klüter H, Bieback K. Comparative analysis of mesenchymal stem cells from bone marrow, umbilical cord blood, or adipose tissue. Stem Cells. 2006 May;24(5):1294-1301.

Kim D, Langmead B, Salzberg SL. HISAT: a fast spliced aligner with low memory requirements. Nat Methods. 2015 Apr;12(4):357-360.

Lammens J, Maréchal M, Delport H, Geris L, Oppermann H, Vukicevic S, Luyten FP. A cell-based combination product for the repair of large bone defects. Bone. 2020 Sep;138:115511.

Lee JH, Hah YS, Cho HY, Kim JH, Oh SH, Park BW, Kang YH, Choi MJ, Shin JK, Rho GJ, Jeon RH, Lee HC, Kim GC, Kim UK, Kim JR, Lee CI, Byun JH. Human umbilical cord blood-derived CD34-positive endothelial progenitor cells stimulate osteoblastic differentiation of cultured human periosteal-derived osteoblasts. Tissue Eng Part A. 2014 Mar;20(5-6):940-953.

Lee JM, Kim MG, Byun JH, Kim GC, Ro JH, Hwang DS, Choi BB, Park GC, Kim UK. The effect of biomechanical stimulation on osteoblast differentiation of human jaw periosteum-derived stem cells. Maxillofac Plast Reconstr Surg. 2017 Mar 5;39(1):7.

Leijten J, Chai YC, Papantoniou I, Geris L, Schrooten J, Luyten FP. Cell based advanced therapeutic medicinal products for bone repair: Keep it simple? Adv Drug Deliv Rev. 2015 Apr;84:30-44.

Leucht P, Kim JB, Amasha R, James AW, Girod S, Helms JA. Embryonic origin and Hox status determine progenitor cell fate during adult bone regeneration. Development. 2008 Sep;135(17):2845-2854.

Li H, Marijanovic I, Kronenberg MS, Erceg I, Stover ML, Velonis D, Mina M, Heinrich JG, Harris SE, Upholt WB, Kalajzic I, Lichtler AC. Expression and function of Dlx genes in the osteoblast lineage. Dev Biol. 2008 Apr 15;316(2):458-470.

Liatsikos SA, Grimbizis GF, Georgiou I, Papadopoulos N, Lazaros L, Bontis JN, Tarlatzis BC. HOX A10 and HOX A11 mutation scan in congenital malformations of the female genital tract. Reprod Biomed Online. 2010 Jul;21(1):126-132.

Lin X, Yang H, Wang L, Li W, Diao S, Du J, Wang S, Dong R, Li J, Fan Z. AP2a enhanced the osteogenic differentiation of mesenchymal stem cells by inhibiting the formation of YAP/RUNX2 complex and BARX1 transcription. Cell Prolif. 2019 Jan;52(1):e12522.

Lindhe J, Bressan E, Cecchinato D, Corrá E, Toia M, Liljenberg B. Bone tissue in different parts of the edentulous maxilla and mandible. Clin Oral Implants Res. 2013 Apr;24(4):372-377.

Mattioli-Belmonte M, Teti G, Salvatore V, Focaroli S, Orciani M, Dicarlo M, Fini M, Orsini G, Di Primio R, Falconi M. Stem cell origin differently affects bone tissue engineering strategies. Front Physiol. 2015 Sep 24;6:266.

Meijer GJ, de Bruijn JD, Koole R, van Blitterswijk CA. Cell based bone tissue engineering in jaw defects. Biomaterials. 2008 Jul;29(21):3053-3061.

Meulemans D, Bronner-Fraser M. Gene-regulatory interactions in neural crest evolution and development. Dev Cell. 2004 Sep;7(3):291-299.

Mimura S, Suga M, Okada K, Kinehara M, Nikawa H, Furue MK. Bone morphogenetic protein 4 promotes craniofacial neural crest induction from human pluripotent stem cells. Int J Dev Biol. 2016;60(1-3):21-28.

Mosmann T. Rapid colorimetric assay for cellular growth and survival: application to proliferation and cytotoxicity assays. J Immunol Methods. 1983 Dec 16;65(1-2):55-63.

Nakahara H, Goldberg VM, Caplan AI. Culture-expanded human periosteal-derived cells exhibit osteochondral potential in vivo. J Orthop Res. 1991 Jul;9(4):465-476.

Noden DM. 1982. Patterns and organization of craniofacial skeletogenic mesenchyme: a perspective, in Factors and Mechanisms Influencing Bone Growth, eds A. D. Dixon and B. G. Sarnat (New York, NY: Alan R. Liss).

Owston HE, Ganguly P, Tronci G, Russell SJ, Giannoudis PV, Jones EA. Colony formation, migratory, and differentiation characteristics of multipotential stromal cells (MSCs) from "clinically accessible" human periosteum compared to donor-matched bone marrow MSCs. Stem Cells Int. 2019 Nov 21;2019:6074245.

Paine-Saunders S, Viviano BL, Zupicich J, Skarnes WC, Saunders S. glypican-3 controls cellular responses to Bmp4 in limb patterning and skeletal development. Dev Biol. 2000 Sep 1;225(1):179-187.

Park HS, Lee YJ, Jeong SH, Kwon TG. Density of the alveolar and basal bones of the maxilla and the mandible. Am J Orthod Dentofacial Orthop. 2008 Jan;133(1):30-37.

Potier E, Ferreira E, Meunier A, Sedel L, Logeart-Avramoglou D, Petite H. Prolonged hypoxia concomitant with serum deprivation induces massive human mesenchymal stem cell death. Tissue Eng. 2007 Jun;13(6):1325-1331.

Raines AM, Magella B, Adam M, Potter SS. Key pathways regulated by HoxA9,10,11/HoxD9,10,11 during limb development. BMC Dev Biol. 2015 Jul 19;15:28.

Risso D, Schwartz K, Sherlock G, Dudoit S. GC-content normalization for RNA-Seq data. BMC Bioinformatics. 2011 Dec 17;12:480.

Roberts SJ, van Gastel N, Carmeliet G, Luyten FP. Uncovering the periosteum for skeletal regeneration: the stem cell that lies beneath. Bone. 2015 Jan;70:10-18.

Robinson MD, McCarthy DJ, Smyth GK. edgeR: a Bioconductor package for differential expression analysis of digital gene expression data. Bioinformatics. 2010 Jan 1;26(1):139-140.

Sacchetti B, Funari A, Remoli C, Giannicola G, Kogler G, Liedtke S, Cossu G, Serafini M, Sampaolesi M, Tagliafico E, Tenedini E, Saggio I, Robey PG, Riminucci M, Bianco P. No identical "mesenchymal stem cells" at different times and sites: human committed progenitors of distinct origin and differentiation potential are incorporated as adventitial cells in microvessels. Stem Cell Reports. 2016 Jun 14;6(6):897-913.

Salgado AJ, Coutinho OP, Reis RL. Bone tissue engineering: state of the art and future trends. Macromol Biosci. 2004 Aug 9;4(8):743-765.

Takimoto A, Kokubu C, Watanabe H, Sakuma T, Yamamoto T, Kondoh G, Hiraki Y, Shukunami C. Differential transactivation of the upstream aggrecan enhancer regulated by PAX1/9 depends on SOX9-driven transactivation. Sci Rep. 2019 Mar 14;9(1):4605.

Tribulo C, Aybar MJ, Nguyen VH, Mullins MC, Mayor R. Regulation of Msx genes by a Bmp gradient is essential for neural crest specification. Development. 2003 Dec;130(26):6441-6452.

Tsai MS, Hwang SM, Chen KD, Lee YS, Hsu LW, Chang YJ, Wang CN, Peng HH, Chang YL, Chao AS, Chang SD, Lee KD, Wang TH, Wang HS, Soong YK. Functional network analysis of the transcriptomes of mesenchymal stem cells derived from amniotic fluid, amniotic membrane, cord blood, and bone marrow. Stem Cells. 2007 Oct;25(10):2511-2523.

van Gastel N, Torrekens S, Roberts SJ, Moermans K, Schrooten J, Carmeliet P, Luttun A, Luyten FP, Carmeliet G. Engineering vascularized bone: osteogenic and proangiogenic potential of murine periosteal cells. Stem Cells. 2012 Nov;30(11):2460-2471.

van Lochem EG, van der Velden VH, Wind HK, te Marvelde JG, Westerdaal NA, van Dongen JJ. Immunophenotypic differentiation patterns of normal hematopoiesis in human bone marrow: reference patterns for age-related changes and disease-induced shifts. Cytometry B Clin Cytom. 2004 Jul;60(1):1-13.

Villanueva S, Glavic A, Ruiz P, Mayor R. Posteriorization by FGF, Wnt, and retinoic acid is required for neural crest induction. Dev Biol. 2002 Jan 15;241(2):289-301.

Wallin J, Wilting J, Koseki H, Fritsch R, Christ B, Balling R. The role of Pax-1 in axial skeleton development. Development. 1994 May;120(5):1109-1121.

Wang W, Huang D, Ren J, Li R, Feng Z, Guan C, Bao B, Cai B, Ling J, Zhou C. Optogenetic control of mesenchymal cell fate towards precise bone regeneration. Theranostics. 2019 Oct 18;9(26):8196-8205.

Wang X, Zheng P, Huang G, Yang L, Zhou Z. Dipeptidyl peptidase-4(DPP-4) inhibitors: promising new agents for autoimmune diabetes. Clin Exp Med. 2018 Nov;18(4):473-480.

Woo J, Miletich I, Kim BM, Sharpe PT, Shivdasani RA. Barx1-mediated inhibition of Wnt signaling in the mouse thoracic foregut controls tracheo-esophageal septation and epithelial differentiation. PLoS One. 2011;6(7):e22493.

Ylönen R, Kyrönlahti T, Sund M, Ilves M, Lehenkari P, Tuukkanen J, Pihlajaniemi T. Type XIII collagen strongly affects bone formation in transgenic mice. J Bone Miner Res. 2005 Aug;20(8):1381-1393.

Zhou Y, Zhou B, Pache L, Chang M, Khodabakhshi AH, Tanaseichuk O, Benner C, Chanda SK. Metascape provides a biologist-oriented resource for the analysis of systems-level datasets. Nat Commun. 2019 Apr 3;10(1):1523.

Chapter 4

Schneiderian membrane derived cells have bone-forming capacities not superior to other hPDCs

Lisanne Groeneveldt [1,2,3], Samuel Ribeiro Viseu [1,2],
Kathleen Bosmans [1,2], Danny Huylebroeck [3,4], Liesbet Geris [1,2,5,6]

[1] Prometheus, Division of Skeletal Tissue Engineering, KU Leuven, Leuven, Belgium;
[2] Skeletal Biology and Engineering Research Center, KU Leuven, Leuven, Belgium;
[3] Department of Cell Biology, Erasmus University Medical Center, Rotterdam, Netherlands;
[4] Department of Development and Regeneration, KU Leuven, Leuven, Belgium;
[5] Biomechanics Research Unit, GIGA-R In Silico Medicine, Université de Liège, Liège, Belgium;
[6] Biomechanics Section, KU Leuven, Leuven, Belgium

In preparation

4.1. Summary

Bone tissue engineering using skeletal stem and progenitor cells (SSPCs) has a high potential to treat large bone defects. Various sources of SSPCs have already been tested, including those obtained from bone marrow, adipose tissue, dental pulp and periosteum. The Schneiderian membrane has also been proposed as an interesting source of cells with bone-forming capacity. Here, we made a comparison between these cells obtained from the maxillary sinus (hSMs) and more regularly used sources of periosteal cells (hPDCs). hSMs showed proliferative characteristics similar to hPDCs and were able to differentiate chondrogenically *in vitro*. They are all positive for SSPC-markers CD90, CD105 and CD164, and negative for CD146, hematopoietic and endothelial lineage markers. However, hPDCs were CD200-positive, whereas hSMs were negative for this additional marker. Histological analysis of *in vivo* bone formation, 8 weeks after ectopic implantation in nude mice, showed some bone formation by hSMs, but tibial as well as mandibular hPDCs scored better, *i.e.* a higher percentage of constructs seeded with these hPDCs showed bone formation. Therefore, hSMs are indeed an alternative source of hPDCs for use in bone tissue engineering. However the surgical procedure needed to harvest hSMs presents with more donor site morbidity than is the case for regular hPDCs.

4.2. Introduction

Large craniofacial bone defects can result from trauma or congenital abnormalities, but also other important conditions such as infection, tumor resection and osteonecrosis. Collectively, these can result in the loss or removal of large parts of bone, causing large bone defects in the craniofacial skeleton. Currently autografts are considered as the standard therapy for filling such bone defects. Grafts can be taken from the mandible in case the bone defect is limited or, in case of larger defects, from iliac crest, fibula, scapula, calvarium or rib (Elsalanty and Genecov, 2009; Neovius and Engstrand, 2010; Patel *et al.*, 2019;). This is accompanied by donor site morbidity such as pain, scar tissue and a risk of infection (Arrington *et al.*, 1996). Also, the transplanted tissue can be or get infected, often resulting in necrosis due to poor vascularization of the graft or in non-union (Mashrah *et al.,* 2021). Therefore, other treatment options have been tested that use non-living osteo-inductive or conductive implants based on hydroxyapatite or other calcium phosphates, demineralized bone, calcium phosphates, and/or added polypeptide growth/differentiation factors. The latter are usually used in high amounts/concentrations in order to obtain an osteo-inductive effect, but in craniofacial or spine surgery may potentially cause complications, *e.g.*, resulting in ectopic bone formation (Elsalanty and Genecov, 2009; Tannoury and An, 2014; Wang and Yeung, 2017). Also, inert materials such as titanium (with or without growth factor coating) are used, but non-living implants themselves cannot fight against a bacterial infection, which can result in complete loss of the implant.

Bone tissue engineering aims to provide additional options for treating bone defects. The constructs are usually composed of a combination of appropriate, well-characterized progenitor cells with expansion potential in cell culture as well as proven differentiation capacity to bone-forming cells; a biomechanical support or scaffold that provides a 3D environment; and an osteo-conductive capacity often supported by added growth/differentiation factors (Leijten *et al.,* 2015). Skeletal stem/progenitor cells (SSPCs) can meanwhile be obtained from various tissues or body locations. The adipose tissue, bone marrow and periosteum are mostly used, but for craniofacial surgery the Schneiderian membrane could also serve as a suitable source for SSPCs. *In vitro* and *in vivo* work has already shown that the cells from this membrane are able to form bone tissue in

specific circumstances (Srouji *et al.,* 2009). Like the periosteum, the Schneiderian membrane lines the bone tissue, but in this case it does so at the inner side of the maxillary sinus cavity. The Schneiderian membrane is a mucous membrane consisting of the aforementioned bone-facing layer, but also a thin layer of pseudo-stratified columnar, ciliated epithelium with vascularized connective tissue (Srouji *et al.,* 2009). Clinical interventions and experiments in larger animals have learned that the lifting of this sinus membrane, and this without insertion of osteo-conductive or inductive materials, results in the augmentation of the floor of the maxillary sinus (Lundgren *et al.,* 2004; Rong *et al.*, 2015; Zahedpasha *et al.*, 2021). Altogether, these observations prompted us to include Schneiderian membrane cells in our studies and compare them to regular hPDCs. In this study, we focused on the proliferation and differentiation potential of the Schneiderian membrane cells, as well as their bone forming capacity upon in vivo ectopic implantation.

4.3. Results

4.3.1. Primary cells obtained from the inner side of the maxillary sinus can readily be expanded in cell culture

The ability to expand sinus-membrane derived cells in cell culture and the comparison to regular hPDCs obtained from tibia, and also maxilla and mandible was made (see **Chapter 3**). While the proliferation rates of hPDCs during *in vitro* expansion were similar, higher proliferation rates were seen for cells obtained from the Schneiderian membrane (**Fig. 4.1A**). Quantification was documented by staining for incorporated EdU after cellular expansion for 6, 9 and 12 weeks, respectively. About 75% of the cells were EdU-positive (+) after 6 and 9 weeks (**Fig. 4.1B**); a significantly higher proliferation rate for maxillary hPDCs was detected after 6 weeks in comparison to tibial and mandibular hPDCs as reported previously (Groeneveldt *et al.,* 2020), but for sinus membrane cells no higher percentage of EdU+ cells was found (**Fig. 4.1B**). Assessment of cellular metabolic activity using the MTT colorimetric assay revealed no statistically significant differences between sinus membrane cells and each of the hPDCs (**Fig. 4.1C**). After 6, 9 and 12 weeks, staining with X-gal for senescence-associated β-Galactosidase was performed. During the first 9 weeks, the average rates of positively stained cells remained below 5% with a higher percentage for membrane-derived cells at 6 weeks (not statistically significant). After 12 weeks, higher rates were found for the hPDCs, up to 28% for individual samples, while the percentage of senescent cells for sinus membrane-derived cells remained low, though no statistical differences were found between the different cell sources (**Fig. 4.1D**).

From this, we conclude that sinus membrane cells are able to proliferate in cell culture similarly, or even slightly better compared to hPDCs obtained from maxilla, mandible or tibia. Furthermore, from previous work, we expected a yield of about 350 million cells after 50 days of proliferation for the hPDCs, which are numbers that are normally sufficient for subsequent bone tissue engineering applications (Lammens *et al.,* 2020). For sinus membrane derived cells, we can expect even slightly more cells after this period, thus making them suitable candidate cells for tissue engineering purposes.

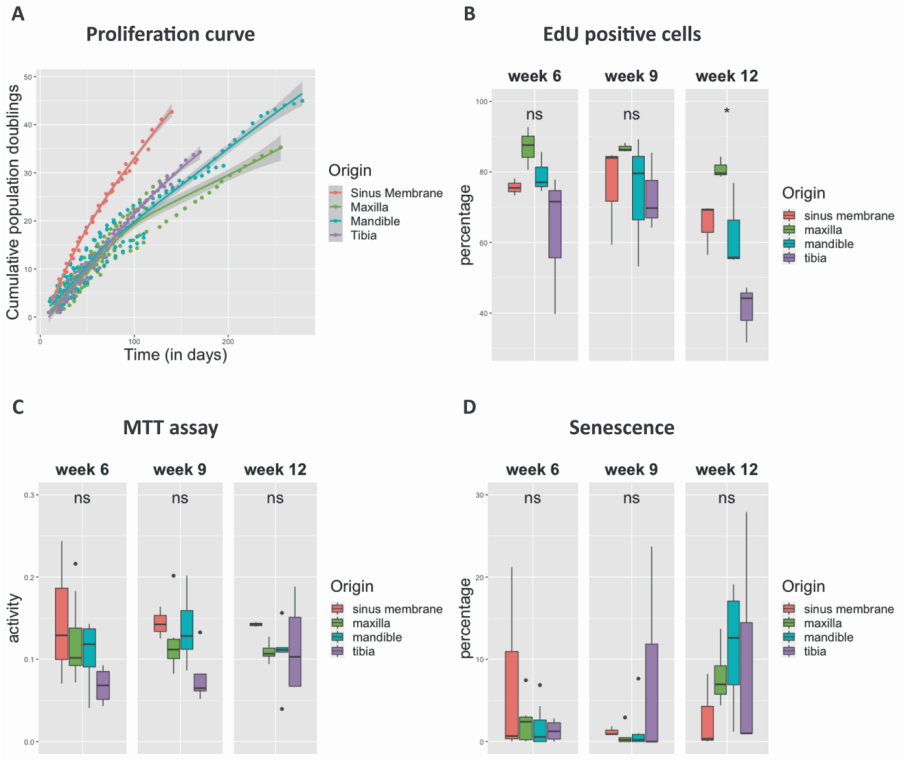

Figure 4.1. Proliferative characteristics of sinus membrane-derived cells in comparison to hPDCs of other origin.

(A) Proliferation curves for cells derived from sinus membrane (in red) and maxillary, mandibular and tibial hPDCs. **(B)** Percentage of Hoechst-positive cells that also stained positive for EdU 72 hours after addition of EdU, as measured after 6, 9 and 12 weeks of cell culture. **(C)** Metabolic activity measured by MTT-assay at weeks 6, 9 and 12 of cell culture. **(D)** Percentage of cells staining positive for b-galactosidase after 6, 9 and 12 weeks of cell cultures. Proliferation curves were compared by a generalized linear model giving $p<0.001$ for sinus membrane cells against the hPDCs. Comparisons for the other assays were made by Kruskal-Wallis test, * $p<0.05$, n=3 in technical triplicates.

4.3.2. Cultured sinus membrane cells can be differentiated towards the chondrogenic and osteogenic lineages

Micromasses were made from the sinus membrane cells, and then cultured for another 7 days in chondrogenic differentiation medium or expansion medium (the latter used as control). Afterwards these micromasses were stained with Alcian Blue (**Fig. 4.2A,B**), which confirmed the capacity of the cells from the Schneiderian membrane, after isolation and then expansion in cell culture, to differentiate towards the chondrogenic lineage, compared to the control setup for which micromasses were cultured in DMEM (**Fig. 4.2B**). As expected, this was also accompanied with upregulation of the chondrogenic gene *COL2A1*, the hypertrophic chondrogenic gene *COL10A1*, and the pre-hypertrophic gene *RUNX2* (**Fig. 4.2G-I).**

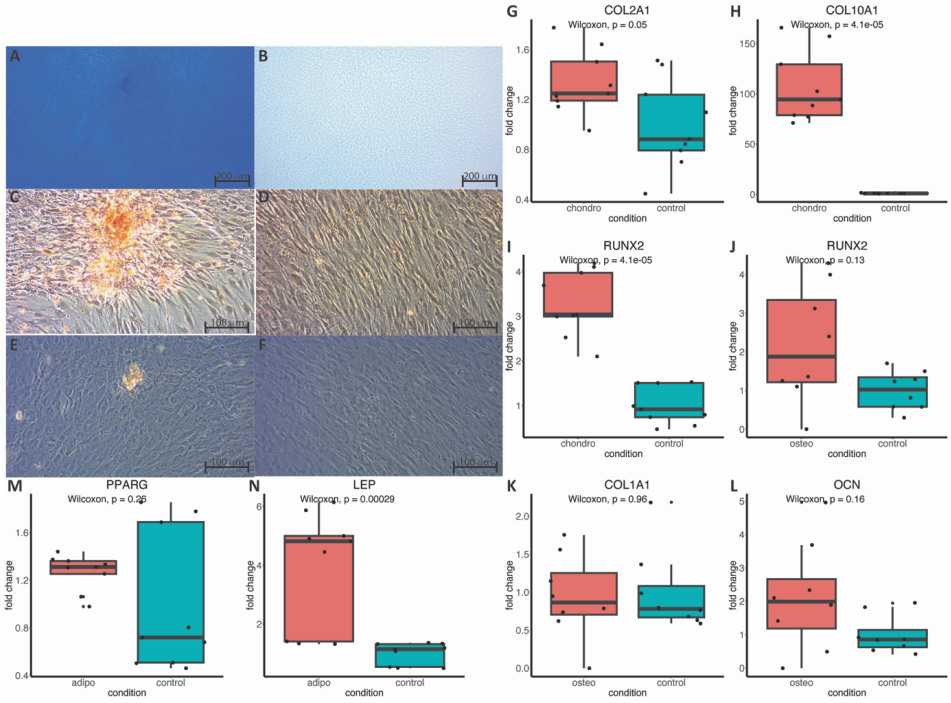

Figure 4.2. Trilineage differentiative capacity of cells obtained from the Schneiderian membrane.

(A,B) Alcian Blue staining of chondrogenic primed sinus membrane-derived cells (panel A) and controls (B), **(C,D)** Alizarin Red staining of osteogenic primed cells (C) and control cells, which remained in expansion medium (D). **(E,F)** Oil Red O staining of adipogenic primed cells (E) and controls (F). **(G-I)** Boxplots of the expression of chondrogenic genes *COL2A1*, *COL10A1* and *RUNX2* in chondrogenic primed cells from the sinus membrane versus controls. **(J-L)** Expression of *RUNX2*, *COL1A1* and *OCN* after osteogenic differentiation for 21 days (in red) or in (control) expansion medium. **(M,N)** Expression of *PPARG* and *LEP* in sinus membrane cells, 14 days primed in adipogenic medium or cultured in (control) expansion medium. N=3 donors with technical triplicates.

The osteogenic differentiation capacity of the cells was also tested, after 21 days of osteogenic priming, by Alizarin Red staining for the calcium phosphate deposition. A few mineral depositions were seen in these osteogenic-primed Schneiderian membrane cells, whereas no mineral deposition was detected in control conditions (**Fig. 4.2C,D**). Comparing osteogenic cultured cells versus control cells, no differences were found in the expression of *RUNX2*, a gene associated with osteoblast formation, or for *COL1A1*, encoding the collagen deposited in bone tissue (**Fig. 4.2J,K**). Also, *OCN*, a gene expressed by more mature osteoblasts, was not upregulated in osteogenic-primed cells derived from the sinus membrane (**Fig. 4.2L**). Staining with Oil Red O revealed limited lipid droplet formation following adipogenic priming (**Figure 4.2E**), while this was not seen in undifferentiated condition (**Fig. 4.2F**). Also, no differences were detected for expression of *PPARG*, a key regulator for adipogenesis, whereas *LEP*, encoding a factor characteristically produced by adipocytes, was up regulated (**Fig. 4.2M,N).**

4.3.3. SSPC-marker analysis in sinus membrane cells

Human SSPCs display specific surface markers (see below) but should neither contain *CD146* (an endothelial cell marker) nor one of the hematopoietic markers CD31, CD45 or CD235ab. FACS confirmed that the cells isolated from the sinus membrane (as well as regular periosteum) do not express any of these 4 markers (**Fig. 4.3A-D).** Markers that positively associate with SSPCs are CD73, CD164 and PDPN (Chan *et al.,* 2018), while CD90 (also named as THY1) and CD105 are known as markers for SSPCs, albeit in mice (**Fig. 4.3E-H;** Chan *et al.,* 2009). CD200 was previously also proposed as a PSC marker (Debnath *et al.,* 2018). FACS showed that the cells from our various sources are positive for CD90, CD164 and CD105 (**Fig. 4.3E-H)**. However, sinus membrane cells have no detectable CD200 on their cell surface, while the hPDCs did (**Fig. 4.3I-L**).

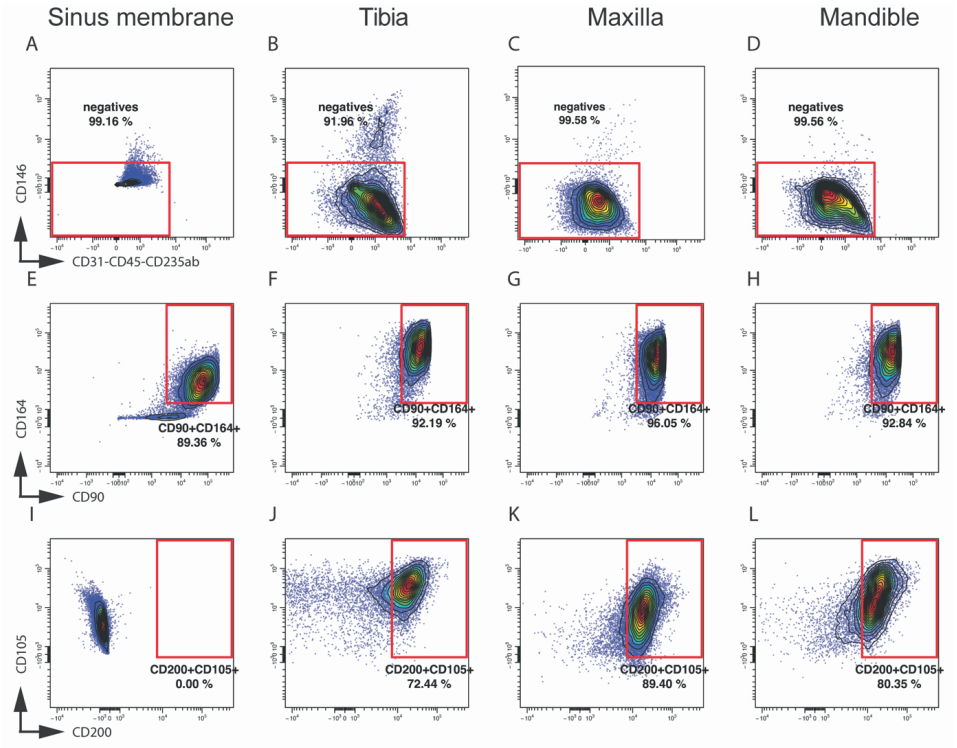

Figure 4.3. Flow-cytometric analysis of markers expressed by sinus membrane cells and other hPDCs.

Flow-cytometric analysis of cells derived from the sinus membrane **(A,E,I)** and hPDCs obtained from tibia **(B,F,J),** maxilla **(C,G,K)** and mandible **(D,H,L)**. Gating was done using FMOs for each channel: (in panels A-D) CD146 versus CD31-CD45-CD235ab, (E-H) negatives gating from previous parent gate plotted as CD164 versus CD90; (I-L) daughter gate from previous gating strategy, showing CD105 versus CD200. Experiments were performed on 3 donors per origin, and representative samples are shown.

4.3.4. *In vivo* bone formation

In order to assess the capacity of sinus membrane derived cells to form bone tissue *in vivo* and compare this to regular hPDCs, the cells were seeded on NuOss scaffolds, ectopically implanted in nude mice and 8 weeks post-implantation analyzed by Nano-CT analysis and histology. As reported previously (Groeneveldt *et al.,* 2020), mandibular and tibial-derived hPDCs showed bone formation, whereas this was not the case for constructs with maxillary-derived hPDCs. Importantly, only a limited volume of bone formation was obtained with constructs seeded with cells obtained from the Schneiderian membrane (**Fig. 4.4A-D**). Nano-CT showed bone tissue formation in 4 out of 12 constructs, with a limited mean of 0.49% of the total construct volume being mineralized (**Fig. 4.4**, inserted table), whereas mandibular hPDCs showed mineralized tissues in half of the constructs, and tibial hPDCs even in 8 out of 13 (**Fig. 4.4.**, inserted table). Similar results were observed in histology using haematoxylin and eosin staining, Alcian Blue staining, and Masson's Trichrome staining.

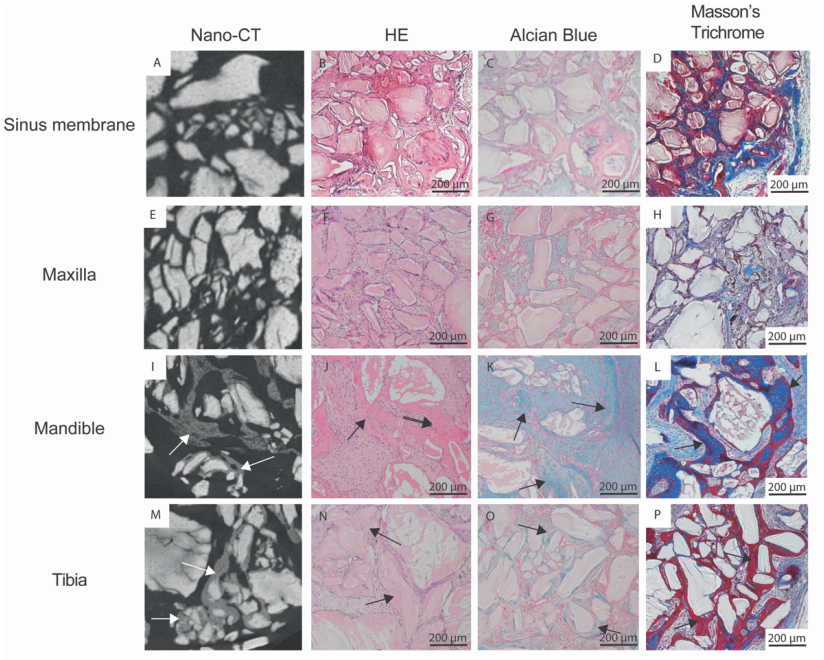

Q

Source	Success	Mean mineralized %	SD
Sinus membrane	4 out of 12 constructs	0,49%	0,51%
Maxilla	0 out of 7 constructs	-	-
Mandible	6 out of 12 constructs	1,10%	1,44%
Tibia	8 out of 13 constructs	1,72%	1,14%

Figure 4.4. Bone formation *in vivo* by hPDCs of various origin (Groeneveldt *et al.,* 2020) and by cells derived from the sinus membrane.

Shown is Nano-CT imaging of scaffolds seeded with hPDCs and cells obtained from the sinus membrane harvested 8 weeks after ectopic implantation with scaffold grains in light gray and mineralized tissue in dark gray **(A, E, I, M)**. Histological imaging of those cell constructs stained with Hematoxylin/Eosin **(B,F,J,N)**, Alcian Blue **(C,G,K,O),** and Masson's Trichrome **(D,H,L,P)** with arrows pointing at bone tissue**.** Volumetric percentage of mineralized tissue in each cell construct **(Q).** N=3 donors and 4 replicates per condition, representative samples are shown.

4.4. Discussion

For the treatment of large bone defects, bone tissue engineering is investigated as a possible treatment strategy (Leijten *et al.,* 2015; see also **Chapter 1**). Bone-lining cells such as hPDCs have been proposed as ideal candidate cells because they are involved in fracture repair *in vivo* (Duchamp de Lageneste *et al.,* 2018), are able to proliferate in cell culture, express SSPC-marker genes, and have the capacity to form bone tissue *in vivo* (Roberts *et al.,* 2015; Nilsson Hall *et al.,* 2019; Groeneveldt *et al.,* 2020). Since the Schneiderian membrane is also a bone-lining tissue, cells from this membrane may serve as a cell source for bone tissue engineering purposes, since lifting of this membrane can result in augmentation of the underlying bone tissue (Lundgren *et al.,* 2004; Rong *et al.,* 2015).

We were able to isolate cells from the Schneiderian membrane using collagenase digestion and to subsequently culture them. The cells were proliferating with similar proliferation rates, metabolic activity and senescence rate compared to regular hPDCs investigated earlier (Groeneveldt *et al.,* 2020). Moreover, those cells are able to differentiate towards the chondrogenic lineage in cell culture, as confirmed by both Alcian Blue staining and *COL2A1* expression, encoding the alpha-1 chain of collagen type-2, which is present in cartilage. Furthermore *RUNX2*, expressed by pre-hypertrophic chondrocytes and *COL10A1*, encoding for collagen type-10 found in hypertrophic cartilage were also up regulated in chondrogenically-primed cells, showing their potential for endochondral ossification (EO). One of the strategies more recently gaining traction in the bone tissue engineering field, is the developmentally inspired approach. Continuing on this approach, our goal is to form bone tissue by EO (Papantoniou et al., 2021), since chondrocytes can thrive well in hypoxic environments and they attract blood vessels during the EO process (Colnot and Helms, 2001). This has the additional benefit that the construct does not necessarily have to be already vascularized prior to implantation. Osteogenic as well as adipogenic differentiation were not very convincing with the Schneiderian membrane cells. However, because the goal of our tissue construct is to form bone tissue by EO, which makes the chances for survival of the construct higher, these two differentiation deficits do not make these cells less suitable.

The membrane derived cells show a marker profile that is known and acknowledged for SSPCs, since they are CD90+, CD105+ and CD164+ (Chan *et al.*, 2018), and negative for CD31, CD45, CD235ab and CD146. These negative markers are otherwise known as hematopoietic lineage markers, present in cells that already differentiated further and hence lost stem cell identity (Van Lochem *et al.,* 2004). However, a difference was found between hPDCs and sinus membrane derived cells for CD200; hPDCs do display this surface marker, while sinus membrane cells were CD200-negative. CD200 has not been included in the list of human SSPC markers, but it was in the list of markers for murine SSPCs (Chan *et al.,* 2015) and in another list of markers for periosteal derived stem cells (Debnath *et al.,* 2018).

The most important result of our study is to take the initial steps to investigate the capacity of sinus membrane derived cells, after their expansion in cell culture, to form bone tissue *in vivo*. This was assessed stringently, *i.e.* by ectopic implantation of NuOss scaffolds seeded with those cells in nude mice. For this purpose, we also included comparisons with NuOss constructs seeded with regular hPDCs obtained from tibia, maxilla and mandible, respectively (Groeneveldt *et al.,* 2020). Eight weeks after cell-scaffold implantation, bone tissue was present in 33% of the implanted constructs for the Schneiderian membrane derived cells, while for mandibular and tibial hPDCs this was 50% and 61.5%, respectively. Furthermore, the mineralized volume (as detected by Nano-CT) was smaller in constructs seeded with sinus membrane derived cells compared to tibial and mandibular hPDCs. It cannot, however, be excluded that the biomaterial

used for the constructs, the addition of growth/differentiation factors, and the actions of local environmental cues, can be responsible for the detected differences (Leucht *et al.,* 2008; Ji *et al.,* 2018).

Taken together, although primary sinus membrane cells can be expanded well in cell culture and can then form bone tissue *in vivo*, this preliminary study leads us to prefer hPDCs , in particular because we obtained more bone tissue *in vivo* for tibial and, importantly for craniofacial applications, mandibular hPDCs. For these cells, bone tissue formation occurred in a higher percentage of the implanted constructs. Furthermore, the surgical procedure to obtain sinus membrane derived cells is in our experience and opinion more complex, and has also been reported to go along with more donor site morbidity than the alternative collection of cells of the mandibular periosteum (Matheny and Duncavage, 2003; Humphreys and Hwang, 2015). In order to improve the bone forming potential of cells obtained from the Schneiderian membrane, the addition of growth/differentiation factors, the biomaterial used for the tissue construct, and the local environmental cues, should be studied (Leucht *et al.,* 2008; Ji *et al.,* 2018). The effects of cellular priming with BMPs prior to implantation have already been studied on tibial-derived hPDCs, as well as the priming with different doses of calcium and the effects of different calcium phosphate scaffolds (Chai *et al.,* 2012; Bolander *et al.,* 2016; Kerckhofs *et al.,* 2016). The effects of scaffold features such as the bio-compatibility, porosity, pore size, surface properties, osteo-inductivity and mechanical properties are also being studied intensively to improve the bone-forming capacity of different types of SSPCs (Salgado *et al.,* 2004; Mattioli-Belmonte *et al.,* 2015; Kim *et al.,* 2017; Wan *et al.,* 2020; Guo *et al.,* 2021). However, since we tested the constructs seeded with sinus membrane derived cells and those with the respective hPDCs from various origins, and this using the same expansion protocol in cell culture and the same type of scaffolds scaffolds without priming with growth/differentiation factors, we conclude that sinus membrane derived SSPCs do not show an overtly higher bone-forming potential than hPDCs.

4.5. Experimental procedures

Isolation and culture of hPDCs

Periosteal samples (5-10 mm) were obtained from the posterior areas of the maxilla and mandible of 16- to 30-year-old healthy female and male patients who underwent bimaxillary orthognathic surgery, after informed consent was obtained (Belgian registration number B322201731127). The tibial samples were harvested by orthopedic surgeons as described previously from 16- to 30-year-old female and male patients undergoing total knee replacement or distraction osteogenesis (Eyckmans and Luyten, 2006). Samples from the Schneiderian membrane were obtained during Le Fort 1 surgery on 16- to 30-year-old healthy patients after informed consent was obtained (Belgian registration number B322201942010).

These samples were digested in medium consisting of Dulbecco's modified Eagle's medium (DMEM) supplemented with 10% Fetal Bovine Serum (FBS; Thermo Fisher Scientific, Waltham, MA, United States) and 1% antibiotics-antimycotics solution (100 units penicillin/ml, 100 µg streptomycin/ml and 0.25 µg amphotericin-B/ml; Invitrogen), from here on referred to as DMEM-complete (DMEM-C), in addition of 4,400 units per 10 ml Collagenase type-IV (Gibco) under constant agitation for 16 h. Cells were from then on cultured in DMEM-C. Population doublings (PD) of these human PDCs (hPDCs) were calculated upon passaging using the formula $\log_2(n_2)-\log_2(n_1)$, with n_1 representing the number of cells seeded in the dish/flask and n_2 the number of cells obtained after trypsinization (TrypLE, Thermo Fisher Scientific) of cells from the same dish/flask at 90% confluency.

Cellular Senescence

For detection of senescent cells, 10^5 cells were plated per well in a 6-well plate in DMEM-C. After one day, the cells were fixed using 4% paraformaldehyde (PFA) for 5 min, rinsed using PBS and stained with 2 ml/well filtered (0.22 µm; Millex-GP) staining solution consisting of 36 mM citric acid, pH 6.0 (Sigma

Aldrich), 4.5 mM potassium ferricyanide (Merck), 0.14 M NaCl, 1.8 mM $MgCl_2$ (Merck) and 1 mg X-gal/ml (Biotium). After 6 h, the cells were imaged using a Primovert inverted microscope (Zeiss).

Cell Proliferation

For detection of proliferating cells, staining for incorporated EdU was performed using the Click-iT™ EdU Alexa Fluor™ 555 Imaging Kit (Thermo Fisher Scientific) according to the manufacturer's protocol. In short, 10^5 cells/well were seeded in a 6-well plate in DMEM-C. The following day, medium was replaced with DMEM-C containing 10 µM EdU, followed by an incubation of 72 h. Next, cells were fixated using 3,7% formaldehyde in PBS (VWR) for 15 min, rinsed twice with 3% bovine serum albumin (BSA, Sigma Aldrich) in PBS and lysed with 0.5% Triton X-100 in PBS (Sigma Aldrich) for 20 min. This was followed by adding the Click-iT reaction cocktail for 30 min in absence of light, quick washing steps of 1 min using subsequently 3% BSA dissolved in PBS and later on in PBS, addition of the Hoechst solution for 30 min in a 1:2,000 dilution in PBS and final washing steps using PBS for 1 min.

Cell Metabolism

Cell metabolic activity was measured by using 3-(4,5-dimethylthiazol-2-yl)-2,5-diphenyltetrazolium bromide (MTT) assay. Living cells contain the mitochondrial reductase enzyme, which reduces MTT toward formazan forming salt crystals. By measuring the amount of reduction of MTT toward formazan, the cell metabolic activity was measured. This was done by removing remaining MTT and solubilizing of the salt crystals in order to get with the different quantities of salt crystals corresponding differences in color intensity (Mosmann *et al.*, 1983). Tests were performed as technical replicates 6 times per donor at 6, 9, and 12 weeks of culture. 10,000 cells were seeded in a 24-well plate in 0.5 ml DMEM-C. After 1 day, DMEM-C was replaced with DMEM containing 250 µg MTT/ml (Sigma Aldrich). After 4 h, medium and remaining MTT were removed and 1 ml absolute ethanol was added to each well in order to solubilize the salt crystals. These solutions were transferred to a 96-well plate and absorbance was read at 570 and 670 nm with a Synergy HT reader (BioTek). In order to calculate the metabolic rate, the background absorbance (at 670 nm) was subtracted from the absorbance at 570 nm and corrected for the blank values which were obtained by performing all steps on wells containing no cells.

Flow Cytometry

10^6 cells were at passage 6 washed in 500 µl PBS + 1% FBS and incubated at the following dilutions with anti-CD90-APC (1:250), anti-CD164-PE (1:250), anti-CD45-FITC (1:1,000), anti-CD31-FITC (1:1,000), anti-CD235ab-FITC (1:1,000; all from BioLegend), anti-CD146-BV711 (1:250), anti-CD73-BV395 (1:250) and anti-PDPN-BV510 (1:100; all from BD Bioscience) in 200 µl PBS + 1% FBS for 15 min in a dark area. The cells were then washed twice with 1% FBS in PBS. Gating was performed using Fluorescence-Minus-One (FMO) controls. Fluorescence measurement was performed on a FACS Calibur (BD Biosciences) using 100,000 events.

Differentiation of hPDCs

Human periosteum-derived cells and cells obtained from the Schneiderian membrane were primed for adipogenic, osteogenic and chondrogenic differentiation for 14, 21, and 7 days, respectively. Analysis was performed by staining with Oil Red O, Alizarin Red and Alcian Blue, respectively.

For adipogenic differentiation of hPDCs, cells were cultured in 24-well plates at a density of 19,000 cells/well in 0.5 ml DMEM-C. After 2 days, the medium was changed for adipogenic differentiation medium, i.e., Minimum Essential Medium Eagle - alpha modification (α-MEM; Invitrogen supplemented with 10% FBS, 1% antibiotics-antimycotics solution, 1 µM dexamethasone + 10 µg human insulin/ml (Sigma Aldrich), 100 µM indomethacin (Sigma Aldrich) and 25 µM 3-isobutyl-1-methylxanthine (Sigma Aldrich). The cells were cultured in a humidified atmosphere at 5% CO2 and 37°C for 14 days and medium was replaced every 2 days. Lipid droplets were stained by Oil Red O. Cells in monolayer were washed in PBS and fixed for 30 min at room temperature in 10% formaldehyde (VWR) diluted in PBS. Next, cells were washed with Milli-Q water and rinsed in 60% isopropanol (VWR) diluted in Milli-Q water. Cells were allowed to dry completely and then stained with 0.2% Oil Red O (Sigma Aldrich) in Milli-Q water for 60 min. These cells were then washed with Milli-Q water before obtaining pictures using the Primovert microscope (Zeiss).

For osteogenic differentiation of hPDCs, cells were cultured in 24-well plates at a density of 8,550 cells per well in 0.5 ml DMEM-C, first allowing them to proliferate. After 1 day, medium was then changed for osteogenic medium consisting of DMEM-C supplied with 100 nM dexamethasone (Sigma Aldrich), 10 mM β-glycerophosphate disodium salt hydrate (Sigma Aldrich) and 50 µg L-ascorbic acid 2-phosphate/ml (Sigma Aldrich). Cells were cultured in a humidified atmosphere at 5% CO_2 and 37°C for 21 days, during

which this medium was replaced every 3 days. Cells in monolayer were washed in PBS, fixed with methanol at −20°C (Fisher Scientific), stored for 1 h at 4°C, and washed again with PBS. Cells were stained for 1 h with a 2% Alizarin-S stain (Sigma Aldrich) in Milli-Q water with pH adjusted to 4.2 (Merck) while the plate was placed on a shaker for constant agitation. After staining, cells were washed with Milli-Q water. Pictures were made using a Discovery.v8 SteREO microscope (Zeiss).

For chondrogenic differentiation of hPDCs, the cells were cultured in micromasses. Micromasses containing 200,000 cells in 10 µl DMEM-C after centrifugation at 260 RCF for 10 min were added to individual wells of 24-well plates. After 2 h, an extra 0.5 ml of DMEM-C was added to each well. After 1 day, this medium was replaced by chondrogenic inductive medium (DMEM-F12 (Invitrogen) containing 2% FBS, antibiotics-antimycotics solution, 1x ITS + premix universal culture supplement (Corning), 100 nM dexamethasone, 10 µM Y27632 (Axon Medchem), 50 µg L-ascorbic acid 2-phosphate /ml, 40 µg proline/ml (Sigma Aldrich) and 10 ng transforming growth factor-β1/ml (TGFβ1; PeproTech). These cells were cultured under humidified conditions at 37°C and 5% CO_2 for 7 days; medium was replaced every 2 days. Sulfated glycosaminoglycans in the micromasses were stained by Alcian Blue (Roth). The cells were rinsed with PBS and fixed with excess ice-cold methanol for 1 h at 4°C. This methanol was removed and cells were rinsed with Milli-Q water prior to adding 0.1% Alcian Blue staining solution (in 0.1 M HCl at pH 2.4) for 1 h on a shaker. Alcian Blue stain was removed and the cells were rinsed with Milli-Q water before pictures were made using the Discovery.v8 SteREO microscope (Zeiss). Micromasses were also obtained for confirmation of chondrogenic differentiation by RT-qPCR. Micromasses were individually lysed in 350 µl RLT buffer (Qiagen) containing 1% β-mercaptoethanol (Sigma Aldrich) and homogenized by thoroughly pipetting up and down. Samples were directly placed on ice and frozen at −80°C until further processing.

RNA Isolation, cDNA Synthesis and Quantitative PCR

RNA was isolated from biological duplicates when a cumulative PD~10 was reached for RT-qPCR and at PD~16 for RNA-seq analysis. 10^6 cells were rinsed twice in PBS and centrifuged at 260 RCF for 10 min. After removing the supernatant, the cell pellet was lysed by adding 350 µl RLT buffer (Qiagen) containing 1% β-mercaptoethanol (Sigma Aldrich) and homogenized by thoroughly pipetting up and down. Samples were directly placed on ice and frozen at −80°C until further processing. The Qiagen RNeasy mini kit was used to isolate RNA according to the manufacturer's instructions. cDNA was obtained by reverse transcription of 500 ng of total RNA, using the PrimeScript™ RT Reagent Kit (Perfect Real Time; Takara Bio)

RT-qPCR was performed on expanded cells with stimulation for chondrogenic differentiated cells for RNA encoding collagen type 2 (*COL2A1*), collagen type 10 (*Col10A1)* and Runt-related transcription factor 2 (*RUNX2*). On osteogenically differentiated cells, the expression of RUNX2, collagen type 1 (*COL1A1*) and bone gamma-carboxyglutamate protein (BGLAP) were measured. For adipogenic primed cells, the expression of peroxisome proliferator activated receptor gamma (*PPARG*) and leptin (*LEP*) were defined and relative differences in expression were calculated using the $2^{-\Delta\Delta Ct}$ method normalized to the housekeeping gene Hypoxanthine Phosphoribosyltransferase 1 (*HPRT*).

Samples were processed and measured in technical duplicates on a on Rotor Gene® 6000 PCR machine (Qiagen) using a Sybr Green detection system (Takara Bio) according to the manufacturer's instructions. The respective primer sequences are listed in **Table S4.1**.

***In vivo* bone formation**

After proliferation, 10^6 cells suspended in 25 µl of DMEM-C were seeded on NuOss scaffolds (21 mm^3; ACEuropa). One hour after seeding, an additional 5 ml of DMEM-C was added. After overnight incubation at 37°C and 5% CO2, scaffolds were randomly implanted subcutaneously over the available mice in triplicates with a maximum of 4 for each mouse at the shoulder and the back in the limb region of 8-week-old female NMRI$^{nu/nu}$ mice (Janvier). All animal procedures were approved by the local ethical committee for Animal Research (KU Leuven, P037-2020). The animals were housed according to the guidelines of the Animal Facilities at Leuven (KU Leuven). Explants were harvested after 8 weeks.

Bone formation was analyzed using the Phoenix NanoTom S CT system (GE measurement) at a voltage of 60 kV and a current of 200 mA. An aluminum filter of 1 mm was used to filter out the low energetic radiation. CTAn and Batch Manager Software programs (Bruker micro-CT, Kontich, Belgium) were used for 3D quantification of the bone volume and calcium phosphate (CaP) grains of the NuOss scaffold. A three-level automatic Otsu segmentation algorithm was used to segment the newly formed bone tissue and CaP-grains from the background in combination with manually chosen thresholds. Noise was reduced by removing black and white speckles smaller than 200 voxels and a closing operation of 2 voxels was performed to solidify the resulting structure, providing binarized images suitable for the 3D analysis. Percentage of bone was calculated with respect to total explant volume (Kerckhofs *et al.,* 2013). After decalcification in EDTA,

dehydration through a series of graded ethanol baths, embedding in paraffin and sectioning, histological stainings were performed.

Staining with hematoxylin and eosin (H&E) was done by a dip in Hematoxylin-solution for 2 min, followed by a wash in H_2O and subsequently a staining in 1% Eosin (Klinipath, Duiven, Netherlands) for 7 min (Bolander *et al.,* 2016). For Alcian Blue staining, samples were rehydrated, stained for 30 min in 0.5% Alcian Blue (Roth) solution in 1 M HCl (pH = 1). Nuclear Fast Red (Vector) was used for staining of the nuclei during 5 min. For staining with Safranin O, samples were dipped in acidic alcohol (1% HCl in 70% ethanol). Next, they were placed in Fast Green (Klinipath) for 3 min, dipped in 1% acetic acid and then stained in 0.1% Safranin O (Sigma Aldrich) for 10 min. Masson's trichrome staining was performed using Bouin's solution (Sigma Aldrich) as mordant followed by 5-minute-dips in Weigert's Iron Hematocxylin Solution, Biebrich Scarlet-Acid Fuchsin, Phosphotungstic/Phosphomolybdic Acid Solution and Aniline Blue Solution (all from Sigma Aldrich), followed by a dip in 1% acetic acid for 2 min. The sections were cleared in HistoClear (National-Diagnostics) and mounted in Pertex (Histolab). Pictures were made using the IX83 microscope (Olympus).

Statistical analysis

Statistical analysis for cellular senescence, quantitative PCR and in vivo bone formation was performed using the Kruskal-Wallis test. The proliferation curve was tested for statistical significant differences by a generalized linear model. In case $p < 0.05$ for Kruskal-Wallis, a two-sided Wilcoxon test was performed to make comparisons for the qPCR validation of the RNA-seq data and to analyze cellular senescence, proliferation and metabolism rate. Student's t-test was used to make comparisons for the chondrogenically differentiated micromasses. The Bonferroni correction was used to correct for multiple testing. All statistical analyses were performed in R (version 3.6.0). Results were considered statistically significant at $p < 0.05$. Data are presented as mean values ± standard deviation (SD) or 95% confidence interval (CI) when stated.

Supplementary table

Table S4.1: Primer sequences used for RT-qPCR.

Gene	Forward	Reverse
BGLAP	GTGCAGCCTTTGTGTCCAA	GCTCACACACCTCCCTCCT
COL1A1	GACGAAGACATCCCACCAAT	AGATCACGTCATCGCACAAC
COL2A1	GGCTTCCATTTCAGCTATGG	AGCTGCTTCGTCCAGATAGG
COL10A1	ACGATACCAAATGCCCACAG	GTGGACCAGGAGTACCTTGC
HPRT	TGAGGATTTGGAAAGGGTGT	GAGCACACAGAGGGCTACAA
LEP	ATGACATTTCACACACGCAGT	GTAGACTGCCAGTGTCTGGTC
PPARG	GCCAAGCTGCTCCAGAAAAT	TGATCACCTGCAGTAGCTGCA
RUNX2	CGCATTCCTCATCCCAGTAT	GCCTGGGGTCTGTAATCTGA

Literature references

Arrington ED, Smith WJ, Chambers HG, Bucknell AL, Davino NA. Complications of iliac crest bone graft harvesting. Clin Orthop Relat Res. 1996 Aug;(329):300-309.

Bolander J, Herpelinck T, Chaklader M, Gklava C, Geris L, Luyten FP. Single-cell characterization and metabolic profiling of in vitro cultured human skeletal progenitors with enhanced in vivo bone forming capacity. Stem Cells Transl Med. 2020 Mar;9(3):389-402.

Chai YC, Roberts SJ, Desmet E, Kerckhofs G, van Gastel N, Geris L, Carmeliet G, Schrooten J, Luyten FP. Mechanisms of ectopic bone formation by human osteoprogenitor cells on CaP biomaterial carriers. Biomaterials. 2012 Apr;33(11):3127-3142.

Chan CK, Seo EY, Chen JY, Lo D, McArdle A, Sinha R, Tevlin R, Seita J, Vincent-Tompkins J, Wearda T, Lu WJ, Senarath-Yapa K, Chung MT, Marecic O, Tran M, Yan KS, Upton R, Walmsley GG, Lee AS, Sahoo D, Kuo CJ, Weissman IL, Longaker MT. Identification and specification of the mouse skeletal stem cell. Cell. 2015 Jan 15;160(1-2):285-298.

Chan CKF, Gulati GS, Sinha R, Tompkins JV, Lopez M, Carter AC, Ransom RC, Reinisch A, Wearda T, Murphy M, Brewer RE, Koepke LS, Marecic O, Manjunath A, Seo EY, Leavitt T, Lu WJ, Nguyen A, Conley SD, Salhotra A, Ambrosi TH, Borrelli MR, Siebel T, Chan K, Schallmoser K, Seita J, Sahoo D, Goodnough H, Bishop J, Gardner M, Majeti R, Wan DC, Goodman S, Weissman IL, Chang HY, Longaker MT. Identification of the human skeletal stem cell. Cell. 2018 Sep 20;175(1):43-56.e21.

Colnot CI, Helms JA. A molecular analysis of matrix remodeling and angiogenesis during long bone development. Mech Dev. 2001 Feb;100(2):245-250.

Debnath S, Yallowitz AR, McCormick J, Lalani S, Zhang T, Xu R, Li N, Liu Y, Yang YS, Eiseman M, Shim JH, Hameed M, Healey JH, Bostrom MP, Landau DA, Greenblatt MB. Discovery of a periosteal stem cell mediating intramembranous bone formation. Nature. 2018 Oct;562(7725):133-139.

Duchamp de Lageneste O, Julien A, Abou-Khalil R, Frangi G, Carvalho C, Cagnard N, Cordier C, Conway SJ, Colnot C. Periosteum contains skeletal stem cells with high bone regenerative potential controlled by Periostin. Nat Commun. 2018 Feb 22;9(1):773.

Elsalanty ME, Genecov DG. Bone grafts in craniofacial surgery. Craniomaxillofac Trauma Reconstr. 2009 Oct;2(3):125-134.

Groeneveldt LC, Herpelinck T, Maréchal M, Politis C, van IJcken WFJ, Huylebroeck D, Geris L, Mulugeta E, Luyten FP. The bone-forming properties of periosteum-derived cells differ between harvest sites. Front Cell Dev Biol. 2020 Nov 25;8:554984.

Guo L, Liang Z, Yang L, Du W, Yu T, Tang H, Li C, Qiu H. The role of natural polymers in bone tissue engineering. J Control Release. 2021 Oct 10;338:571-582.

Humphreys IM, Hwang PH. Avoiding Complications in endoscopic sinus surgery. Otolaryngol Clin North Am. 2015 Oct;48(5):871-881.

Ji W, Kerckhofs G, Geeroms C, Marechal M, Geris L, Luyten FP. Deciphering the combined effect of bone morphogenetic protein 6 and calcium phosphate on bone formation capacity of periosteum derived cells-based tissue engineering constructs. Acta Biomater. 2018 Oct 15;80:97-107.

Kerckhofs G, Chai YC, Luyten FP, Geris L. Combining microCT-based characterization with empirical modelling as a robust screening approach for the design of optimized CaP-containing scaffolds for progenitor cell-mediated bone formation. Acta Biomater. 2016 Apr 15;35:330-340.

Kim HD, Amirthalingam S, Kim SL, Lee SS, Rangasamy J, Hwang NS. Biomimetic materials and fabrication approaches for bone tissue engineering. Adv Healthc Mater. 2017 Dec;6(23).

Lammens J, Maréchal M, Delport H, Geris L, Oppermann H, Vukicevic S, Luyten FP. A cell-based combination product for the repair of large bone defects. Bone. 2020 Sep;138:115511.

Leijten J, Chai YC, Papantoniou I, Geris L, Schrooten J, Luyten FP. Cell based advanced therapeutic medicinal products for bone repair: Keep it simple? Adv Drug Deliv Rev. 2015 Apr;84:30-44.

Leucht P, Kim JB, Amasha R, James AW, Girod S, Helms JA. Embryonic origin and Hox status determine progenitor cell fate during adult bone regeneration. Development. 2008 Sep;135(17):2845-2854.

Lundgren S, Andersson S, Gualini F, Sennerby L. Bone reformation with sinus membrane elevation: a new surgical technique for maxillary sinus floor augmentation. Clin Implant Dent Relat Res. 2004;6(3):165-173.

Mashrah MA, Aldhohrah T, Abdelrehem A, Sakran KA, Ahmad H, Mahran H, Abu-Lohom F, Su H, Fang Y, Wang L. Survival of vascularized osseous flaps in mandibular reconstruction: A network meta-analysis. PLoS One. 2021 Oct 22;16(10):e0257457.

Matheny KE, Duncavage JA. Contemporary indications for the Caldwell-Luc procedure. Curr Opin Otolaryngol Head Neck Surg. 2003 Feb;11(1):23-26.

Mattioli-Belmonte M, Teti G, Salvatore V, Focaroli S, Orciani M, Dicarlo M, Fini M, Orsini G, Di Primio R, Falconi M. Stem cell origin differently affects bone tissue engineering strategies. Front Physiol. 2015 Sep 24;6:266.

Neovius E, Engstrand T. Craniofacial reconstruction with bone and biomaterials: review over the last 11 years. J Plast Reconstr Aesthet Surg. 2010 Oct;63(10):1615-1623.

Nilsson Hall G, Mendes LF, Gklava C, Geris L, Luyten FP, Papantoniou I. Developmentally engineered callus organoid bioassemblies exhibit predictive in vivo long bone healing. Adv Sci (Weinh). 2019 Dec 10;7(2):1902295.

Papantoniou I, Nilsson Hall G, Loverdou N, Lesage R, Herpelinck T, Mendes L, Geris L. Turning Nature's own processes into design strategies for living bone implant biomanufacturing: a decade of Developmental Engineering. Adv Drug Deliv Rev. 2021 Feb;169:22-39

Patel SY, Kim DD, Ghali GE. Maxillofacial reconstruction using vascularized fibula free flaps and endosseous implants. Oral Maxillofac Surg Clin North Am. 2019 May;31(2):259-284.

Roberts SJ, van Gastel N, Carmeliet G, Luyten FP. Uncovering the periosteum for skeletal regeneration: the stem cell that lies beneath. Bone. 2015 Jan;70:10-18.

Rong Q, Li X, Chen SL, Zhu SX, Huang DY. Effect of the Schneiderian membrane on the formation of bone after lifting the floor of the maxillary sinus: an experimental study in dogs. Br J Oral Maxillofac Surg. 2015 Sep;53(7):607-612.

Salgado AJ, Coutinho OP, Reis RL. Bone tissue engineering: state of the art and future trends. Macromol Biosci. 2004 Aug 9;4(8):743-765.

Srouji S, Kizhner T, Ben David D, Riminucci M, Bianco P, Livne E. The Schneiderian membrane contains osteoprogenitor cells: in vivo and in vitro study. Calcif Tissue Int. 2009 Feb;84(2):138-145.

Tannoury CA, An HS. Complications with the use of bone morphogenetic protein 2 (BMP-2) in spine surgery. Spine J. 2014 Mar 1;14(3):552-559.

van Lochem EG, van der Velden VH, Wind HK, te Marvelde JG, Westerdaal NA, van Dongen JJ. Immunophenotypic differentiation patterns of normal hematopoiesis in human bone marrow: reference patterns for age-related changes and disease-induced shifts. Cytometry B Clin Cytom. 2004 Jul;60(1):1-13.

Wan Z, Zhang P, Liu Y, Lv L, Zhou Y. Four-dimensional bioprinting: Current developments and applications in bone tissue engineering. Acta Biomater. 2020 Jan 1;101:26-42.

Wang W, Yeung KWK. Bone grafts and biomaterials substitutes for bone defect repair: A review. Bioact Mater. 2017 Jun 7;2(4):224-247.

Zahedpasha A, Ghassemi A, Bijani A, Haghanifar S, Majidi MS, Ghorbani ZM. Comparison of bone formation after sinus membrane lifting without graft or using bone substitute "Histologic and radiographic evaluation". J Oral Maxillofac Surg. 2021 Jun;79(6):1246-1254.

Chapter 5

Human periosteum-derived cells do expand and retain bone-forming properties in platelet lysate

Lisanne C. Groeneveldt [1,2,3], Samuel Ribeiro Viseu [1,2], Kathleen Bosmans [1,2], Janne Vleminckx[1,2], Carla Geeroms[1,2], Orely Vanborren[1,2], Danny Huylebroeck [3,4], Liesbet Geris [1,2,5,6*]

[1] Prometheus, Division of Skeletal Tissue Engineering, KU Leuven, Leuven, Belgium;
[2] Skeletal Biology and Engineering Research Center, KU Leuven, Leuven, Belgium;
[3] Department of Cell Biology, Erasmus University Medical Center, Rotterdam, Netherlands;
[4] Department of Development and Regeneration, KU Leuven, Leuven, Belgium;
[5] Biomechanics Research Unit, GIGA-R In Silico Medicine, Université de Liège, Liège, Belgium;
[6] Biomechanics Section, KU Leuven, Leuven, Belgium

In preparation

5.1. Summary

Current methods for treating large bone defects involve the use of autologous bone tissue, allogeneic or xenogenic biomaterials, and growth factors, but they have limitations and complications. This study explores the potential of using human platelet lysate (hPL) as an alternative to fetal bovine serum (FBS). Despite its widespread use in research, FBS is associated with ethical concerns and translational complications related to the use of animal-derived products in the expansion of hPDCs in cell culture. The results show that replacing FBS with hPL in the culture medium for hPDCs does not significantly affect their proliferative capacity over time. However, there is a decrease in the percentage and number of proliferating cells when FBS is replaced by hPL. Nonetheless, there are no significant differences in DNA quantity, senescence rate, or apoptotic marker expression between hPL and FBS conditions. In terms of *in vitro* differentiation, the substitution of FBS with hPL does not have a significant impact on chondrogenic differentiation. However, osteogenic differentiation is enhanced when higher concentrations of hPL are used. *In vivo* experiments show a higher volume of mineralized tissue for hPDCs expanded in hPL-containing medium compared to those cultured in FBS-supplemented medium when seeded on a calcumphosphate-based scaffold. Overall, these findings suggest that hPL can serve as a suitable alternative to FBS for expanding hPDCs in cell culture without compromising their bone-promoting abilities.

5.2. Introduction

Following the historical success of bone marrow and keratinocyte transplantations, research by stem cell biologists over the last 20 years has raised the hope to use stem/ progenitor cells, including such cells isolated from various adult tissues, in cell-based therapies in human regenerative medicine. This research is usually incorporated in multi-disciplinary approaches involving experts in biomaterials, small and larger animal models, organoids and organs-on-a-chip, but also systems biologists and of course transplantation surgeons, under the generic term tissue engineering. One of these domains to which many efforts have been dedicated is this of bone tissue engineering. Specifically, at this moment, craniofacial bone defects are treated by using autologous bone tissue, allogeneic or xenogenic biomaterials such as demineralised bone, addition of cell-instructive growth/differentiation factors, use of metals like titanium or ceramics such as Bio-Oss, still with risk for complications and limitations (Fisher *et al.*, 2019; Al-Sabahi *et al.*, 2022; Stevanovic *et al.,* 2022). Bone tissue engineering, however, presents also a possible alternative treatment option for craniofacial bone defects. Inspired by other fields, such as developmental biology, a major focus is on recapitulating developmental principles of signaling between and fate determination of early embryonic and fetal (including in organogenesis) cells in adult regenerative processes (Papantoniou *et al.,* 2021). This is definitely the case for fracture healing of long bones in orthopedic surgery context, exploiting skeletal stem/precursor cells (SSPCs) from sources such as bone marrow and periosteum, using in the latter case hPDCs (Colnot, 2009). As part of this research, we have demonstrated the different properties of hPDCs depending on their body site of harvesting, showing mandibular hPDCs as the more favorable cell source for the use in tissue engineering approaches for craniofacial bone defects (Groeneveldt *et al.,* 2020).

Creating tissue engineered constructs continues to require lots of cells, usually in the range of millions, in order to create a construct of even only 1 cm^3, hence necessitating their expansion first in cell culture, while mainaininge their cell identity and their responsiveness to chondro- and/or osteogenic cues. The medium to proliferate cells traditionally consists of Dulbecco's

Modified Eagle Medium (DMEM), and addition of antibiotics/antimycotics and, very importantly, fetal bovine serum (FBS) (Chen *et al.,* 2009), which is nowadays frequently irradiated before use. In order to produce FBS, pregnant cows are slaughtered including their foetuses. It also goes along with a risk of contamination by endotoxins, mycoplasma, viral contaminants or even prion proteins, imposing stringent quality control of used animals as well as the obtained FBS. FBS furthermore is prone to batch-to-batch variation and has also been reported to sometimes prevent chondrogenesis (Brindley *et al.,* 2012; Gstraunthaler *et al.* 2013; Ren *et al.,* 2018). Therefore, many groups attempt to design FBS-free media and use alternative supplements and chemically defined media (CDM). As far as we know, no CDM has been developed yet for *ex vivo*, cell culture based expansion of hPDCs.

Medium containing human platelet lysate (hPL) may provide a suitable alternative. It contains platelet-derived growth factors (PDGFs), basic fibroblast growth factor (bFGF), transforming growth factor type-β (TGFβ), insulin-like growth factor-1 (IGF-1), epidermal growth factor (EGF), vascular endothelial growth factor (VEGF) and proteins involved in haemostasis (such as fibronectin and fibrinogen) (Doucet *et al.,* 2005; Müller *et al.,* 2009; Gupta *et al.,* 2019). hPL still has a batch-to-batch variation, but ethical concerns and some of the safety concerns can be avoided. DMEM supplemented with hPL has already been tested in cell culture on mesenchymal stromal cells (MSCs) obtained from adipose tissue or bone marrow. It was shown to lead to higher cellular proliferation rate and higher viability, and to elicit higher anti-inflammatory activities, beneficial to improved healing. The differentiation capabilities in cell culture towards osteogenic and chondrogenic lineages were found to be at least similar compared to the starting MSCs cultured in FBS, while adipogenic differentiation capacity was reduced (Barro *et al.,* 2019; Mareschi *et al.,* 2020; Chen *et al.,* 2023). With tibial-derived hPDCs higher proliferation rates were obtained when expanded in hPL-supplemented medium compared to those supplemented with FBS, as well as better bone-promoting capacity in combination with ectopic implantation of the used constructs (Gupta *et al.,* 2019).

In this part of our research, we tested and documented the substitution of FBS in FBS-enriched DMEM by different concentrations of hPL in expansion protocols for mandibular hPDCs.

5.3. Results

5.3.1. Proliferation of cultured hPDCs in the presence of hPL

Mandibular hPDCs of 3 individual donors were expanded in DMEM + 10% FBS during a two-week period to obtain sufficient cell numbers to start off with in the first place. Then, cells were cultured in DMEM + 10% FBS or in serum-free DMEM supplemented with 5%, 7.5% or 10% hPL. The latter condition showed a trend towards a higher proliferative capacity, but this trend was not statistically significant over longer time, *e.g.*, at day 31 (**Fig. 5.1A**). Additional documentation of hPDCs grown in the different conditions was performed by staining of incorporated EdU. Remarkably and unexpectedly, a statistically significant drop in the percentage and numbers of EdU-postive (+) cells was seen after replacement of FBS by any of the tested concentrations of hPL (mixed nested two-way ANOVA effect of hPL $p<0.001$), while a similar trend was seen in the level of proliferation-associated marker KI67 (**Fig. 5.1B,C**). DNA-quantification showed no differences between the medium conditions (**Fig. 5.1F**), and neither the senescence rate nor the apoptotic marker CASP3 were higher in 10% hPL compared to 10% FBS-supplemented medium (**Fig. 5.1D,E**).

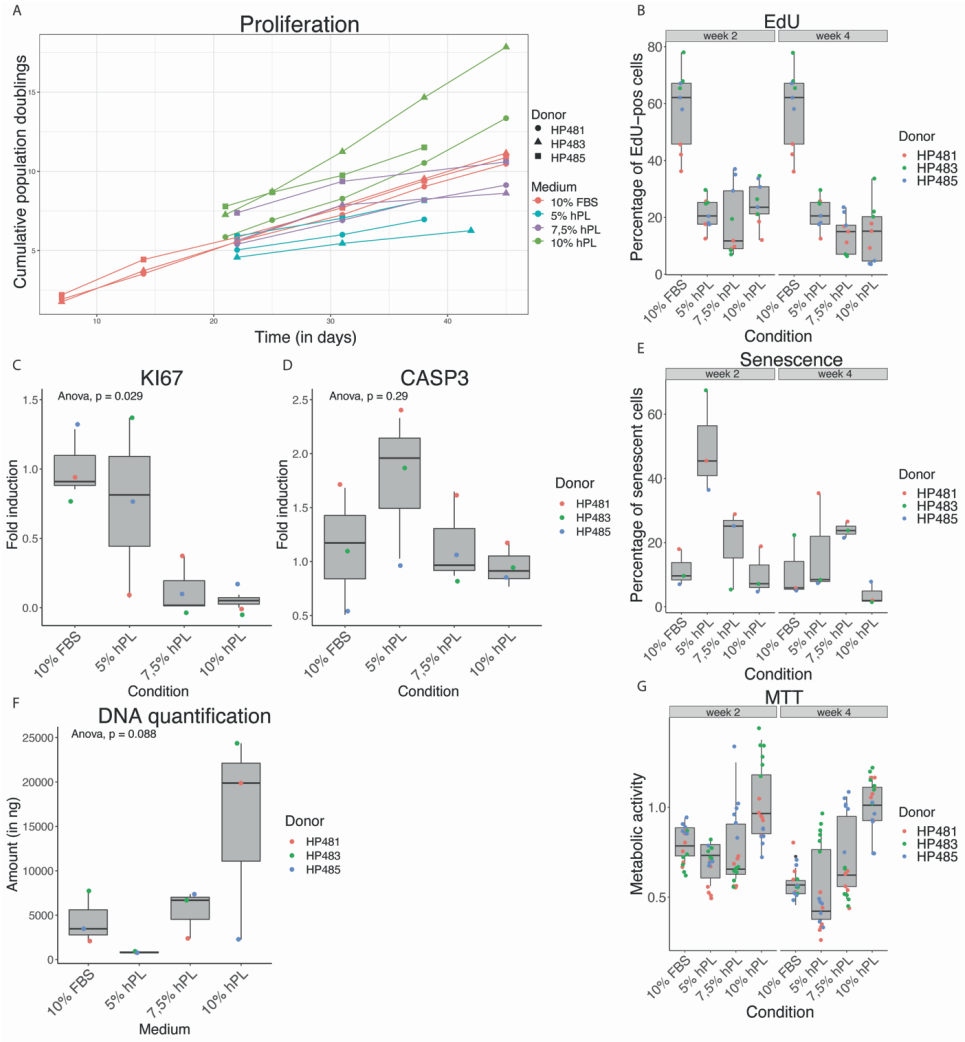

Figure 5.1. Characterization during the expansion of human periosteum-derived cells in hPL versus FBS (control). (A) Proliferation curve of hPDCs cultured in FBS-containing DMEM during 2 weeks before medium was replaced for the different indicated doses of hPL. **(B)** Percentage of EdU+ cells after 48 hours after EdU addition to cells cultured first for 2 and 4 weeks in hPL-containing DMEM. **(C)** Expression of the proliferative marker KI67 measured by RT-qPCR. **(D)** The level of apoptosis marker CASP3. **(E)** Percentage of senescent cells after 2 and 4 weeks proliferation in DMEM+hPL. **(F)** Quantification of DNA per 250,000 initially seeded cells per condition. **(G)** Metabolic activity of hPDCs cultured for 2 or 4 weeks in DMEM+hPL compared to DMEM+FBS, as measured in an MTT-assay. N=3 donors with technical triplicates.

5.3.2. *In vitro* differentiation

Osteogenic differentiation of hPDCs in cell culture showed no statistically higher expression of *RUNX2* when replacing 10% FBS by 5% hPL, but by adding the higher doses (of 10% as well as 7.5%) of hPL, a statistically significant difference was seen ($p<0.01$). This was the case in osteogenic primed cells as well as in control cells cultured without β-glycerophosphate, L-ascorbic acid and dexamethasone. The osteogenic differentiation was confirmed by Alizarin Red Staining (**Fig. 5.3A,B**). Chondrogenic differentiation was also confirmed by upregulated expression of *SOX9* and the hypertrophic marker gene *COL10A1* in chondrogenic primed conditions versus controls, but no differences were found between FBS and hPL-enriched media (**Fig. 5.3C,D**). Alcian Blue staining in chondrogenic primed cultures showed no differences either (**Fig. 5.3E).** For adipogenic differentiation, also no differences were found (see **Fig. S5.1**).

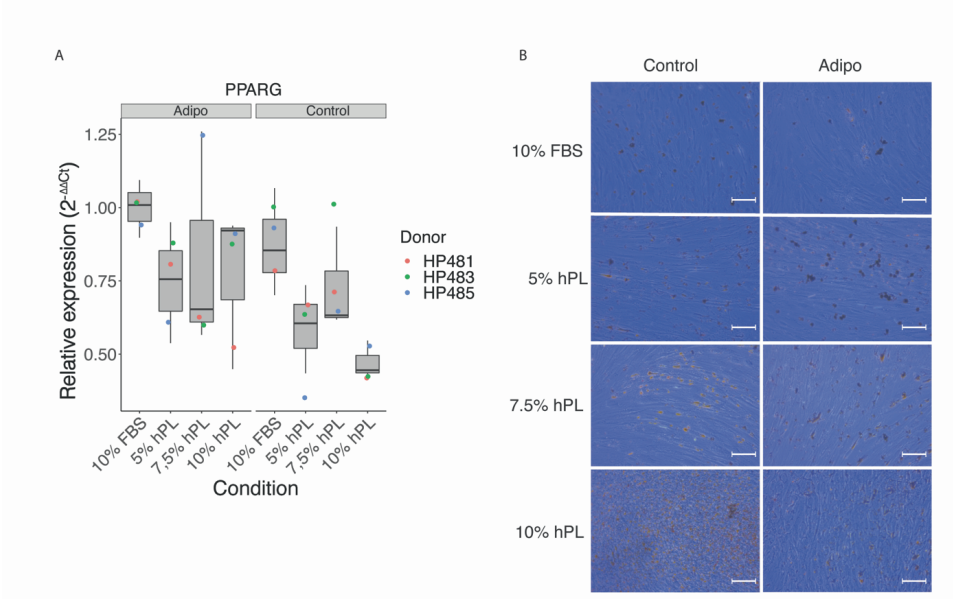

Figure S5.1. Adipogenic differentiation capacities of cultured hPDCs, including in hPL-supplemented DMEM.
(A) Steady-state mRNA levels of early adipogenic marker gene *PPARG* as determined by RT-qPCR. **(B)** Oil Red O staining on adipogenically primed hPDCs grown for 7 days, staining fat droplet deposition; scale bars represent 200 µm. N=3 donors, representative images are shown for technical triplicates.

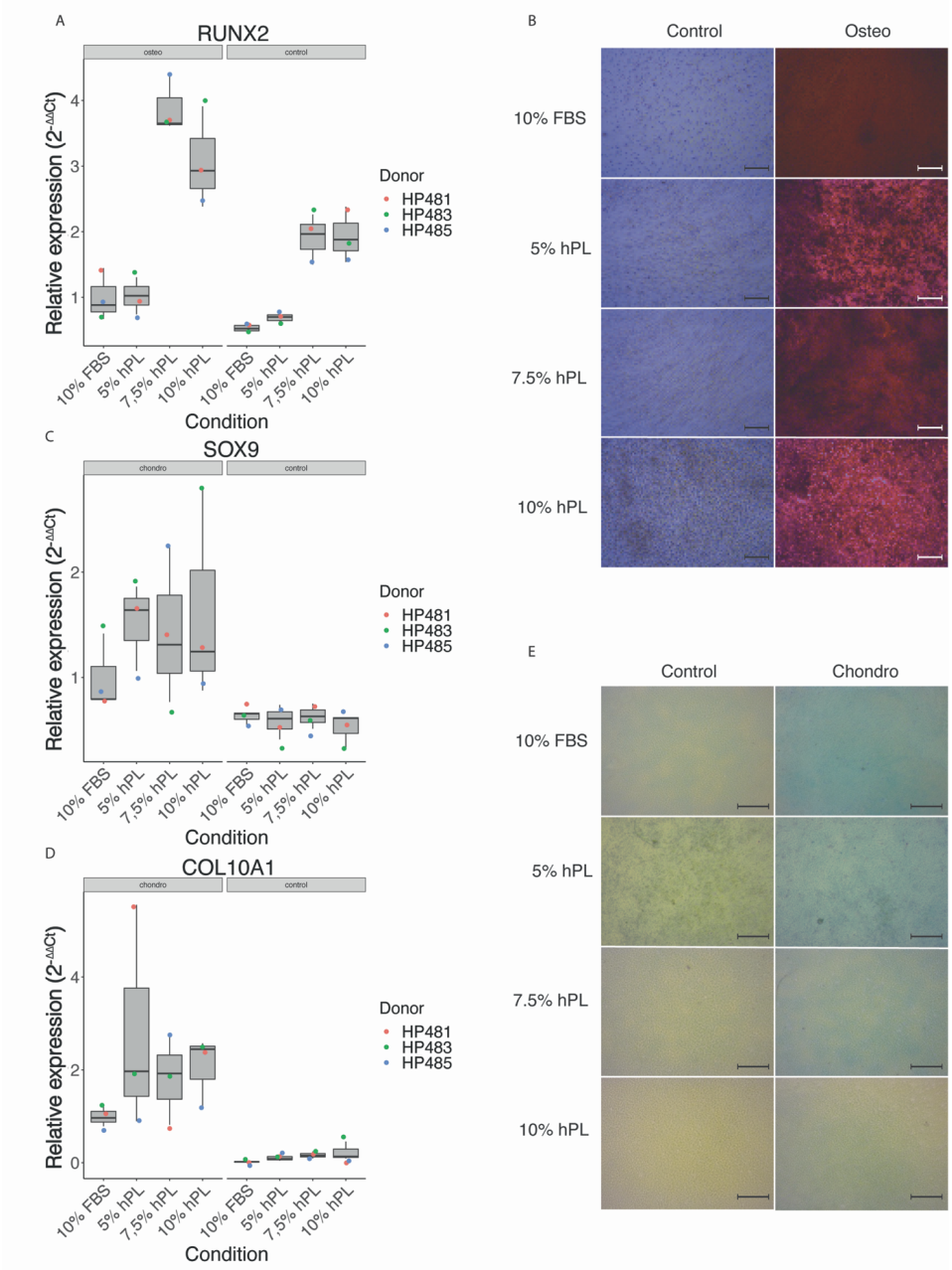

Figure 5.2. **Differentiation capacities of cultured hPDCs, including in hPL-supplemented DMEM.** **(A)** Steady-state mRNA levels of early osteogenic marker gene *RUNX2* as determined by RT-qPCR. **(B)** Alizarin Red staining on osteogenic primed hPDCs grown for 14 days, staining calcium phosphate deposition; scale bars represent 200 µm. **(C,D)** mRNA level of chondrogenesis-related marker gene *SOX9* (panel C) and hypertrophic marker gene *COL10A1* (D) in chondrogenic primed hPDCs grown in hPL-supplemented (FBS-free) DMEM. **(E)** Alcian Blue staining in chondrogenically primed hPDCs grown for 21 days, staining glycosaminoglycans in the sample. N=3 donors, representative images are shown for technical triplicates.

5.3.3. *In vivo* bone formation

Mandibular hPDCs were loaded on NuOss scaffolds and then implanted ectopically in nude mice. After 8 weeks, Nano-CT analysis was performed. The analysis of the amount of mineralized tissue showed a higher mineralized volume in scaffolds seeded with cells that were expanded in DMEM+hPL compared to those DMEM+FBS ($p<0.01$; **Fig. 5.4A**), and an effect of hPL concentration was found ($p<0.05$). Representative examples of CT-slides are shown in **Fig. 5.4B**. The mineralized bone tissue seen on CT-scans was confirmed as bone tissue (by staining with hematoxilin/eosin; **Fig. 5.4C-F**). Alcian blue staining showed that bone tissue formation occurred via endochondral ossification (**Fig. 5.4G-J**); Masson's Trichrome showed the newly formed bone tissue nicely around the calciumphosphate granules from the scaffold itself (**Fig. 5.4K-N**).

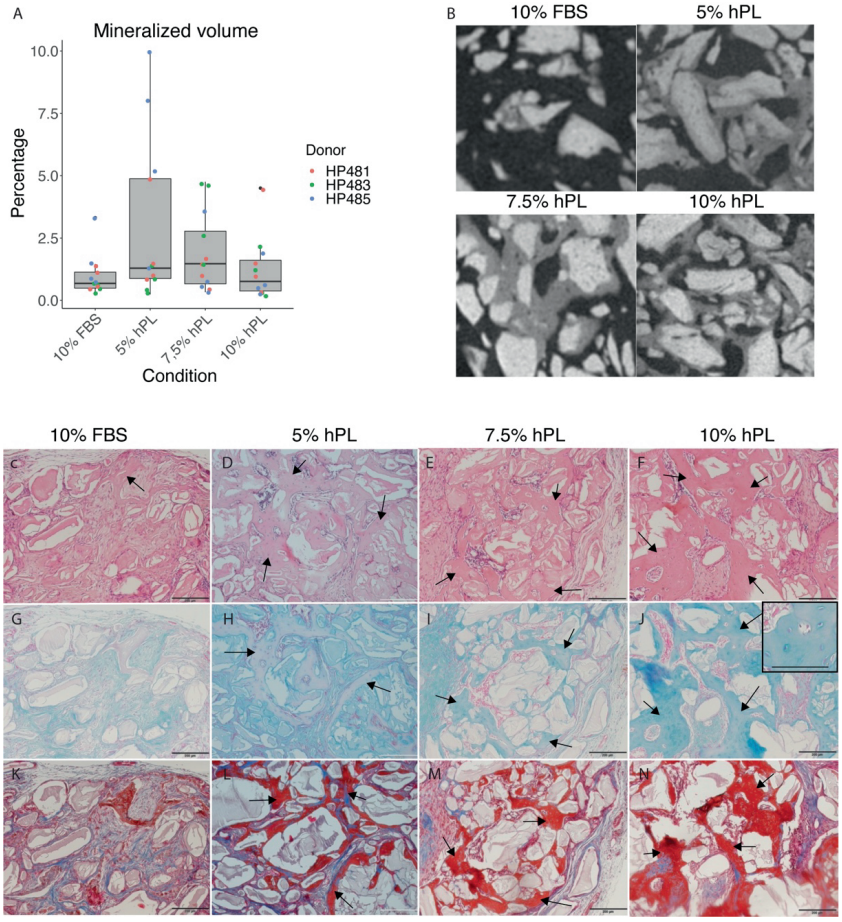

Figure 5.3. ***In vivo*** **bone-forming capacity of hPDCs expanded in hPL-supplemented DMEM.**
(A) Percentage of scaffold volume that is mineralized, **(B)** Typical CT-scan slides of NuOss scaffolds with their remaining calcium phosphate grains (white) and mineralization around (grey). **(C-F)** Histological imaging of those cell constructs stained with Hematoxylin/Eosin, **(G-J)** Alcian Blue with higher magnification inserted in **(J)** and **(K-N)** Masson's Trichrome staining. Scale bars represent 200 µm, for the higher magnification scale bar represents 100 µm, arrows point at bone tissue. N=3 donors, representative images are shown for technical quadruplicates.

5.4. Discussion

In this part of the PhD research, we documented the effects of replacing FBS by a presumptively safer product, *i.e*. hPL, in order to meet ethical concerns and facilitate translation to the clinic by avoiding the risk of complications linked to the use of animal-based products for human cell culture (Jochems *et al.,* 2002). Chemically-defined growth media have not been worked-out for our mandibula-derived hPDCs or did still contain FBS (Al Hoshni *et al.,* 2020). This study demonstrates that replacement of FBS by hPL shows promising results regarding the maintenance of bone-promoting capacities of the hPL-grown mandibular hPDCs both in cell culture and *in vivo*. Although some differences were seen in the proliferative properties between DMEM + 10% FBS and DMEM + (5%, 7.5% or 10%) hPL, no statistically significant deviations were seen indicative of negative effects of hPL. Those differences were also not detected by flow-cytometric analysis of the cell cycle, for which the same time of incubation for EdU was used. For the *in vitro* differentiation towards osteogenic or chondrogenic lineages, more osteogenic differentiation was seen when the addition of 10% FBS was substituted by 7.5% or 10% hPL, and no inferior results were seen for chondrogenic differentiation of the mandibular hPDCs. *In vivo* even superior results were obtained for cells cultured in DMEM supplemented with 7,5% or 10% hPL, based on the higher 78roviding78d contents and the appearance of endochondral ossification.

The use of hPL may still be prone to batch effects. However, risks for contamination by prion proteins and viruses seen in cows are eliminated, and hPL could be produced with risk levels of contaminations similar to those of blood transfusion (Schallmoser *et al.,* 2020). Moreover, ethical concerns associated with the slaughter of pregnant cows are absent when using hPL. Furthermore, it has been reported that FBS sometimes prevents chondrogenesis (Ren *et al.,* 2018), while this was not seen in our *in vitro* chondrogenic differentiation study.

However, more in depth analyses on the effects of hPL on hPDCs should still be performed since hPL exerts different effects on pathways that are important for proliferation and bone formation compared to FBS. A down-regulation of Wnt and TGFb pathways is already described, while the CREB signaling gets activated (Al Hoshni *et al.,* 2020). When Wnt3A is eliminated from the expansion medium, a 3-times higher proliferation can be noted for hPDCs. However, Wnt is also required for bone repair, shown by the effects of a mutation in *Axin2* that works downstream of Wnt3 in a negatively manner, or *in vitro* osteogenic differentiation (De Boer *et al.,* 2004; Komiya and Habas, 2008; Minear *et al.,* 2020; Ma *et al,* 2023). TGFb is more known to stimulate bone formation by pushing cells towards differentiation by interacting with SMAD 2/3 and SMAD4 (Pauklin and Vallier, 2015; Al Hoshni *et al.,* 2020, Loh *et al.,* 2023). Classical bone tissue engineering strategies use a combination of cells, carriers and growth or differentiation factors to accomplish bone tissue formation *in vivo*. Since the properties of the cells are possibly changed, the effects of the replacement of FBS by hPL on the *in vivo* bone forming potential of hPDCs should be examined before already gathered knowledge on FBS-expanded cells can be used on hPL-expanded cells.

All together, hPL is a good candidate to replace FBS in expansion medium of hPDCs for translational bone tissue engineering approaches. The cell product can become safer compared to FBS-cultured cells, but further research is required to investigate the effects of hPL on cell priming strategies.

5.5. Experimental procedures

Isolation and culture of hPDCs

The mandibular samples were harvested by maxillofacial surgeons after informed consent was obtained (Belgian registration number B322201731127) as described previously (Groeneveldt *et al.*, 2020). These samples were digested in medium consisting of Dulbecco's modified Eagle's medium (DMEM) supplemented with 10% Fetal Bovine Serum (FBS; Thermo Fisher Scientific, Waltham, MA, United States) and 1% antibiotics-antimycotics solution (100 units penicillin/ml, 100 µg streptomycin/ml and 0.25 µg amphotericin-B/ml; Invitrogen), from here on referred to as FBS-DMEM (FBS-DMEM), in addition of 4,400 units per 10 ml Collagenase type-IV (Gibco) under constant agitation for 16 h. Cells were from then on cultured in FBS-DMEM for 2 weeks, obtaining a sufficient amount of cells to perform the experiment on cells from the same donor. Then, instead of 10% FBS, different concentrations (5%, 7.5% or 10%) of hPL were added to the cells. Population doublings (PD) of these hPDCs were calculated upon passaging using the formula $\log_2(n_2)-\log_2(n_1)$, with n_1 representing the number of cells seeded in the dish/flask and n_2 the number of cells obtained after trypsinization (TrypLE, Thermo Fisher Scientific) of cells from the same dish/flask at 90% confluency.

Cellular senescence

In order to detect cells in senescence, 100,000 cells were plated per well of a 6-well plate in DMEM in addition of FBS or hPL. After one day of cell proliferation, the cells were fixed using 4% paraformaldehyde (PFA) for 5 min. Cells were rinsed using PBS and stained with 2 ml staining solution containing 36 mM citric acid (pH 6.0; Sigma Aldrich), 4.5 mM potassium ferricyanide (Merck), 4.5 mM potassium ferrocyanide (Biomedicals, Santa Ana, USA), 0.14M NaCl, 1.8 mM MgCl2 (Merck) and 1ml X-gal/ml (Biotium, Fremont, USA). After 6 hours, the pictures were made using the Primovert microscope (Zeiss).

Cellular proliferation

For detection of proliferating cells, staining for incorporated EdU was performed using the Click-iTTM EdU Alexa FluorTM 555 Imaging Kit (Thermo Fisher Scientific) according to the manufacturer's protocol and as described before (Groeneveldt *et al.,* 2020). In short, 10,000 cells/well were seeded in a 6-well plate in DMEM supplemented with the experimental dose of FBS or hPL. The following day, medium was replaced with DMEM containing 10% FBS or 5%, 7.5% or 10% hPL containing 10 µM EdU, followed by an incubation of 48 h. Next, cells were fixated using 3,7% formaldehyde in PBS (VWR) for 15 min, rinsed twice with 3% bovine serum albumin (BSA, Sigma Aldrich) in PBS and lysed with 0.5% Triton X-100 in PBS (Sigma Aldrich) for 20 min. This was followed by adding the Click-iT reaction cocktail for 30 min in absence of light, quick washing steps of 1 min using subsequently 3% BSA dissolved in PBS and PBS, addition of the Hoechst solution for 30 min in a 1:2,000 dilution in PBS and final washing steps using PBS for 1 min.

Metabolism

Cell metabolic activity was measured by using 3-(4,5-dimethylthiazol-2-yl)-2,5-diphenyltetrazolium bromide (MTT) assay as described previously (Groeneveldt *et al.,* 2020). Living cells contain the mitochondrial reductase enzyme, which reduces MTT toward formazan forming salt crystals. By measuring the amount of reduction of MTT toward formazan, the cell metabolic activity was measured. This was done by removing remaining MTT and solubilizing of the salt crystals in order to get with the different quantities of salt crystals corresponding differences in color intensity (Mosmann, 1983). Tests were performed as technical replicates 6 times per donor at 2 and 4 weeks of culture in DMEM in addition of FBS or hPL. 10,000 cells were seeded in a 24-well plate in 0.5 ml FBS/hPL-DMEM. After 1 day, this medium was replaced with DMEM containing 250 µg MTT/ml (Sigma Aldrich) without FBS or hPL. After 4 h, medium and remaining MTT were removed and 1 ml absolute ethanol was added to each well in order to solubilize the salt crystals. These solutions were transferred to a 96-well plate and absorbance was read at 570 and 670 nm with a Synergy HT reader (BioTek). In order to calculate the metabolic rate, the background absorbance (at 670 nm) was subtracted from the absorbance at 570 nm and corrected for the blank values which were obtained by performing all steps on wells containing no cells.

***In vitro* trilineage differentiation**

Human periosteum-derived cells were primed for adipogenic, osteogenic and chondrogenic differentiation for 14, 21, and 7 days, respectively. Analysis was performed by staining with Oil Red O, Alizarin Red and Alcian Blue, respectively as described previously (Groeneveldt *et al.,* 2020). For these experiments, instead

of 10% FBS the selected dose of hPL for the corresponding experimental condition was added to the DMEM as described above.

For adipogenic differentiation of hPDCs, cells were cultured in 24-well plates at a density of 19,000 cells/well in 0.5 ml FBS/hPL-DMEM. After 2 days, the medium was changed for adipogenic differentiation medium, i.e., Minimum Essential Medium Eagle – alpha modification (α-MEM; Invitrogen supplemented with 10% FBS or the selected dose of hPL for the hPL-conditions, 1% antibiotics-antimycotics solution, 1 µM dexamethasone + 10 µg/ml human insulin (Sigma Aldrich), 100 µM indomethacin (Sigma Aldrich) and 25 µM 3-isobutyl-1-methylxanthine (Sigma Aldrich). The cells were cultured in a humidified atmosphere at 5% CO2 and 37°C for 14 days and medium was replaced every 2 days. Lipid droplets were stained by Oil Red O. Cells in monolayer were washed in PBS and fixed for 30 min at room temperature in 10% formaldehyde (VWR) diluted in PBS. Next, cells were washed with Milli-Q water and rinsed in 60% isopropanol (VWR) diluted in Milli-Q water. Cells were allowed to dry completely and then stained with 0.2% Oil Red O (Sigma Aldrich) in Milli-Q water for 60 min. These cells were then washed with Milli-Q water before obtaining pictures using the Primovert microscope (Zeiss).

For osteogenic differentiation of hPDCs, cells were cultured in 24-well plates at a density of 8,550 cells per well in 0.5 ml FBS-DMEM or hPL-DMEM, first allowing them to proliferate. After 1 day, medium was then changed for osteogenic medium consisting of FBS/hPL-DMEM supplied with 100 nM dexamethasone (Sigma Aldrich), 10 mM β-glycerophosphate disodium salt hydrate (Sigma Aldrich) and 50 µg/ml L-ascorbic acid 2-phosphate (Sigma Aldrich). Cells were cultured in a humidified atmosphere at 5% CO2 and 37°C for 21 days, during which this medium was replaced every 3 days. Cells in monolayer were washed in PBS, fixed with methanol at −20°C (Fisher Scientific), stored for 1 h at 4°C, and washed again with PBS. Cells were stained for 1 h with a 2% Alizarin-S stain (Sigma Aldrich) in Milli-Q water with pH adjusted to 4.2 (Merck) while the plate was placed on a shaker for constant agitation. After staining, cells were washed with Milli-Q water. Pictures were made using a Discovery.v8 SteREO microscope (Zeiss).

For chondrogenic differentiation of hPDCs, the cells were cultured in micromasses. Micromasses containing 200,000 cells in 10 µl DMEM after centrifugation at 260 RCF for 10 min were added to individual wells of 24-well plates. After 2 h, an extra 0.5 ml of FBS-DMEM or hPL-DMEM was added to each well. After 1 day, this medium was replaced by chondrogenic inductive medium (DMEM-F12 (Invitrogen) containing 2% FBS or 2% hPL for the hPL-conditions, antibiotics-antimycotics solution, 1x ITS + premix universal culture supplement (Corning), 100 nM dexamethasone, 10 µM Y27632 (Axon Medchem), 50 µg L-ascorbic acid 2-phosphate/ml, 40 µg proline/ml (Sigma Aldrich) and 10 ng transforming growth factor-β1/ml (TGFβ1; PeproTech). These cells were cultured under humidified conditions at 37°C and 5% CO2 for 7 days; medium was replaced every 2 days. Sulfated glycosaminoglycans in the micromasses were stained by Alcian Blue (Roth). The cells were rinsed with PBS and fixed with excess ice-cold methanol for 1 h at 4°C. This methanol was removed and cells were rinsed with Milli-Q water prior to adding 0.1% Alcian Blue staining solution (in 0.1 M HCl at pH 2.4) for 1 h on a shaker. Alcian Blue stain was removed and the cells were rinsed with Milli-Q water before pictures were made using the Discovery.v8 SteREO microscope (Zeiss). At days 1 (control), 3, 5 and 7, micromasses were also obtained for confirmation of chondrogenic differentiation by RT-qPCR. Micromasses were individually lysed in 350 µl RLT buffer (Qiagen) containing 1% β-mercaptoethanol (Sigma Aldrich) and homogenized by thoroughly pipetting up and down. Samples were directly placed on ice and frozen at −80°C until further processing.

RNA isolation, DNA quantification, cDNA synthesis and quantitative PCR

Cells were rinsed twice in PBS, lysed by adding 350 µl of RLT buffer (Qiagen) containing 1% β-mercaptoethanol (Sigma Aldrich) per well, and homogenized by thoroughly pipetting up and down. Samples were directly placed on ice and frozen at −80°C until further processing. DNA quantification was performed using a 0.5% Quant-it™ dsDNA HS reagent solution in the accompanied buffer solution and fluorometric measurement on the Qubit fluorometer (Invitrogen). The Qiagen Rneasy mini kit was used to isolate RNA. cDNA was obtained by reverse transcription of 500 ng of total RNA, using the PrimeScript™ RT Reagent Kit (Takara Bio) according to manufacturer's manual. For RT-qPCR, primers were designed for mRNAs of Marker Of Proliferation Ki-67 (KI67), Caspase 3 (CASP3), RUNX Family Transcription Factor 2 (RUNX2), SRY-Box Transcription Factor 9 (SOX9), Collagen Type X Alpha 1 Chain (COL10A1) and peroxisome proliferator activated receptor gamma (*PPARG)*.Relative differences in expression were calculated using the $2^{-\Delta\Delta Ct}$ method normalized to the housekeeping gene Hypoxanthine Phosphoribosyltransferase 1 (*HPRT*). Samples were processed and measured in technical duplicates on a on Rotor Gene® 6000 PCR machine (Qiagen) using a Sybr Green detection system (Takara Bio) according to the manufacturer's instructions, and normalized using as a housekeeping gene. The respective primer sequences are listed in the **Table S5.1**.

CT analysis

Bone formation was analysed using the Phoenix NanoTom S CT system (GE measurement) at a voltage of 60 kV and a current of 200 mA. An aluminium filter of 1 mm was used to filter out the low energetic radiation. CTAn and Batch Manager Software programs (Bruker micro-CT, Kontich, Belgium) were used for 3-D quantification of the bone volume and calcium phosphate (CaP) grains of the NuOss scaffold. A three-level automatic Otsu segmentation algorithm was used to segment the newly formed bone tissue and CaP-grains from the background in combination with manually chosen thresholds. Noise was reduced by removing black and white speckles smaller than 200 voxels and a closing operation of 2 voxels was performed to solidify the resulting structure, providing binarized images suitable for the 3-D analysis (Kerckhofs *et al.,* 2013).

Histology

After decalcification in EDTA, dehydration through series of graded ethanol, then embedding in paraffin, and sectioning in 5-µm thick slices, histological staining was carried out. Staining with hematoxylin and eosin (H&E) was done by a dip in hematoxylin-solution for 2 min, followed by a brief wash in water, and subsequently staining in 1% Eosin (Klinipath, Duiven, Netherlands) for 7 min.

For Alcian Blue staining, samples were rehydrated, stained for 30 min in 0.5% Alcian Blue (Roth) solution in 1 M HCl (pH = 1). Nuclear Fast Red (Vector) was used for staining of the nuclei during 5 min. For staining with Safranin O, samples were dipped in acidic alcohol (1% HCl in 70% ethanol). Next, they were placed in Fast Green (Klinipath) for 3 min, dipped in 1% acetic acid and then stained in 0.1% Safranin O (Sigma Aldrich) for 10 min. Masson's trichrome staining was performed using Bouin's solution (Sigma Aldrich) as mordant followed by 5-minute-dips in Weigert's Iron Hematocxylin Solution, Biebrich Scarlet-Acid Fuchsin, Phosphotungstic/ Phosphomolybdic Acid Solution and Aniline Blue Solution (all from Sigma Aldrich), followed by a dip in 1% acetic acid for 2 min. The sections were cleared in HistoClear (National-Diagnostics) and mounted in Pertex (Histolab). Pictures were made using the IX83 microscope (Olympus).

Statistical Analysis

Statistical analysis for cellular senescence, quantitative PCR and *in vivo* bone formation was done using the mixed nested two-way ANOVA where analysis of variance was based on the linear mixed model fit by REML. T-tests used Satterthwaite's method. All statistical analyses were performed in R (version 4.1.1). Results were considered statistically significant at $p < 0.05$. Data are presented typed as mean values ± standard deviation (SD) or as boxplots with median and interquartile range.

Supplementary table

Table S5.1: Primer sequences used for RT-qPCR.

Gene	Forward	Reverse
CASP3	GGCGGTTGTAGAAGAGTTTCG	TCACGGCCTGGGATTTCAAG
COL10A1	ACGATACCAAATGCCCACAG	GTGGACCAGGAGTACCTTGC
HPRT	TGAGGATTTGGAAAGGGTGT	GAGCACACAGAGGGCTACAA
KI67	CTTTGGGTGCGACTTGACGA	GCAAATTTACAACTCTTCCACTGGG
PPARG	GCCAAGCTGCTCCAGAAAAT	TGATCACCTGCAGTAGCTGCA
RUNX2	CGCATTCCTCATCCCAGTAT	GCCTGGGGTCTGTAATCTGA
SOX9	TGGAGACTTCTGAACGAGAGC	CGTTCTTCACCGACTTCCTC

Literature references

Al Hosni R, Shah M, Cheema U, Roberts HC, Luyten FP, Roberts SJ. Mapping human serum-induced gene networks as a basis for the creation of biomimetic periosteum for bone repair. Cytotherapy. 2020 Aug;22(8):424-435.

Al-Sabahi ME, Jamali OM, Shindy MI, Moussa BG, Amin AA, Zedan MH. Aesthetic reconstruction of onco-surgical mandibular defects using free fibular flap with and without CAD/CAM customized osteotomy guide: a randomized controlled clinical trial. BMC Cancer. 2022 Dec 2;22(1):1252.

Barro L, Su YT, Nebie O, Wu YW, Huang YH, Koh MB, Knutson F, Burnouf T. A double-virally-inactivated (Intercept-solvent/detergent) human platelet lysate for in vitro expansion of human mesenchymal stromal cells. Transfusion. 2019 Jun;59(6):2061-2073.

Brindley DA, Davie NL, Culme-Seymour EJ, Mason C, Smith DW, Rowley JA. Peak serum: implications of serum supply for cell therapy manufacturing. Regen Med. 2012 Jan;7(1):7-13.

Chen C, Hou X, Jing F, Wang T, Feng L, Kang YJ. Alteration of Transcriptomic Profile and Antiseptic Efficacy of Adipose-Derived Mesenchymal Stromal/Stem Cells Under Different Culture Conditions. Stem Cells Dev. 2023 Feb;32(3-4):75-86.

Chen HH, Decot V, Ouyang JP, Stoltz JF, Bensoussan D, de Isla NG. In vitro initial expansion of mesenchymal stem cells is influenced by the culture parameters used in the isolation process. Biomed Mater Eng. 2009;19(4-5):301-309.

Colnot C. Skeletal cell fate decisions within periosteum and bone marrow during bone regeneration. J Bone Miner Res. 2009 Feb;24(2):274-282.

De Boer J, Wang HJ, Van Blitterswijk C. Effects of Wnt signaling on proliferation and differentiation of human mesenchymal stem cells. Tissue Eng. 2004 Mar-Apr;10(3-4):393-401.

Doucet C, Ernou I, Zhang Y, Llense JR, Begot L, Holy X, Lataillade JJ. Platelet lysates promote mesenchymal stem cell expansion: a safety substitute for animal serum in cell-based therapy applications. J Cell Physiol. 2005 Nov;205(2):228-236.

Fisher M, Yee K, Alba B, Tanna N, Bastidas N, Bradley JP. Applications of Bone Morphogenetic Protein-2: alternative therapies in craniofacial reconstruction. J Craniofac Surg. 2019 Oct;30(7):1952-1959.

Groeneveldt LC, Herpelinck T, Maréchal M, Politis C, van Ijcken WFJ, Huylebroeck D, Geris L, Mulugeta E, Luyten FP. The bone-forming properties of periosteum-derived cells differ between harvest sites. Front Cell Dev Biol. 2020 Nov 25;8:554984.

Gstraunthaler G, Lindl T, van der Valk J. A plea to reduce or replace fetal bovine serum in cell culture media. Cytotechnology. 2013 Oct;65(5):791-793.

Gupta P, Hall GN, Geris L, Luyten FP, Papantoniou I. Human platelet lysate improves bone forming potential of human progenitor cells expanded in microcarrier-based dynamic culture. Stem Cells Transl Med. 2019 Aug;8(8):810-821.

Jochems CE, van der Valk JB, Stafleu FR, Baumans V. The use of fetal bovine serum: ethical or scientific problem? Altern Lab Anim. 2002 Mar-Apr;30(2):219-227.

Komiya Y, Habas R. Wnt signal transduction pathways. Organogenesis. 2008 Apr;4(2):68-75.

Loh HY, Norman BP, Lai KS, Cheng WH, Nik Abd Rahman NMA, Mohamed Alitheen NB, Osman MA. Post-Transcriptional Regulatory Crosstalk between MicroRNAs and Canonical TGF-β/BMP Signalling Cascades on Osteoblast Lineage: A Comprehensive Review. Int J Mol Sci. 2023 Mar 29;24(7):6423.

Ma J, Chen P, Deng B, Wang R. Kynurenic acid promotes osteogenesis via the Wnt/β-catenin signaling. In Vitro Cell Dev Biol Anim. 2023 Jun 8.

Mareschi K, Castiglia S, Adamini A, Rustichelli D, Marini E, Banche Niclot AGS, Bergallo M, Labanca L, Ferrero I, Fagioli F. Inactivated platelet lysate supports the proliferation and immunomodulant characteristics of mesenchymal stromal cells in GMP culture conditions. Biomedicines. 2020 Jul 17;8(7):220.

Minear S, Leucht P, Jiang J, Liu B, Zeng A, Fuerer C, Nusse R, Helms JA. Wnt proteins promote bone regeneration. Sci Transl Med. 2010 Apr 28;2(29):29ra30.

Müller AM, Davenport M, Verrier S, Droeser R, Alini M, Bocelli-Tyndall C, Schaefer DJ, Martin I, Scherberich A. Platelet lysate as a serum substitute for 2D static and 3D perfusion culture of stromal vascular fraction cells from human adipose tissue. Tissue Eng Part A. 2009 Apr;15(4):869-875.

Pauklin S, Vallier L. Activin/Nodal signalling in stem cells. Development. 2015 Feb 15;142(4):607-19.

Ren J, Ward D, Chen S, Tran K, Jin P, Sabatino M, Robey PG, Stroncek DF. Comparison of human bone marrow stromal cells cultured in human platelet growth factors and fetal bovine serum. J Transl Med. 2018 Mar 14;16(1):65.

Papantoniou I, Nilsson Hall G, Loverdou N, Lesage R, Herpelinck T, Mendes L, Geris L. Turning Nature's own processes into design strategies for living bone implant biomanufacturing: a decade of Developmental Engineering. Adv Drug Deliv Rev. 2021 Feb;169:22-39

Schallmoser K, Henschler R, Gabriel C, Koh MBC, Burnouf T. Production and Quality Requirements of Human Platelet Lysate: A Position Statement from the Working Party on Cellular Therapies of the International Society of Blood Transfusion. Trends Biotechnol. 2020 Jan;38(1):13-23.

Stevanovic M, Selakovic D, Vasovic M, Ljujic B, Zivanovic S, Papic M, Zivanovic M, Milivojevic N, Mijovic M, Tabakovic SZ, Jokanovic V, Arnaut A, Milanovic P, Jovicic N, Rosic G. Comparison of hydroxyapatite/poly(lactide-co-glycolide) and hydroxyapatite/polyethyleneimine composite scaffolds in bone regeneration of swine mandibular critical size defects: in vivo study. Molecules. 2022 Mar 4;27(5):1694.

Chapter 6

Human periosteum-derived cells primed with BMP2 can heal a large bone defect *in vivo*

Lisanne C. Groeneveldt [1,2,3], Liesbeth Ory [1,2], Kathleen Bosmans [1,2], Ayse Kose [1,2], Tim Herpelinck [1,2], Carla Geeroms [1,2], Wilfred F. J. van Ijcken [3,4], Danny Huylebroeck [3], Liesbet Geris [1,2,5,6*]

[1] Prometheus, Division of Skeletal Tissue Engineering, KU Leuven, Leuven, Belgium;
[2] Skeletal Biology and Engineering Research Center, KU Leuven, Leuven, Belgium;
[3] Department of Cell Biology, Erasmus University Medical Center, Rotterdam, Netherlands;
[4] Center for Biomics, Erasmus University Medical Center, Rotterdam, Netherlands;
[5] Biomechanics Research Unit, GIGA-R In Silico Medicine, Université de Liège, Liège, Belgium;
[6] Biomechanics Section, KU Leuven, Leuven, Belgium

Work in progress

6.1. Summary

Bone tissue engineering is a strong candidate for addressing the problems associated with the current standard therapies to treat large bone defects in craniofacial area. In this study, combinations of priming techniques and scaffolds to create biomechanical support for mandibular-derived skeletal stem and progenitor cells (hPDCs) were explored and compared.

The effects of hPDC-priming with BMP2 and BMP6 were assessed by RNA sequencing showing a stronger effect in downstream pathways related to bone formation for BMP2. The roles of highly upregulated transcription factors DLX5 and DLX6 herein were further tested by silencing experiments, pointing towards a negative feedback loop for BMP2. Next, the *in vivo* bone formation capacity of primed hPDCs on several scaffolds, and even a scaffold-free method using extracellular matrix produced by the cells themselves were tested ectopically, showing the most promising bone formation by BMP2-primed cells seeded on a collagen-based scaffold with hydroxyapatite. The final bone-defect healing potential of this construct was tested on an in-house developed orthotopic rat model with a critical size mandibular bone defect. Overall, this study demonstrated that constructs consisting of mandibular-derived hPDCs primed with BMP2 on a CopiOs scaffold, show enhanced bone-forming properties compared to other constructs and that they have the ability to heal critically sized mandibular bone defects in rats.

6.2. Introduction

Currently, tissue autografts are the standard surgical interventions for treating cranio-maxillofacial large bone defects, which are often caused by trauma, osteonecrosis, oncologic resections or congenital malformations. These interventions create a secondary surgical site and are accompanied by high risk for donor site morbidity, pain at this site, and possibly may cause major complications such as post-operative infection or necrosis of the transplanted tissue, the latter due to poor vascularisation of the graft (Arrington *et al.*, 1996; Mashrah *et al.*, 2021). Bone tissue engineering has emerged as an early field of cell-based regenerative therapy to repair bone defects. For this approach a multi-disciplinary expert knowledge is used to select appropriate cells that are able to expand *ex vivo* and retain their capacity to differentiate. To these cells, suitable polypeptide growth/differentiation factors are added to instruct cell differentiation, also after implantation, and biomaterials that provide a 3D environment for biomechanical support (Leijten *et al.*, 2015). For this, skeletal stem and progenitor cells (SSPCs) have been and are still being obtained and characterized from various sources. Depending on their adult tissue of origin, differences in the properties of SSPCs have been documented regarding cellular proliferation and differentiation mostly in cell culture, as well as cell survival and senescence, cytokine production and release, and more recently gene/mRNA expression profiles (Dominici *et al.*, 2006; Kern *et al.*, 2006; Tsai *et al.*, 2007). The bone-forming cells most predominant in the callus of long bone fractures are the periosteal-derived SSPCs (PDCs). Therefore, many workers in the field including ourselves concur that PDCs are a clinically relevant, available and expandable cell source for bone tissue engineering. This is thought, since PDCs are able to contribute to mimic natural fracture repair (Colnot *et al.*, 2012; de Bari *et al.*, 2006; van Gastel *et al.*, 2012). In previous research we have shown that the donor site for hPDCS co-determines this outcome (Groeneveldt *et al.* , 2020). Based on this work, mandibular-derived PDCs were selected here to continue the testing of priming strategies and different 3D scaffolds for improved bone-forming properties.

In order to steer and/or promote progenitor cells towards bone-producing cells, priming with polypeptide growth/differentiation factors such as bone morphogenetic proteins (BMPs) is commonly used (Shu *et al.*, 2011; Salazar *et al.,* 2016; Bolander *et al.*, 2016). For BMP2 and BMP7, the respective approvals for clinical use in the bone field have been given. However, BMP7 is being withdrawn from the market (Vukecivic *et al.*, 2014; Gillman and Jayasuriya, 2021). For BMP6, promising results have already been and still are being obtained (Bolander *et al.*, 2016; Pecin *et al.*, 2021) following exploration of its effects on endochondral ossification in fracture repair (Mendes *et al.*, 2016; Freyria and Mallein-Gerin, 2012). BMP2 and BMP6 ligand homodimers both bind to tetrameric complexes of two type-1 and two type-2 receptors of a larger family of TGFβ/BMP serine/threonine kinase receptors (Salazar *et al.,* 2016; Halloran *et al.,* 2020). Examples of ligand-activated type-1 receptors are, and notably here, BMPR-IA (also named ALK3) and BMPR-IB (ALK6) (Aoki *et al.,* 2001). Furthermore, they phosphorylate SMAD1/5/9 (SMAD8 being renamed SMAD9; for reviews, see Schmierer and Hill, 2007; Salazar *et al.,* 2016) and activate effector proteins that act in the nucleus as DNA-binding transcription factors. Of note the ligand-activated receptor complexes also activate downstream non-SMAD signalling involving protein kinases, such as p38MAPK, Erk and Tak1 (Salazar *et al.,* 2016; Aoki *et al.,* 2001; Zhang *et al.,* 2009). For the entire larger subfamily of BMP ligands, the ligand-receptor complex affinities do vary, but overall BMP2 tends to signal via the ALK3 and ALK6 receptor-containing complexes, while BMP6 often binds also to ALK2 receptor-complexes (Heldin and Moustakas, 2016). ALK2 and ALK3 are present throughout cartilage and bone formation, while ALK6 is expressed during chondrogenesis and late osteogenesis, but not during the phase with hypertrophic cartilage (Haaijman *et al.*, 2000; Lin *et al.,* 2016). Furthermore, in mice BMP2 is necessary for endochondral bone formation and fracture repair (as shown by using appropriate conditional and/or cell-type specific knockout mice; Shu *et al.,* 2011; Tsuji *et al.,* 2006), while BMP6 is necessary for periosteal bone formation and the function of the growth plate (as shown in *Bmp6-null* mice; Perry *et al.,* 2008). From this, we infer that both BMP2 and BMP6 are important candidate factors to direct PDCs towards bone formation.

The goal of biomechanical support in the form of scaffolds to the cell-based constructs is to provide a 3D structure where the cells can reside on in treated bone defects. Many materials have been tested for bone tissue engineering purposes, including natural and synthetic polymers. Natural polymers, like those based on proteins (such as gelatin, collagen, fibrin) or polysaccharides (hyaluronic acid, chondroitin sulphate, alginate) are biocompatible and biodegradable. The use of synthetic polymers (polyethylene glycol, polyvinyl alcohol, polyacrylamide) offers high controllability of the end product and adaptable mechanical properties (Li *et al.,* 2018). We investigated the use of three types of constructs. The first one is a collagen-based scaffold with hydroxyapatite (indicated as CopiOs); the second scaffold is gelatin-based and addition of methacryloyl (GelMA) enables subsequent crosslinking by UV-light and further tuning of its physical properties and biodegradability (Agten *et al.*, 2022; Van Den Bulcke *et al.*, 2000). The third type consists of assembled chondrogenic-primed cell aggregates, since these do already form extracellular matrix and circumvent the need for an additional, non-cell-based scaffold (Nilsson Hall *et al.*, 2019). These constructs are compared to data that is already obtained with Nuoss, which are calciumphosphate-based scaffolds (Groeneveldt *et al.,* 2020).

Taken together, in this study we test the bone-forming properties of mandibular-derived hPDCs primed with BMP2 or BMP6, and this in combination with the aforementioned three types of constructs.

6.3. Results

6.3.1. RNA-sequencing of BMP2 and BMP6-primed hPDCs in cell culture

hPDCs obtained from the mandibular periosteum are responsive to BMP2 (from 10 ng/ml) and to BMP6 (100 ng/ml), as documented by increased p-SMAD1/5/9 (**Fig. 6.1A**). Using BMP2 (at 50 ng/ml) and BMP6 (at 100 ng/ml) for 6 hours priming, we obtained the respective profiles of differentially expressed genes (DEGs) as determined by bulk RNA-sequencing (RNA-seq). 73% of the variance in the principal component analysis (PCA) is explained by differences observed between the priming conditions, as revealed by upregulation of Inhibitor Of DNA Binding 1 (*ID1)*, *SMAD1* and Atonal BHLH Transcription Factor 8 (*ATOH8)* (**Fig. 6.1B,C;** see also **Fig. 6.2A,B**). The effects of BMP6 are mostly similar to those of BMP2 as compared to the controls, but for BMP2 more upregulated DEGs are obtained (**Fig. 6.1D**).

Pathways that were upregulated after priming by BMP2 included artery morphogenesis and development, and the top-10 upregulated pathways consisted completely of those involved in ossification and biomineralization, as well as Wnt regulation. Downregulated were pathways like interleukin-10 production (**Fig. 6.1E**). The pathways downregulated after priming by BMP6 compared to hPDCs primed with BMP2, and furthermore notably upregulated in BMP2-primed cells compared to cells without priming, include body morphogenesis, artery development, skeletal system morphogenesis, ossification, and skeletal system development (**Fig. 6.1F**).

Looking at expression levels of individual genes, an upregulation of the early chondrogenic markers *SOX9* and *ACAN* was detected (**Fig. 6.2C,D**). *RUNX2*, a marker for early osteogenesis, was upregulated too (**Fig. 6.2E**), together with *COL1A1* and Secreted Protein Acidic And Cysteine Rich (*SPARC;* **Fig. 6.2F,G**). From this, we conclude that in cultured hPDCs BMP2 was able to upregulate higher numbers of important pathways as well as genes for bone regeneration, when compared to BMP6.

6.3.2. Knockdown studies

We have previously shown that mandibular hPDCs have the capacity to form bone tissue ectopically *in vivo,* while maxillary hPDCs lacked this property (Groeneveldt *et al.*, 2020). In this context, we noticed *DLX5* and *DLX6* as interesting DEGs and well-established BMP-responsive genes (Luo *et al.,* 2001; Ohta *et al.,* 2016). Our prioritized interest in *DLX5* and *DLX6* also comes from research by others into epigenetic signatures, further concluding that cells that are capable to form endochondral bone tissue *in vivo* showed a high upregulation for *DLX5* and *DLX6* (Hochmann *et al.,* 2023). Our mandibular hPDCs expressed both genes at high level, while maxillary-derived hPDCs did not express them. *DLX5* and *DLX6* are important for bone formation, since their dual genetic inactivation results in severe craniofacial, axial and appendicular skeletal abnormalities, ultimately leading to perinatal lethality (Robledo *et al.*, 2002). *DLX5* is known to act early downstream of the BMP-cascade as a transcriptional activator in the nucleus, stimulating the cells towards osteogenic differentiation. After priming with BMP2 or BMP6, the expression of both these *DLX* genes was markedly higher (see **Fig. 5.2H,I**).

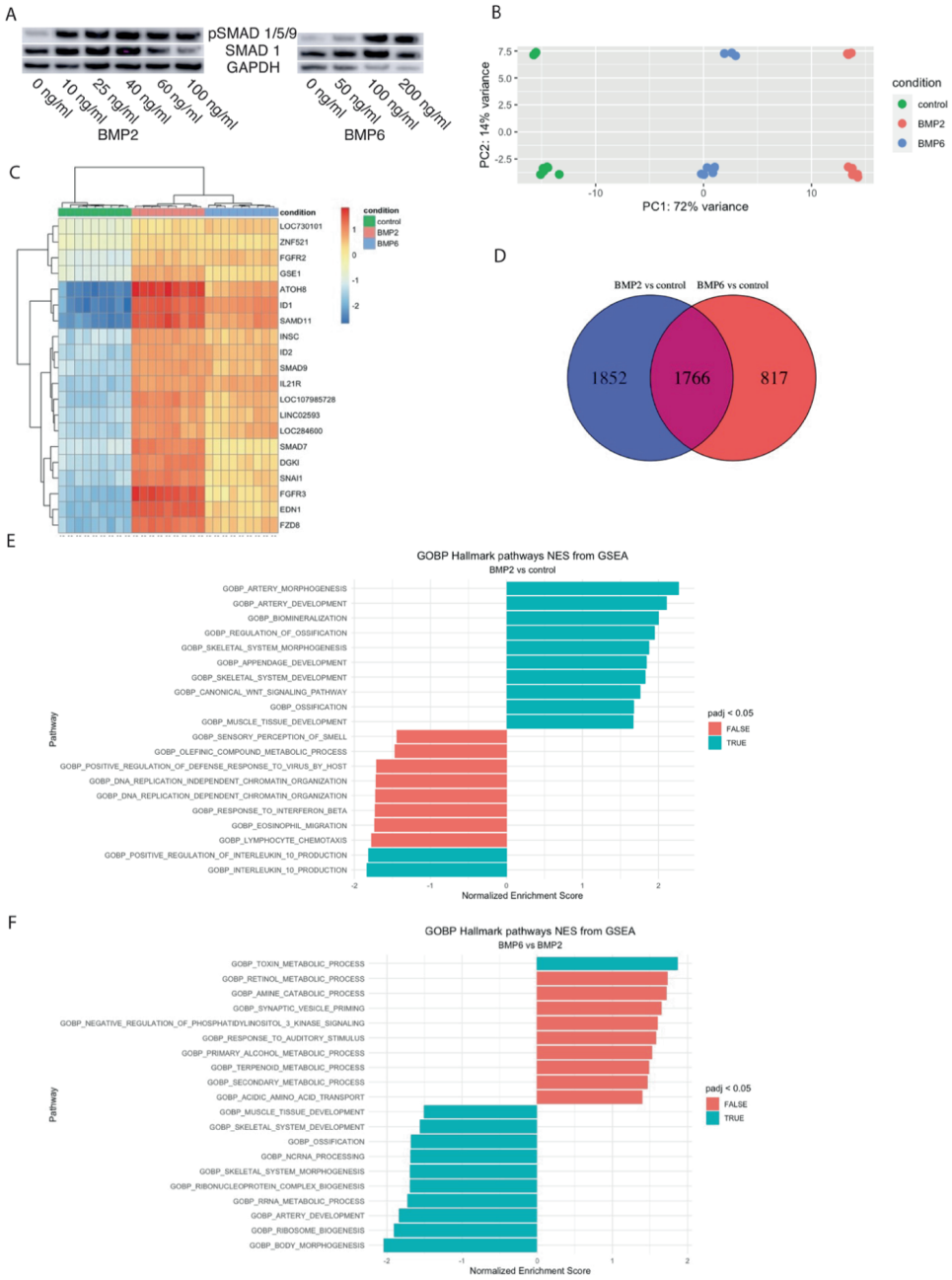

Figure 6.1. RNA-seq profiling of BMP2 and BMP6 primed hPDCs in cell culture.

(A) Western blot in hPDC extracts. The cells were primed with different doses of BMP2 or BMP6; results are shown for p-SMAD1/5/9, total SMAD and control GAPDH, respectively. **(B)** PCA showing the variance between the treatment groups. **(C)** Heatmap showing up (in red) and down (in blue) regulated genes. **(D)** Venn diagram of the number of statistically significant (padj<0.05) upregulated genes. **(E)** Gene-set enrichment analysis (GSEA) for the comparison of hPDCs treated with BMP2 versus control or **(F)** BMP6 versus BMP2.

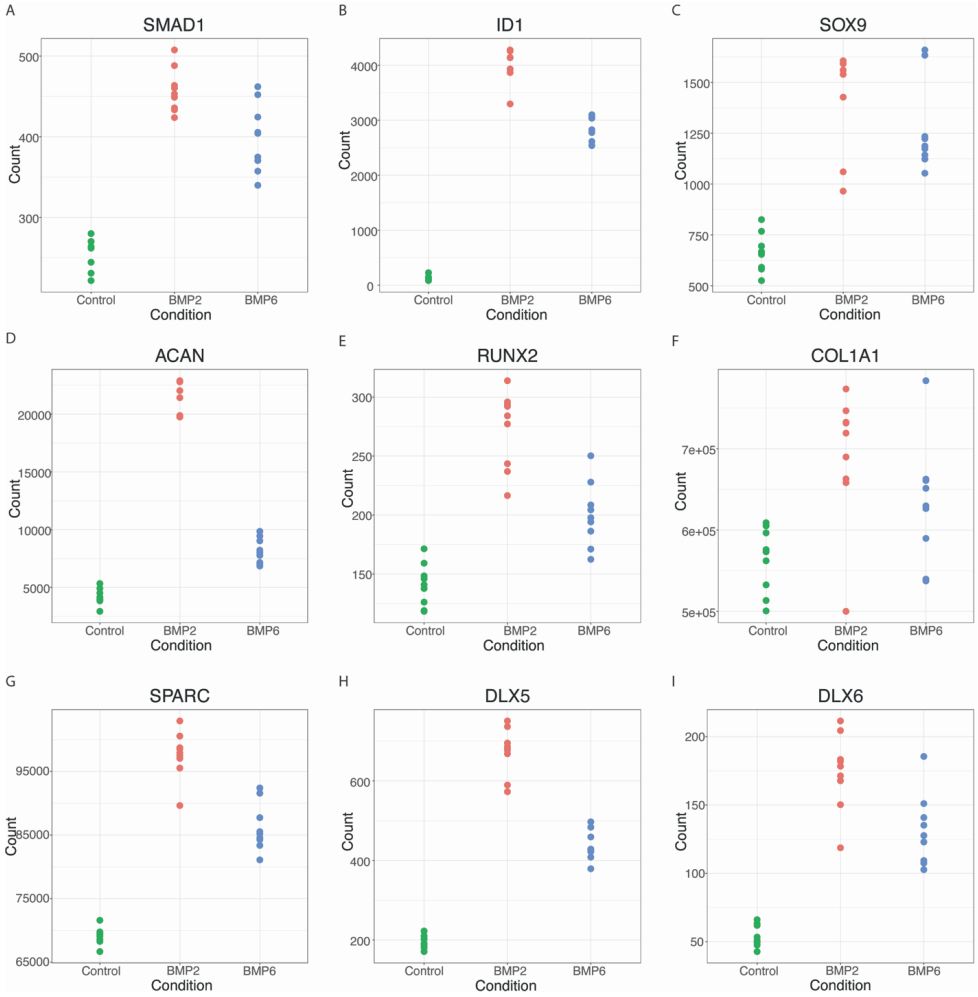

Figure 6.2. Comparative expression levels of individual genes in unprimed (control) or BMP-primed mandibular hPDCs based on RNA-seq.

Expression level of **(A)** SMAD1, **(B)** ID1, **(C)** SOX9, **(D)** ACAN, **(E)** RUNX2, **(F)** COL1A1, **(G)** SPARC, **(H)** DLX5 and **(I)** DLX6 on mandibular hPDCs after expansion in DMEM-C unprimed (control) or after priming with BMP2 or BMP6 at PD = 10, *n* = 3 in biological duplicates for each origin.

Hence, we proceeded with DLX5 and DLX6 knockdown using siRNAs, reaching 70% (for DLX5) and 80% (for DLX6) reduction of their expression (**Fig. 6.3A,B**). The upregulation of *ID1*, a well-established BMP-SMAD target gene in most cell types, and seen in the bulk RNA-seq too, was confirmed by RT-qPCR after priming with BMPs (**Fig. 6.3C**). However, this effect was even more prominent after DLX5 or DLX6 knockdown (**Fig. 6.3D**).

In addition, a negative feedback of the added BMP2 on the expression of its own gene is seen after 6 hours (**Fig. 6.3E**). A drop in *BMP2* expression is also seen after knockdown of *DLX5*, suggesting a stronger negative feedback by factors likely acting epistatically between BMP2 addition and DLX5 action response, while for *BMP6* an upregulation was seen when BMP2 and

BMP6 were combined (**Fig. 6.3F; Fig. S6.1A**). *SOX9* expression increased after priming with BMP; for BMP2 this is even more the case than for BMP6 (**Fig. 6.3G**), while knockdown of *DLX5* or *DLX6* did not influence *SOX9* expression (**Fig. 6.3H**). A similar response was seen for known BMP-responsive genes such as *MSX1* and *RUNX2* (Vieux-Rochas *et al.,* 2013; Phimphilai *et al.,* 2006) (**Fig. 6.3I, J**), however no differences were observed for *MSX2* (**Fig. S6.1B**).

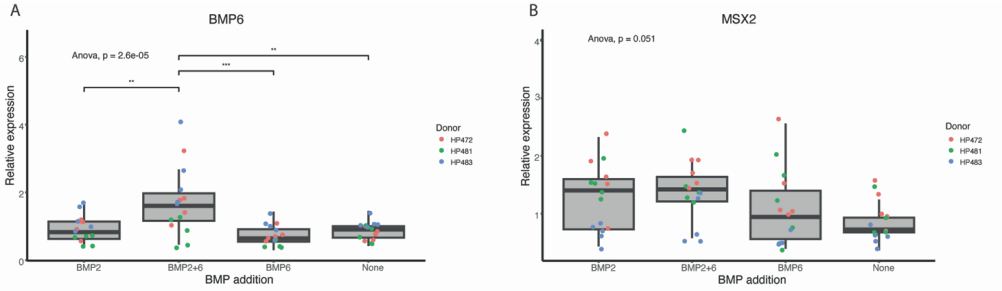

Figure S6.1. Gene expression levels after knockdown of DLX5 and/or DLX6, including in BMP2 and/or BMP6 priming conditions.

RT-qPCR data for the expression of **(A)** *BMP6* and **(B)** *MSX* transcripts after siRNA-treatment and priming with BMP2, BMP2 in combination with BMP6, BMP6 alone or none.

6.3.3. *In vivo* ectopic bone formation

Mandibular hPDCs were first cultured in DMEM + 10% FBS (see Materials and Methods) for proliferation and then seeded on NuOss scaffolds, BMP6-loaded CopiOs scaffolds, suspended in 10% GelMA together with BMP6, or cultured as spheroids for 21 days in presence of BMP2 and BMP6 and thereafter assembled in aggregates, respectively. Those respective construct types were implanted ectopically (see Materials and Methods), and CT-scans were then made after explantation at 8 weeks (**Fig. 6.4A-F**). The highest bone volumes were obtained using constructs consisting of CopiOs + 1.6 mg of BMP2/scaffold (**Fig 6.4G**). Histological analysis after haematoxylin/eosin staining showed no bone-like tissue formation using NuOss constructs or the GelMA-construct primed with BMP2 (**Fig. 6.4L,M**). The constructs consisting of CopiOs or aggregates showed bone had formed including signs of a bone marrow compartment (**Fig. 6.4H-J**). It should be noted that the bone-like tissue formation seen in the GelMA+BMP6 construct , is located outside the GelMA construct itself (**Fig. 6.4K**).

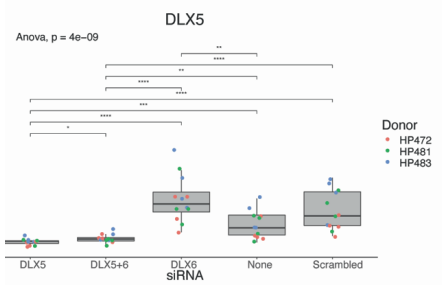
DLX5
Anova, p = 4e−09
Relative expression
DLX5
DLX5+6
DLX6
None
Scrambled
siRNA
Donor
HP472
HP481
HP483

B

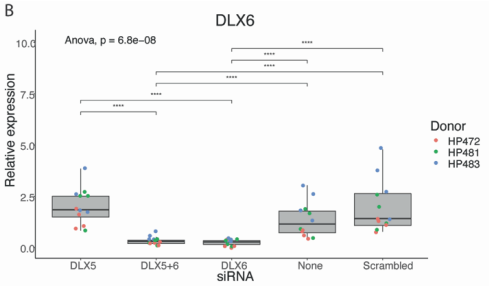
DLX6
Anova, p = 6.8e−08
Relative expression
10.0
7.5
5.0
2.5
0.0
DLX5
DLX5+6
DLX6
None
Scrambled
siRNA
Donor
HP472
HP481
HP483

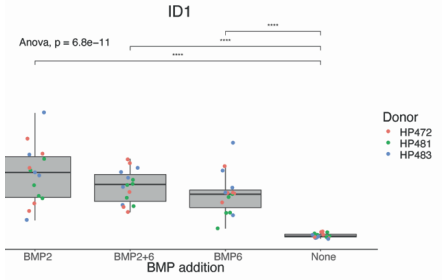
ID1
Anova, p = 6.8e−11
Relative expression
BMP2
BMP2+6
BMP6
None
BMP addition
Donor
HP472
HP481
HP483

D

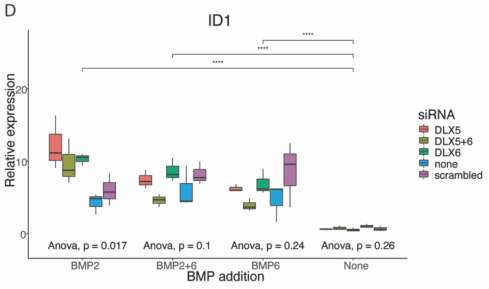
ID1
Relative expression
20
10
0
Anova, p = 0.017
Anova, p = 0.1
Anova, p = 0.24
Anova, p = 0.26
BMP2
BMP2+6
BMP6
None
BMP addition
siRNA
DLX5
DLX5+6
DLX6
none
scrambled

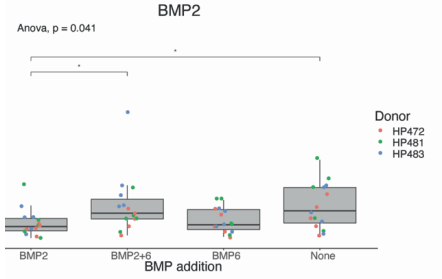
BMP2
Anova, p = 0.041
BMP2
BMP2+6
BMP6
None
BMP addition
Donor
HP472
HP481
HP483

F

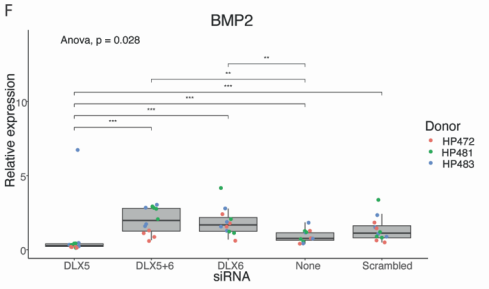
BMP2
Anova, p = 0.028
Relative expression
10
5
0
DLX5
DLX5+6
DLX6
None
Scrambled
siRNA
Donor
HP472
HP481
HP483

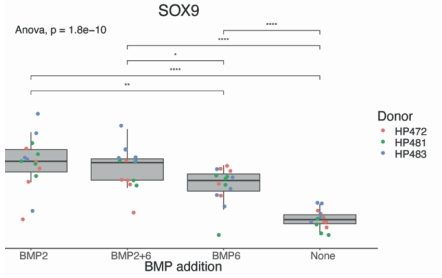
SOX9
Anova, p = 1.8e−10
BMP2
BMP2+6
BMP6
None
BMP addition
Donor
HP472
HP481
HP483

H

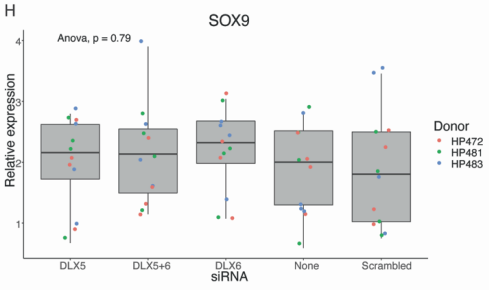
SOX9
Anova, p = 0.79
Relative expression
4
3
2
1
DLX5
DLX5+6
DLX6
None
Scrambled
siRNA
Donor
HP472
HP481
HP483

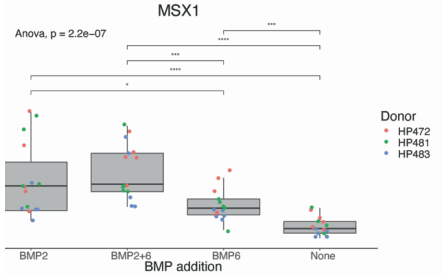
MSX1
Anova, p = 2.2e−07
BMP2
BMP2+6
BMP6
None
BMP addition
Donor
HP472
HP481
HP483

J

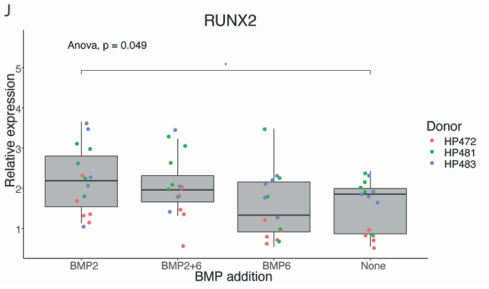
RUNX2
Anova, p = 0.049
Relative expression
5
4
3
2
1
BMP2
BMP2+6
BMP6
None
BMP addition
Donor
HP472
HP481
HP483

Figure 6.3. (***previous page***). **Gene expression levels after knockdown of DLX5 and/or DLX6, including in BMP2 and/or BMP6 priming conditions.** RT-qPCR data for the expression of **(A)** *DLX5* and **(B)** *DLX6* transcripts after siRNA-treatment. **(C,D)** *ID1* expression levels shown for individual or combinatorial priming with BMPs, as well as upon DLX-targeting siRNA. **(E,F)** *BMP2* expression shown for each BMP-priming method and for DLX knockdown. **(G,H)** Same as in E+F, for *SOX9* and for priming with BMP for **(I)** *MSX1* (BMP-priming) and **(J)** *RUNX2*. Pairwise comparisons were made by Wilcoxon test + Bonferroni correction for multiple testing. * p<0.05, **p<0.01, ***p<0.001, **** p<0.0001, n=3 donors.

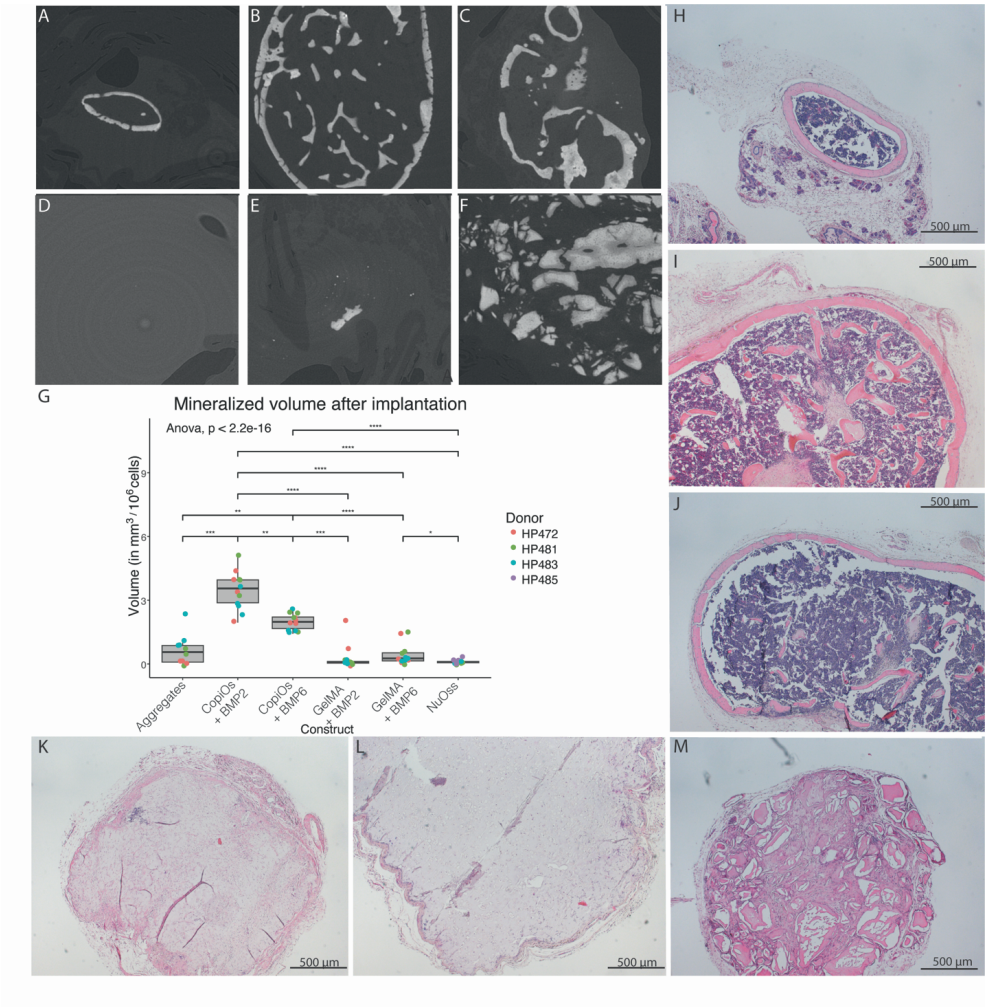

Figure 6.4. ***In vivo*** **bone formation results 8 weeks after implantation of constructs.**

(A-F) NanoCT images of the constructs consisting of aggregates (A), CopiOs with BMP2-priming (B), CopiOs with BMP6-priming (C), GelMA including BMP2 (D), GelMA including BMP6 (E), and NuOss (F). **(G)** Measurement of mineralized volume based on nanoCT-images, comparisons made per 1,000,000 cells. **(H-M)** HE stainings of the constructs based on aggregates (H), CopiOs with BMP2-priming (I), CopiOs with BMP6-priming (J), GelMA including BMP2 (K), GelMA including BMP6 (L), and NuOss (M). Pairwise comparisons were made by Wilcoxon test + Bonferroni correction for multiple testing. * p<0.05, **p<0.01, ***p<0.001, **** p<0.0001, n=3 donors for technical quadruplicates.

6.4. Discussion

Bone tissue engineering approaches using cell-based constructs have increasingly focused on selecting the best body location source(s) and cell status/lineage origin(s). Bone-marrow-derived SSPCs (BM-SSPCs) have gotten much of the initial attention. However, periosteal-derived SSPCs have become important because they are involved in fracture repair *in vivo*, as shown by a transplantation study using fluorescent labelled cells (Duchamp de Lageneste *et al.*, 2018). Hence, hPDCs have gained prime attention for bone tissue engineering purpose (Colnot *et al.*, 2012; de Bari *et al.*, 2006; van Gastel *et al.*, 2012; Roberts *et al.,* 2015; Bolander *et al.,* 2020). We have previously obtained hPDCs from maxilla and mandible, and compared these to hPDCs from tibia, the latter being the more routine source in the field (Groeneveldt *et al.,* 2020). Mandibular hPDCs were shown to be a promising source of *ex vivo* expandable cells included in bone tissue engineering constructs intended for promotion of bone-tissue formation in the craniofacial area. The respective gene expression profiles also revealed *DLX5* and *DLX6* among the top DEGs in mandibular hPDCs, and the relevance of both *DLX* gene family members to the bone forming process has been convincingly demonstrated (Robledo *et al.*, 2002). In order to further optimise the *in vivo* bone-forming capacity of cultured mandibular hPDCs, we tested priming methods with BMP2 and/or BMP6, and applied such cells in 3 different types of construct, comparing each of these preparations to cells seeded on a NuOss construct without prior treatment by BMPs.

Bulk RNA-seq revealed a higher potential for BMP2 than BMP6 with respect to stimulating cells towards bone regenerative pathways. The number of upregulated genes for BMP2-primed cells was higher, while the GO-terms that came up for BMP2-treated cells involved mostly bone developmental/regenerative pathways such as skeletal system development, ossification and biomineralization. Well-established marker genes for chondrogenic and osteogenic differentiation were upregulated to higher expression levels after priming with BMP2 compared to BMP6.

Upon *DLX5* and/or *DLX6* knockdown, an upregulation of *ID1* was seen. *ID1* is a directly induced BMP-SMAD-dependent target gene, whereas *DLX5* has been proposed to act downstream of p38 kinase phosphorylation. This gene also gets activated by BMP, resulting in upregulation of *OSX,* encoding a DNA-binding zinc-finger transcription factor also known as Sp7, which regulates the expression of a set of ECM proteins. Those ECM proteins are involved in BMP-induced terminal osteoblast differentiation (Hojo and Ohba, 2022; Ludwig *et al.*, 2022; for a recent review, see Wang *et al.,* 2023). Furthermore, *DLX5* also stimulates the intramembranous ossification (Ulsamer *et al.,* 2008; Sinha and Zhou, 2013). *SOX9,* which promotes chondrogenic differentiation of osteo/chondro-progenitors, was also upregulated by BMPs, most prominently by BMP2. This can occur again by the p38 pathway, but *SOX9* can also be up regulated by p-SMADs, bypassing *DLX5*-dependent activation (Pan *et al.*, 2008; Vu *et al.*, 2021).

In vivo tests showed a higher capacity for BMP2-containing CopiOs to form ectopic bone compared to the same scaffolds containing BMP6. This is opposite to reports from Vukicevic and co-workers. A possible explanation is that they have tested BMP6 only *in vivo* and did so in other types of construct than ours (Vukicevic *et al.*, 2014). We also observe differences in DEGs between BMP2 and BMP6 addition, even in conditions of comparable p-SMAD1/5/9 status. Moreover, we report big differences in the bone-forming capabilities of the construct types, depending on the scaffold that was used. Noteworthy, in the GelMA constructs, more mineralisation was seen in the constructs primed with BMP6 when compared to BMP2. However, this mineralisation occurred outside the GelMA construct, and could thus possibly result from stimulation of the neighbouring cells of the host tissue by BMPs released from the carrier material.

To conclude, priming of mandibular hPDCs with BMP2 showed more upregulation of genes involved in skeletal system development and fracture repair and showed the best bone forming properties *in vivo* after ectopic implantation when used in combination with a CopiOs collagen-based scaffold.

6.5. Experimental procedures

Isolation and culture of hPDCs

The mandibular samples were harvested by maxillofacial surgeons after informed consent was obtained (Belgian registration number B322201731127) as described previously (Groeneveldt *et al.*, 2020). These samples were digested in medium consisting of Dulbecco's modified Eagle's medium (DMEM) supplemented with 10% Fetal Bovine Serum (FBS; Thermo Fisher Scientific, Waltham, MA, United States) and 1% antibiotics-antimycotics solution (100 units penicillin/ml, 100 µg streptomycin/ml and 0.25 µg amphotericin-B/ml; Invitrogen), from here on referred to as DMEM-complete (DMEM-C), in addition of 4,400 units per 10 ml Collagenase type-IV (Gibco) under constant agitation for 16 h. Cells were from then on cultured in DMEM-C. Population doublings (PD) of these human PDCs (hPDCs) were calculated upon passaging using the formula $\log_2(n_2)-\log_2(n_1)$, with n_1 representing the number of cells seeded in the dish/flask and n_2 the number of cells obtained after trypsinization (TrypLE, Thermo Fisher Scientific) of cells from the same dish/flask at 90% confluency.

Priming with BMP2 or BMP6 in cell culture

BMP2 or BMP6-priming was performed on hPDCs obtained from 3 different patients, cultured in DMEM-C at a density of 200,000 cells/ well of a 6-well plate, when a cumulative PD~10 was reached. Then the selected doses of BMP2 (Medtronic) or BMP6 (Peprotech) were added after 16 hours of serum deprivation consisting of DMEM and 1% antibiotics-antimycotics solution, and read-out 6 hours after stimulation with BMP. For western blot read-outs, multiple doses were selected for BMP2 (0, 10, 25, 40, 60 and 100 ng/ml) and BMP6 (0, 50, 100 and 200 ng/ml). For RNA isolation, 50 ng BMP2/ml or 100 ng BMP6/ml were used.

Protein extraction and western blots

Proteins were obtained using a cell extraction buffer (CEB) (ThermoFisher Scientific) containing 0.03 mM phenylmethylsulfonyl fluoride (PMSF), 4.66 mM sodium fluoride (NaF), 0.25 mM sodium orthovanadate (Na_3VO_4) and protease inhibitor cocktail (PIC) (Sigma-Aldrich, Bornem, BE). Protein quantification was performed using the BCA Protein assay kit (Pierce). Equal protein quantities were loaded on a NuPAGE 4-12% Bis-Tris Gel (Invitrogen) and electrophoresed in a running buffer containing 5% NuPAGE MES (Invitrogen). These proteins were transferred to a Polyvinylidene fluoride (PVDF) membrane by wet transfer; the transfer buffer contained 40 mM glycine, 50 mM Tris base, 1 mM SDS, 10% methanol and 0.1% antioxidant (ThermoFisher Scientific). Primary antibodies were diluted 1:1000. Rabbit polyclonal phospho-SMAD1 (Ser463/465)/SMAD5 (Ser463/465)/SMAD8 (Ser426/428)(9516), rabbit polyclonal SMAD1 (6944) (Cell Signalling, Leiden, NL), mouse monoclonal glyceraldehyde-3-phosphate dehydrogenase (Abcam), HRP-conjugated secondary antibodies were each used at 1:2000 dilution (Jackson, Pennsylvania, US); SuperSignal® West Femto (Thermo Scientific) was used as substrate. For development of the images, a LAS3000 Imaging System (FUJI) was used.

RNA isolation, RNA-sequencing, cDNA synthesis and quantitative PCR

Cells were rinsed twice in PBS, lysed by adding 350 µl of RLT buffer (Qiagen) containing 1% β-mercaptoethanol (Sigma Aldrich) per well, and homogenized by thoroughly pipetting up and down. Samples were directly placed on ice and frozen at −80°C until further processing. The Qiagen RNeasy mini kit was used to isolate RNA. RNA-seq was performed on samples from 3 different donors (*i.e.* HP472, HP481 and HP483) after treatment with 50 ng BMP2/ml, 100 ng BMP6/ml or no added BMP, each in triplicate.

cDNA libraries were generated using the Illumina TruSeq Stranded mRNA Library Prep Kit. These libraries were then sequenced (50-bp lengths) according to the Illumina TruSeq Rapid v2 protocol in 5 runs, using 2 lanes per run, on an Illumina HiSeq 2500 sequencer. Low-quality reads and contaminants (*e.g.*, sequence adapters) were removed using Trimmomatic (Bolger et al., 2014). Sequences were then aligned to the GRCh38 genome using STAR (version 2.7.9a) (Dobin *et al.*, 2013), and counts were obtained using samtools and GNU Parallel (Danecek *et al.*, 2021). Normalization of the data and differentially expressed genes (DEGs) were listed using the edgeR v.3.34.1 (Chen *et al.,* 2016) and DESeq2 v.1.32.0 packages (Love *et al,.* 2014).

Correction for batch-effect caused by the donors was performed by using the Surrogate Variable Analysis (sva) v.3.40.0 package (Leek *et al*, 2022). GeneSetEnrichment scores were calculated based on the fgsea v.1.18.0 package (Korotkevich *et al.*, 2019)

Silencing of target proteins

For knockdown of DLX5 and/or DLX6, siRNAs were used: for DLX5, a combination of pre-designed siRNAs (s4148 and s534292) was used, for DLX6, the combination consisted of s4149 and s223427. We used Lipofectamine™ RNAiMAX Transfection Reagent and opti-MEM (all from Thermofisher) according to manufacturer's protocol/dose recommendations. As controls, cells cultured in DMEM-C and treated with Select Negative Control No. 1 siRNA (Thermofisher) were used. Cells cultured in DMEM-C without scrambled siRNAs were used as a blanc control. After 4 hours, the opti-MEM medium including siRNAs was replaced by DMEM-C. 28 hours later, the DMEM-C was replaced for DMEM including 1% antibiotics/antimycotics, but without FBS for overnight serum starvation and 50 ng BMP2/ml or 100 ng BMP6/ml were added. After 6 hours, RNA isolation was carried out as described above.

cDNA was obtained by reverse transcription of 500 ng of total RNA, using the PrimeScript™ RT Reagent Kit (Takara Bio) according to manufacturer's manual. For RT-qPCR, primers were designed for mRNAs of BMP2, BMP6, Distal-Less Homeobox-5 (DLX5), Distal-Less Homeobox-6 (DLX6), Msh Homeobox-1 (MSX1), Msh Homeobox-2 (MSX2), SRY (sex determining region Y)-box-9 (SOX9), Runt-related transcription factor-2 (RUNX2), Inhibitor of DNA Binding-1 (ID1), Tumor Protein P63 (TP63) and BMP Binding Endothelial Regulator (BMPER) (Thermofisher). Samples were processed and measured in technical triplicates on a Rotor Gene® 6000 PCR machine (Qiagen) using a SYBR Green detection system (Takara Bio) according to the manufacturer's instructions, and normalizing using hypoxanthine phosphoribosyltransferase-1 (HPRT1). The respective primer sequences are listed in **Table S6.1**.

***In vivo* ectopic bone formation**

After proliferation, cells were seeded on NuOss or CopiOs scaffolds or seeded in agarwells for differentiation. For the NuOss constructs, 10^6 cells suspended in 25 µl of DMEM-C were seeded on the scaffolds (21 mm^3; ACEuropa). One hour after seeding, an additional 5 ml of DMEM-C was added. After overnight incubation at 37°C and 5% CO2, scaffolds were implanted. For the CopiOs constructs, 20 µl DMEM containing 1,6 µg of BMP2 or 3,2 µg of BMP6 was loaded per construct. After 1 hour, 10^6 cells in 25 µl of DMEM-C were seeded on the primed scaffolds (Zimmer). An hour later, an additional of 5 ml DMEM-C was added and 4 hours after seeding, the scaffolds were implanted. For the GelMA constructs, 10% bovine GelMA constructs were made with a bloom strength of 225 and the degree of functionalization of 85% derived from bovine type B gelatin (Agten *et al.,* 2022), size 3x3x3 mm, containing each 10^6 cells and 1.6 µg BMP2 or 3.2 µg BMP6 and incubated overnight at 37°C and 5% CO2 in 5 ml DMEM-C.

For the microaggregates, 300,000 cells were seeded per well in an AggreWell 800 platform (STEMCELL Technologies) after coating with an anti-adherence rinsing solution according to manufacturer's instructions. Cells were cultures for 21 days in a differentiation medium of LG-DMEM (Gibco) containing 1% antibiotic-antimycotics solution (100 units penicillin/ml, 100 µg streptomycin/ml and 0.25 µg amphotericin-B/ml; Invitrogen), 1mM ascorbate-2 phosphate (Sigma), 40 µg proline/ml (Sigma), 1% ITS + (Corning), 100 nM dexamethasone (Sigma), 20 µM Rho-kinase inhibitor Y27632 (Axon Medchem), 100 ng BMP2/ml (Medtronic), 10 ng TGFβ1/ml (Peprotech), 100 ng GDF5/ml (Peprotech), 1 ng BMP6/ml (Peprotech) and 0,2 ng FGF2/ml (Peprotech) (Mendes *et al.*, 2016). Half of the media was carefully replaced twice a week. After differentiation, the macrotissues were formed by combining 3 wells with spheroids into a macrowell formed by a PCR-tube in 3% agarose (Invitrogen) in the same differentiation medium. After 24 hours, those tissues were implanted.

The structures were randomly implanted subcutaneously over the available mice in quadruplicates with a maximum of 4 for each mouse at the shoulder and the back in the limb region of 8-week-old female NMRI nu/nu mice (Janvier). All animal procedures were approved by the local ethical committee for Animal Research (KU Leuven, P037-2020). The animals were housed according to the guidelines of the Animal Facilities at Leuven (KU Leuven). Explants were harvested after 8 weeks.

***In vivo* orthotopic bone formation**

Mandibular bone defects were created with a 6mm outer diameter trephine bur (Henry Schein) in adult (12-14 weeks old) Hsd:RH-Foxn1rnu rats (Envigo). In those bone defects the structure consisting of CopiOs (5mm punchout) in addition of 3,8 mg BMP2 and $2{,}4*10^6$ cells was implanted after 4 hours incubation. The structure was made as described above for the ectopic bone formation test. The procedure was performed under general anesthesia with intraperitoneal ketamine/xylazine and vetergesic as painkiller. After 0, 4 and

8 weeks, *in vivo* CT-scans were made under inhalation anesthesia with isoflurane. Explantation of the mandible was done 8 weeks after surgery and an additional micro-CT imaging procedure was performed on them. The animal procedures were approved by the local ethical committee for Animal Research (KU Leuven, P037-2020), animals were housed according to the guidelines of the Animal Facilities at Leuven (KU Leuven).

CT analysis

Bone formation was analysed using the Phoenix NanoTom S CT system (GE measurement) at a voltage of 60 kV and a current of 200 mA. An aluminium filter of 1 mm was used to filter out the low energetic radiation. CTAn and Batch Manager Software programs (Bruker micro-CT, Kontich, Belgium) were used for 3-D quantification of the bone volume and calcium phosphate (CaP) grains of the NuOss scaffold. A three-level automatic Otsu segmentation algorithm was used to segment the newly formed bone tissue and CaP-grains from the background in combination with manually chosen thresholds. For CopiOs, gelMA and macroaggregtes, only segmentation between newly formed bone tissue and background was necessary. Noise was reduced by removing black and white speckles smaller than 200 voxels and a closing operation of 2 voxels was performed to solidify the resulting structure, providing binarized images suitable for the 3-D analysis (Kerckhofs *et al.,* 2013).

Histology

After decalcification in EDTA, dehydration through a series of graded ethanol, embedding in paraffin, and sectioning in 5-µm thick slices, histological stainings were carried out. Staining with hematoxylin and eosin (H&E) was done by a dip in hematoxylin-solution for 2 min, followed by a brief wash in water, and subsequently staining in 1% Eosin (Klinipath, Duiven, Netherlands) for 7 min.

For Alcian Blue staining, samples were rehydrated, stained for 30 min in 0.5% Alcian Blue (Roth) solution in 1 M HCl (pH = 1). Nuclear Fast Red (Vector) was used for staining of the nuclei during 5 min. For staining with Safranin O, samples were dipped in acidic alcohol (1% HCl in 70% ethanol). Next, they were placed in Fast Green (Klinipath) for 3 min, dipped in 1% acetic acid and then stained in 0.1% Safranin O (Sigma Aldrich) for 10 min. Masson's trichrome staining was performed using Bouin's solution (Sigma Aldrich) as mordant followed by 5-minute-dips in Weigert's Iron Hematocxylin Solution, Biebrich Scarlet-Acid Fuchsin, Phosphotungstic/ Phosphomolybdic Acid Solution and Aniline Blue Solution (all from Sigma Aldrich), followed by a dip in 1% acetic acid for 2 min. The sections were cleared in HistoClear (National-Diagnostics) and mounted in Pertex (Histolab). Pictures were made using the IX83 microscope (Olympus).

Statistical Analysis

Statistical analysis for cellular senescence, quantitative PCR and *in vivo* bone formation was done using the Kruskal-Wallis test. In case $p < 0.05$ for Kruskal-Wallis, a two-sided Wilcoxon test was performed. The Bonferroni correction was used to correct for multiple testing. All statistical analyses were performed in R (version 4.1.1). Results were considered statistically significant at $p < 0.05$. Data are presented typed as mean values ± standard deviation (SD) or as boxplots with median and interquartile range.

Supplementary table

Table S6.1: Primer sequences used for RT-qPCR.

Gene	Forward	Reverse
BMP2	GGAACGGACATTCGGTCCTT	CACCATGGTCGACCTTTAGGA
BMP6	GCTCAACCGCAAGAGCCTTC	TGTCGTACTCCACCAGGTTC
BMPER	GCTTGTGTGAAAGGCAGGAC	TTGAGAATTTTGCCCTGTGGG
DLX5	CACGGCTACTGCTCTCCTAC	CTTCTTTCTCTGGCTGGTTGGTG
DLX6	GAGGGGACGACACAGATCA	GTTCGGCTCTCTCTGGAAGG
HPRT	TGAGGATTTGGAAAGGGTGT	GAGCACACAGAGGGCTACAA
ID1	AATCCGAAGTTGGAACCCCC	GATCTGGATCTCACCTCGGC
MSX1	TCCGCAAACACAAGACGAAC	TACTGCTTCTGGCGGAACTT
MSX2	TTCAGAAGATGGAGCGGCGT	TCATATGTCCTCCTACTCCTGCC
RUNX2	CGCATTCCTCATCCCAGTAT	GCCTGGGGTCTGTAATCTGA
SOX9	TGGAGACTTCTGAACGAGAGC	CGTTCTTCACCGACTTCCTC
TP63	GGAAACCAGAGATGGGCAAG	TCGTACCATCACCGTTCTTTG

Literature references

Agten H, Van Hoven I, Viseu SR, Van Hoorick J, Van Vlierberghe S, Luyten FP, Bloemen V. In vitro and in vivo evaluation of 3D constructs engineered with human iPSC-derived chondrocytes in gelatin methacryloyl hydrogel. Biotechnol Bioeng. 2022 Oct;119(10):2950-2963.

Aoki H, Fujii M, Imamura T, Yagi K, Takehara K, Kato M, Miyazono K. Synergistic effects of different bone morphogenetic protein type I receptors on alkaline phosphatase induction. J Cell Sci. 2001 Apr;114(Pt 8):1483-1489.

Arrington ED, Smith WJ, Chambers HG, Bucknell AL, Davino NA. Complications of iliac crest bone graft harvesting. Clin Orthop Relat Res. 1996 Aug;(329):300-309.

Bolander J, Chai YC, Geris L, Schrooten J, Lambrechts D, Roberts SJ, Luyten FP. Early BMP, Wnt and Ca(2+)/PKC pathway activation predicts the bone forming capacity of periosteal cells in combination with calcium phosphates. Biomaterials. 2016 Apr;86:106-118.

Bolander J, Herpelinck T, Chaklader M, Gklava C, Geris L, Luyten FP. Single-cell characterization and metabolic profiling of in vitro cultured human skeletal progenitors with enhanced in vivo bone forming capacity. Stem Cells Transl Med. 2020 Mar;9(3):389-402.

Bolger AM, Lohse M, Usadel B. Trimmomatic: a flexible trimmer for Illumina sequence data. Bioinformatics. 2014 Aug 1;30(15):2114-2120.

Chen Y, Lun AT, Smyth GK. From reads to genes to pathways: differential expression analysis of RNA-Seq experiments using Rsubread and the edgeR quasi-likelihood pipeline. F1000Res. 2016 Jun 20;5:1438.

Colnot C, Zhang X, Knothe Tate ML. Current insights on the regenerative potential of the periosteum: molecular, cellular, and endogenous engineering approaches. J Orthop Res. 2012 Dec;30(12):1869-1878.

Danecek P, Bonfield JK, Liddle J, Marshall J, Ohan V, Pollard MO, Whitwham A, Keane T, McCarthy SA, Davies RM, Li H. Twelve years of SAMtools and BCFtools. Gigascience. 2021 Feb 16;10(2):giab008.

de Bari C, Dell'Accio F, Vanlauwe J, Eyckmans J, Khan IM, Archer CW, Jones EA, McGonagle D, Mitsiadis TA, Pitzalis C, Luyten FP. Mesenchymal multipotency of adult human periosteal cells demonstrated by single-cell lineage analysis. Arthritis Rheum. 2006 Apr;54(4):1209-1221.

Dobin A, Davis CA, Schlesinger F, Drenkow J, Zaleski C, Jha S, Batut P, Chaisson M, Gingeras TR. STAR: ultrafast universal RNA-seq aligner. Bioinformatics. 2013 Jan 1;29(1):15-21.

Dominici M, Le Blanc K, Mueller I, Slaper-Cortenbach I, Marini F, Krause D, Deans R, Keating A, Prockop Dj, Horwitz E. Minimal criteria for defining multipotent mesenchymal stromal cells. The International Society for Cellular Therapy position statement. Cytotherapy. 2006;8(4):315-317.

Duchamp de Lageneste O, Julien A, Abou-Khalil R, Frangi G, Carvalho C, Cagnard N, Cordier C, Conway SJ, Colnot C. Periosteum contains skeletal stem cells with high bone regenerative potential controlled by Periostin. Nat Commun. 2018 Feb 22;9(1):773.

Freyria AM, Mallein-Gerin F. Chondrocytes or adult stem cells for cartilage repair: the indisputable role of growth factors. Injury. 2012 Mar;43(3):259-265.

Gillman CE, Jayasuriya AC. FDA-approved bone grafts and bone graft substitute devices in bone regeneration. Mater Sci Eng C Mater Biol Appl. 2021 Nov;130:112466.

Groeneveldt LC, Herpelinck T, Maréchal M, Politis C, van IJcken WFJ, Huylebroeck D, Geris L, Mulugeta E, Luyten FP. The bone-forming properties of periosteum-derived cells differ between harvest sites. Front Cell Dev Biol. 2020 Nov 25;8:554984.

Haaijman A, Burger EH, Goei SW, Nelles L, ten Dijke P, Huylebroeck D, Bronckers AL. Correlation between ALK-6 (BMPR-IB) distribution and responsiveness to osteogenic protein-1 (BMP-7) in embryonic mouse bone rudiments. Growth Factors. 2000;17(3):177-192.

Halloran D, Durbano HW, Nohe A. Bone Morphogenetic Protein-2 in Development and Bone Homeostasis. J Dev Biol. 2020 Sep 13;8(3):19. doi: 10.3390/jdb8030019. PMID: 32933207; PMCID: PMC7557435.

Heldin CH, Moustakas A. Signaling Receptors for TGF-β Family Members. Cold Spring Harb Perspect Biol. 2016 Aug 1;8(8):a022053

Hochmann S, Ou K, Poupardin R, Mittermeir M, Textor M, Ali S, Wolf M, Ellinghaus A, Jacobi D, Elmiger JAJ, Donsante S, Riminucci M, Schäfer R, Kornak U, Klein O, Schallmoser K, Schmidt-Bleek K, Duda GN, Polansky JK, Geissler S, Strunk D. The enhancer landscape predetermines the skeletal regeneration capacity of stromal cells. Sci Transl Med. 2023 Mar 22;15(688):eabm7477.

Hojo H, Ohba S. Sp7 Action in the Skeleton: Its Mode of Action, Functions, and Relevance to Skeletal Diseases. Int J Mol Sci. 2022 May 18;23(10):5647.

Kerckhofs G, Sainz J, Wevers M, Van de Putte T, Schrooten J. Contrast-enhanced nanofocus computed tomography images the cartilage subtissue architecture in three dimensions. Eur Cell Mater. 2013 Feb 7;25:179-189.

Kern S, Eichler H, Stoeve J, Klüter H, Bieback K. Comparative analysis of mesenchymal stem cells from bone marrow, umbilical cord blood, or adipose tissue. Stem Cells. 2006 May;24(5):1294-1301.

Korotkevich G, Sukhov V, Budin N, Shpak B, Artyomov MN, Sergushichev A. Fast gene set enrichtmens analysis. bioRxiv 2019;060012

Leek JT. svaseq: removing batch effects and other unwanted noise from sequencing data. Nucleic Acids Res. 2014 Dec 1;42(21):e161.

Leijten J, Chai YC, Papantoniou I, Geris L, Schrooten J, Luyten FP. Cell based advanced therapeutic medicinal products for bone repair: Keep it simple? Adv Drug Deliv Rev. 2015 Apr;84:30-44.

Li X, Sun Q, Li Q, Kawazoe N, Chen G. Functional Hydrogels With Tunable Structures and Properties for Tissue Engineering Applications. Front Chem. 2018 Oct 22;6:499.

Lin S, Svoboda KK, Feng JQ, Jiang X. The biological function of type I receptors of bone morphogenetic protein in bone. Bone Res. 2016 Apr 5;4:16005.

Love MI, Huber W, Anders S. Moderated estimation of fold change and dispersion for RNA-seq data with DESeq2. Genome Biol. 2014;15(12):550.

Ludwig K, Ward LM, Khan N, Robinson ME, Miranda V, Bardai G, Moffatt P, Rauch F. Dominant osteogenesis imperfecta with low bone turnover caused by a heterozygous SP7 variant. Bone. 2022 Jul;160:116400.

Luo T, Matsuo-Takasaki M, Lim JH, Sargent TD. Differential regulation of Dlx gene expression by a BMP morphogenetic gradient. Int J Dev Biol. 2001 Jun;45(4):681-684.

Mashrah MA, Aldhohrah T, Abdelrehem A, Sakran KA, Ahmad H, Mahran H, Abu-Lohom F, Su H, Fang Y, Wang L. Survival of vascularized osseous flaps in mandibular reconstruction: A network meta-analysis. PLoS One. 2021 Oct 22;16(10):e0257457.

Mendes LF, Tam WL, Chai YC, Geris L, Luyten FP, Roberts SJ. Combinatorial Analysis of Growth Factors Reveals the Contribution of Bone Morphogenetic Proteins to Chondrogenic Differentiation of Human Periosteal Cells. Tissue Eng Part C Methods. 2016 May;22(5):473-486.

Nilsson Hall G, Mendes LF, Gklava C, Geris L, Luyten FP, Papantoniou I. Developmentally Engineered Callus Organoid Bioassemblies Exhibit Predictive In Vivo Long Bone Healing. Adv Sci (Weinh). 2019 Dec 10;7(2):1902295.

Ohta S, Wang B, Mansour SL, Schoenwolf GC. BMP regulates regional gene expression in the dorsal otocyst through canonical and non-canonical intracellular pathways. Development. 2016 Jun 15;143(12):2228-2237.

Pan Q, Yu Y, Chen Q, Li C, Wu H, Wan Y, Ma J, Sun F. Sox9, a key transcription factor of bone morphogenetic protein-2-induced chondrogenesis, is activated through BMP pathway and a CCAAT box in the proximal promoter. J Cell Physiol. 2008 Oct;217(1):228-241.

Pecin M, Stokovic N, Ivanjko N, Smajlovic A, Kreszinger M, Capak H, Vrbanac Z, Oppermann H, Maticic D, Vukicevic S. A novel autologous bone graft substitute containing rhBMP6 in autologous blood coagulum with synthetic ceramics for reconstruction of a large humerus segmental gunshot defect in a dog: The first veterinary patient to receive a novel osteoinductive therapy. Bone Rep. 2021 Feb 25;14:100759.

Perry MJ, McDougall KE, Hou SC, Tobias JH. Impaired growth plate function in bmp-6 null mice. Bone. 2008 Jan;42(1):216-225.

Phimphilai M, Zhao Z, Boules H, Roca H, Franceschi RT. BMP signaling is required for RUNX2-dependent induction of the osteoblast phenotype. J Bone Miner Res. 2006 Apr;21(4):637-646.

Roberts SJ, van Gastel N, Carmeliet G, Luyten FP. Uncovering the periosteum for skeletal regeneration: the stem cell that lies beneath. Bone. 2015 Jan;70:10-18.

Robledo RF, Rajan L, Li X, Lufkin T. The Dlx5 and Dlx6 homeobox genes are essential for craniofacial, axial, and appendicular skeletal development. Genes Dev. 2002 May 1;16(9):1089-1101.
Salazar VS, Gamer LW, Rosen V. BMP signalling in skeletal development, disease and repair. Nat Rev Endocrinol. 2016 Apr;12(4):203-21.

Schmierer B, Hill CS. TGFbeta-SMAD signal transduction: molecular specificity and functional flexibility. Nat Rev Mol Cell Biol. 2007 Dec;8(12):970-82

Shu B, Zhang M, Xie R, Wang M, Jin H, Hou W, Tang D, Harris SE, Mishina Y, O'Keefe RJ, Hilton MJ, Wang Y, Chen D. BMP2, but not BMP4, is crucial for chondrocyte proliferation and maturation during endochondral bone development. J Cell Sci. 2011 Oct 15;124(Pt 20):3428-3440.

Sinha KM, Zhou X. Genetic and molecular control of osterix in skeletal formation. J Cell Biochem. 2013 May;114(5):975-984.

Tsuji K, Bandyopadhyay A, Harfe BD, Cox K, Kakar S, Gerstenfeld L, Einhorn T, Tabin CJ, Rosen V. BMP2 activity, although dispensable for bone formation, is required for the initiation of fracture healing. Nat Genet. 2006 Dec;38(12):1424-1429.

Ulsamer A, Ortuño MJ, Ruiz S, Susperregui AR, Osses N, Rosa JL, Ventura F. BMP-2 induces Osterix expression through up-regulation of Dlx5 and its phosphorylation by p38. J Biol Chem. 2008 Feb 15;283(7):3816-3826.

Van Den Bulcke AI, Bogdanov B, De Rooze N, Schacht EH, Cornelissen M, Berghmans H. Structural and rheological properties of methacrylamide modified gelatin hydrogels. Biomacromolecules. 2000 Spring;1(1):31-38.

van Gastel N, Torrekens S, Roberts SJ, Moermans K, Schrooten J, Carmeliet P, Luttun A, Luyten FP, Carmeliet G. Engineering vascularized bone: osteogenic and proangiogenic potential of murine periosteal cells. Stem Cells. 2012 Nov;30(11):2460-2471.

Vieux-Rochas M, Bouhali K, Mantero S, Garaffo G, Provero P, Astigiano S, Barbieri O, Caratozzolo MF, Tullo A, Guerrini L, Lallemand Y, Robert B, Levi G, Merlo GR. BMP-mediated functional cooperation between Dlx5;Dlx6 and Msx1;Msx2 during mammalian limb development. PLoS One. 2013;8(1):e51700.

Vu TH, Takechi M, Shimizu M, Kitazawa T, Higashiyama H, Iwase A, Kurihara H, Iseki S. Dlx5-augmentation in neural crest cells reveals early development and differentiation potential of mouse apical head mesenchyme. Sci Rep. 2021 Jan 22;11(1):2092.

Vukicevic S, Oppermann H, Verbanac D, Jankolija M, Popek I, Curak J, Brkljacic J, Pauk M, Erjavec I, Francetic I, Dumic-Cule I, Jelic M, Durdevic D, Vlahovic T, Novak R, Kufner V, Bordukalo Niksic T, Kozlovic M, Banic Tomisic Z, Bubic-Spoljar J, Bastalic I, Vikic-Topic S, Peric M, Pecina M, Grgurevic L. The clinical use of bone morphogenetic proteins revisited: a novel biocompatible carrier device OSTEOGROW for bone healing. Int Orthop. 2014 Mar;38(3):635-647.

Wang JS, Tokavanich N, Wein MN. SP7: from Bone Development to Skeletal Disease. Curr Osteoporos Rep. 2023 Apr;21(2):241-252.

Zhang YE. Non-Smad pathways in TGF-beta signaling. Cell Res. 2009 Jan;19(1):128-139.

Chapter 7

Discussion, and some perspectives

7.1. Background

With this PhD research, and inspired by my training in medicine and dentistry, I have tried to contribute to the establishment of cell-based implants for future treatment of large defects in cranio-maxillofacial bone. Limited fractures heal naturally *in vivo* by activation of periosteal cells and their eventual differentiation towards chondrocytes, enabling to make new bone tissue through a process that resembles endochondral ossification observed during development. The use of human periosteum-derived cells (hPDCs) got my prime attention for this. The Prometheus team at KU Leuven had already initiated research on hPDCs and had gained insight in the isolation and cell culture of these cells from adult bone, and were combining this with expertise in biomaterials, bioprinting, bioinformatics and in silico medicine. This connected well with the instructed cell differentiation know-how and the use of multi-omics approaches at Erasmus MC (including RNA-sequencing I applied in this PhD research) to study embryonic and adult BMP signal interpretation in the nucleus of embryonic stem cells and multiple tissues/organs, aiming at understanding action mechanisms in transcriptional target gene regulation in a dynamic chromatin context. Such integrative and multi-disciplinary approach will ultimately lead to stark improvement of stimulated *in vivo* repair of devastating bone defects in patients. Notably, and understandably, the focus in this field is mainly on bone tissue repair of defects in extremities, such as the tibia and femur (see **Chapter 1**).

Most future craniofacial bones originate from transient, multi-potent neural crest cells in the embryo, whereas *e.g.*, tibial and femural bones originate from precursor cells of a region of the embryonic mesoderm. We hypothesized that periosteal cells obtained from accessible adult craniofacial areas may intrinsically differ and have a different repair potential compared to tibial-derived periosteal cells (see **Chapter 2**). Therefore, we decided to start comparing for the first time the properties of hPDCs isolated from maxilla and mandible, respectively, with those taken from tibial hPDCs. The experimental work is quite broad and diverse, and required in the field, *i.e.* (i) cell expansion in the dish needs verification and possibly optimization, (ii) the cells need the supply of the appropriate differentiation signals and (iii) ideally are tested also *in vivo* with regard to *de novo* bone formation, which is often done first in ectopic (and thereafter orthotopic) locations in animal models. Importantly, we found that the mandibular hPDCs have very good potential to serve bone formation by endochondral ossification (**Chapter 3**).

In a parallel project, we included cells from the Schneiderian membrane, also known as the membrane in the maxillary sinus. We were aware that a thickening of the bone of the upper jaw is seen in some of these cases where the membrane is elevated and a blood cloth forms. It has been proposed that that the Schneiderian membrane is responsible for this bone-thickening effect (Srouji *et al.*, 2008). We first needed to gain expertise in isolating these cells from the Schneiderian membrane and to culture them in the dish. They were also differentiating *in vitro* towards chondroblasts and, to a lesser degree, osteoblasts. However, they proved – at least in our hands – less successful in *in vitro* differentiation and *in vivo* bone formation than mandibular and tibial hPDCs (**Chapter 4**). In another parallel project, we tried to culture mandibular hPDCs in the dish without the use of FBS, but a ready-to-use chemically defined medium is not available for these cells. We succeeded to replace the FBS by hPL and achieved even better osteogenic differentiation, at least *in vitro* (**Chapter 5**).

Another important aim of this PhD research was to improve bone-forming properties *in vivo* by first priming the mandibular hPDCs with BMPs and then seeding them on the best available

scaffolds. We observed that the effects after priming with BMP2 were more pronounced compared to the setup with BMP6. In addition, CopiOs as scaffold gave more *in vivo* bone formation than GelMA-constructs or assemblies of spheroids cultured in the presence of of BMP2 and BMP6, according to the protocol for tibial hPDCs optimized by colleagues (Mendes *et al.,* 2018; **Chapter 6**).

7.2. *In vitro* culture of cells

In this PhD research, the desired cells have been obtained from the donor tissues by enzymatic digestion using collagenase type-IV. This invariably works well with our cells and was adopted from previous research performed with tibial hPDCs. Other options are available such as the egression method or the use of other collagenase enzymes (*e.g.*, collagenase type-I or type-XI) (Olbrich et al., 2012; Ceccarelli *et al.*, 2016; Ude et al., 2021). However, for the described egression method also part of the cortical bone is harvested together with the desired periosteum, resulting in a biopsy with tissue of higher complexity. To limit the post-operative discomfort for the patient, we have chosen to use the enzymatic method (using collagenase type-IV; de Bari *et al.*, 2001).

Furthermore, we decided to expand our cells standard in DMEM supplemented with 10% FBS (Roberts *et al.,* 2011), which in the future might be replaced by hPL (see **Chapter 5**). The success of hPL also depends on the availability and the preparation itself, which was unsecure at the time we started this work. In order not to compromise the timing of our experiments, the DMEM+FBS option was chosen.

The intermittent use of added growth/differentiation factors to hPDC cultures is still under debate. Fibroblast Growth Factor-2 (FGF2) could be used in order to stimulate the proliferation of hPDCs (Ma *et al.*, 2019; Ude *et al.*, 2021). However, FGF2 plays a role in chondrogenic differentiation of (mouse) cells in the growing limb, and provokes mesenchymal condensation prior to this when used in a low dose, while the goal is still to expand cell numbers(Sabbieti *et al.*, 2009; Su *et al.*, 2014). In our hands, a basal medium consisting of DMEM+FBS (hopefully in the future with hPL as the alternative to FBS) did work well, so we decided not to change this for the other chapters and focus instead on the selection of the cell origin, priming strategy, selection of scaffolds, and the additional setup of an orthotopic model, specifically designed for studying for craniofacial bone defect regeneration.

7.3. Priming of cells

From the moment that sufficient numbers of cells are available to make the tissue-engineered construct, cell differentiation along the endochondral pathway or intramembranous ossification pathway should be pushed. The endochondral pathway is favored, since chondroblasts and chondrocytes are used to living in a hypoxic environment, making the scaling up less difficult since a bigger construct goes along with a more pronounced gradient of nutrients, metabolites and oxygen (Söhling *et al.,* 2020).

Different strategies can push cells towards endochondral ossification. In this PhD research thesis, we have chosen to test 3 different strategies to prime: BMP2, BMP6 and – in part – a combination of growth/differentiation factors including BMP2, BMP6, FGF2 and GDF5, at a dosage

co-determined by previous work in the Prometheus team (Mendes *et al.,* 2016). BMP2 is already approved by the European Medicine Agency (EMA) and the food and drug administration (FDA) in the United States for use in induction of bone formation. For BMP6 clinical studies are ongoing, making the clinical translation using this priming strategy more straightforward compared to other factors (Chiari *et al.,* 2020; Durdevic *et al.,* 2020).

7.3.1. Priming with BMPs

As described in **Chapter 1**, several BMPs exist (BMP2 up till BMP15). Expression of the genes encoding for and/or the presence of the ligands BMP2, -3, -4, -5, -6, -7, GDF5 (also named BMP14 and CDMP1) and -6 (also named BMP13, sometimes still KFS, KFS1, SGM1) has been documented in the human skeleton (Salazar *et al.,* 2016; Lowery and Rosen, 2018). BMP1 is not a cognate BMP subfamily ligand and is a metalloproteinase whose action is to cleave thrombospondin-1 (TSP1) in the ECM, so that the C-terminal part of TSP1 is released so it can activate certain forms of latent TGFb. Notably, mutations in *BMP1* result in brittle bones, as part of *e.g.*, osteogenesis imperfecta (Syx *et al.,* 2015; Anastasi *et al.*, 2020).

BMP2 plays a role in osteo- and chondrogenesis (Wozney *et al.*, 1988) and has been approved by the FDA and EMA for use in the clinic for spinal bone grafts and tibial bone defects. BMP3 is needed for patterning the early skeleton and antagonizes the function of osteogenic BMPs (Rosen *et al.,* 1989; Daluiski *et al.,* 2001; Kang *et al.,* 2004). BMP4 plays a role in osteogenesis, angiogenesis and in many other embryonic and adult processes, including in soft tissues. It can form heterodimers with BMP2, and skeletal defects result from mutation of either *BMP4* or *BMP2*, but *BMP4* is dispensable for bone formation and fracture healing (Tsuji *et al.*, 2008; Lowery and Rosen, 2018; Rezzola *et al.*, 2019; Nakatsu *et al.*, 2023). BMP5 promotes neural development by dendritic growth and induces dopaminergic neurons, but also plays a role in cartilage and bone formation. Mutations in *BMP5* in mice only yield a mild phenotype resulting in an abnormal geometry of the bone tissue (Mikić *et al.*, 1996; Beck *et al.*, 2001; Jovanovic *et al.*, 2018) *BMP6* is essential for ossification and cartilage formation; ossification in mice is delayed in case inactivating mutations occur in this gene (Solloway *et al.,* 1998). Furthermore, BMP6 is also related to iron overload diseases, whereas BMP7 together with BMP2 (and BMP4), plays a role in skeletal morphogenesis, but also in neurogenesis and haematopoiesis, and cardiovascular abnormalities when mutated (Kim *et al.,* 2001; Kim *et al.,* 2019).

GDF5 and GDF6 act in cartilage formation, adipogenesis and neurogenesis (den Hollander *et al.*, 2010; Degenkolbe *et al.*, 2013; Wang *et al.*, 2013; Wang *et al.*, 2016; Wu *et al.*, 2018; Zhang *et al.*, 2019). Mutation of *GDF5* causes specific types of brachydactyly, whereas the combination with *GDF6* mutation also gives skeletal patterning defects (Storm *et al.*, 1994; Settle *et al.*, 2003). When all phenotypes of mutations are compared, *BMP2* and *BMP6* can give severe skeletal malformations by themselves, while in case of mutations in *BMP4* or *BMP7* an interplay between several BMPs is required (Lowery and Rosen, 2018). BMP2, BMP6 and BMP7 are known to give a higher bone mass in rats upon systemic administration (Simic *et al.*, 2006; Dumic-Cule *et al.*, 2014).

BMP2 is approved by the FDA and EMA to treat spinal fusions and tibial bone defects. For BMP6 the clinical studies are ongoing and await approval, whereas BMP7 has been withdrawn from the market, because its beneficial effect in randomized controlled clinical trials is very limited or even giving poorer outcomes for long bone defects (Technology Assessment Report,

2010). These are, in brief, the major reasons why we decided to test BMP2 and BMP6 on hPDCs here. As discussed briefly in **Chapter 6** their intracellular signal transduction involves Ser/Thr-kinase receptor activity including of the ligand-bound type-I BMP receptors in the type-I/II tetrameric receptor complex (activating SMADs1/5/9 to the respective p-SMADS) and/or they act via non-SMAD signalling pathways involving other kinases such as Erk, p38MAPK or Tak1 (Aoki *et al.,* 2001). Although ALK3 (BMPR-IA), ALK6 (BMPR-IB) and ALK2 (ActR-IA) are required for endochondral bone formation, mutation in one of these receptors only results in milder skeletal phenotypes, because of receptor redundancy (Yoon *et al.,* 2005). The effects of BMP stimulation at a given dosage are not always the same in different cell types or even in different conditions for similar cells. Affinities of the BMP subfamily of ligands for receptor ectodomain binding vary, the interplay between SMAD-dependent and non-SMAD-dependent pathways will co-determine the final effect under specific conditions (Zhang *et al.,* 2009). In addition, and par excellence, many SMAD-interacting transcription factors and their ratios will co-determine the cellular response to BMPs as well as the massive forward/feedback, autoregulation and synexpression regulation of components of the BMP system itself. This is in addition to the crosstalk with other signalling pathways, in particular WNT, but also Activin/Nodal and TGFβ pathways. Wnt signalling normally induces differentiation of pre-osteoblasts to osteoblasts, but BMP-signalling generally upregulates Wnt-inhibitors, while BMP signalling is also known to stimulate bone formation, making the prediction and translation of results when using other cell types or cellular context even more difficult (**Figure 7.1**; Kamiya *et al.,* 2011).

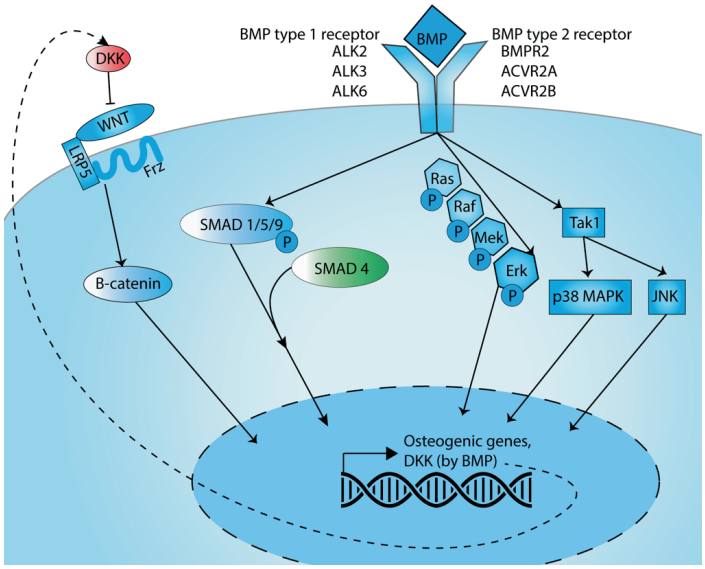

Figure 7.1. BMP signalling and its crosstalk with WNT
BMP can activate canonical signalling through SMADs1/5/9, but also non-canonical signalling such as Erk, p38MAPK or JNK. BMP-signalling upregulates Wnt-inhibitors *e.g.* DKK resulting in an inhibition of Wnt-stimulated osteogenic differentiation of pre-osteoblasts

7.3.2. Angiogenesis

In the field, and also in this PhD research, good results have been obtained when using BMP2, in particular regarding the mineralized volume of the newly formed tissue, and the histological images showing the presence of bone marrow compartments. However, blood vessel formation was not shown in the images. Angiogenesis, a form of vasculogenesis that involves the growth by sprouting of pre-existing blood vessels, is started by hypertrophic chondrocytes for endochondral ossification. These produce besides BMP2 also vascular endothelial growth factor (VEGF; i.e. $VEGF_{121}$ and $VEGF_{165}$) in order to attract endothelial cells (Petersen *et al.*, 2002). Matrix metalloproteinase-9 (MMP9) degrades mineralised cartilage, so that vascularization can be facilitated. Absence of the gene coding for this protein results in less cartilage degradation, and an impaired vascularization, leading to a larger callus and delayed fracture healing (Colnot *et al.*, 2003). Due to the vascularization, hematopoietic stem cells can enter the newly formed tissue, but also osteoclasts and some osteoblasts do so (Kodama *et al.*, 2022).

One could argue to add additional (and appropriate type and splice form of) VEGF to the construct in order to stimulate the vascularization or to add MMP9. However, it cannot be excluded that MMP9 would result in precocious degradation of the scaffold, thereby affecting the structural stability of the construct already in an early phase after transplantation. VEGF stimulates sprouting by endothelial cells, but high dosing ultimately leads to a dense vessel network with low perfusion capacity. VEGF furthermore stimulates besides angiogenesis also osteoclastogenesis, and plays a role in chondrocyte and osteoblast differentiation, requiring a careful titration of its dose (Nakagawa *et al.,* 2000; Stegen and Carmeliet, 2018). Vascularization after implantation could also be stimulated by culturing the cells *in vitro* under hypoxic conditions (as low as 1% oxygen). Both in the fields of cardiac regeneration and neurology, increased angiogenesis is seen when cells were cultured under hypoxic conditions *in vitro* (Lee *et al.*, 2010; Hu *et al.*, 2014). Hypoxia results in the upregulation and increased activity of hypoxia-inducible factor-1a (HIF-1a, a transcription factor) and subsequently to increased production of secreted VEGF by osteoblasts (Gerber *et al.*, 1999; Westra *et al.*, 2010; Tsai *et al.*, 2011; Chai *et al.*, 2020; Loopmans *et al.*, 2022). The timing of implantation of the construct should be planned very carefully, since mineralization of the matrix reduces the production of VEGF by chondrocytes and hence also angiogenesis, while VEGF plays a role in osteoblast and chondrocyte differentiation too (Nakagawa *et al.,* 2000; Ji *et al.*, 2023). In addition to the angiogenic response of cells to hypoxia, SSPCs could be proliferating faster when cultured in hypoxic conditions (Loopmans *et al.,* 2012).

Another possibility to stimulate angiogenesis is apparently via the addition of statins such as atorvastatin. This statin did not affect the viability or the presence of markers at the cell surface for bone-marrow derived MSCs, but increased VEGF levels via the phosphatidylinositol 3-kinase (PI3K)/AKT/mammalian target of rapamycin (mTOr) pathway (Karar and Maity, 2011; Adamićková *et al.*, 2023). The co-culture of SSPCs with endothelial cells would present another option to increase angiogenesis in the newly formed bone tissue. Peripheral blood-derived SSPCs can for example stimulate the proliferation of endothelial progenitor cells and their angiogenesis, while these progenitors stimulate bone formation (Wang *et al.*, 2023). However, to our knowledge, only osteogenic differentiation *in vitro* and ectopic bone formation *in vivo* have been tested.

7.4. Perspectives

Currently, the expansion of cells in the petri dish is still time consuming and expensive. In addition, our constructs of 5.25 mm diameter need 2.4 million cells. When we scale this up to a construct measuring 8cm^3 we would need ~175 million cells. This implies an additional cumulative population doubling of more than 6, requiring about 3 additional weeks of culture, in 84 additional culture flasks, using more than 4 liter of medium, more than 400 ml of undiluted serum, and several hours of intense work. These cell numbers would be achievable, although definitely requiring many handlings, labor hours, medium and serum. Adaptations of the protocols may help here, certainly when these operations are needed for cells of multiple patients. Static protocols also result in gradients of temperature, nutrients, metabolites and oxygen. Bioreactors could offer a solution here (Warnock and Al-Rubeai, 2006; Rodrigues *et al.*, 2011; dos Santos *et al.*, 2013) where cells could also be grown in suspension culture, as aggregates, or as an adherent layer on a substrate-like degradable or polystyrene beads (Gupta *et al.,* 2018; Van Beylen *et al.,* 2021). For satisfactory cell expansion of periosteum derived cells, the separation of hPDCs from other cells of the periosteum relies on the fact that hPDCs are adherent, whereas other cell types are not. This means that the hPDCs will adhere in reasonably short time to the polystyrene bottom of the culture flasks, and other cells will be readily washed away during media changes. Microcarriers may also be used by cells to adhere to in spinner flasks, also leaving the option to wash away other cells. Initial tests comparing the effect of microcarriers on tibial-derived hPDCs have already been performed, but tests on mandibular hPDCs are still required (dos Santos *et al.*, 2013; Van Beylen *et al.*, 2021). Further, the biomechanical requirements such as agitation rate and geometry of the impeller could be tailored to the use of hPDCs (Gupta *et al.,* 2018).

For clinical translation, the consistency and efficacy of the combined product (*e.g.*, cells in combination with BMP2 and the CopiOs scaffold, as proposed here) needs to be proven. *In vivo* studies in this thesis have shown variability in the bone forming capacities of cells between priming strategies and scaffolds, but also between technical replicates. Constructs were randomly implanted in the mice to minimize the effect of the animals on the results obtained from the *in vivo* experiments. However, we are aware that local environmental cues, the distribution of calciumphoshate grains in the scaffolds, and also donor characteristics, together influence the ability of these cells to form bone. The effects of the microenvironment have already been shown by periosteal grafting experiments, as well as the influence of scaffold material on bone forming properties (Leucht *et al.,* Ji *et al.,* 2018). The efficacy of the combined product is ideally proven in a small (first) and/or large animal model, with evaluation of longer-term risks, before true clinical studies can start. It is not clear yet as to whether in this field the need for animal models can be replaced by alternatives such as organoids or organ-on-a-chip approaches. In addition, the tumorigenicity and chromosomal integrity/stability needs to be checked for cultured hPDCs before these cells can be tested in human. EMA has, besides their recommendations for the use of stem cells in human, also stated recommendations for the use of stem cells in tissue-engineered products, and these recommendations also include tests of the pharmacodynamics and -kinetics. Tests on pharmacodynamics should investigate the mechanisms of action and the local environment, while tests on pharmacokinetics should focus on the donor age, culture passage and culture conditions for the used cells (Salvadori *et al.,* 2019). So, although the use of BMP2 and CopiOs have already been separately approved by the FDA and EMA for clinical use, additional studies still need to be performed before this tissue- engineering approach can make it into the clinics.

For this PhD research, hPDCs were used since they are no longer too difficult to obtain from a patient, can be expanded in an affordable way for research purposes, and they are progenitors for cartilage and bone. However, still a time frame of several weeks must be envisaged in order to isolate hPDCs from the patient's own periosteal tissue, to expand these cells, and to create the combined product ready for implantation via a second surgical procedure. An alternative option could be to use allogeneic hPDCs or to consider induced pluripotent stem cells (iPSCs). Many studies on establishing and growing iPSCs have been performed, but the major hurdle remains the transcription factor cocktail-assisted reprogramming of somatic cells to robust iPSCs (Takahashi *et al.*, 2007). In addition, iPSCs are pluripotent, while hPDCs are more restricted, and both may have tumorigenic potential still. Human iPSCs seem to proliferate at a higher rate than hPDCs, and can be obtained from various somatic cells, including peripheral blood cells (Kato *et al.*, 2022), and ready-to-use reference iPSC lines exist (Rivera *et al.*, 2020). In principle, by using iPSCs the number of surgical events could be minimized to only one, *i.e.,* the one to put the construct in the bone defect.

IPSCs could in the longer term offer a promising alternative to SSPCs (such as hPDCs), but their cell culture and processing could end up being more complex. hPDC cultures only require simple enzymatic digestion. The differentiation of iPSCs towards bone-producing hypertrophic chondrocytes differs from the protocol for hPDCs, and iPSCs likely need other biomechanical conditions than hPDCs do, which may necessitate a change of scaffold material too. We suggest that hPDCs expanded in hPL-containing medium could offer a promising route as cell culture source for bone tissue engineering, including as therapy for craniofacial large bone defects, in particular when primed with BMP2 and seeded on a NuOss scaffold. Their success is already shown in a small animal model (*e.g.*, rats). Upscaling of such cultures and constructs would be the next logical step, together with using a careful, non-invasive method to observe the function of such grown and applied cells, and also to prove the safety of their use in patients.

To conclude, satisfactory results are shown in this PhD thesis in bone tissue engineering for craniofacial applications, contributing to driving this approach more and more towards its clinical translation. Culture conditions for different origins or even types of cells have been established, and the most promising cells - mandibular hPDCs - were selected. Attempts were made to improve safety and efficacy of culture techniques by replacing animal-drived FBS by human platelet lyasate, and lastly, the combination of products was tested showing the bone forming potential for the best performing construct consisting of BMP2-primed cells seeded on CopiOs scaffolds.

Literature references

Adamičková A, Chomaničová N, Gažová A, Maďarič J, Červenák Z, Valášková S, Adamička M, Kyselovic J. Effect of Atorvastatin on Angiogenesis-Related Genes VEGF-A, HGF and IGF-1 and the Modulation of PI3K/AKT/mTOR Transcripts in Bone-Marrow-Derived Mesenchymal Stem Cells. Curr Issues Mol Biol. 2023 Mar 10;45(3):2326-2337.

Anastasi C, Rousselle P, Talantikite M, Tessier A, Cluzel C, Bachmann A, Mariano N, Dussoyer M, Alcaraz LB, Fortin L, Aubert A, Delolme F, El Kholti N, Armengaud J, Fournié P, Auxenfans C, Valcourt U, Goff SV, Moali C. BMP-1 disrupts cell adhesion and enhances TGF-β activation through cleavage of the matricellular protein thrombospondin-1. Sci Signal. 2020 Jul 7;13(639):eaba3880.

Aoki H, Fujii M, Imamura T, Yagi K, Takehara K, Kato M, Miyazono K. Synergistic effects of different bone morphogenetic protein type I receptors on alkaline phosphatase induction. J Cell Sci. 2001 Apr;114(Pt 8):1483-9.

Beck HN, Drahushuk K, Jacoby DB, Higgins D, Lein PJ. Bone morphogenetic protein-5 (BMP-5) promotes dendritic growth in cultured sympathetic neurons. BMC Neurosci. 2001;2:12

Ceccarelli, G., Graziano, A., Benedetti, L., Imbriani, M., Romano, F., Ferrarotti, F., Aimetti, M., & Cusella De Angelis, G. M. (2016). Osteogenic Potential of Human Oral-Periosteal Cells (PCs) Isolated From Different Oral Origin: An In Vitro Study. *Journal of Cellular Physiology*, *231*(3), 607–612.

Chai M, Gu C, Shen Q, Liu J, Zhou Y, Jin Z, Xiong W, Zhou Y, Tan W. Hypoxia alleviates dexamethasone-induced inhibition of angiogenesis in cocultures of HUVECs and rBMSCs via HIF-1α. Stem Cell Res Ther. 2020 Aug 6;11(1):343.

Chiari C, Grgurevic L, Bordukalo-Niksic T, Oppermann H, Valentinitsch A, Nemecek E, Staats K, Schreiner M, Trost C, Kolb A, Kainberger F, Pehar S, Milosevic M, Martinovic S, Peric M, Sampath TK, Vukicevic S, Windhager R. Recombinant Human BMP6 Applied Within Autologous Blood Coagulum Accelerates Bone Healing: Randomized Controlled Trial in High Tibial Osteotomy Patients. J Bone Miner Res. 2020 Oct;35(10):1893-1903.

Colnot C, Thompson Z, Miclau T, Werb Z, Helms JA. Altered fracture repair in the absence of MMP9. Development. 2003 Sep;130(17):4123-33.

Daluiski A, Engstrand T, Bahamonde ME, Gamer LW, Agius E, Stevenson SL, Cox K, Rosen V, Lyons KM. Bone morphogenetic protein-3 is a negative regulator of bone density. Nat Genet. 2001 Jan;27(1):84-8.

De Bari, C., Dell'Accio, F., & Luyten, F. P. (2001). Human periosteum-derived cells maintain phenotypic stability and chondrogenic potential throughout expansion regardless of donor age. *Arthritis and Rheumatism*, *44*(1), 85–95.

Degenkolbe E, König J, Zimmer J, Walther M, Reißner C, Nickel J, Plöger F, Raspopovic J, Sharpe J, Dathe K, Hecht JT, Mundlos S, Doelken SC, Seemann P. A GDF5 point mutation strikes twice--causing BDA1 and SYNS2. PLoS Genet. 2013;9(10):e1003846.

den Hollander AI, Biyanwila J, Kovach P, Bardakjian T, Traboulsi EI, Ragge NK, Schneider A, Malicki J. Genetic defects of GDF6 in the zebrafish out of sight mutant and in human eye developmental anomalies. BMC Genet. 2010 Nov 11;11:102.

dos Santos FF, Andrade PZ, da Silva CL, Cabral JM. Bioreactor design for clinical-grade expansion of stem cells. Biotechnol J. 2013 Jun;8(6):644-54.

Dumic-Cule I, Brkljacic J, Rogic D, Bordukalo Niksic T, Tikvica Luetic A, Draca N, Kufner V, Trkulja V, Grgurevic L, Vukicevic S. Systemically available bone morphogenetic protein two and seven affect bone metabolism. Int Orthop. 2014 Sep;38(9):1979-85.

Durdevic D, Vlahovic T, Pehar S, Miklic D, Oppermann H, Bordukalo-Niksic T, Gavrankapetanovic I, Jamakosmanovic M, Milosevic M, Martinovic S, Sampath TK, Peric M, Grgurevic L, Vukicevic S. A novel autologous bone graft substitute comprised of rhBMP6 blood coagulum as carrier tested in a randomized and controlled Phase I trial in patients with distal radial fractures. Bone. 2020 Nov;140:115551.

Gerber HP, Vu TH, Ryan AM, Kowalski J, Werb Z, Ferrara N. VEGF couples hypertrophic cartilage remodeling, ossification and angiogenesis during endochondral bone formation. Nat Med. 1999 Jun;5(6):623-8.

Gupta P, Geris L, Luyten FP, Papantoniou I. An Integrated Bioprocess for the Expansion and Chondrogenic Priming of Human Periosteum-Derived Progenitor Cells in Suspension Bioreactors. Biotechnol J. 2018 Feb;13(2)

Hu X, Wu R, Shehadeh LA, Zhou Q, Jiang C, Huang X, Zhang L, Gao F, Liu X, Yu H, Webster KA, Wang J. Severe hypoxia exerts parallel and cell-specific regulation of gene expression and alternative splicing in human mesenchymal stem cells. BMC Genomics. 2014 Apr 23;15:303.

Ji E, Leijsten L, Witte-Bouma J, Rouchon A, Di Maggio N, Banfi A, van Osch GJVM, Farrell E, Lolli A. In Vitro Mineralisation of Tissue-Engineered Cartilage Reduces Endothelial Cell Migration, Proliferation and Tube Formation. Cells. 2023 Apr 20;12(8):1202.

Jovanovic VM, Salti A, Tilleman H, Zega K, Jukic MM, Zou H, Friedel RH, Prakash N, Blaess S, Edenhofer F, Brodski C. BMP/SMAD Pathway Promotes Neurogenesis of Midbrain Dopaminergic Neurons *In Vivo* and in Human Induced Pluripotent and Neural Stem Cells. J Neurosci. 2018 Feb 14;38(7):1662-1676

Kamiya N, Kaartinen VM, Mishina Y. Loss-of-function of ACVR1 in osteoblasts increases bone mass and activates canonical Wnt signaling through suppression of Wnt inhibitors SOST and DKK1. Biochem Biophys Res Commun. 2011 Oct 22;414(2):326-30.

Kang Q, Sun MH, Cheng H, Peng Y, Montag AG, Deyrup AT, Jiang W, Luu HH, Luo J, Szatkowski JP, Vanichakarn P, Park JY, Li Y, Haydon RC, He TC. Characterization of the distinct orthotopic bone-forming activity of 14 BMPs using recombinant adenovirus-mediated gene delivery. Gene Ther. 2004 Sep;11(17):1312-20.

Karar J, Maity A. PI3K/AKT/mTOR Pathway in Angiogenesis. Front Mol Neurosci. 2011 Dec 2;4:51.

Kato H, Watanabe K, Saito A, Onodera S, Azuma T, Takano M. Bone regeneration of induced pluripotent stem cells derived from peripheral blood cells in collagen sponge scaffolds. J Appl Oral Sci. 2022 Feb 21;30:e20210491.

Kim RY, Robertson EJ, Solloway MJ. Bmp6 and Bmp7 are required for cushion formation and septation in the developing mouse heart. Dev Biol. 2001 Jul 15;235(2):449-66.

Kim HS, Neugebauer J, McKnite A, Tilak A, Christian JL. BMP7 functions predominantly as a heterodimer with BMP2 or BMP4 during mammalian embryogenesis. Elife. 2019 Sep 30;8:e48872.

Kodama J, Wilkinson KJ, Iwamoto M, Otsuru S, Enomoto-Iwamoto M. The role of hypertrophic chondrocytes in regulation of the cartilage-to-bone transition in fracture healing. Bone Rep. 2022 Aug 28;17:101616.

Lee SH, Lee YJ, Song CH, Ahn YK, Han HJ. Role of FAK phosphorylation in hypoxia-induced hMSCS migration: involvement of VEGF as well as MAPKS and eNOS pathways. Am J Physiol Cell Physiol. 2010 Apr;298(4):C847-56.

Loopmans S, Stockmans I, Carmeliet G, Stegen S. Isolation and *in vitro*characterization of murine young-adult long bone skeletal progenitors. Front Endocrinol (Lausanne). 2022 Aug 1;13:930358.

Lowery JW, Rosen V. The BMP Pathway and Its Inhibitors in the Skeleton. Physiol Rev. 2018 Oct 1;98(4):2431-2452.

Ma, Y., Kakudo, N., Morimoto, N., Lai, F., Taketani, S., & Kusumoto, K. (2019). Fibroblast growth factor-2 stimulates proliferation of human adipose-derived stem cells via Src activation. *Stem Cell Research and Therapy*, *10*(1), 1–9.

Mendes LF, Tam WL, Chai YC, Geris L, Luyten FP, Roberts SJ. Combinatorial Analysis of Growth Factors Reveals the Contribution of Bone Morphogenetic Proteins to Chondrogenic Differentiation of Human Periosteal Cells. Tissue Eng Part C Methods. 2016 May;22(5):473-86.

Mikić B, Van der Meulen MC, Kingsley DM, Carter DR. Mechanical and geometric changes in the growing femora of BMP-5 deficient mice. Bone. 1996 Jun;18(6):601-7.

Nakagawa M, Kaneda T, Arakawa T, Morita S, Sato T, Yomada T, Hanada K, Kumegawa M, Hakeda Y. Vascular endothelial growth factor (VEGF) directly enhances osteoclastic bone resorption and survival of mature osteoclasts. FEBS Lett. 2000 May 12;473(2):161-4.

Nakatsu D, Kunishige R, Taguchi Y, Shinozaki-Narikawa N, Osaka K, Yokomizo K, Ishida M, Takei S, Yamasaki S, Hagiya K, Hattori K, Tsukamoto T, Murata M, Kano F. BMP4-SMAD1/5/9-RUNX2 pathway activation inhibits neurogenesis and oligodendrogenesis in Alzheimer's patients' iPSCs in senescence-related conditions. Stem Cell Reports. 2023 Mar 14;18(3):688-705.

Olbrich, M., Rieger, M., Reinert, S., & Alexander, D. (2012). Isolation of Osteoprogenitors from Human Jaw Periosteal Cells: A Comparison of Two Magnetic Separation Methods. *PLOS ONE*, *7*(10), e47176.

Petersen W, Tsokos M, Pufe T. Expression of VEGF121 and VEGF165 in hypertrophic chondrocytes of the human growth plate and epiphyseal cartilage. J Anat. 2002 Aug;201(2):153-7.

Rezzola S, Di Somma M, Corsini M, Leali D, Ravelli C, Polli VAB, Grillo E, Presta M, Mitola S. VEGFR2 activation mediates the pro-angiogenic activity of BMP4. Angiogenesis. 2019 Nov;22(4):521-533.

Rivera T, Zhao Y, Ni Y, Wang J. Human-Induced Pluripotent Stem Cell Culture Methods Under cGMP Conditions. Curr Protoc Stem Cell Biol. 2020 Sep;54(1):e117.

Roberts SJ, Chen Y, Moesen M, Schrooten J, Luyten FP. Enhancement of osteogenic gene expression for the differentiation of human periosteal derived cells. Stem Cell Res. 2011 Sep;7(2):137-44.

Rodrigues CA, Diogo MM, da Silva CL, Cabral JM. Microcarrier expansion of mouse embryonic stem cell-derived neural stem cells in stirred bioreactors. Biotechnol Appl Biochem. 2011 Jul-Aug;58(4):231-42.

Rosen V, Wozney JM, Wang EA, Cordes P, Celeste A, McQuaid D, Kurtzberg L. Purification and molecular cloning of a novel group of BMPs and localization of BMP mRNA in developing bone. Connect Tissue Res. 1989;20(1-4):313-9.

Sabbieti, M. G., Agas, D., Xiao, L., Marchetti, L., Coffin, J. D., Doetschman, T., & Hurley, M. M. (2009). Endogenous FGF-2 is critically important in PTH anabolic effects on bone. *Journal of Cellular Physiology*, *219*(1)

Salazar VS, Gamer LW, Rosen V. BMP signalling in skeletal development, disease and repair. Nat Rev Endocrinol. 2016 Apr;12(4):203-21.

Salvadori M, Cesari N, Murgia A, Puccini P, Riccardi B, Dominici M. Dissecting the Pharmacodynamics and Pharmacokinetics of MSCs to Overcome Limitations in Their Clinical Translation. Mol Ther Methods Clin Dev. 2019 May 17;14:1-15.

Settle SH Jr, Rountree RB, Sinha A, Thacker A, Higgins K, Kingsley DM. Multiple joint and skeletal patterning defects caused by single and double mutations in the mouse Gdf6 and Gdf5 genes. Dev Biol. 2003 Feb 1;254(1):116-30.

Simic P, Culej JB, Orlic I, Grgurevic L, Draca N, Spaventi R, Vukicevic S. Systemically administered bone morphogenetic protein-6 restores bone in aged ovariectomized rats by increasing bone formation and suppressing bone resorption. J Biol Chem. 2006 Sep 1;281(35):25509-21.

Storm EE, Huynh TV, Copeland NG, Jenkins NA, Kingsley DM, Lee SJ. Limb alterations in brachypodism mice due to mutations in a new member of the TGF beta-superfamily. Nature. 1994 Apr 14;368(6472):639-43.

Söhling N, Neijhoft J, Nienhaus V, Acker V, Harbig J, Menz F, Ochs J, Verboket RD, Ritz U, Blaeser A, Dörsam E, Frank J, Marzi I, Henrich D. 3D-Printing of Hierarchically Designed and Osteoconductive Bone Tissue Engineering Scaffolds. Materials (Basel). 2020 Apr 13;13(8):1836.

Solloway MJ, Dudley AT, Bikoff EK, Lyons KM, Hogan BL, Robertson EJ. Mice lacking Bmp6 function. Dev Genet. 1998;22(4):321-39.

Stegen S, Carmeliet G. The skeletal vascular system - Breathing life into bone tissue. Bone. 2018 Oct;115:50-58.

Su, N., Jin, M., & Chen, L. (2014). Role of FGF/FGFR signaling in skeletal development and homeostasis: learning from mouse models. *Bone Research*, *2*.

Syx D, Guillemyn B, Symoens S, Sousa AB, Medeira A, Whiteford M, Hermanns-Lê T, Coucke PJ, De Paepe A, Malfait F. Defective Proteolytic Processing of Fibrillar Procollagens and Prodecorin Due to Biallelic BMP1 Mutations Results in a Severe, Progressive Form of Osteogenesis Imperfecta. J Bone Miner Res. 2015 Aug;30(8):1445-56.

Takahashi K, Okita K, Nakagawa M, Yamanaka S. Induction of pluripotent stem cells from fibroblast cultures. Nat Protoc. 2007;2(12):3081-9.

Tsai CC, Chen YJ, Yew TL, Chen LL, Wang JY, Chiu CH, Hung SC. Hypoxia inhibits senescence and maintains mesenchymal stem cell properties through down-regulation of E2A-p21 by HIF-TWIST. Blood. 2011 Jan 13;117(2):459-69.

Tsuji K, Cox K, Bandyopadhyay A, Harfe BD, Tabin CJ, Rosen V. BMP4 is dispensable for skeletogenesis and fracture-healing in the limb. J Bone Joint Surg Am. 2008 Feb;90 Suppl 1:14-8

Ude, C. C., Sharma, G. G., Shen, J., & O'Keefe, R. J. (2021). Isolation and Culture of Periosteum-Derived Progenitor Cells from Mice. *Methods in Molecular Biology*, *2230*, 397–413.

Van Beylen K, Papantoniou I, Aerts JM. Microcarrier Screening and Evaluation for Dynamic Expansion of Human Periosteum-Derived Progenitor Cells in a Xenogeneic Free Medium. Front Bioeng Biotechnol. 2021 May 24;9:624890.

Wang SS, Huang HY, Chen SZ, Li X, Zhang WT, Tang QQ. Gdf6 induces commitment of pluripotent mesenchymal C3H10T1/2 cells to the adipocyte lineage. FEBS J. 2013 Jun;280(11):2644-51.

Wang J, Yu T, Wang Z, Ohte S, Yao RE, Zheng Z, Geng J, Cai H, Ge Y, Li Y, Xu Y, Zhang Q, Gusella JF, Fu Q, Pregizer S, Rosen V, Shen Y. A New Subtype of Multiple Synostoses Syndrome Is Caused by a Mutation in GDF6 That Decreases Its Sensitivity to Noggin and Enhances Its Potency as a BMP Signal. J Bone Miner Res. 2016 Apr;31(4):882-9.

Wang H, Li X, Lai S, Cao Q, Liu Y, Li J, Zhu X, Fu W, Zhang X. Construction of Vascularized Tissue Engineered Bone with nHA-Coated BCP Bioceramics Loaded with Peripheral Blood-Derived MSC and EPC to Repair Large Segmental Femoral Bone Defect. ACS Appl Mater Interfaces. 2023 Jan 11;15(1):249-264.

Warnock JN, Al-Rubeai M. Bioreactor systems for the production of biopharmaceuticals from animal cells. Biotechnol Appl Biochem. 2006 Jul;45(Pt 1):1-12.

Westra J, Molema G, Kallenberg CG. Hypoxia-inducible factor-1 as regulator of angiogenesis in rheumatoid arthritis - therapeutic implications. Curr Med Chem. 2010;17(3):254-63.

Wozney JM, Rosen V, Celeste AJ, Mitsock LM, Whitters MJ, Kriz RW, Hewick RM, Wang EA. Novel regulators of bone formation: molecular clones and activities. Science. 1988 Dec 16;242(4885):1528-34.

Wu H, Li J, Xu D, Zhang Q, Cui T. Growth Differentiation Factor 5 Improves Neurogenesis and Functional Recovery in Adult Mouse Hippocampus Following Traumatic Brain Injury. Front Neurol. 2018 Jul 23;9:592.

Yoon BS, Ovchinnikov DA, Yoshii I, Mishina Y, Behringer RR, Lyons KM. Bmpr1a and Bmpr1b have overlapping functions and are essential for chondrogenesis in vivo. Proc Natl Acad Sci U S A. 2005 Apr 5;102(14):5062-7.

Zhang YE. Non-Smad pathways in TGF-beta signaling. Cell Res. 2009 Jan;19(1):128-39.

Zhang W, Wu X, Pei Z, Kiess W, Yang Y, Xu Y, Chang Z, Wu J, Sun C, Luo F. GDF5 Promotes White Adipose Tissue Thermogenesis via p38 MAPK Signaling Pathway. DNA Cell Biol. 2019 Nov;38(11):1303-1312.

https://www.accessdata.fda.gov/cdrh_docs/pdf4/h040004b.pdf

https://www.cms.gov/medicare/coverage/determinationprocess/downloads/id75ta.pdf

https://www.ema.europa.eu/en/documents/scientific-guideline/reflection-paper-clinical-aspects-related-tissue-engineered-products_en.pdf

https://www.ema.europa.eu/en/documents/scientific-guideline/reflection-paper-stem-cell-based-medicinal-products_en.pdf

Summary

Bone grafts are commonly used in orthopedics, traumatology, and oral and maxillofacial surgery for treating bone defects caused by trauma, oncologic resection, congenital malformations, and prosthetic treatments. There are still limitations and complications associated with the current standard of using autologous bone tissue as grafts. These include donor site morbidity, inadequate quantities of available donor tissue, ultimate poor tissue integration, and risk of complications as a consequence of donor tissue withdrawal. Therefore, the field is intensively investigating alternative bone graft materials.

Bones have multiple functions, providing structure, stability, and mobility with retention of flexibility via joints, to the body. The skeleton also protects internal organs, has endocrine functions and bones contain bone marrow. Bone can consist of compact cortical bone and less dense trabecular bone tissue, both of which contain mineralized tissue, osteocytes and bone-lining cells. Osteoblasts are responsible for depositing collagen and mineralizing the bone, while osteoclasts are involved in bone resorption. Bone tissue, depending on its location in the embryo and the adult body, forms through one of these two processes: intramembranous ossification (IO) and endochondral ossification (EO). IO involves the differentiation of skeletal stem and progenitor cells (SSPCs) into osteoblasts, leading to the deposition of bone matrix and subsequent vascularization of the bone. EO involves the formation of cartilage as an intermediate tissue, with SSPCs differentiating into chondroblasts that produce a cartilage matrix. The chondrocytes then become hypertrophic and subsequently either undergo cell death and allow invasion of osteoprogenitor cells and blood vessels, or they transdifferentiate into osteoblasts. Long bones are primarily formed through EO, and bone fracture healing recapitulates this process to a large extent.

Bone tissue engineering aims to provide an alternative treatment option for bone defects. It is using engineered constructs composed of appropriate cells, polypeptide growth/differentiation factors, and a 3-D environment. This approach is not yet giving totally satisfactory results required to enter the clinic. It needs to select the best source of appropriate progenitor cells, which will be combined with scaffolds, and the cells ideally can be expanded *ex vivo* whilst retaining their bone-forming properties. Both natural polymers and synthetic polymers have been considered for scaffold materials, and polypeptide growth/differentiation factors, particularly bone morphogenetic proteins (BMPs), are already being used to promote cell differentiation towards bone-forming cells. BMPs are multi-potent embryonic and adult cytokines that act in soft tissues of the embryo and the adult, but also play a role in bone formation. BMP2 and BMP6 direct human periosteum-derived cells towards bone formation. Engineering bone tissue via IO has limitations, since the lack of sufficiently speedy vascularization is a major hurdle, which could result in tissue necrosis. EO, via its cartilage intermediate is more adapted to a hypoxic environment and has shown promising results for bone tissue engineering. Craniofacial bones, such as those in the face and jaws, have different embryonic origins and bone formation mechanisms compared to long bones. Craniofacial bones differ in terms of their turnover rate, expression of osteoblast marker genes, and their potency of tissue mineralization. Cells that are multi-potent, particularly SSPCs, are commonly used for bone tissue engineering due to both their proliferation and differentiation capabilities. SSPCs can be obtained from various sources, including bone marrow, adipose tissue, dental pulp, and periosteum.

In this PhD thesis, the focus is primarily on periosteal-derived cells (hPDCs) including the bone-lining cells found in the maxillary sinus, and on their potential for bone tissue repair when combined with bone-promoting factors and bone-supporting biomaterials. The present study combines expertise in hPDCs, biomaterials, systems biology and transcriptomics to characterize and explore hPDCs for future clinical use. In the first part, hPDCs are isolated from different craniofacial areas (maxilla, mandible) and from the tibia, respectively. We hypothesized that these cells may have intrinsic differences and display varying bone-forming potential. We show they each have comparable proliferative capacities in cell culture, but their transcriptome, including of genes that are involved in skeletal system development, differs. Ectopic *in vivo* testing for *de novo* bone formation shows that mandibular-derived hPDCs have – both *in vitro* and *in vivo* – differentiation potentials towards cartilage and bone tissue, and present a strong potential for bone formation through EO.

In a separate, smaller project, similar investigations were conducted using cells from the Schneiderian membrane, which are bone-lining cells found in the maxillary sinus. While the Schneiderian membrane cells show good proliferative capacities and *in vitro* differentiation capabilities towards chondrogenic and osteogenic lineages, they were found *in vivo* to be less successful in bone formation compared to mandibular and tibial hPDCs.

Another separate objective was to replace the used fetal bovine serum (FBS) containing cell culture medium by a xenogeneic-free medium. For this, we tested chemically defined media (CDM) and medium supplemented with human platelet lysate (hPL). While the CDM tested for this thesis showed no successes because of excess cell death, the replacement of FBS by hPL led to improved osteogenic differentiation *in vitro* and more mineralized bone tissue *in vivo*.

The next objective of this PhD research was to enhance bone-forming properties *in vivo* by priming mandibular hPDCs with BMPs, seeding the cells on scaffolds and implant the constructs. Our work demonstrated that priming with BMP2 yields more pronounced effects regarding the upregulation of genes associated with the development of the skeletal system, when compared to BMP6. Among the tested scaffolds, CopiOs showed the most promising results in terms of ectopic *in vivo* bone formation. Furthermore, a rat model was developed for a critically-sized large bone defect in the mandible, and in this animal model the cell construct consisting of mandibular hPDCs, primed with BMP2, and then seeded on a CopiOs scaffold, was tested for its bone-regenerative abilities in a relevant environment.

Overall, this PhD research will contribute to the field of bone tissue engineering, with focus on cranio-maxillofacial bone repair, by exploring the potential of hPDCs, investigating different cell sources and culture conditions, and optimizing the use of BMPs and scaffolds for enhanced bone formation.

Samenvatting

Bottransplantaten worden vrijwel routinematig gebruikt in orthopedie, traumatologie, en orale en maxillofaciale chirurgie om botdefecten te behandelen die het gevolg zijn van trauma, chirurgische verwijdering van kwaadaardige tumoren, aangeboren afwijkingen, en prothetische behandelingen. Er zijn echter nog altijd beperkingen en complicaties verbonden aan de huidige standaard van het gebruik van autoloog botweefsel als transplantaten. Deze omvatten morbiditeit op de donorplaats, onvoldoende hoeveelheden beschikbaar donorweefsel, slechte ultieme weefselintegratie, en het risico op complicaties als gevolg van wegnamen van donorweefsel. Daarom is er behoefte aan alternatieve behandelingen voor botdefecten.

Botten hebben meerdere functies: ze bieden structuur, stabiliteit en mobiliteit met behoud van flexibiliteit via gewrichten, aan het lichaam. Het skelet beschermt ook inwendige organen, endocriene functies, en beenderen bevatten ook beenmerg. Botten bestaan uit compact corticaal bot en minder dichtmazig trabeculair botweefsel, die beide gemineraliseerd weefsel, botcellen en bot-omgevende cellen bevatten. Osteoblasten zijn verantwoordelijk voor het afzetten van collageen en het mineraliseren van het bot, terwijl osteoclasten betrokken zijn bij botresorptie. Botweefsel kan zich, afhankelijk van zijn locatie in het embryo en het adulte lichaam, via twee processen vormen, nl. intramembraneuze (IO) en endochondrale ossificatie (EO). IO behelst de differentiatie van skeletale stam- en voorlopercellen (SSPCs) in osteoblasten, wat leidt tot de afzetting van botmatrix en daaropvolgende vascularisatie. EO omvat de vorming van kraakbeen als intermediair weefsel, met SSPCs die differentiëren tot chondroblasten die kraakbeenmatrix produceren. De kraakbeencellen raken dan gezwollen en ondergaan dan vervolgens celdood en maken invasie van osteoprogenitorcellen en bloedvaten mogelijk, of ze *trans*differentiëren tot osteoblasten. Lange botten worden voornamelijk gevormd door EO, en de genezing van botbreuken herhaalt dit proces.

Botweefsel engineering biedt een veelbelovende behandelingsoptie voor botdefecten. Het maakt gebruik van constructen die zijn samengesteld uit geschikte cellen, polypeptide groei- en differentiatiefactoren en een 3-D draagstructuur. De huidige benaderingen geven echter nog geen bevredigende resultaten voor gebruik in de kliniek. Er is nog altijd de noodzaak om de beste bron van progenitorcellen te selecteren, en deze efficiënt te combineren met biomaterialen en 3D draagstructuren, en idealiter kunnen de cellen efficiënt worden geëxpandeerd *ex vivo* met behoud van hun botvormende eigenschappen. Zowel natuurlijke als synthetische polymeren zijn overwogen voor deze 3D draagstructuren, en polypeptide groei- en differentiatiefactoren, zoals de been morfogenetische eiwitten (BMPs). Deze worden nu al gebruikt om celdifferentiatie van SSPCs tot botvormende cellen te bevorderen. BMPs zijn multi-potente embryonale en adulte cytokines die tevens effecten hebben in zachte weefsels, maar ook een rol spelen bij botvorming. BMP2 en BMP6 sturen cellen van het human beenvlies (hPDCs) naar botvorming. IO heeft beperkingen in botweefsel engineering, omdat er geen vascularisatie mee gepaard gaat, wat kan leiden tot weefselnecrose. EO, met het intermediair kraakbeenweefsel dat wordt gevormd en geadapteerd is aan een zuurstofarme omgeving, heeft veelbelovende resultaten opgeleverd voor botweefsel engineering. Craniofaciale botten, zoals die in het aangezicht en de kaken, hebben een andere embryonale oorsprong en botvormingsmechanisme dan lange botten. Craniofaciale botten tonen verschillen in celdelingssnelheid, expressie van osteoblast merkergenen, en hun potentie van weefselmineralisatie. Cellen die multi-potent zijn, zoals de SSPCs, worden vaak gebruikt voor botweefsel engineering vanwege hun proliferatie- en differentiatiecapaciteiten. SSPCs kunnen uit

verschillende bronnen worden verkregen, waaronder beenmerg, vetweefsel, tandpulp, en periosteum.

In dit doctoraatsproefschrift ligt de focus vooral op cellen uit het beenvlies (hPDCs) en ook op de bot-bekledende cellen in de maxillaire sinus, en op hun potentieel voor botweefselherstel in combinatie met bot bevorderende factoren en bot ondersteunende draagstructuren. Deze studie combineert expertise van hPDCs, biomaterialen, systeembiologie en transcriptomics om de hPDCs te karakteriseren en te exploreren voor toekomstig gebruik in de kliniek. In het eerste deel van deze thesis worden hPDCs respectievelijk geïsoleerd uit verschillende craniofaciale locaties (met name boven- en onderkaak) en uit het onderbeen. Onze hypothese hierbij was dat deze cellen intrinsieke verschillen en een verschillend botvormend potentieel hebben. Wij tonen aan dat de celdelingscapaciteiten van elk van die hPDCs vergelijkbaar zijn, maar hun transcriptoom, inbegrepen genen die betrokken zijn bij de skeletontwikkeling, verschilt. Stringente *in vivo* testen voor *de novo* botvorming tonen aan dat de mandibulaire hPDCs - zowel in celcultuur als *in vivo* – een sterk differentiatiepotentieel hebben naar kraakbeen- en botweefsel door EO.

In een apart, kleiner project onderzochten we eveneens cellen van het Schneider-membraan, dit zijn botbeklede cellen die worden aangetroffen in de sinus van de bovenkaak. Niettegenstaande deze cellen goed delen en in celcultuur differentiëren naar kraakbeen- en botvormende cellen, zijn ze *in vivo* minder succesvol in botvorming in vergelijking met hPDCs van de onderkaak en het onderbeen. Een ander, afzonderlijke ambitie was om onze celcultuurmedia met foetaal runderserum (FBS) te vervangen door een dierproduct-vrij medium. Daarom werden chemisch gedefinieerde media (CDM) en medium aangevuld met humaan bloedplaatjeslysaat (hPL) getest. De CDM die voor dit proefschrift werd uitgeprobeerd, liet geen succes zien door de aanzienlijke celdood, maar de vervanging van FBS door hPL leidt tot verbeterde differentiatie richting bot *in celcultuur* en meer gemineraliseerd botweefsel *in vivo*.

Het volgende doel van dit doctoraatsonderzoek was om botvormende eigenschappen *in vivo* te verbeteren door hPDCs van de onderkaak te stimuleren met BMPs en deze cellen dan op 3D draagstructuren uit te zaaien en te gebruiken in transplantatie. Ons onderzoek toont aan dat stimulatie met BMP2 meer uitgesproken effecten oplevert met betrekking tot de productie van genen die geassocieerd zijn met de ontwikkeling van het skeletstelsel, in vergelijking met BMP6. Van de geteste draagstructuren laat CopiOs de meest veelbelovende resultaten zien met betrekking tot botvorming. Verder werd een rattenmodel ontwikkeld voor een kritisch-groot botdefect in de onderkaak, waarin het celconstruct bestaande uit hPDCs van de onderkaak, gestimuleerd met BMP2 en gezaaid op een CopiOs-draagstructuur, getest kon worden op zijn botherstellend vermogen in een relevante context.

Alles samen draagt dit doctoraatsonderzoek bij tot het gebied van cranio-maxillofaciaal botherstel door het potentieel van hPDCs te onderzoeken, verschillende celbronnen en kweekomstandigheden te onderzoeken, en het gebruik van BMPs en draagstructuren voor verbeterde botvorming te optimaliseren.

Curriculum vitae and PhD portfolio

Personal information

Name	**Lisanne** Caroline **Groeneveldt**
Date of birth	March 6, 1992
Nationality	Dutch
E-mail	lisanne.groeneveldt@kuleuven.be l.c.groeneveldt@erasmusmc.nl l.groeneveldt@gmail.com

Education

2018-current (fulltime since 2019)	**KU Leuven en Erasmus Universiteit Rotterdam** Joint PhD with FWO personal PhD Fellowship (ref. 1193020) > Promotors: Prof. Liesbet Geris (KU Leuven) and Prof. Danny Huylebroeck (Erasmus University Rotterdam)
2016-2019	**KU Leuven** Master in Dentistry (magna cum laude)
2015-2017	**KU Leuven** Bachelor in Dentistry (cum laude)
2012-2017 (parttime)	**Erasmus University Rotterdam** Master Molecular Medicine
2012-2015	**Erasmus University Rotterdam** Master in Medicine
2009-2012	**Erasmus University Rotterdam** Bachelor in Medicine

Research projects

PhD Thesis 2018- current	Bone tissue engineering: Exploring human periosteal-derived cells obtained from different origins and optimizing cell delivery methods. > Prometheus, Division of Skeletal Tissue Engineering, KU Leuven, Leuven, Belgium > Department of Cell Biology, Erasmus University Medical Center, Rotterdam, the Netherlands
Master Thesis Dentistry 2019	Bone tissue engineering: different gene expression levels between tibial, maxillary and mandibular-derived periosteal cells > Prometheus, Division of Skeletal Tissue Engineering, KU Leuven, Leuven, Belgium
Master Thesis Molecular Medicine 2017	Bone tissue engineering: mapping and testing differences between periosteal cells from craniofacial and long bones > Prometheus, Division of Skeletal Tissue Engineering, KU Leuven, Leuven, Belgium > Department of Cell Biology, Erasmus University Medical Center, Rotterdam, the Netherlands
Small internship Molecular Medicine 2013	The effects of EMD on chondrogenic differentiation of bone-marrow derived mesenchymal stem cells > Department of Oral and Maxillofacial Surgery, Special Dental Care and Orthodontics Erasmus University Medical Center Rotterdam, the Netherlands.

Certificates

2021	Interdisciplinary Program in Healthcare Innovation, I3Health,
2019	Brussels, Belgium
2016	IHC Good clinical practice
2015	Radiation protection certificate, KU Leuven, Leuven, Belgium
2012	Certificate B of the Federation of European Laboratory Animal Science Association KU Leuven, Leuven, Belgium
2009-2011	Masterclass surgical anatomy of the head and neck region (result: excellent), Erasmus MC Anatomy Research Project (EARP), Rotterdam, the Netherlands
2007-2008	Honours Class, Erasmus MC, Rotterdam, the Netherlands Junior Med School, Erasmus MC, Rotterdam, the Netherlands

Additional Courses

2022	Biostatistics I, NIHES, Rotterdam, the Netherlands
2020	Scientific Integrity II, KU Leuven, Leuven, Belgium
2019	Presentation Skills for Biomedical Researchers, Leuven Language Institute (ILT), Leuven, Belgium
2018	Scientific Integrity I, KU Leuven, Leuven, Belgium

Publications

Published

Groeneveldt LC, Herpelinck T, Maréchal M, Politis C, van IJcken WFJ, Huylebroeck D, Geris L, Mulugeta E, Luyten FP. The bone-forming properties of periosteum-derived cells differ between harvest sites. ***Front Cell Dev Biol.*** 2020 Nov 25;8:554984. doi: 10.3389/fcell.2020.554984. PMID: 33324630. (*This thesis*).

Smeets M, Gemels B, **Groeneveldt L**, Politis C. Is there need for technical investigations in order to predict potential length of hospital stay of oral infections? ***Am J Emerg Med.*** 2019 Feb;37(2):231-236. doi: 10.1016/j.ajem.2018.05.034. PMID: 29898830.

Spiegelberg L, Braks JA, **Groeneveldt LC**, Djasim UM, van der Wal KG, Wolvius EB. Hyperbaric oxygen therapy as a prevention modality for radiation damage in the mandibles of mice. ***J Craniomaxillofac Surg.*** 2015 Mar;43(2):214-219. doi: 10.1016/j.jcms.2014.11.008. PMID: 25523397.

Groeneveldt LC, Knuth C, Witte-Bouma J, O'Brien FJ, Wolvius EB, Farrell E. Enamel Matrix derivative has no effect on the chondrogenic differentiation of mesenchymal stem cells. ***Front Bioeng Biotechnol.*** 2014 Sep 2;2:29. doi: 10.3389/fbioe.2014.00029. PMID: 25229057.

Manuscripts submitted or in preparation

Borgiani E, Nasello G, Ory L, Herpelinck T, **Groeneveldt L**, Bucher C, Schmidt-Bleek K, Geris L. COMMBINI: an experimentally-informed COMputational Model of the Bone INjury Immuno-response. *In revision.*

Mukherjee S, Mandal S, Barzegari M, Perez-Boerema F, Liang B, Sadeghian Dekhord E, **Groeneveldt L**, Geris L. In silico design and optimization of mesoscopic and macroscopic properties of additively manufactured scaffolds: applications in skeletal tissue engineering. *In preparation*.

Groeneveldt LC, Ribeiro Viseu S, Bosmans K, Vleminckx J, Geeroms C, Vanborren O, Huylebroeck D, Geris L. Human periosteum-derived cells do expand and retain their bone-forming properties in platelet lysate. *In preparation*.

Groeneveldt LC, Ory L, Bosmans K, Kose A, Herpelinck T, Geeroms C, van Ijcken WFJ, Huylebroeck D, Geris L. Human periosteum-derived cells primed with BMP2 can heal a large bone defect in rats. *In preparation*.

International conference talks

Sept. 2022	Bones & Teeth Gordon Research Seminar (GRS), Ventura, USA
Nov. 2021	Tissue Engineering and Regenerative Medicine International Society (TERMIS) 6th World Congress, Maastricht, the Netherlands
Feb. 2020	Craniofacial Morphogenesis and Tissue Regeneration Gordon Research Conference (GRC), Lucca, Italy

International poster presentations

Oct. 2022	13th BMP Conference, Dubrovnik, Croatia
Sept. 2022	Bones & Teeth Gordon Research Conference (GRC), Ventura, USA
Feb. 2020	Craniofacial Morphogenesis and Tissue Regeneration Gordon Research Conference (GRC), Lucca, Italy
Feb. 2020	Craniofacial Morphogenesis and Tissue Regeneration Gordon Research Seminar (GRS), Lucca, Italy

Teaching

Oral and Maxillofacial physical examination, 2nd Master Medicine

Acknowledgments

I am deeply grateful to everyone who has contributed to the completion of this doctoral thesis. Without their unwavering support, encouragement, feedback and guidance, this work would not have been possible.

First and foremost, I extend my heartfelt gratitude to my supervisors, Lies Geris and Danny Huylebroeck for their invaluable mentorship, patience, and expertise throughout this research journey. Their insightful feedback and constant motivation have been instrumental in shaping this thesis.

Danny, we know each other already from earlier master theses; you guided me through my second and third master theses (the ones for Molecular Medicine and Dentistry). You taught me to write a research proposal containing many different techniques I could learn, you initiated connections enabling next steps in both my research and career and introduced me to the fields of RNA-sequencing and of course BMP-signaling. A whole new world opened for me, a world that I didn't think I was good enough to step into, but that I really enjoyed exploring.

Lies, what else can I say? Thank you for being my promotor. You helped me to grow as a researcher; you supported me a lot during the application for funding and made clear that proper research goes hand in hand with a good work-life balance (and that some work during the nights can fit into that balance too). You let me work independently, but were there as a pillar of support on the important moments.

Frank, you introduced me into the Prometheus platform after only 1 conversation, enabling me to start my master theses in your lab and subsequently my PhD. Whenever I contacted you, you always responded immediately. Thank you for believing in me and my capabilities.

I would also like to express my sincere thanks to the members of my thesis committees for their valuable insights and constructive criticisms that have strengthened the quality of this work; Because this thesis is the work for a joint PhD, committees were set up for both universities.

For my PhD in Rotterdam, I would like to thank Gert Jansen, Peter ten Dijke and Geert Carmeliet for reading the whole manuscript and their fast feedback on it. Peter ten Dijke, when you asked me to put figures in my discussion-chapter my first response included thoughts like “it is a doctoral thesis, not a graphic novel”, but I am glad you gave me this feedback. It has been a challenge for me I didn’t expect to encounter during a PhD journey, but I think it made my discussion consisting of 6 full pages with only text livelier and more attractive to read. Hans van Leeuwen, Petra Knaus and Robbert Rottier, thank you sincerely for taking part in my doctoral committee.

For my PhD in Leuven my sincere appreciation goes to Geert Carmeliet and Patrick Callaerts. You were available each year again to attend my presentations, to provide suggestions for improvements both in research skills, data analysis skills and presentation skills. Above all, you made me feel everything would be all right while I was stressing about whether I was good enough to do a PhD. Geert Carmeliet, thank you for your presence during my Prometheus data sessions. You came with very careful commentary about my research methods and data. Of course I also would like to thank Celine Colnot and France Lambert for their critical assessment and feedback on my thesis. You have read the whole thesis for a student from another university which alone is already worth a big thank you, and in addition you gave me very thoughtfull comments to improve my thesis and made time available to attend my defence.

Besides my committte members, I would also thank all the (former) faculty members and staff at Erasmus MC and KU Leuven who provided a conducive environment for learning and research, but above all also an environment which made I enjoyed going to work.

From Erasmus MC I would like to especially thank Eskeww for his help and data analysis of the first RNA sequencing experiment that was performed and the Biomics team with Wilfred van IJcken and Mirjam van den Hout for their assistance. Marike, without your help, this joint PhD would never have been possible at the Erasmus MC. You really took care of everything for me; contracts, registrations for applications, all steps in Hora Finita; you guided me through all the steps and arranged a lot for my defence in Rotterdam.

From KU Leuven and Liege university, I would like to thank Jenny, for all the troubleshooting when something was not working as planned. Marina, thank you for your guidance throughout my master theses and all steps we had to take regarding the achievement of patient samples and animal experiments. Louca, Johanna, Tim and Hannah, my dear colleagues I met during my labwork for my master theses outside office hours. Thanks to your enthusiasm and support I decided to start this PhD journey in Leuven. Louca, you made me understand the principles of flowcytometry. Even after defending your own thesis and while you were working else, you still stayed available for me and helped me with new research questions I wanted to solve with flowcytometry. Tim, thanks for sharing your knowledge, for explaining the BMP-pathways to me and last but not least, for teaching me how to analyse RNA sequencing data so that I could do the second RNA sequencing experiment totally by myself. I did also sincerely appreciate you as a travelmate to the conferences in California and Croatia; working hard, but also taking some time to enjoy life. Hannah, thanks a lot for all discussions we have had about immunohistochemical stainings and all the inspiring, supportive, and social talks we have had. Hanna, the one who was always busy with labwork as a postdoctoral researcher, thanks a lot for sharing your expertise in immunohistochemical stainings and your supportive talks. Gabriele, I really appreciated your help when I (again) encountered problems with jupyter notebook. Thank you Raphaele for your help and support regarding the PhD thesis and all social talks we have had. Liesbeth, words are not sufficient to thank you for everything we have encountered during our PhD journeys. All the coffee breaks, the surgeries we have done together, the animal care,... you have done a lot for me, the small things in the lab you did so that I could focus on this thesis and very importantly: being a friend. Ayse, Isaak, Ehsan, Mahtab, Edoardo, Satanik, Claire, Fernando, Rodrigo and all other team members from the Biomech, Prometheus and SBE teams; you also helped me a lot with your support, encouragement and inspirational and motivational talks.

Ik ben mijn familie veel dank verschuldigd voor hun onvoorwaardelijke liefde, begrip en voortdurende aanmoediging gedurende deze reis waarin ik, op dit moment al 14 jaar, ingeschreven ben als student aan de universiteit. Jullie vroegen mij niet constant waarom ik een tweede of derde master wilde studeren, of waarom ik bepaalde keuzes maakte, jullie vertrouwden mij en waren er om me te steunen. Papa, Mama en Stephanie; ondanks dat de afstand inmiddels wat groter is geworden dan aan het begin van mijn universitaire carrière, stonden jullie altijd voor mij klaar. Marco, jij hebt als rots in de branding zowel de successen met mij gevierd als mij gesteund bij tegenslagen. In het weekend nog even langs het lab rijden om cellen of dieren te verzorgen was nooit een probleem, net als alle keren dat ik 's avonds nog zat te werken omdat ik zo nodig iets af wilde hebben.

To everyone who has played a part, big or small, in shaping this thesis and my academic career, I offer my heartfelt gratitude. Your contributions have made a significant impact, and I am truly blessed to have you in my life.

Thank you.

Lisanne

It is time for the next adventure.

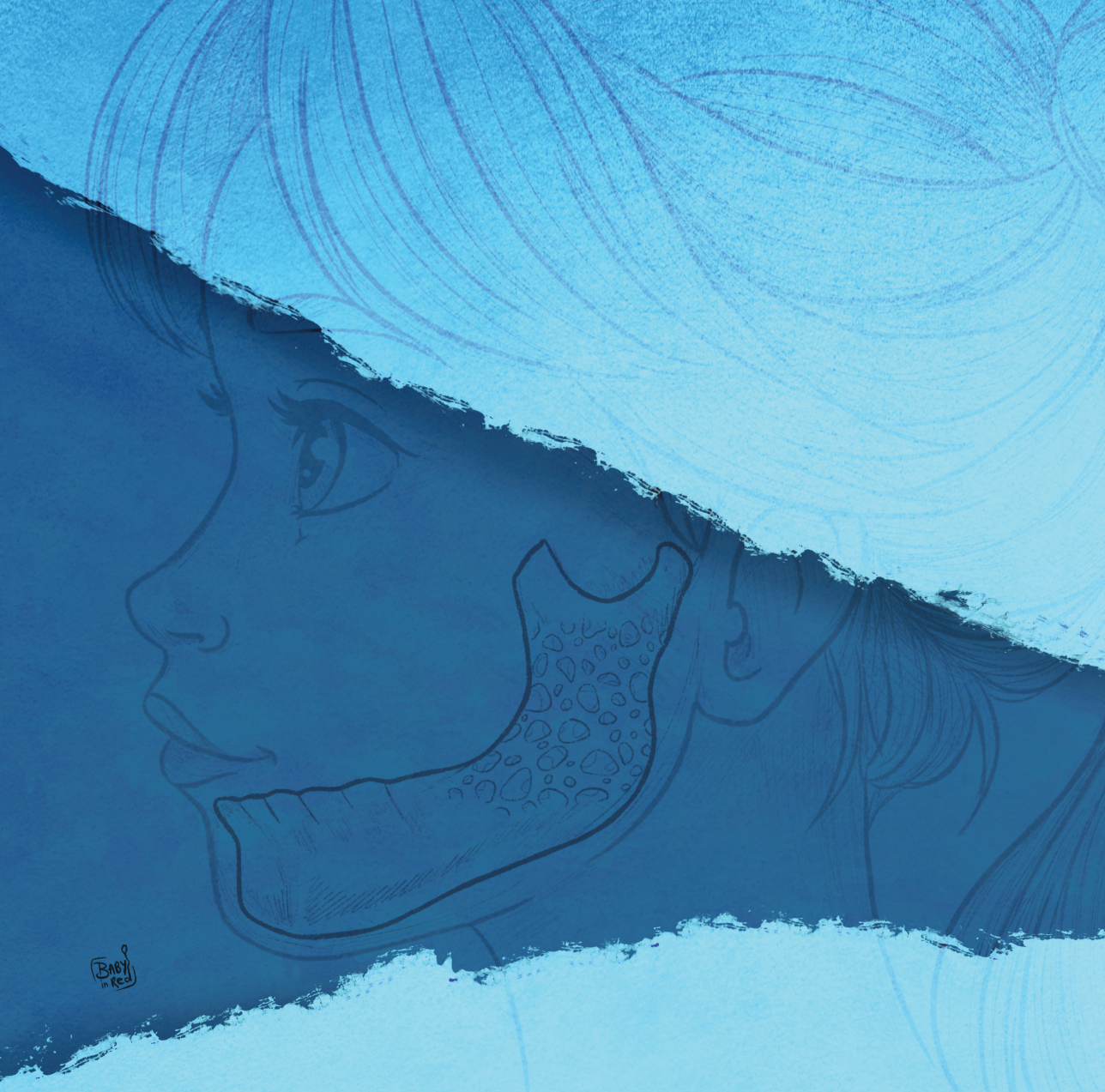

Faculty of Medicine KU Leuven
Department of Development and Regeneration
Laboratory for Tissue Engineering

Erasmus University Medical Center
Department of Cell Biology

KU LEUVEN
DOCTORAL SCHOOL
BIOMEDICAL SCIENCES

Erasmus